PARAMETER ESTIMATION IN NON-LINEAR ROTOR-BEARING SYSTEMS THROUGH VOLTERRA AND WIENER THEORIES

by

AHMAD ALI KHAN

DEPARTMENT OF MECHANICAL ENGINEERING
INDIAN INSTITUTE OF TECHNOLOGY KANPUR

JANUARY, 1999

PARAMETER ESTIMATION IN NON-LINEAR ROTOR-BEARING SYSTEMS THROUGH VOLTERRA AND WIENER THEORIES

A Thesis Submitted
in Partial Fulfilment of the Requirements
for the Degree of
DOCTOR OF PHILOSOPHY

by

AHMAD ALI KHAN

to the

DEPARTMENT OF MECHANICAL ENGINEERING
INDIAN INSTITUTE OF TECHNOLOGY KANPUR
JANUARY, 1999

CERTIFICATE

It is certified that the work contained in the thesis entitled, "**PARAMETER ESTIMATION IN NONLINEAR ROTOR-BEARING SYSTEMS THROUGH VOLTERRA AND WIENER THEORIES**" has been carried out under my supervision and that this work has not been submitted elsewhere for the award of a degree.

Nalinaksh Vyas. 4.2.99

Dr. Nalinaksh S. Vyas
Associate Professor
Department of Mechanical Engineering
Indian Institute of Technology, Kanpur

SYNOPSIS

Name of the student Ahmad Ali Khan **Roll No** 9510561

Degree for which submitted Ph.D. **Department** Mechanical Engineering

Thesis Title PARAMETER ESTIMATION IN NON-LINEAR ROTOR-BEARING SYSTEMS THROUGH VOLTERRA AND WIENER THEORIES

Name of the thesis supervisor Dr. Nalinaksh S. Vyas

The response and stability of a rotor system are critically dependent on bearing characteristics. Problems involving nonlinear characteristics of bearings - both, rolling element and fluid film, arise quite frequently in rotors (Ragulskis et al, 1974; Harris, 1984; Dimentberg, 1988; Bendat, 1990; Stolarski, 1990; Choy et al, 1992; Childs, 1993; Soong and Grigoriu, 1993; Lin and Cai, 1995; Zhou and Hashimoto, 1995). It has become evident in recent years that an important class of rotor bearing phenomenon cannot be studied without adequately accounting for the nonlinear forces produced by the bearings. Bearing nonlinearity assumes a greater role for high speed and low weight rotor applications, where the vibration amplitudes tend to be relatively large. In comparison to the amount of work done in recent years, in the area of characterisation of linear elastic parameters of bearings, research in identification and estimation of the nonlinear parameters has been relatively scarce. This is true for fluid film bearings as well as rolling element bearings, which, despite their mechanical simplicity, are known to display highly nonlinear behaviour and present some very complex rotor problems.

Parameter estimation is an inverse problem of determination of the elements of the system from measures of the forcing function induced upon it and the resultant response. Inverse problems in nonlinear analysis require techniques with rigorous theoretical base, which can provide valid routes to parameter estimation. The structure of Volterra series (Volterra; 1889, 1930, 1959) and Wiener series (Wiener, 1958), which model the relationship between the system response and the input in terms of a series of first and higher order convolution integrals, provide analytical platforms which can be utilised for parameter estimation.

The present study attempts to employ the kernel form of response representation of nonlinear systems, developed by Volterra and Wiener, for estimation of nonlinear stiffness parameters of rotor-bearing systems. These theories have been in engineering literature for quite some time and have been used by researchers, mainly in electrical control systems area, for kernel identification and synthesis. However, Volterra and Wiener theories have been scarcely used in mechanical engineering applications. An engineering approach is adopted in the present work, whereby these theories have been utilised beyond first and higher order kernel identification, to the problem of estimation of both linear and nonlinear stiffness parameters of rotor-bearing systems.

The Volterra series, recognised as a powerful tool for nonlinear analysis of systems (Billings, 1980; Rugh, 1981; Korenburg and Hunter, 1990), employs multidimensional kernels, which upon convolution with the applied excitation, express the response in the form of a power series. The kernels of the system are understood as multi-dimensional unit impulse response functions. Two basic difficulties associated with practical application of Volterra series are the convergence of the series and measurement of Volterra kernels of the given system. Their measurement is possible only if the contributions of each of the system's Volterra operators can be separated from the total response. These difficulties are circumvented in the Wiener theory. Wiener functionals are formed by a set of orthogonal functionals from the Volterra functionals for an input, which is a white Gaussian time function. The Wiener kernels can be determined through cross-correlation techniques, which can be carried out in time domain or the frequency domain. Reference can be made to the works of Lee and Schetzen (1965), Harris and Lapidus (1967), French and Butz (1973), Frentch and Butz (1974), Bedrosian and Rice (1975), Crum (1975), Gifford and Tomlinson (1989), Bendat (1990, 1998), Bendat and Piersol (1993), for kernel and higher order FRF measurements. The frequency domain treatment of Volterra and Wiener series offers an easier computation and more intuitive interpretation, in comparison to time domain treatment.

A frequency domain methodology has been developed, in the present study, for nonlinear rotor-bearing systems, whereby the Wiener kernels are estimated from measurements of the system response and applied white (broad band) excitation. Excitation is applied at the bearing stations and resultant vibration responses are picked up at the bearings and other required stations along the rotor. Volterra form of response representation is employed to synthesise mathematical expressions of the kernels in terms of linear and nonlinear parameters of the system. The relationships between Volterra and Wiener kernels of identical order, based on orthogonality conditions, are then employed to obtain estimates of the system parameters.

The parameter estimation procedure is developed and illustrated for the following rotor configurations --

(i) rigid rotor in bearings without cross-coupling

(ii) rigid rotor in bearings with cross-coupling

(iii) flexible rotors

The case of a rigid rotor supported in bearings with negligible cross-coupling effects, as in the case of ball bearings, has been modeled as a single-degree-of-freedom system. The analytical development, though general in form, is done through an assumption of a cubic type of nonlinearity in the system. An engineering approach is suggested through a third order response representation of Volterra and Wiener series. Damping is taken as linear. Using frequency domain analysis, the first to third order kernels are extracted from measurements of the applied force and response. A third order kernel factor is synthesised from the first order kernel transform and is processed along with the measured third order kernel transform for nonlinear stiffness estimation. The procedure is illustrated through numerical simulation.

The Volterra kernels are obtained from the Wiener kernels for a white Gaussian excitation. However, in practice, a broad band excitation can be provided and finite samples of data are used to obtain an estimate of a kernel. Though, the estimates are expected to differ from the true values, by amounts dependent on the variance of the

means, formed from the finite samples, errors can be made to diminish by averaging over more data. The analysis is developed in terms of nondimensional parameters. A numerical simulation of the response and subsequent parameter estimation is carried out and errors involved are illustrated for various sets of nondimensional parameters.

A rigid rotor supported in bearings with cross-coupling effects, as in the case of fluid film bearings, is modeled as a two-degree-of-freedom system. This case is more involved, since in addition to the set of direct kernels, cross-kernels also need to be defined in this case, which can be convolved with the applied excitation for response representation in terms of Volterra and Wiener series. Starting with the equations of motion, Laplace transforms are employed to derive expressions for the first and higher order direct and cross-kernels. Again, analytical modeling is carried out for a cubic type of nonlinearity. Damping is taken as linear and without cross-coupling, in order to keep the model simple. The first and third order kernels are extracted from the force and response measurements. Third order direct and cross-kernel factors are synthesised from the measured first order kernel transforms. These are subsequently processed with the measured third order kernel transforms for parameter estimation. The procedure is illustrated through numerical simulation, for various sets of nondimensional parameters and the effect of approximations and errors involved are discussed.

The procedure has been further developed to incorporate the influence of shaft flexibility. Influence coefficient concepts are employed to obtain shaft stiffness for the analysis. In order to reduce algebraic complexities, the shaft stiffness is assumed to be linear and only the bearing nonlinearity has been included. The analysis has been carried out in matrix form, to the extent possible, in order to retain the generality of approach. The parameter estimation procedure is numerically illustrated for a set of nondimensional parameters.

The application aspects of the procedure are studied through experimental investigations on a laboratory rotor rig. The experimental work has been restricted to a simple configuration, a rotor supported in ball bearings, which is treated as a single-degree-of-freedom system. The excitation mechanism, instrumentation and the results obtained are

discussed. The estimates of the parameters are compared with those obtained from a previous study based on Markov process approach. The results are also validated through an independent check, which employs Hertzian contact theory for obtaining stiffness estimates of bearings in isolation of the shaft.

To summarize, linear and non-linear bearing stiffness estimation procedures have been developed for cases of rigid rotors in bearings with and without cross-coupling and flexible rotors. The procedures are based on the theoretical foundations of the kernel form of nonlinear response representation of the Volterra and Wiener series. The procedures, though analytically developed for cubic type nonlinearity, have a general form and can be employed for estimation of a general polynomial form of nonlinearity. The procedures are also applicable to multi-degree freedom systems. The algorithms are illustrated through numerical simulation and experiments on a laboratory rotor-bearing test rig. The results and errors involved due to various engineering approximations are discussed.

ACKNOWLEDGEMENTS

I feel fortunate to have worked with Dr. N. S. Vyas. He was source of encouragement, direction and help, all along my association with him. I am extremely thankful to him for the tremendous amount of support he provided at every stage of my thesis.

I thank Prof. A. K. Mallik for introducing me to nonlinear vibrations. I also thank Mr. Animes Chatterjee, Mr. Goutam Chakarborty, Mr. Goutam Pohit, Mr. Atul Agarwal, Mr. N. Chandrashekhar and Mr. S. N. Vardha for useful discussions with them during the course of this work and to Mr. M. M. Singh for his timely and valuable help.

I liked the homely atmosphere created by family members of Dr. N. S. Vyas, Mr. M. M. Singh, Mr. A. Chatterjee, Mr. G. Pohit and my neighbours.

I am deeply indebted to my wife Samina who has shown immense understanding and patience during my preoccupation with the present work. My children Ateeb and Zain also deserve special thanks as they were deprived of the usual attention due to my absence from home.

AHMAD ALI KHAN

CONTENTS

LIST OF FIGURES

LIST OF TABLES

NOMENCLATURE

c	Damping coefficient
c_{xx}, c_{yy}	Direct damping coefficients
$f(t)$, $f_1(t)$, $f_2(t)$	Random forces
$\bar{f}(\tau)$, $\bar{f}_1(\tau)$, $\bar{f}_2(\tau)$	Normalised forces
g	Preload
$h_1(\tau_1)$	First order Volterra kernel
$h_2(\tau_1, \tau_2)$	Second order Volterra kernel
$h_3(\tau_1, \tau_2, \tau_3)$	Third order Volterra kernel
k	Linear stiffness term
$k_{b_1}^L$, $k_{b_2}^L$	Linear stiffness terms for bearings 1 and 2 respectively
k_{ij}	Shaft stiffness parameters
k^N	Nonlinear stiffness term
k_{xx}, k_{yy}	Direct linear stiffness terms
k_{xy}, k_{yx}	Cross-coupled linear stiffness terms
k_{xx}^N, k_{yy}^N	Direct nonlinear stiffness terms
k_{xy}^N, k_{yx}^N	Cross-coupled nonlinear stiffness terms
m	Mass of the system considered
$w_{0(2)}$	Zeroth order derived Wiener kernel
$w_1(\tau_1)$	First order Wiener kernel
$w_{1(3)}(\tau_1)$	First order derived Wiener kernel
$w_2(\tau_1, \tau_2)$	Second order Wiener kernel
$w_3(\tau_1, \tau_2, \tau_3)$	Third order Wiener kernel
x^*	Response parameter
x, y	Response in x-and y-directions respectively

$x, \dot{x}, \ddot{x}$	Displacement, velocity and acceleration, respectively
$x-y-z$	Rectangular coordinate system
$z(\tau)$	Output of the exponential filter
A, A_1, A_2	Variance of the forces $\bar{f}(\tau)$, $\bar{f}_1(\tau)$, and $\bar{f}_2(\tau)$ respectively
$F_{\max}$, $F_{\max_1}$	Maximum of the input $f(t)$ and $f_1(t)$ respectively
$\overline{F}(\omega)$	Fourier transform of the force $\bar{f}(\tau)$
$\overline{F}^*(\omega)$	Complex conjugate of $\overline{F}(\omega)$
$F(s)$ $F_1(s)$, $F_2(s)$	İaplace transforms of $\bar{f}(\tau)$, $\bar{f}_1(\tau)$ and $\bar{f}_2(\tau)$ respectively
$H_1(\omega)$	First order Volterra kernel transform
${}^{x}H_1^{(1)}(\omega)$	First order direct Volterra kernel transform with input $\bar{f}_1(\tau)$
${}^{x}H_1^{(2)}(\omega)$	First order cross Volterra kernel transform with input $\bar{f}_2(\tau)$
${}^{y}H_1^{(1)}(\omega)$	First order cross Volterra kernel transform with input $\bar{f}_1(\tau)$
${}^{y}H_1^{(2)}(\omega)$	First order direct Volterra kernel transform with input $\bar{f}_2(\tau)$
$H_2(\omega_1, \omega_2)$	Second order Volterra kernel transform
$H_3(\omega_1, \omega_2, \omega_3)$	Third order Volterra kernel transform
${}^{x}H_3^{(1)}(\omega, \omega, \omega)$	Third order direct Volterra kernel transform with excitation $\bar{f}_1(\tau)$
${}^{x}H_3^{(2)}(\omega, \omega, \omega)$	Third order cross Volterra kernel transform with excitation $\bar{f}_2(\tau)$
${}^{y}H_3^{(1)}(\omega, \omega, \omega)$	Third order cross Volterra kernel transform with excitation $\bar{f}_1(\tau)$
${}^{y}H_3^{(2)}(\omega, \omega, \omega)$	Third order direct Volterra kernel transform with excitation $\bar{f}_2(\tau)$
${}^{x_1}H_3^{(1)}(\omega, \omega, \omega)$	Third order direct Volterra kernel transform for station 1 with excitation $\bar{f}_1(\tau)$
${}^{x_1}H_3^{(2)}\omega, \omega, \omega)$	Third order cross Volterra kernel transform for station 1 with excitation $\bar{f}_2(\tau)$
${}^{x_2}H_3^{(1)}(\omega, \omega, \omega)$	Third order cross Volterra kernel transform for station 2 with excitation $\bar{f}_1(\tau)$

${}^{x_2}H_3^{(2)}(\omega,\omega,\omega)$	Third order direct Volterra kernel transform for station 2 with excitation $\bar{f}_2(\tau)$
${}^{x_3}H_3^{(1)}(\omega,\omega,\omega)$	Third order cross Volterra kernel transform for station 3 with excitation $\bar{f}_1(\tau)$
${}^{x_3}H_3^{(2)}(\omega,\omega,\omega)$	Third order cross Volterra kernel transform for station 3 with excitation $\bar{f}_2(\tau)$
$S_{ff}(\omega)$	Power-spectrum of the input force
$W_1(\omega)$	First order Wiener kernel transform
$W_2(\omega_1,\omega_2)$	Second order Wiener kernel transform
$W_3(\omega_1,\omega_2,\omega_3)$	Third order Wiener kernel transform
${}^{x}W_3^{(1)}(\omega,\omega,\omega)$	Third order direct Wiener kernel transform with excitation $\bar{f}_1(\tau)$
${}^{x}W_3^{(2)}(\omega,\omega,\omega)$	Third order cross Wiener kernel transform with excitation $\bar{f}_2(\tau)$
${}^{x_1}W_3^{(1)}(\omega,\omega,\omega)$	Third order direct Wiener kernel transform for station 1 with excitation $\bar{f}_1(\tau)$
${}^{x_1}W_3^{(2)}(\omega,\omega,\omega)$	Third order cross Wiener kernel transform for station 1 with excitation $\bar{f}_2(\tau)$
${}^{x_2}W_3^{(1)}(\omega,\omega,\omega)$	Third order cross Wiener kernel transform for station 2 with excitation $\bar{f}_1(\tau)$
${}^{x_2}W_3^{(2)}(\omega,\omega,\omega)$	Third order direct Wiener kernel transform for station 2 with excitation $\bar{f}_2(\tau)$
${}^{x_3}W_3^{(1)}(\omega,\omega,\omega)$	Third order cross Wiener kernel transform for station 3 with excitation $\bar{f}_1(\tau)$
${}^{x_3}W_3^{(2)}(\omega,\omega,\omega)$	Third order cross Wiener kernel transform for station 3 with excitation $\bar{f}_2(\tau)$

${}^{y}W_3^{(1)}(\omega,\omega,\omega)$	Third order cross Wiener kernel transform with excitation $\bar{f}_1(\tau)$
${}^{y}W_3^{(2)}\omega,\omega,\omega)$	Third order direct Wiener kernel transform with excitation $\bar{f}_2(\tau)$
δ	Dirac-delta function
$\eta(\tau)$	Nondimensional response
η,η',η''	Nondimensional displacement, velocity and acceleration respectively
${}^{x}\eta(\tau)$, ${}^{y}\eta(\tau)$	Nondimensional responses for x- and y- coordinates respectively
${}^{x}\eta(s)$, ${}^{y}\eta(s)$	Laplace transforms of ${}^{x}\eta(\tau)$ and ${}^{y}\eta(\tau)$
${}^{x_1}\eta(\tau)$, ${}^{x_2}\eta(\tau)$, ${}^{x_3}\eta(\tau)$	Nodimensional responses at stations 1, 2 and 3 respectively
λ	Nonlinear nondimensional parameter
$\lambda_{b_1}^{L}$, $\lambda_{b_2}^{L}$	Linear nondimensional bearing stiffness parameters
$\lambda_{b_1}^{N}$, $\lambda_{b_2}^{N}$	Nonlinear nondimensional bearing stiffness parameters
λ_{xx}^{L}, λ_{yy}^{L}	Linear nondimensional direct stiffness parameters
λ_{xx}^{N}, λ_{yy}^{N}	Nonlinear nondimensional direct stiffness parameters
λ_{xy}^{L}, λ_{yx}^{L}	Linear nondimensional cross stiffness parameters
λ_{xy}^{N}, λ_{yx}^{N}	Nonlinear nondimensional cross stiffness parameters
μ_1,μ_2	Effective bearing mass to disc mass ratios
τ	Nondimensional time
ω_n	Natural frequency
ξ, ξ_{ii}	Damping ratios
$\Psi_3(\omega,\omega,\omega)$	Third order kernel factor
${}^{xx}\Psi_3^{(l-i,j,k)}(\omega,\omega,\omega)$; ${}^{x_1x_1}\Psi_3^{(l-i,j,k)}(\omega,\omega,\omega)$ etc.	Third order kernel factors

CHAPTER 1

INTRODUCTION

Dynamic characterization of bearings constitutes a major area in rotordynamic studies. The response and stability of a rotor system are critically dependent on bearing characteristics. It has become evident in recent years, that an important class of rotor bearing phenomenon cannot be studied without adequately accounting for the nonlinear forces produced by the bearings. Bearing nonlinearity assumes a greater role for high speed and low weight rotor applications, where vibration amplitudes tend to be relatively large.

While considerable amount of work has been done in recent years in estimation of linear elastic parameters of bearings, research in identification and estimation of the nonlinear parameters has been relatively scarce. This is true for fluid film bearings as well as rolling element bearings, which despite their mechanical simplicity, are known to display highly nonlinear behaviour and present some very complex rotor problems. The approximations, thus involved in the dynamic characterisation of bearings are responsible for some of the unreliability in prediction of the response and stability of a rotor system. Parameter estimation is an inverse problem of determination of the elements of the system from measures of the forcing functions induced upon it and the resultant response. Estimation of linear parameters of rotor-bearing systems has been mostly carried out within the framework of classical dynamics, where closed form solutions are generally available to model the system response. Work in nonlinear parameter estimation has been handicapped, due to absence of such general models to exactly represent the system response.

The present study attempts to employ the kernel form of response representation of nonlinear systems, developed by Volterra and Wiener, for estimation of nonlinear stiffness parameters of rotor-bearing systems. These theories have been in engineering

literature for quite some time and used by researchers, mainly in electrical control systems area, for kernel identification and synthesis. However, they have been scarcely used in mechanical engineering applications. An engineering approach is adopted in the present work, whereby these theories have been utilised beyond first and higher order kernel identification to the problem of estimation of both linear and nonlinear stiffness parameters of rotor-bearing systems.

The structure of Volterra and Wiener series offers a rigorous theoretical platform for analysis of the response of a nonlinear system for parameter estimation. The Volterra series models the relationship between the system response and input by a series of first and higher order convolution integrals. The convolution is carried out between the applied excitation and the kernels of the system. The kernels of the system are understood as multi-dimensional unit impulse response functions. The response can be represented as a series of linear, bilinear, trilinear terms and so on. Two basic difficulties associated with the practical application of the Volterra series are the convergence of the series and the measurement of the Volterra kernels of the given system. Their measurement is possible only if the contributions of each of the system's Volterra operators can be separated from the total response. These difficulties are circumvented in the Wiener theory. Wiener functionals are formed by a set of orthogonal functionals from the Volterra functionals, for an input which is a white Gaussian time function. The Wiener kernels can be determined through cross-correlation techniques. This determination can be carried out in the time domain or frequency domain.

A general procedure has been developed in the present study, whereby the Wiener kernels are estimated from measurements of the system response and applied white (broad band) excitation. Volterra form of response representation is employed to synthesise mathematical expressions of the kernels in terms of the linear and nonlinear parameters of the system. Relationships between Volterra and Wiener kernels of identical order, based on orthogonality conditions, are then employed to obtain estimates of the system parameters. A frequency domain approach is adopted for analysis.

The problem is initially attempted for a rigid rotor supported in bearings with negligible cross-coupling effects, as in the case of ball bearings. Such a rotor-bearing configuration is modeled as a single-degree-of-freedom system. The analytical development, though general in form, is done through an assumption of a cubic type of stiffness nonlinearity in the system. An engineering approach is suggested using a third order response representation of Volterra and Wiener series. Damping is taken as linear. Using frequency domain analysis, the first and third order kernels are extracted from measurements of the applied force and response. A third order kernel factor is synthesised from the first order measured kernel transforms and is processed along with the measured third order kernel transform for nonlinear stiffness estimation. The procedure is illustrated through numerical simulation. Volterra kernels are developed from the Wiener kernels for a white Gaussian excitation. However, in practice, a broad band excitation can be provided and finite samples of data can be used to obtain an estimate of a kernel. Though, the estimates are expected to differ from the true values, by amounts dependent on the variance of means formed from the finite samples, errors can be made to diminish by averaging over more number of samples. The analysis is done in terms of nondimensional parameters and numerical simulation of the response is carried out. Subsequent parameter estimation and the errors involved are illustrated for various sets of nondimensional parameters.

The procedure is developed further for treatment of a rigid rotor supported in bearings with cross-coupling effects, as in the case of fluid film bearings. This case is more involved and is modeled as a two-degree-of-freedom system. In addition to the set of direct kernels, such a system needs cross-kernels to be defined, which can be convolved with the applied excitation for response representation in terms of Volterra and Wiener series. Starting with the equations of motion, Laplace transforms are employed to derive expressions for the first and higher order direct and cross-kernel transforms. Analytical modeling is carried out for a cubic type of nonlinearity. Damping is taken as linear and without cross-coupling, for simplicity. The first and third order kernels are extracted from force and response measurements. Third order direct and cross-kernel factors are synthesised from the measured first order kernel transforms. These are subsequently

processed with the measured third order kernel transforms for parameter estimation. The procedure is illustrated through numerical simulation, for various sets of nondimensional terms and the approximations and errors involved are discussed.

The case of parameter estimation in flexible rotors is considered next. In the cases mentioned above, the rotor shaft is taken as rigid. The treatment has been further extended to incorporate the influence of shaft flexibility. Influence coefficient concepts are employed to incorporate shaft flexibility. In order to reduce algebraic complexities, shaft stiffness is assumed to be linear and only the bearing nonlinearity has been incorporated. Analysis has been carried out in matrix form to the extent possible, in order to retain the generality of the approach. Parameter estimation procedure is developed along the route described in the previous cases. Numerical illustration is carried out for a set of nondimensional parameters.

Experimental investigations have been carried out on a laboratory rotor rig, to further study the application aspects of the procedures developed. The experimental work has been restricted to a simple configuration of a rotor supported in ball bearings, which is treated as a single-degree-of-freedom system. The excitation mechanism, instrumentation and results obtained are discussed. Estimates of the parameters are compared with those obtained from a previous study based on the Markov process approach. The results are also validated through an independent check, which employs Hertzian contact theory for obtaining stiffness estimates of bearings in isolation of the shaft.

CHAPTER 2

LITERATURE REVIEW

Analysis of the response of non-linear systems subjected to random excitation have attracted considerable attention in the recent past, mainly due to growing awareness of the significance of the random nature of forces produced by a number of physical phenomena like wind, sea waves, earthquakes etc., which must be considered in limit design of aircrafts, buildings, off-shore structures, ships etc. The present study, deals with the *inverse problem* of the estimation of system parameters from a knowledge of the applied force and the resultant system response. Inverse problems in nonlinear analysis require techniques with rigorous theoretical base, which can provide valid routes to parameter estimation. Volterra series (Volterra; 1889, 1930, 1959), provides a basis for these requirements. It has, by now, been well established as a powerful tool in the analysis of nonlinear systems (Billings, 1980; Rugh, 1981; Korenburg and Hunter, 1990). The theory of Volterra series involves modeling the relationship between system response and input force in terms of a series of first and higher order convolution integrals. Wiener series (Wiener, 1958) circumvents the problems associated with Volterra series, i.e. convergence of the series and measurement of individual kernels. The Wiener series is formed by an orthogonal set of functionals from the Volterra series for a white Gaussian input. Such white noise analysis is considered to be an effective method for gaining a maximum of information with a minimum number of assumptions about the system.

Volterra and Wiener approaches are adopted, in the present work, for linear and nonlinear parameter estimation of rotor-bearing systems. Problems involving nonlinear vibrations arise quite frequently in rotordynamics, especially those caused through random vibrations of bearings - both, rolling element and fluid film, excited by random loads (Ragulskis et al., 1974; Harris, 1984; Dimentberg, 1988; Bendat, 1990; Stolarski, 1990; Choy et al., 1992; Childs, 1993; Soong and Grigoriu, 1993; Lin and Cai, 1995; Zhou and Hashimoto, 1995). In some cases, deterministic models prove to be inadequate or at least,

extremely complex and the phenomenon can be adequately described only within the framework of statistical models. Statistical dynamics, concerned with the study of various random phenomena in dynamic systems, enriches the classical basic theory of oscillations and extends the possibilities for its applications.

A review, of the various approaches to analysis of nonlinear random vibrations, followed by a discussion on the ongoing research on dynamic characterization of rotor bearings, is presented here.

2.1 VOLTERRA AND WIENER SERIES

Volterra series has been in engineering literature for quite some time now. However, there have been few attempts towards its application to mechanical systems. Volterra series represents the response of a system in a functional form, through a series of first and higher order convolution integrals, involving explicit operations on the input to the system. The alternative form of Volterra series is the operator form. In the functional form, the emphasis is on the output at a specific time instant, for a given input function, while in operator form the focus of attention is the complete output function. The response is represented as a series of linear, bilinear, trilinear terms and so on. A linear operator is one for which the response to a linear combination of signals is same as the linear combination of the response to each individual signal. The functional form of the linear operator is a first order integral involving convolution between the first order kernel and input. The first order kernel is a unit impulse response function. The second order operator is one for which the response to a linear combination of signals is a bilinear operation on individual input signals. The functional representation of the bilinear operator is a two dimensional integral involving convolution of a second order kernel with the input. The second order kernel can be interpreted as a two dimensional impulse response. The trilinear and higher operators are similar extensions to higher dimensions. There have been many articles devoted to theoretical issues such as existence of Volterra series (Leon, 1978; Lesiak, 1978; Sandberg, 1982), computation of Volterra kernels of special systems, composition, feedback configurations, nonlinear circuits etc. (Brilliant, 1958; Barret, 1963; Flake, 1963; Lubbock, 1969; Chua, 1979, 1979a; Boyd et

al., 1983) and the formal frame work for Volterra series (Halme, 1971; DeFigueiredo, 1980; Sandberg, 1982). Volterra series can be treated in both – the time domain and the frequency domain. The frequency domain treatment provides a logical and appropriate way of extending the linear system theory to higher order Frequency Response Functions (FRFs). The higher order FRFs are calculated using techniques similar to those applied to linear systems. The obvious advantage of the frequency domain treatment over time domain treatment is that frequency domain kernels are easier to compute and have an easier interpretation. Two basic difficulties are associated with practical application of the Volterra series. The first concerns measurement of the Volterra kernels of the given system. Measurement is possible only if contributions of each of the system's Volterra operators can be separated from the total response. No exact method of isolating an individual Volterra operator exists, for a system not predefined to be restricted to a finite order. The second difficulty is that Volterra series representation of a physical system may converge for only a limited range of the system input amplitude. Volterra series is a power series with memory, similar to Taylor series, and suffers from the same limitations as the Taylor series. These difficulties with the Volterra series are circumvented in the Wiener theory.

Wiener functionals involve forming a set of orthogonal functionals from the Volterra functionals. These functionals are orthogonal when the input is a white Gaussian time function. The convergence of an orthogonal series is a convergence in the mean and Wiener functionals describe a larger class of nonlinear systems (Schetzen, 1980). The Wiener kernels render themselves to individual determination through means of cross-correlation. This determination can be carried out in the time domain or the frequency domain. White Gaussian excitation provides a means of exciting all possible nonlinear behaviour of a system, within a certain amplitude limit. However, in practice, a broad band excitation can be provided and finite samples of data can be used to obtain an estimate of a kernel. Though, the estimates differ from the expected values, by amounts dependent on the variance of the means formed from finite samples (Fakhouri et al., 1981), errors can be made to diminish by averaging over more data.

Considerable amount of research has been carried out on various aspects of Volterra and Wiener series analysis of nonlinear systems. Some of the salient works are discussed below.

Early studies:

Fretchet (1910) developed a functional series, called as Fretchet-Volterra series, for representation of a continuous nonlinear system. Wiener (1958) considered the identification of nonlinear systems by representing each functional term by a Fourier-Hermite series in conjunction with Laguerre functions. Brilliant (1958) has used the frequency domain approach in the analysis of various systems composed of cascade, feedback, inversion, addition, and subtraction of the elements. A number of studies stemmed from this work, for synthesis of a system to be equated to an unknown system. Amorocho and Orlob (1961) used the basis functional approach in finding the kernels of rainfall-runoff process. Jacoby (1966) introduced a decomposition model for hydrologic systems, A number of calculation methods were developed by later investigators using direct solution, basis functions, time domain, and frequency domain approaches, a review of which has been made by Hung and Stark (1977).

Time domain approach:

Schetzen (1965) presented a method for measuring the Volterra kernels of a finite order nonlinear system. The kernels are obtained individually as a multi-dimensional impulse response. Multi-dimensional kernel transforms can also, be obtained by the method described. As an extension, a technique of obtaining Volterra kernels from a multi-dimensional step response was presented. This technique is useful for nonlinear systems which can be considered to be of a given finite order, for only a limited range of input amplitudes. In a subsequent paper (1965(a)), he has presented a method for synthesis of Volterra kernels. Later, Lee and Schetzen (1965) developed a practical and relatively simple method for measuring Wiener kernels of a nonlinear system. The method is based upon cross correlation techniques and does not involve orthogonal expansion of basis functions as in the Wiener method.

Katzenelson and Gould (1962) developed an iterative method for obtaining kernels that can represent a system. They posed the system equivalently in terms of the solution needed for an optimum filter. Korenberg (1973) considered identification of differential systems having a Volterra series expansion, using a slowly exponentially decaying sum of sinusoids as input. The terms of the differential expansion are determined orthogonally using linear regression and simple averaging procedures. A method of directly identifying the Volterra kernels using an exponentially decaying function multiplied by a bounded zero-mean independent process, was also developed by Korenberg (1973). Identification is orthogonal, and the kernels are obtained by averaging procedure. Marmarelis and Naka (1973, a-c) and Watanabe (1975) discussed two input approach to extract kernel information. Krausz (1975) developed an identification method based on a random impulse train (Poisson process) rather than white Gaussian input. This method appears to be especially applicable to study of neuronal interactions, where the input is stimulation of a nerve axon. Klein and Yasui (1976) proposed the concept of 'dual-space' basis functions, which are then expanded in terms of Volterra kernels and further, related to Wiener kernels. Fakhouri (1978) developed an algorithm for identification of discrete Volterra kernels in terms of multidimensional z-transforms using higher order correlation functions and coloured Gaussian inputs. Fakhouri (1980) and Billings and Fakhouri (1980) analysed the nonlinear feedback system and developed an identification algorithm for open and closed loop nonlinear systems based upon pseudorandom excitation, which provides estimates of the individual component subsystems from measurement of the input and noise corrupted output.

Frequency domain approach:

After the initial works of Brilliant (1958) and George (1959), a number of studies were carried out employing the frequency domain approach. Tick (1961) developed a measure of quadratic coherence, which is used to indicate the amount of quadratic effect on the output due to input. Barret (1963) introduced the use of functional expansions for calculation of output when the input is sinusoidal or random. Korenberg (1973) developed a general method for explicit solution of the transfer functions of a random-stimulus-input cascade system containing a chain of alternating linear and static nonlinear

systems. Brillinger (1970) developed a procedure for an asymptotically unbiased and asymptotically normal estimation of the jth degree frequency transfer function for identification of a general unknown system.

French and Butz (1973) developed a general frequency-domain method for calculation of higher degree Wiener kernels, analogous to the cross correlation method of Lee and Schetzen (1965) for the time-domain case. They have used complex exponential functions as a set of orthogonal functions for expanding the kernels. In another work Frentch and Butz (1974) have developed an algorithm based on expansion of Wiener kernels in terms of Walsh functions. The nonlinear system is described in terms of a set of kernels, which contain dyadic convolution operation, and identification is performed using the fast Walsh-Fourier transform. Crum (1975) presented a simple procedure for the simultaneous reduction and expansion of multidimensional Laplace-transform kernels.

Bedrosian and Rice (1971, 1975) illustrated frequency domain methods for solution of some simple nonlinear combination of elements by means of harmonic probing, which involves simple harmonic functions as inputs and employs direct-expansion method. Gifford and Tomlinson (1989) illustrated the technique of calculation of higher order FRF's, for systems with more than one degree of freedom. The technique involving correlation measurements using random excitation is illustrated by analysis of a nonlinear beam. They also introduced higher order FRF models of a discrete structural system and showed how this model can be used as a basis for curve fitting and extracting a parametric model of multi-degree of freedom nonlinear system.

Nam et al. (1990) have presented a frequency domain approach for digitally estimating the system parameters, based on input/output measurements, of a nonlinear system which can be approximately characterised in terms of the first three transfer functions of Volterra series. As an extension of the work of previous investigators (Tick, 1961; Koh, 1985; Nikias, 1987; Powers, 1987; Kim, 1988), they presented a unified approach for handling cubic systems with stationary random inputs, by providing a quantitative

measure of power transfer between the system input and output. Odiari and Ewins (1992) have presented a procedure for identifying the vibration parameters of nonlinear vibratory systems, with particular emphasis on rotor-stator systems. They have derived the equations for calculating the Wiener and Volterra kernels in the frequency domain.

Modal techniques (Ewins, 1984) form the basis of most of structural analysis of general degree of freedom systems. Bendat and Piersol (1982, 1986), have derived equations based on bispectral analysis techniques for finite memory square law systems. Later, Bendat (1990, 1998); Bendat and Piersol (1993) derived a range of formulae for finding the first order, second order and third order FRF's through spectral analysis. Application of bispectral analysis methods to quadratic type system has also been reported by Yamamouchi (1974), for describing ocean wave characteristics and by Choi et al. (1985) and Vandiver and Jong (1986) for flow induced problems. Rice and Fitzpatric (1988) have given a generalized method for identification of a large range of nonlinear systems subjected to random excitations using spectral method in frequency domain. Rice and Fritzpatic (1991) have also discussed a situation where the modal technique becomes unsatisfactory and an inversion approach has been adopted. Recently, Worden et al. (1997) have extended the conventional harmonic probing algorithm of Bedrosian and Rice (1975) to deal with multi-input multi-output form of Volterra series.

System Characterisation:

There have been two approaches to the system characterization problems. The first approach is the differential equation method (Eykhoff et al. 1966; Eykhoff, 1974), where the topology of a system is assumed to be known, so that a set of differential equations can be used to represent the system. Identification, therefore, reduces to determination of various parameters in the equations. The second approach (Hung, et al., 1977) is the integral equation method, where little or no a-priori assumptions are made about the topology of the system. Instead, the form of integral equations is fixed, and the identification method reduces to determination of values within the integrals, called kernels. When the internal structure of a system is known, the differential equation method is usually preferred to the integral method. Only a few parameters need to be

identified in the set of differential equations, since often only a finite number of kernels need to be estimated. Another advantage of differential over integral equation approach is that the former is usually easier to interpret. On the other hand the power of the integral equation approach lies in its canonical nature (Wiener, 1958). The method can be applied to a wide class of systems, which are essentially time-invariant and have finite memory. Ho and Stark (1973) and Watanabe and Stark (1975) carried out interpretation of their estimated kernels. They have also emphasised the examination of the response dynamics of the kernel models to transient inputs, such as pulses, steps, and ramps etc.

As mentioned in the introductory part of this chapter, statistical methods have also served as powerful tools for analysis of stochastic dynamics of nonlinear systems. A brief discussion of such methods is presented here.

2.2 STATISTICAL METHODS

Statistical Dynamics, concerned with study of various random phenomena in dynamic systems, extends the possibilities for application of the classical basic theory of oscillations to situations where deterministic models are inadequate. Recognition of white noise excitation as an efficient tool for extracting maximum information about the system, with least number of assumptions has served to underline the significance of such procedures for parameter estimation.

Markov process approach:

The significance of the Markov process approach in parameter estimation lies in the fact that exact solutions of a limited class of vibratory systems can be obtained. A process, whose present probability distribution depends on only one previous time instant, is called a Markov process. The structure of a Markov process is completely determined, for all future times, by the distribution at some initial time and by a transition probability density function, which satisfies a linear partial differential equation known as the Fokker-Planck-Kolmogorov (Fokker, 1914; Planck, 1917; Kolmogorov, 1931) equation. The Fokker-Planck equation was derived and exact stationary response was obtained for certain cases of two-degree-of-freedom non-linear dynamic systems, by Ariaratnam

(1960). The theory was generalized later by Caughey (1963) for multi-degree of freedom cases. The drift and diffusion coefficients in the FPK equation can be derived from the nonlinear equations of motion of the dynamic system (Crandall, 1966). A general, closed form solution to FPK equation is yet to be found. However, the first order probability distribution for the stationary response distribution is readily obtained for a limited class of vibratory systems with nonlinear restoring forces and special forms of nonlinear damping (Fuller, 1969; Caughey, 1971; Caughey and Ma, 1983; Pradlwarter et al., 1991). Exact stationary solution in terms of probability density function, for a class of non-linear systems driven by a non-normal-delta-correlated process has been obtained by Vasta (1995).

For the response to be approximated by a Markov process, it is necessary that the excitation be approximated by ideal white noise. This restriction can be, in principle, removed at the price of increasing the complexity of the system, by introducing linear filters between the ideal white-noise excitations and the system. It can be shown by using stochastic averaging principles that, under certain conditions, the response of a nonlinear dynamic system to non-white excitation can be approximated by a Markov process. Relevant works in this field are by Stratonovitch (1967), Khasminskii (1966), Papanicolaou and Kohler (1974), Dimentberg (1980), Roberts (1983), Spanos (1983) and Zhu (1983). These works involve extensive applications to nonlinear random vibration of mechanical and structural systems.

Perturbation methods:

Perturbation methods are generally employed, when the amount of nonlinearity in a system is controlled by a small scaling parameter. The solution is sought in terms of a power series in a small scaling parameter and successive terms are evaluated as linear responses to nonlinear functions of the preceding terms. This classical approach for deterministic nonlinear problems (Stoker, 1950) was extended to random vibration problems by Crandall (1963). In practice, calculations are seldom carried beyond the first perturbation. Functional series methods offer an alternative approach to developing an expansion, based on the linear solution. An example of application of this method is the

work of Orabi and Ahmadi (1987). They used a Wiener-Hermite expansion and presented a formal procedure for deriving the deterministic equations governing kernel functions, arising in the expansion (Roy and Spanos, 1990).

Method of moments:

A set of differential equations for various statistical moments, or related quantities known as cumulants (or semi-invariants) and quasi-moments (Stratonovitch, 1967) of the response, as function of time, can be obtained by multiplying the FPK equation by suitable functions and integrating over the probability space. Equivalent sets of equations can be derived directly from the dynamic equations of motions or the equivalent Ito equations. Approximate solutions have been proposed, based on ad-hoc closure assumption (Bolotin, 1979; Ibrahim and Roberts, 1978; Roberts, 1981, Crandall, 1985).

Method of equivalent nonlinear equations:

An alternative generalization of statistical linearization has been proposed by Caughey (1986). The idea is to replace the original set of nonlinear differential equations by an equivalent nonlinear set, where the latter belong to a class of problems, which can be solved exactly. This class is, at present, very limited, and thus the range of applicability of the technique is correspondingly restricted. Results have been obtained for oscillators with nonlinearity in damping and stiffness (Caughey, 1986; Cai and Lin, 1988; Zhu and Yu, 1989). Equivalent statistical quadratization methods have been applied to non-linear multi-degree-of-freedom systems subjected to random excitation by Spanos and Donley (1991, 1992). It has been demonstrated that the method is very effective as a means of predicting the probability distribution of response, with reasonable accuracy.

Method of computer simulation:

Numerical simulation or the Monte Carlo method (Shinozuka, 1972; Bolotin, 1979; Spanos, 1981; Rubinstein, 1981; Spanos and Mignolet, 1989) consists of generating a large number of sample excitations, computing the corresponding response samples and processing them to obtain the desired response statistics. The backbone, of any digital

simulation study, is an algorithm, which provides a set of pseudo-random numbers, belonging to a population with specified probability density function. Proper processing of this set of numbers can yield values of sample functions of random process excitations, with pre-selected frequency content and temporal variation of intensity, at successive discrete equi-spaced times. Upon generating a single sample of excitation, commonly available subroutines for numerical integration of differential equations can be employed to obtain the system response. Another sample of excitation can then be generated and the computed values of system response can be used to update its statistics. The procedure, in principle, is very general and applicable to stationary or non-stationary response of systems of any degree of complication.

2.3 ROTOR-BEARING CHARACTERISATION

Parameter estimation of the elastic parameters of bearings involves establishing a relationship between the incident load on the bearing and its resultant deformation. Some of the relevant studies available in literature in the area of dynamic characterisation of rolling element and fluid-film bearings are discussed in this section.

Rolling element bearings:

Hertzian contact theory (Hertz, 1896) for the solution of local stress and deformation of two elastic bodies apparently contacting at a single point provides a platform for determination of the elastic parameters of rolling element bearings. Hertz's analysis is applied to surface stresses caused by a concentrated force, applied perpendicular to the surface. In determination of the contact deformation versus load curve, concentrated load applied normal to the surface alone, is considered, for most rolling element bearing applications. Methods of calculation of surface and subsurface stresses under a combination of normal and tangential (traction) stresses are complex, (Zwirlein and Schlicht, 1980). Owing to infinitesimally small irregularities in the basic surface geometries of the rolling contact bodies, neither uniform normal stress field nor a uniform shear field are likely to occur in practice (Sayler et al., 1981; Kalker, 1982). Rigorous mathematical/numerical methods have been developed to calculate the distribution and

magnitude of surface stresses in any line contact situation, that is, including the effects of crowning of rollers, raceways, and combinations thereof (Kunert, 1961; Reusner, 1977). Additionally, finite element methods (FEM) have been employed (Fredriksson, 1980) to perform the same analysis.

It is possible to determine how bearing load is distributed among the balls or rollers, after having determined how each ball or roller in a bearing carries load. To do this, it is necessary to develop load-deflection relationships for rolling elements contacting raceways. Most rolling bearing applications involve steady-state rotation of either the inner or outer raceways or both. Rolling element centrifugal forces, gyroscopic moments and frictional forces and moments do not significantly influence this load distribution in most applications. Theoretical models (Palmgren, 1959; Ragulskis et al., 1974; Harris, 1984; Eschamann et al. 1985; Stolarski, 1990) are available for estimation of bearing stiffnesses under static loading conditions. Recently, Chen and Lee (1997) presented a method for estimating linearised coefficients of rolling element bearings, which uses relations of unbalance responses and known system parameters in the construction of an estimator.

Bearing vibrations caused due to geometric imperfections of contact surfaces were first analyzed by Lohman (1953) and Gustavsson (1962). Comprehensive investigations have been carried out on the high frequency response of bearings (McFadden and Smith, 1984) and its relation to surface irregularities (Sunnesjo, 1985; McFadden and Smith, 1985; Su et al., 1993). Lim and Singh have analyzed the vibration transmission through rolling element bearings in series of publications (1990a, 1990b, 1991, 1992, 1994).

A method for determination of the nonlinear characteristics of bearings using the procedure of Krylov-Bogoliubov-Mitropolsky has been suggested by Kononenko and Plakhtienko (1970). Honrath (1960) and Elsermans et al. (1975) have experimentally examined the stiffness and damping of rolling element bearings. Walford and Stone (1980) designed and fabricated a test rig for direct measurement of the relative displacement of the shaft and bearing housing for the oscillating force applied to the

bearing housing, which is used to obtain the stiffness parameters. They found that the interfacial play between races and housing and shaft play a significant role in the determination of bearing stiffness and damping. Kraus et al. (1987) presented a method for extraction of rolling element bearing stiffness and damping under operating conditions. The method is based on experimental modal analysis combined with a mathematical model of the rotor-bearing-support system. Effects of speed, preload and free outer race bearings on stiffness and damping have been investigated. Muszynska (1990) has developed a perturbation technique for estimation of these parameters. The technique involves a controlled input excitation to be given to the bearings. Goodwin (1991) reviewed the experimental approaches to rotor support impedance measurement, with particular emphasis on fluid film bearing impedance measurement. A general procedure for identification of restoring force nonlinearity from system's response to a white-noise excitation has been discussed by Dimentberg and Sokolov (1991). Nonlinear stochastic contact vibrations and friction at a Hertzian contact have been studied by Hess et al. (1992). Analytical and experimental studies are carried out by them, using the Fokker-Planck equation and simulating the vibrations to the contact region, either externally by a white Gaussian random normal load or internally by a rough surface input.

Tiwari and Vyas (1995, 1997, 1997a, 1998) in a series of papers described procedures for estimation of non-linear elastic parameters of bearings based on the analysis of random response signals picked up from the bearing caps. The procedures did not require an a-priori knowledge of the random excitation force induced on the system. The dynamics of the rotor-bearing system was modeled as a Markov process and Fokker-Planck equations are formulated. The Fokker-Planck equations were solved and the response was processed, for the inverse problem of parameter estimation. The procedure was developed for cases of rigid rotors; single disc flexible rotors and multi-disc flexible rotors. The study was extended further, to include harmonic excitation to the non-linear system along with random excitation and the case of an unbalanced rigid rotor was discussed. The algorithms were also verified experimentally, for a laboratory rotor-bearing test rig.

Fluid-film bearings:

Vast amount of literature is available on the linear aspects of rotors supported in fluid film bearings. Reference can be made to the texts by Fuller (1984), Childs (1993) and Rao (1998) for a detailed study. Some of the relevant works are discussed below.

The idea of representing the dynamic response characteristics of a journal bearing by means of stiffness and damping coefficients originates with Stodola (1925) and Hummel (1926). Their aim was to improve the calculation of the critical speed of a rotor by including the flexibility of the bearing oil film. Concurrently, Newkirk (1924, 1925) described the phenomenon of bearing induced instability, which he called oil whip. Robertson (1946) analysed the whirling of a journal in a sleeve bearing. The influence of fluid film journal bearing on the stability of rotors was reported by Hagg (1946).

The bearings have been approximated, in the initial stages, as short bearings (Ocvirk, 1952) or as infinitely long bearings (Gross, 1962; Booker, 1965). Both types of approximations have been usefully employed by researchers for bearing analysis. The analytic finite length bearing model is given by Warner (1963). Later works include those of Kirk and Gunter (1970, 1975, 1975a) who employed the short bearing model for rotor dynamic analysis; Simandri and Hahn (1975) and Tonneson (1975) used the short bearing model in the analysis of squeeze film dampers. Vance and Kearton (1975) examined the appropriateness of the long bearing model for long squeeze film dampers with end seals.

Several investigators have investigated the combined transient rotor bearing dynamic problem by numerically solving the Reynold's equation for the bearing reaction force, while simultaneously integrating the rotor equations of motion. Lund and Sternlicht (1962) initially calculated the linear stiffness and damping coefficients through numerical differentiation of a finite difference solution to the Reynold's equation. Blok (1965) solved the Reynold's equation directly via finite differences to obtain mobility descriptions for finite length bearings. The numerical approach is also followed in the works of Kirk and Gunter, mentioned earlier, for the short bearing model and by Myrick and Rylander (1975) for finite length bearing. Orcutt and Arwas (1967) used a similar

analysis approach to obtain stiffness and damping coefficients for both laminar and turbulent conditions.

Lund (1968) developed a perturbation solution to the Reynold's equation, which eliminates the requirement of numerical differentiation. A direct analytic method for deriving a complete set of analytic stiffness and damping coefficients from impedance descriptions is developed and demonstrated for the cavitating finite length bearing impedances by Childs et al. (1977). The development of the concept of spring and damping coefficients for journal bearing is briefly reviewed by Lund (1987). Baheti and Kirk (1994, 1994a) used finite element method to solve the nonlinear coupled hydrodynamic and thermal equations to obtain the stiffness and damping coefficients of seals.

The direct experimental determination of stiffness and damping coefficients of journal bearing was initiated by Glienicke (1966) and Morton (1971). They used the technique of excitation of bush sinusoidally in two mutually perpendicular directions, and in each case measuring the amplitude and phase of the resulting motions. One way of improving the accuracy of measurement of stiffness and damping coefficients is to collect experimental data over a wide range of forcing frequencies, and to use all of this data to determine the coefficient values. In publications by Stanway et al. (1979), by Burrows et al. (1981), and by Burrows and Sahinkya (1982) the system is forced at all frequencies within the range of interest, simultaneously in horizontal and vertical directions. A method of treating the unbalance response data from a test rig to determine bearing stiffness and damping coefficients was suggested by Sahinkaya and Burrows (1984). A similar approach through the transient response to an impulse or step force was given by Nordman and Schollhorn (1980). Goodwin (1991) has given a concise account of the experimental techniques available for use in the measurement of bearing impedances and discussed the potential advantages and disadvantages of each approach. The frequency swept rotating input perturbation techniques, for identification of fluid film rotor bearing system dynamic characteristics are described by Muszynska and Bentley (1990). The method developed by Rouvas and Childs (1993) is designed to account for an unmeasurable input

to the system, namely the force generated by turbulence and cavitation in fluid film, by assuming that the applied excitation and the fluid film induced forces are statistically independent.

Krodkiewski and Ding (1993) developed an on site identification algorithm for multi-bearing rotor systems based on monitoring the trajectories of the relative motion of the journals with respect to the bearings. Arumugam et al. (1997) have carried out experimental investigations to identify static and dynamic characteristics of journal bearings under the influence of various cases of twisting misalignment. Goodwin et al. (1997) described a combined theoretical and experimental investigation of linear fluid film stiffness and damping coefficients. A multi-frequency force signal was used to excite the bearing and measurements of the relative movement between the shaft and journal have been made.

Investigations into the nonlinear aspects of fluid-film bearing dynamics have been relatively few and recent. Choy et al. (1992) have examined the nonlinear characteristics and their effects on the dynamic performance of a hydrodynamic journal bearing at various operating conditions. Krodkiewski and Ding (1993a) considered the problem of static indetermination in the mathematical model for nonlinear dynamic analysis of multi-bearing systems. Recently, Chu et al. (1998) have described a nonlinear dynamic model for hydrodynamic bearings which incorporates the nonlinear stiffness and damping parameters as functions of static bearing stiffness. A finite difference approach is used to solve for these coefficients. For a detailed account on available experimental data on hydrodynamic bearings, reference can be made to the extensive survey by Swanson and Kirk (1997), which catalogues about a 100 published experimental works.

CHAPTER 3

PARAMETER ESTIMATION IN RIGID-ROTORS SUPPORTED IN BEARINGS WITH NO CROSS-COUPLING

A rigid-rotor supported in bearings with no cross-coupling effects is considered as a first exercise in linear and nonlinear parameter estimation. This may be the case for a rotor supported in rolling element bearings, where the cross-coupled stiffness terms are negligible in comparison to the direct stiffness terms. Similarly, damping is taken to be comprising of the direct terms only. The effect of the rotor shaft flexibility is also not accounted for, in this chapter. Rolling element bearings are generally characterized by a cubic nonlinearity. For algebraic ease, only stiffness nonlinearity is considered. Damping is taken to be linear. This reduces the rotor-bearing set-up to a single-degree-of-freedom system with cubic stiffness nonlinearity. An engineering approach for parameter estimation is developed through a third order Volterra kernel representation of the system response. Using frequency domain analysis, the first to third order kernels are extracted from measurements of the applied force and response. A third order kernel factor is synthesised from the first order kernel transform and is processed along with the third order measured kernel transform for estimation of the nonlinear parameter. The procedure is illustrated through numerical simulation. The assumptions involved and the approximations are discussed. The influence of excitation force, linear damping parameter and probable measurement noise on the estimates is illustrated through nondimensional simulation.

3.1 Governing Equation And Volterra Series Representation of Response

For the rotor-bearing system shown in Fig. 3.1, modeled as a single-degree-of-freedom system, the governing equation of motion can be written as

$$m\ddot{x} + c\dot{x} + kx + k^N x^3 = f(t) \tag{3.1}$$

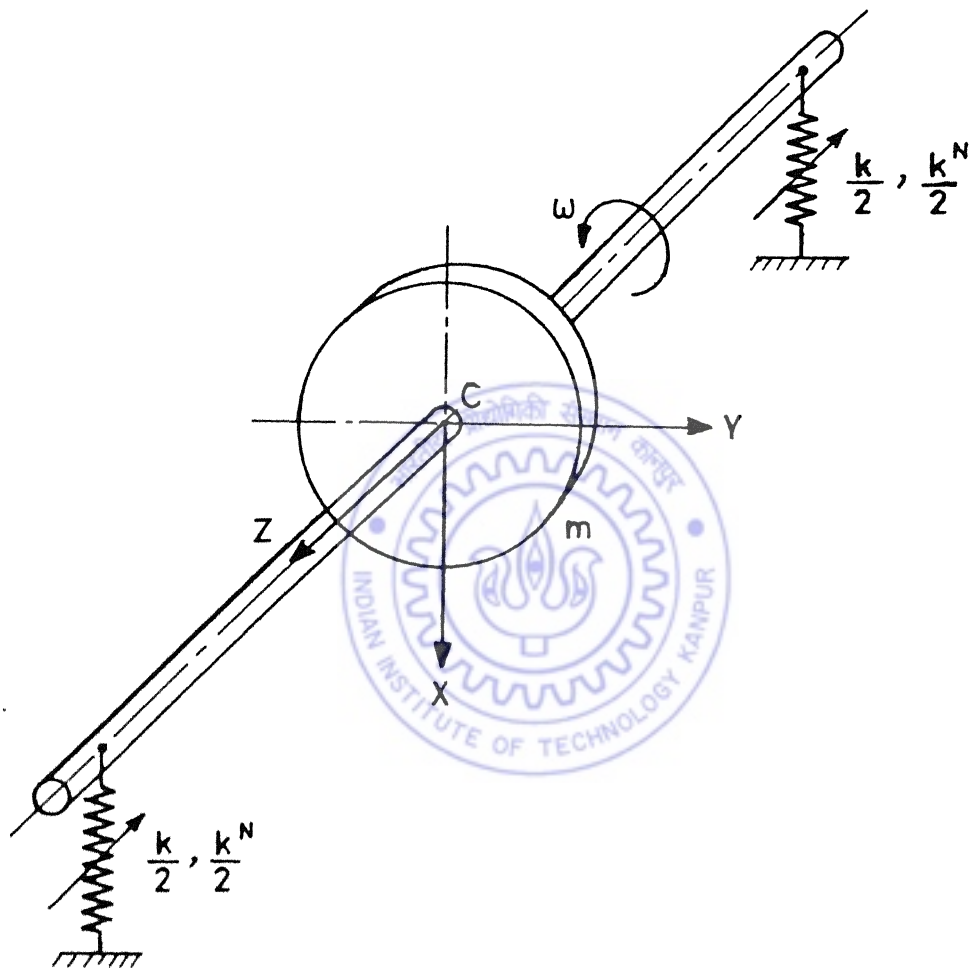

Figure 3.1 Rigid rotor in bearings without cross-coupling.

where m is the mass, k^N is the unknown non-linear stiffness, while c and k are the unknown linear damping and stiffness terms. $f(t)$ in the above equation represents the random excitation given to the system.

The equation (3.1) is rewritten in nondimensional form as

$$\eta''(\tau)+2\xi\eta'(\tau)+\eta(\tau)+\lambda\eta^3(\tau)=\bar{f}(\tau) \tag{3.2}$$

where ($'$) denotes differentiation with respect to τ, and

$$\tau=\omega_n t$$
$$\omega_n=\sqrt{k/m} \qquad \xi=c/2m\omega_n \qquad \eta=x/x^* \tag{3.3}$$
$$x^*=F_{\max}/k \qquad \lambda=k^N F_{\max}^2/k^3 \qquad \bar{f}(\tau)=f(\tau)/F_{\max}$$

Employing Volterra theory the system response is taken to be of the following kernel form

$$\eta(\tau)=h_0+\int_{-\infty}^{\infty}h_1(\tau_1)\bar{f}(\tau-\tau_1)d\tau_1+\int_{-\infty}^{\infty}\int_{-\infty}^{\infty}h_2(\tau_1,\tau_2)\bar{f}(\tau-\tau_1)\bar{f}(\tau-\tau_2)d\tau_1 d\tau_2$$
$$+\int_{-\infty}^{\infty}\int_{-\infty}^{\infty}\int_{-\infty}^{\infty}h_3(\tau_1,\tau_2,\tau_3)\bar{f}(\tau-\tau_1)\bar{f}(\tau-\tau_2)\bar{f}(\tau-\tau_3)d\tau_1 d\tau_2 d\tau_3+..... \tag{3.4}$$
$$....+\int_{-\infty}^{\infty}.....\int_{-\infty}^{\infty}h_n(\tau_1,.....,\tau_n)\bar{f}(\tau-\tau_1).....\bar{f}(\tau-\tau_n)d\tau_1.....d\tau_n+.....$$

where h_0 is a constant and the n^{th} order Volterra kernel

$$h_n(\tau_1,.....\tau_n)=0 \quad \text{for} \quad \tau_j<0, \quad j=1,2.....n$$

The response can be, alternatively expressed, in operator form as

$$\eta(\tau)=\mathbf{H}[\bar{f}(\tau)]$$
$$=\sum_{n=0}^{\infty}H_n[\bar{f}(\tau)] \tag{3.5}$$

where

$$H_n[\bar{f}(\tau)]=\int_{-\infty}^{\infty}.....\int_{-\infty}^{\infty}h_n(\tau_1,.....,\tau_n)\bar{f}(\tau-\tau_1).....\bar{f}(\tau-\tau_n)d\tau_1.....d\tau_n \tag{3.6}$$

3.2 Synthesis of Higher Order Volterra Kernel Factors

The approach suggested by Schetzen (1980) is employed to define the Laplace transform of the first-order kernel, $H_1(s)$, in terms of the linear parameters of the system, namely ω_n and ξ. The expressions for higher order kernel transforms $H_2(s)$, $H_3(s)$ etc. are consequently synthesised from the first-order transform, $H_1(s)$, and the nonlinear parameter λ.

Replacing the applied force $\bar{f}(\tau)$ by $c\bar{f}(\tau)$, the system response, from equation (3.4) is

$$\sum_{n=1}^{\infty} c^n H_n[\bar{f}(\tau)] = \sum_{n=1}^{\infty} c^n \eta_n(\tau) \tag{3.7}$$

where, c being a constant and for convenience

$$\eta_n(\tau) = H_n[\bar{f}(\tau)]. \tag{3.8}$$

Substituting the new force and the response of equation (3.7) in equation (3.2) gives

$$\left\{\sum_{n=1}^{\infty} c^n \eta_n(\tau)\right\}'' + 2\xi\left\{\sum_{n=1}^{\infty} c^n \eta_n(\tau)\right\}' + \left\{\sum_{n=1}^{\infty} c^n \eta_n(\tau)\right\} + \lambda\left\{\sum_{n=1}^{\infty} c^n \eta_n(\tau)\right\}^3 = c\bar{f}(\tau) \tag{3.9}$$

The above power series representation of the governing equation is solved by equating the coefficients of like powers of c.

Equating the coefficients of the first power of c, one obtains

$$\eta_1''(\tau) + 2\xi\eta_1'(\tau) + \eta_1(\tau) = \bar{f}(\tau). \tag{3.10}$$

Noting from equation (3.4) that $\eta_1(\tau)$, the first term in the Volterra representation of $\eta(\tau)$, is the solution of the linear part of the differential equation (3.2), i.e.

$$H_1[\bar{f}(\tau)] = \eta_1(\tau) \tag{3.11}$$

the Laplace transform of H_1, is

$$H_1(s) = 1/(s^2 + 2\xi s + 1). \tag{3.12}$$

Similarly, equating the coefficients of c^2 gives

$$\eta_2''(\tau) + 2\xi\eta_2'(\tau) + \eta_2(\tau) = 0 \tag{3.13}$$

The above requires the second order kernel h_2 to be identically to be zero, i.e.

$$h_2(\tau_1, \tau_2) = 0 \tag{3.14}$$

Equating the coefficients of c^3 gives

$$\eta_3''(\tau) + 2\xi\eta_3'(\tau) + \eta_3(\tau) = -\lambda\eta_1^3(\tau) \tag{3.15}$$

Similar to that in the case of equation (3.10), the above requires

$$\eta_3(\tau) = -\lambda H_1[\eta_1^3(\tau)] \tag{3.16}$$

Now, since

$$\eta_3(\tau) = H_3[\tilde{f}(\tau)] \tag{3.17}$$

one gets

$$H_3[\tilde{f}(\tau)] = -\lambda H_1[\eta_1^3(\tau)] \tag{3.18}$$

and in terms of Laplace transforms (refer the block diagram representation of equation (3.18) in Fig. 3.2)

$$H_3(s_1, s_2, s_3) = \lambda\left[\Psi_3(s_1, s_2, s_3)\right] \tag{3.19}$$

where $\Psi_3(s_1, s_2, s_3)$, has been christened as the synthesised third order kernel factor and is mathematically expressed as

$$\Psi_3(s_1, s_2, s_3) = -H_1(s_1)H_1(s_2)H_1(s_3)H_1(s_1 + s_2 + s_3). \tag{3.20}$$

3.3 Wiener Kernel Representation of Response

The practical application of Volterra series analysis is known to present two major problems, namely, measurement of individual kernels and convergence of the series. Wiener (1958)

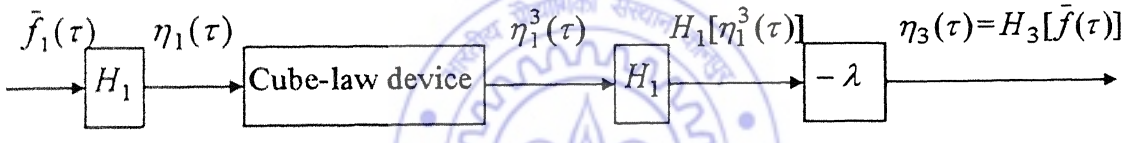

Fig. 3.2 Block diagram representation for the operator, H_3.

suggested a set of orthogonal functionals in order to circumvent the above problems. If $\bar{f}(\tau)$ is a stationary Gaussian white noise excitation with variance A (which is same as the power spectrum, $S_{ff}(\omega)$, of input force for a Gaussian process), the nth order Wiener kernel written as

$$g_n[w_n, w_{n-1(n)}, \ldots\ldots, w_{0(n)}; \bar{f}(\tau)] \tag{3.21}$$

is an orthogonal functional formed from Volterra functionals such that it is orthogonal to any homogeneous Volterra functional of degree less than n, i.e.

$$\overline{H_m[\bar{f}(\tau)]\, g_n[w_n, w_{n-1(n)}, \ldots\ldots, w_{0(n)}; \bar{f}(\tau)]} = 0 \tag{3.22}$$

The system response can be readily written in terms of the Wiener functionals, as below (Lee et. al., 1964)

$$\begin{aligned}\eta(\tau) = w_0 &+ \int_{-\infty}^{\infty} w_1(\tau_1)\bar{f}(\tau-\tau_1)d\tau_1 \\ &+ \int_{-\infty}^{\infty}\int_{-\infty}^{\infty} w_2(\tau_1,\tau_2)\bar{f}(\tau-\tau_1)\bar{f}(\tau-\tau_2)d\tau_1 d\tau_2 - A\int_{-\infty}^{\infty} w_2(\tau_1,\tau_1)d\tau_1 \\ &+ \int_{-\infty}^{\infty}\int_{-\infty}^{\infty}\int_{-\infty}^{\infty} w_3(\tau_1,\tau_2,\tau_3)\bar{f}(\tau-\tau_1)\bar{f}(\tau-\tau_2)\bar{f}(\tau-\tau_3)d\tau_1 d\tau_2 d\tau_3 \\ &- 3A\int_{-\infty}^{\infty}\int_{-\infty}^{\infty} w_3(\tau_1,\tau_1,\tau_2)\bar{f}(\tau-\tau_2)d\tau_1 d\tau_2 + \ldots\ldots\ldots\ldots\end{aligned} \tag{3.23}$$

whereby owing to the orthogonality property the Wiener and Volterra kernels can be shown to bear the following mutual relations (for a third order system response representation; Schetzen (1980))

$$\begin{aligned} h_3(\tau_1,\tau_2,\tau_3) &= w_3(\tau_1,\tau_2,\tau_3) \\ h_2(\tau_1,\tau_2) &= w_2(\tau_1,\tau_2) \\ h_1(\tau_1) &= w_1(\tau_1) + w_{1(3)}(\tau_1) \\ h_0 &= w_0 + w_{0(2)} \end{aligned} \tag{3.24}$$

with

$$w_{1(3)}(\tau_1) = -3A\int_{-\infty}^{\infty} w_3(\tau_1,\tau_2,\tau_2)d\tau_2$$

$$w_{0(2)} = -A\int_{-\infty}^{\infty} w_2(\tau_1,\tau_1)d\tau_1$$

3.4 Extraction of Wiener Kernels from Measured Response

In view of the stated difficulties in the measurement of Volterra kernels, the measured system response is employed to extract the Wiener kernels. These Wiener kernels are then employed to generate the Volterra kernels, using the relationships of equations (3.24).

Extraction of Wiener kernels from measured response involves enormous amount of data processing, since the kernels are multi-dimensional. The Laguerre filters proposed by Wiener (1958) or the alternative approach of using cross-correlation techniques and time delay filters suggested by Lee and Schetzen (1965), present formidable amount of data processing. Use of a complex filter, in the frequency domain (French and Butz, 1973), reduces the computational effort and is also suitable for such analysis since the Wiener kernel theory involves multidimensional convolutions. The scheme, employing a complex exponential filter, is graphically shown in Fig. 3.3. The Fourier transform representation for the variables in equation (3.23) may be expressed as,

$$\bar{f}(\tau) = \int_{-\infty}^{\infty} \bar{F}(\omega) e^{j\omega\tau} d\omega \qquad \eta(\tau) = \int_{-\infty}^{\infty} \eta(\omega) e^{j\omega\tau} d\omega$$

$$w_1(\tau_1) = \int_{-\infty}^{\infty} W_1(\omega_1) e^{j\omega_1\tau_1} d\omega_1 \qquad w_2(\tau_1,\tau_2) = \int_{-\infty}^{\infty} W_2(\omega_1,\omega_2) e^{j(\omega_1\tau_1+\omega_2\tau_2)} d\omega_1 d\omega_2$$

$$w_3(\tau_1,\tau_2,\tau_3) = \int_{-\infty}^{\infty} W_3(\omega_1,\omega_2,\omega_3) e^{j(\omega_1\tau_1+\omega_2\tau_2+\omega_3\tau_3)} d\omega_1 d\omega_2 d\omega_3 \tag{3.25}$$

Substituting equation (3.25) into equation (3.23) and using the relationship that

$$\int_{-\infty}^{\infty} e^{j\omega\tau} d\tau = \delta(\omega), \text{ the Dirac Delta function,} \tag{3.26}$$

one obtains

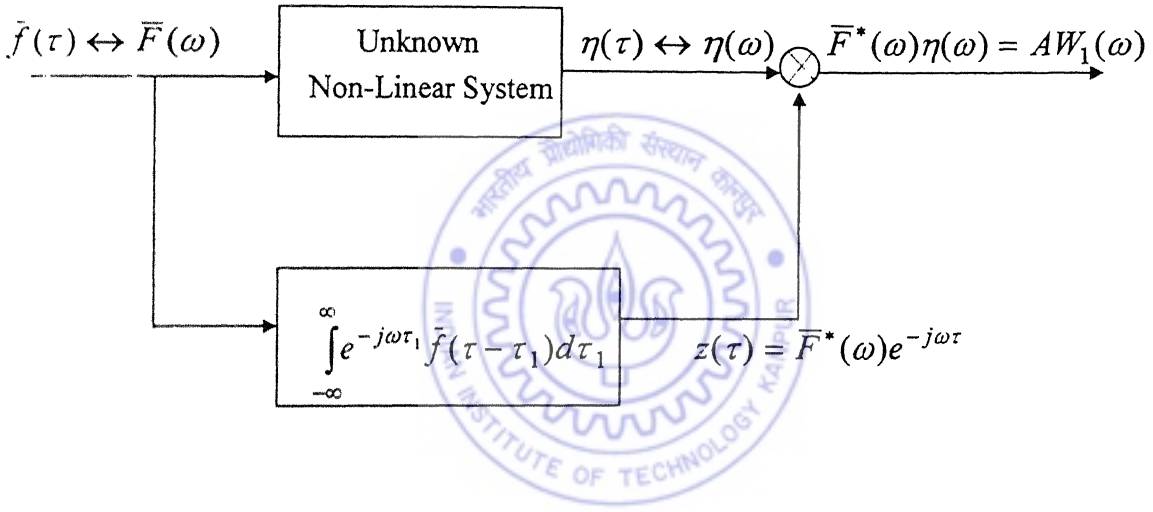

Fig. 3.3 Scheme for evaluation of the first order Wiener kernel transform, $W_1(\omega)$.

$$\eta(\tau) = W_0 + \int_{-\infty}^{\infty} W_1(\omega_1)\bar{F}(\omega_1)e^{j\omega_1\tau}d\omega_1$$
$$+ \int_{-\infty}^{\infty}\int_{-\infty}^{\infty} W_2(\omega_1,\omega_2)\bar{F}(\omega_1)\bar{F}(\omega_2)e^{j(\omega_1+\omega_2)\tau}d\omega_1 d\omega_2 - A\int_{-\infty}^{\infty} W_2(\omega_2,-\omega_2)d\omega_2$$
$$+ \int_{-\infty}^{\infty}\int_{-\infty}^{\infty}\int_{-\infty}^{\infty} W_3(\omega_1,\omega_2,\omega_3)\bar{F}(\omega_1)\bar{F}(\omega_2)\bar{F}(\omega_3)e^{j(\omega_1+\omega_2+\omega_3)\tau}d\omega_1 d\omega_2 d\omega_3 \quad (3.27)$$
$$-3A\int_{-\infty}^{\infty}\int_{-\infty}^{\infty} W_3(\omega_1,\omega_2,-\omega_2)\bar{F}(\omega_1)d\omega_1 d\omega_2 + \ldots\ldots\ldots\ldots$$

The output $z(\tau)$, from the exponential filter, can be written as

$$z(\tau) = \int_{-\infty}^{\infty} e^{j\omega\tau_1}\bar{f}(\tau-\tau_1)d\tau_1$$
$$= \bar{F}^*(\omega)e^{-j\omega\tau_1} \quad (3.28)$$

The ensemble average of the output of the circuit (Fig. 3.3) is obtained as

$$\langle\eta(\tau)z(\tau)\rangle = \langle\bar{F}^*(\omega)\rangle e^{-j\omega\tau}W_0$$
$$+ \int_{-\infty}^{\infty} W_1(\omega_1)\langle\bar{F}(\omega_1)\bar{F}^*(\omega)\rangle e^{-j\tau(\omega_1-\omega)}d\omega_1$$
$$+ \int_{-\infty}^{\infty}\int_{-\infty}^{\infty} W_2(\omega_1,\omega_2)\langle\bar{F}(\omega_1)\bar{F}(\omega_2)\bar{F}^*(\omega)\rangle e^{-j\tau(\omega_1+\omega_2-\omega)}d\omega_1 d\omega_2$$
$$- A\langle\bar{F}^*(\omega)\rangle e^{-j\omega\tau}\int_{-\infty}^{\infty} W_2(\omega_2,-\omega_2)d\omega_2 \quad (3.29)$$
$$+ \int_{-\infty}^{\infty}\int_{-\infty}^{\infty}\int_{-\infty}^{\infty} W_3(\omega_1,\omega_2,\omega_3)\langle\bar{F}(\omega_1)\bar{F}(\omega_2)\bar{F}(\omega_3)\bar{F}^*(\omega)\rangle e^{-j\tau(\omega_1+\omega_2+\omega_3-\omega)}d\omega_1 d\omega_2 d\omega_3$$
$$- 3A\int_{-\infty}^{\infty}\int_{-\infty}^{\infty} W_3(\omega_1,\omega_2,-\omega_2)\langle\bar{F}(\omega_1)\bar{F}^*(\omega)\rangle e^{-j\tau(\omega_1-\omega)}d\omega_1 d\omega_2$$
$$+ \ldots\ldots\ldots\ldots$$

Since $\bar{f}(\tau)$ is stationary Gaussian white noise with zero mean and variance A, the Fourier transform, $\bar{F}(\omega)$, is also a stationary Gaussian white noise process and the ensemble averages of the products transformed functions are (Raemer, 1969)

$$\langle \bar{F}(\omega) \rangle = 0$$

$$\langle \bar{F}(\omega_1)\bar{F}(\omega_2) \rangle = A\delta(\omega_1 + \omega_2)$$

$$\langle \bar{F}(\omega_1)\bar{F}(\omega_2)\bar{F}(\omega_3) \rangle = 0$$

$$\langle \bar{F}(\omega_1)\bar{F}(\omega_2)\bar{F}(\omega_3)\bar{F}(\omega_4) \rangle = A^2[\delta(\omega_1+\omega_2)\delta(\omega_3+\omega_4)] + A^2[\delta(\omega_1+\omega_3)\delta(\omega_2+\omega_4)] + A^2[\delta(\omega_1+\omega_4)\delta(\omega_2+\omega_4)] \quad (3.30)$$

The relations of equation (3.30) reduce equation (3.29) to

$$\langle \eta(\tau)z(\tau) \rangle = AW_1(\omega) \quad (3.31)$$

However, due to the equivalence of time and ensemble averages, the ensemble average $\langle \eta(\tau)z(\tau) \rangle$ can also be written as

$$\langle \eta(\tau)z(\tau) \rangle = \lim_{T\to\infty} \frac{1}{T} \int_{-T/2}^{T/2} \eta(\tau)z(\tau)d\tau \quad (3.32)$$

giving

$$\langle \eta(\tau)z(\tau) \rangle = \bar{F}^*(\omega)\eta(\omega) \quad (3.33)$$

Equations (3.31) and (3.33) give

$$AW_1(\omega) = \bar{F}^*(\omega)\eta(\omega)$$

from which the expression for the Fourier transform of the first order Wiener kernel is be obtained as

$$W_1(\omega) = \bar{F}^*(\omega)\eta(\omega)/A \quad (3.34)$$

For measurement of third order kernel transform, a circuit involving three exponential delay filters as shown in Fig. 3.4 is considered. The output, $z(\tau)$, from the exponential filters is

$$z(\tau) = \int_{-\infty}^{\infty} e^{-j\omega_1\tau_1}\bar{f}(\tau-\tau_1)d\tau_1 \int_{-\infty}^{\infty} e^{-j\omega_2\tau_2}\bar{f}(\tau-\tau_2)d\tau_2 \int_{-\infty}^{\infty} e^{-j\omega_3\tau_3}\bar{f}(\tau-\tau_3)d\tau_3 \quad (3.35)$$

The above, after some algebraic manipulations, reduces to

$$z(\tau) = \bar{F}(-\omega_1)\bar{F}(-\omega_2)\bar{F}(-\omega_3)e^{-j(\omega_1+\omega_2+\omega_3)\tau}$$

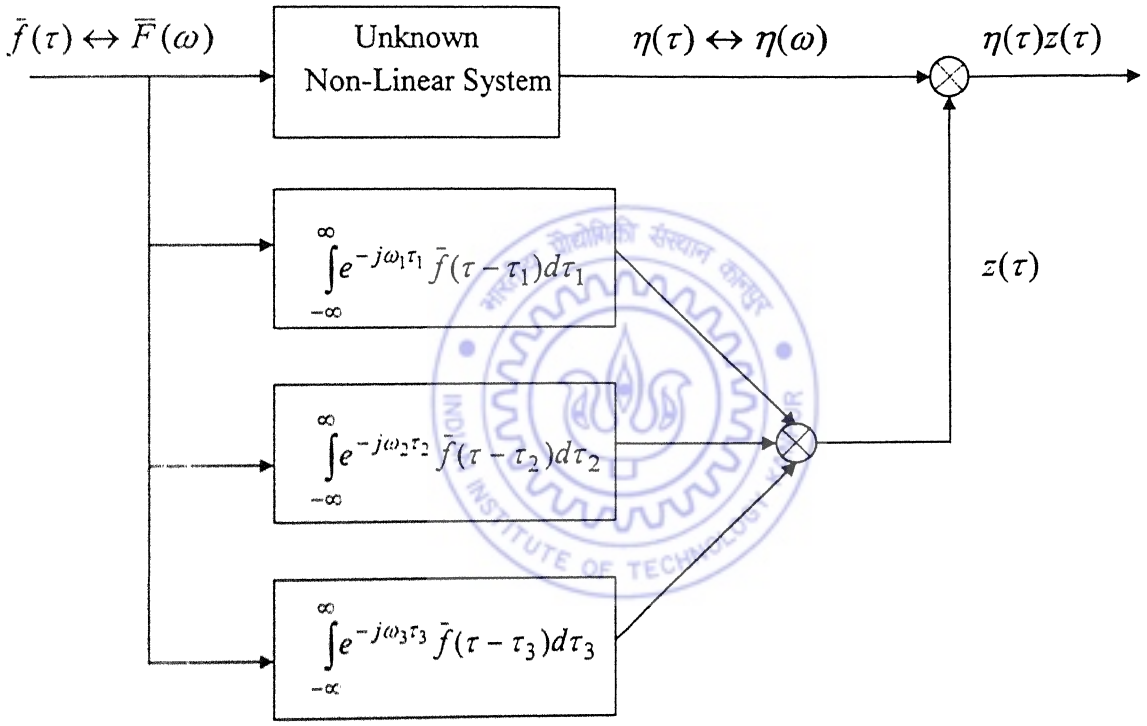

Fig. 3.4 Scheme for evaluation of the third order Wiener kernel transform, $W_3(\omega,\omega,\omega)$

The ensemble average of the output of the circuit can be expressed as

$$\begin{aligned}\langle \eta(\tau)z(\tau)\rangle = A^2[&W_1(\omega_1)\delta(-\omega_2-\omega_3)e^{j(-\omega_2-\omega_3)\tau}\\ &+W_1(\omega_2)\delta(-\omega_1-\omega_3)e^{j(-\omega_1-\omega_3)\tau}\\ &+W_1(\omega_3)\delta(-\omega_1-\omega_2)e^{j(-\omega_1-\omega_2)\tau}\ ]+6A^3W_3(\omega_1,\omega_2,\omega_3)\end{aligned} \tag{3.36}$$

The equivalence of time and ensemble averages gives

$$\langle \eta(\tau)z(\tau)\rangle = \lim_{T\to\infty}\frac{1}{T}\int_{-T/2}^{T/2}\eta(\tau)z(\tau)d\tau \tag{3.37}$$

giving

$$\langle \eta(\tau)z(\tau)\rangle = \overline{F}(-\omega_1)\overline{F}(-\omega_2)\overline{F}(-\omega_3)\eta(\omega_1+\omega_2+\omega_3) \tag{3.38}$$

Equations (3.36) and (3.38) give the expression for the measurement of the Fourier transform of the third order Wiener Kernel as

$$\begin{aligned}W_3(\omega_1,\omega_2,\omega_3) = (1/6A^3)&\left[\overline{F}^*(\omega_1)\overline{F}^*(\omega_2)\overline{F}^*(\omega_3)\eta(\omega_1+\omega_2+\omega_3)\right]\\ &-(1/6A)\left[W_1(\omega_1)\delta(\omega_2+\omega_3)+W_1(\omega_2)\delta(\omega_1+\omega_3)+W_1(\omega_3)\delta(\omega_1+\omega_2)\right]\end{aligned} \tag{3.39}$$

$W_3(\omega_1,\omega_2,\omega_3)$ forms a multi-dimensional surface on the $(\omega_1,\omega_2,\omega_3)$ axes. Measurements are made for special trispectral kernels with $\omega_1=\omega_2=\omega_3=\omega$. These kernels are functions of only one variable ω and are much easier to compute and interpret. (Bendat (1990) has termed such single function transforms for Volterra series as Special Trispectral Kernel Transforms). The Special Trispectral Wiener Kernel Transform can be readily written from (3.39) as

$$W_3(\omega,\omega,\omega) = (1/6A^3)\left[\{\overline{F}^*(\omega)\}^3\eta(3\omega)\right]-(1/2A)\left[W_1(\omega)\delta(\omega)\right] \tag{3.40}$$

3.5 Parameter Estimation

The Special Trispectral Wiener kernel Transforms can be extracted from the measurement of the applied random force and system response and employing equations (3.34) and (3.40).

Subsequently, for a third order representation of the system response, noting the equivalence between the Volterra and Wiener kernels (Eqn. 3.24), the third order Special Trispectral Volterra kernel transform can be computed from

$$H_3(\omega,\omega,\omega) = W_3(\omega,\omega,\omega)$$
$$= (1/6A^3)\left[\{\bar{F}^*(\omega)\}^3\eta(3\omega)\right] - (1/2A)\left[W_1(\omega)\delta(\omega)\right] \tag{3.41}$$

Similarly, from the relations of equations (3.24), the expression for the first order Volterra kernel transform, in terms of the measured Wiener kernel transforms, becomes

$$H_1(\omega) = W_1(\omega) + W_{1(3)}(\omega) \tag{3.42}$$

where $W_1(\omega)$ is as given in equation (3.34) and $W_{1(3)}(\omega)$ is the first order derived kernel transform,

$$W_{1(3)}(\omega) = -3A\int_{-\infty}^{\infty} W_3(\omega,\omega_2,-\omega_2)d\omega_2 \tag{3.43}$$

The linear parameters, ω_n and ξ can be readily obtained by equating the measured first order Volterra kernel (of equation (3.42)) to its analytical expression given in equation (3.12). Standard curve fitting techniques can be used. These, estimated linear parameters, ω_n and ξ, are employed further in the estimation of the nonlinear parameter λ.

The estimate for λ is obtained by equating the synthesized expression (Eqn. 3.20) and the measured value (Eqn. 3.41) of the third order Volterra kernels of the system. Thus

$$\lambda = \left\{(1/6A^3)\left[\{\bar{F}^*(\omega)\}^3\eta(3\omega)\right] - (1/2A)\left[W_1(\omega)\delta(\omega)\right]\right\} \Big/ \left[\Psi_3(\omega,\omega,\omega)\right] \tag{3.44}$$

3.6 Computer Simulation

The procedure is illustrated through numerical simulation of the response of the nondimensional equation with cubic nonlinearity, Eqn.(3.2). Owing to the statistical nature of the estimation procedure, illustration is carried out for various values of the nonlinearity parameter, λ. The procedure is repeated for various values of the damping ratio, ξ.

The forcing function in equation (3.2) is a normalised random force, $\bar{f}(\tau)$, with zero mean value. The excitation force is simulated through random number generating subroutine and is normalised with respect to its maximum value F_{max} . A typical sample of this excitation force is shown in Fig. 3.5(a), while Fig. 3.5(b) shows a typical nondimensional response, $\eta(\tau)$, for nonlinear parameter λ=0.1 and a damping ratio, $\xi = 0.01$. The response has been numerically generated for 4096 number of instances in the nondimensional time (τ) range 0-2048, using standard fourth-order Runge-Kutta subroutine. The response is computed for 2000 number of samples of the simulated random force (The influence of the number of samples in the ensemble is discussed later).

3.6.1 Estimates of Linear Parameters

Fig. 3.6(a) depicts the power spectrum of the random force averaged over the ensemble of 2000 samples. The corresponding ensemble average of the power spectrum of the response can be seen in Fig. 3.6(b). The first order Volterra kernel, $H_1(\omega)$, Fig. 3.7(a), is then computed, using the expression of equation (3.42), over the ensembles of the force and response. The linear parameters ω_n and ξ are computed from $H_1(\omega)$, through routine modal analysis procedures (Ewins, 1984). The linear parameters, thus estimated are

ω_n = 0.1606 (cycles / τ) = 1.009 (rad / τ)

and ξ = 0.012.

The curve of Fig. 3.7(b) shows the error incurred in the estimate of $H_1(\omega)$, due to the statistical nature of the Fast Fourier Transform computational procedure and the finite length of an individual sample (4096 in the present case). The normalised random error, as known (Bendat and Piersol, 1986), can be seen to be the maximum in the vicinity of natural frequency of the linear part of the system (1rad / τ i.e. 0.1592 cycles / τ). The error in the frequency range 0.0 - 0.10, is less than 4%. It can be readily inferred that the normalised error for the higher order kernels would show a similar trend and the error in the estimate of the nonlinear parameter λ can be expected to be less in the frequency zone 0.0-0.10 cycles / τ.

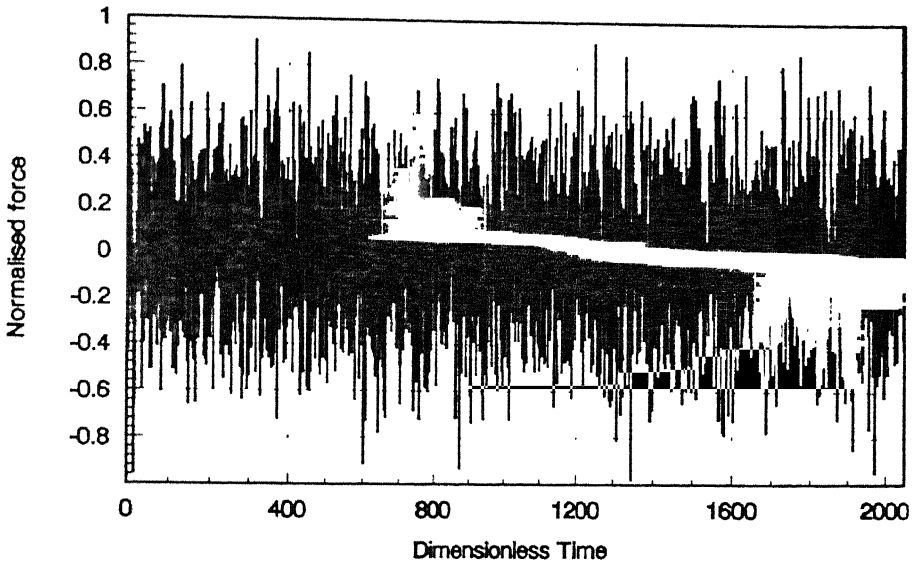

Fig. 3.5(a) Typical sample of random input force .

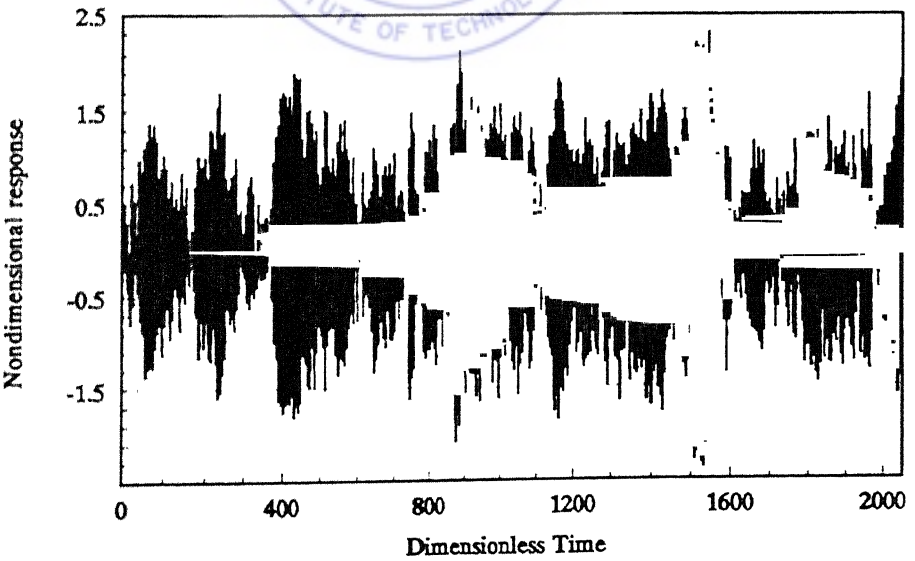

Fig. 3.5(b) Typical sample of nondimensional response ($\lambda = 0.10,\ \xi = 0.01$).

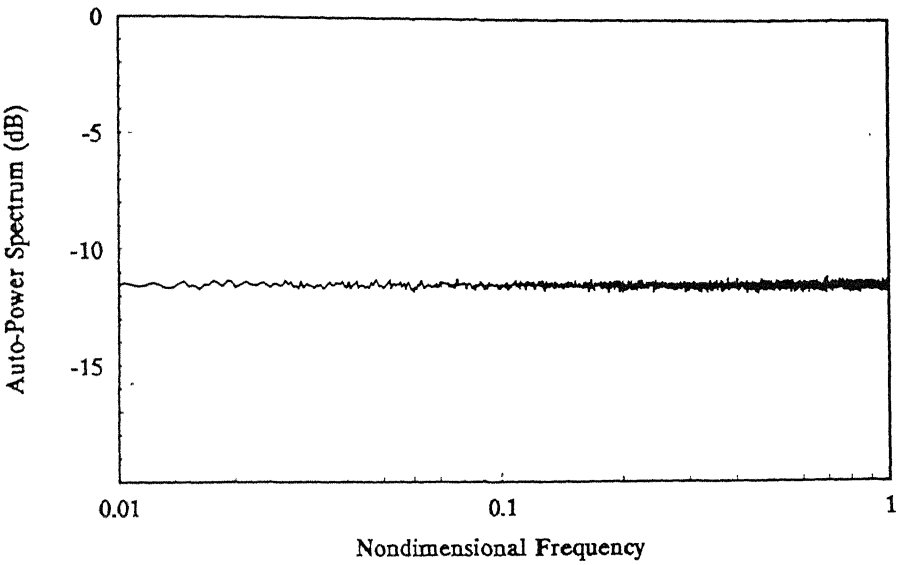

Fig. 3.6(a) Power spectrum of the input force (averaged over 2000 samples).

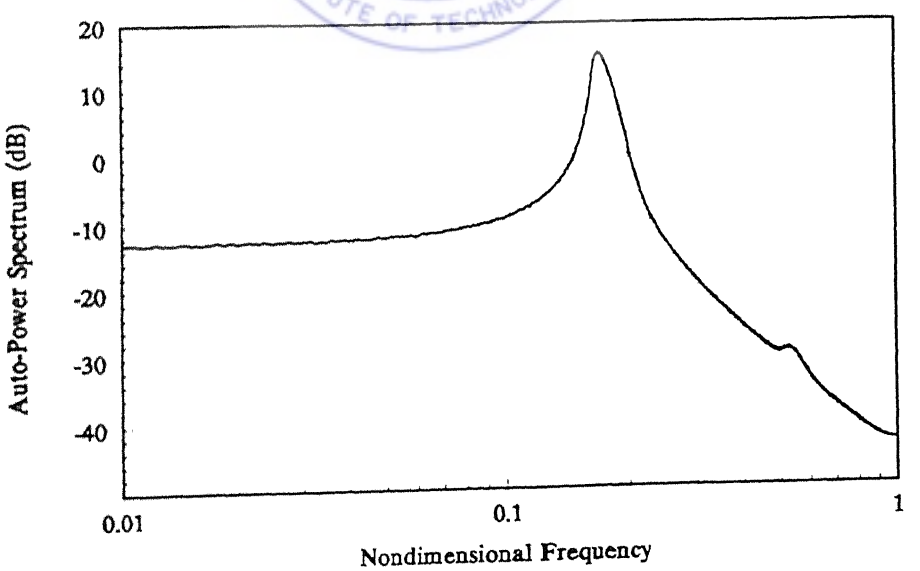

Fig. 3.6(b) Power spectrum of the response (averaged over 2000 samples) (for simulation values of $\lambda = 0.10$; $\xi = 0.01$).

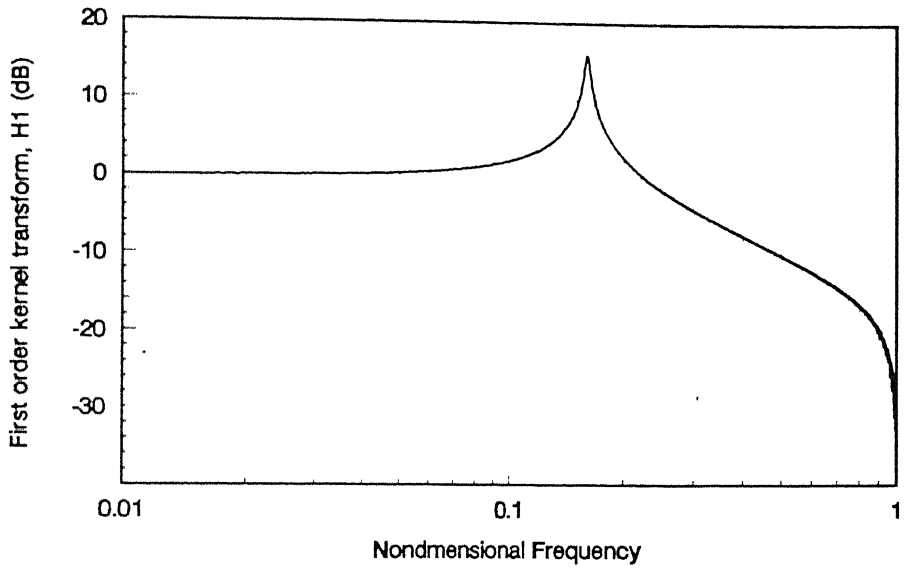

Fig. 3.7(a) Estimate of first order Volterra kernel transform, $H_1(\omega)$ (for simulation values of $\lambda = 0.10$; $\xi = 0.01$).

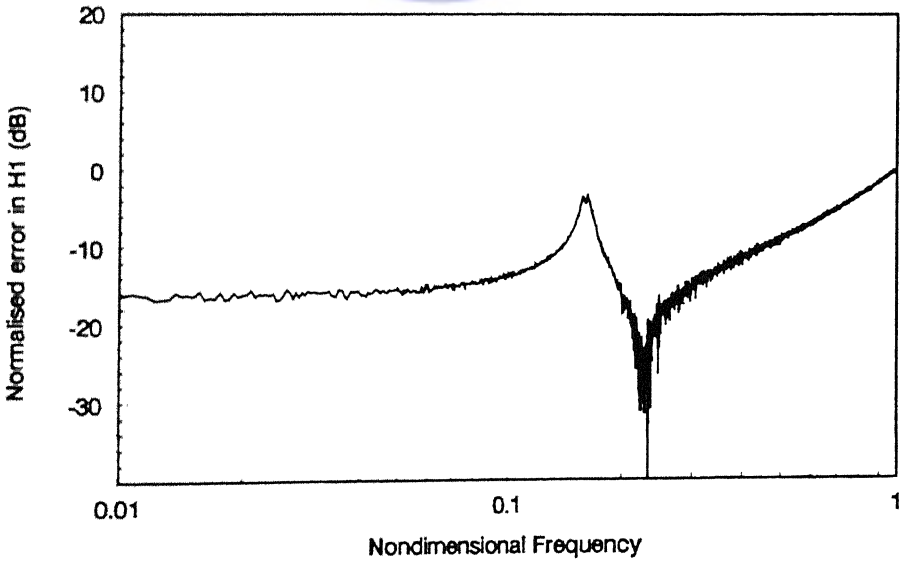

Fig. 3.7(b) Error in the estimate of $H_1(\omega)$.

3.6.2 Estimates of the Nonlinear Parameter

Nonlinear estimation is carried out for a range of values of the nonlinear parameter λ, and damping ratios ξ. The response of the nondimensional equation (3.2) is numerically simulated for λ = 1.00, 0.10 and 0.01, while keeping the damping ratio ξ fixed at 0.01. It may be noted from equation (3.3) that λ includes both, the nonlinear stiffness term k^N and F_{max}, the maximum value of the applied force. A low value of λ, for a fixed value of k^N implies a low value of F_{max}, while a high value of λ, for the same k^N implies a high F_{max} and vice-versa. The results for such a nondimensional parameter can be readily employed to design experiments and decide the excitation level for an expected nonlinearity of a given system.

The estimated results for the third order kernel are depicted in Fig. 3.8. The third order kernel factor $\Psi_3(\omega,\omega,\omega)$, synsthesised from the measured first order kernel transform $H_1(\omega)$, and the measured third order kernel transform $H_3(\omega,\omega,\omega)$ are shown in Fig. 3.8 (a), 3.9(a) and 3.10(a) for λ = 1.00, 0.1 and 0.01 respectively (ξ= 0.01). It is to be noted here, that while the first order kernel is estimated in the entire available frequency range 0.0 - 1.0, the third order kernels, involving a 3ω factor, have to be restricted to one-third of this frequency zone (i.e. 0.0 - 0.33). It can be observed, from the figures, that while the measured third order kernel transform $H_3(\omega,\omega,\omega)$ is reasonably accurate in showing the harmonic at $\omega_n/3$ (at nondimensional frequency = 0.053), the identification of the harmonic at ω_n (at nondimensional frequency = 0.159) is weak, the best approximation being in the case of λ = 1.0. The estimation of λ, from these kernels, is therefore restricted to the frequency zone of 0.0 - 0.10. The estimates of the nonlinear parameter λ, obtained in accordance with the relationship (3.44), are shown in Figs. 3.8(b), 3.9(b), 3.10(b). A fourth order polynomial curve regressed through the estimates of λ, over the frequency range, is also shown in Figures 3.8(b), 3.9(d) and 3.10(b). The mean values of the estimates of λ are found to be 1.08, 0.14 and 0.05 respectively. The order of the magnitude can be seen to be estimated correctly in all three cases, while a good accuracy can be seen to be obtained for λ=1.0 (Fig. 3.8(b)). It is to be noted here that the response representation of equation (3.23) has been

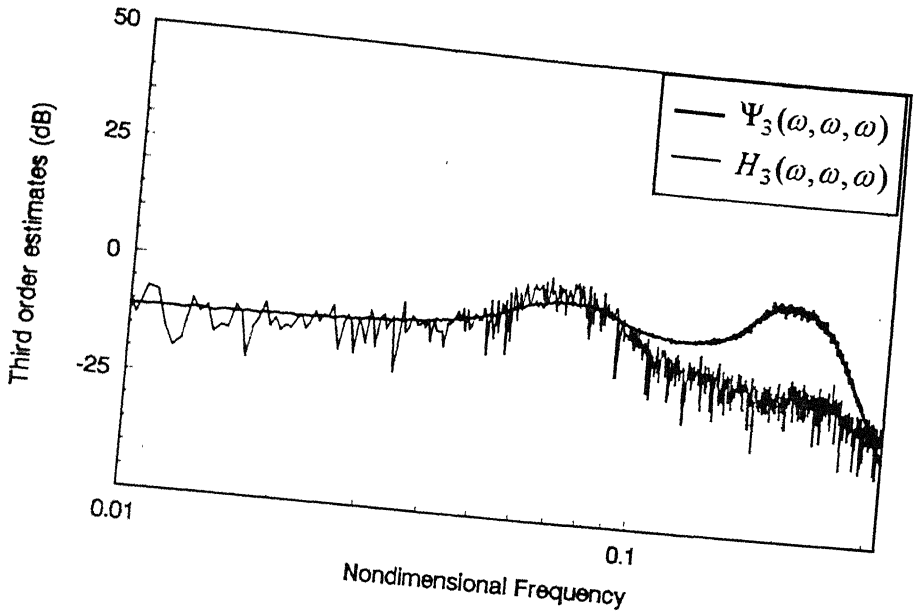

(a) Estimates of $\Psi_3(\omega,\omega,\omega)$ and $H_3(\omega,\omega,\omega)$.

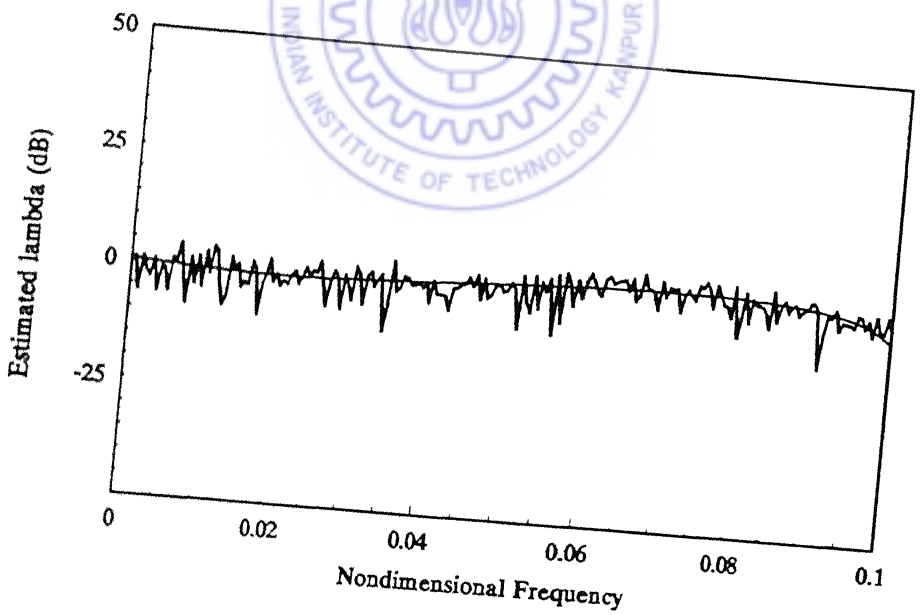

(b) Estimate of λ.

Fig. 3.8 Estimates of third order kernel transforms and nonlinearity parameter λ (for simulation values of $\lambda = 1.00$; $\xi = 0.01$).

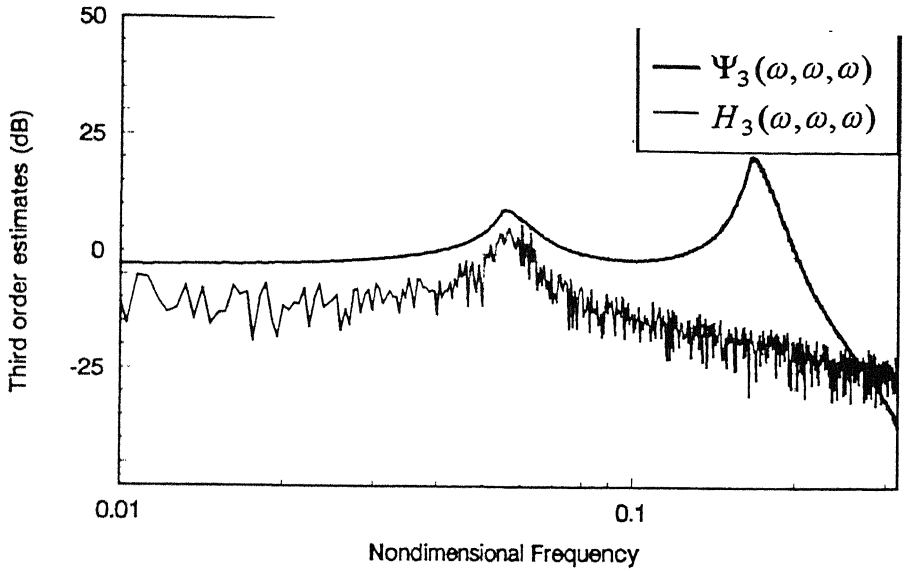

(a) Estimates of $\Psi_3(\omega,\omega,\omega)$ and $H_3(\omega,\omega,\omega)$.

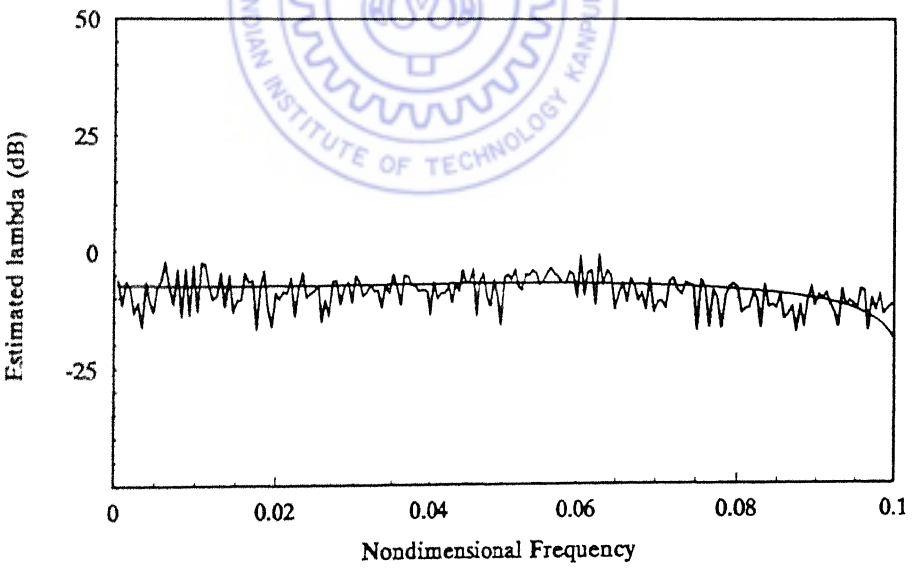

(b) Estimate of λ.

Fig. 3.9 Estimates of third order kernel transforms and nonlinearity parameter λ (for simulation values of $\lambda = 0.10$; $\xi = 0.01$).

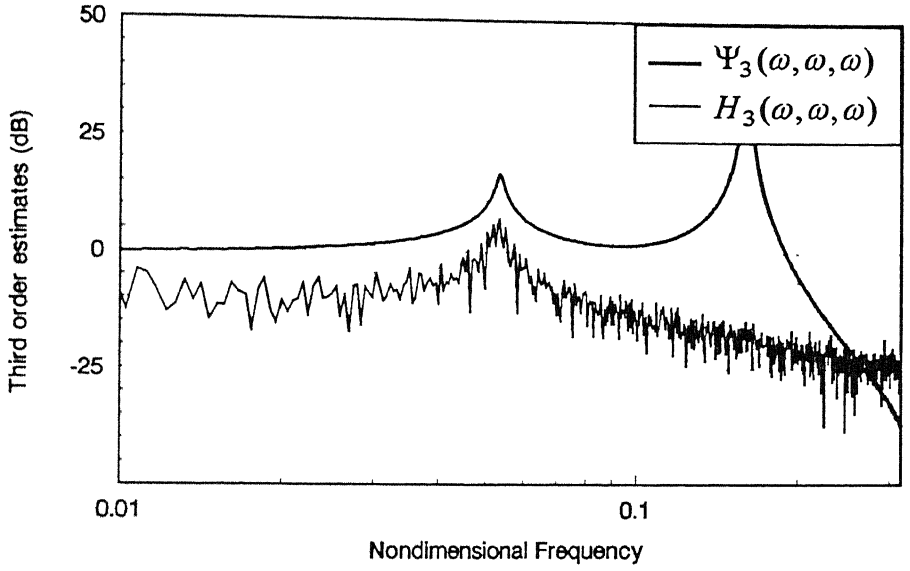

(a) Estimates of $\Psi_3(\omega,\omega,\omega)$ and $H_3(\omega,\omega,\omega)$.

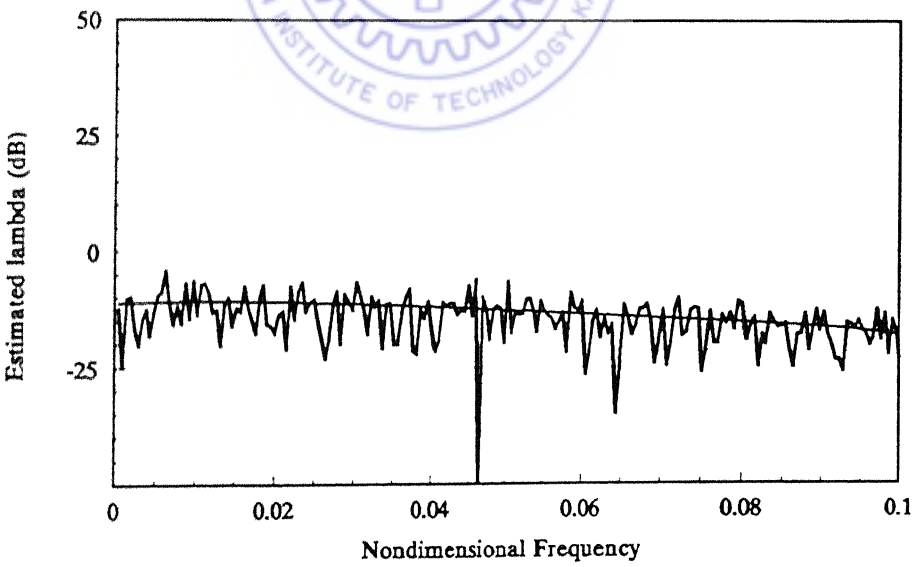

(b) Estimate of λ.

Fig. 3.10 Estimates of third order kernel transforms and nonlinearity parameter λ (for simulation values of $\lambda = 0.01$; $\xi = 0.01$).

restricted to include kernels only up to the third order, in order to keep the computations to a manageable level. Inclusion of higher order kernels (5^{th}., 7^{th} order) in the response representation can be expected to improve the accuracy of the estimates at increased computational effort. Another source of inaccuracy in the estimates is the finite length of samples and the ensemble size. The nondimensional time interval for sampling has been taken as 0.5 and 4096 response instants are collected for a sample data set which gives a frequency bandwidth of $\pm$ 1.0 cycles / τ and a frequency resolution of 0.488×10^{-3} cycles / τ. Additionally it may also be noted that the numerical fourth order Runge-Kutta procedure of response simulation is also a source of error.

3.6.3 Influence of the Number of Samples

It was observed that while increasing the sample size beyond 500 has insignificant influence on the first order estimates, the influence on the third order estimates can be seen from the curves of Figs. 3.11(a) - (d). The figures show the power spectrum of the input for ensemble sizes 500, 1000, 1500 and 2000 along with the corresponding third order kernel factor $\Psi'_3(\omega,\omega,\omega)$ and the measured third order Wiener kernel transform, $H_3(\omega,\omega,\omega)$, which are both observed to get refined with increasing number of samples in the ensemble. In the present study the ensemble size has been limited to 2000.

3.6.4 Influence of Measurement Noise

Errors can be expected during an experiment, in the measurement of the excitation force and the response. The influence of measurement noise is studied by contaminating the simulated force and response signals, individually and simultaneously, with 5% simulated random noise. The frequency range is split into two and Fig. 3.12(a) shows the third order kernel transform $H_3(\omega,\omega,\omega)$ and the third order kernel factor $\Psi_3(\omega,\omega,\omega)$ (for 5% noise in both input and output), in the frequency zone of interest 0.00-0.03 cycles / τ , on a magnified scale, while the remaining portions of the curves are shown in Fig. 3.12(b). Other estimates are also observed to be similarly robust to measurement noise influence.

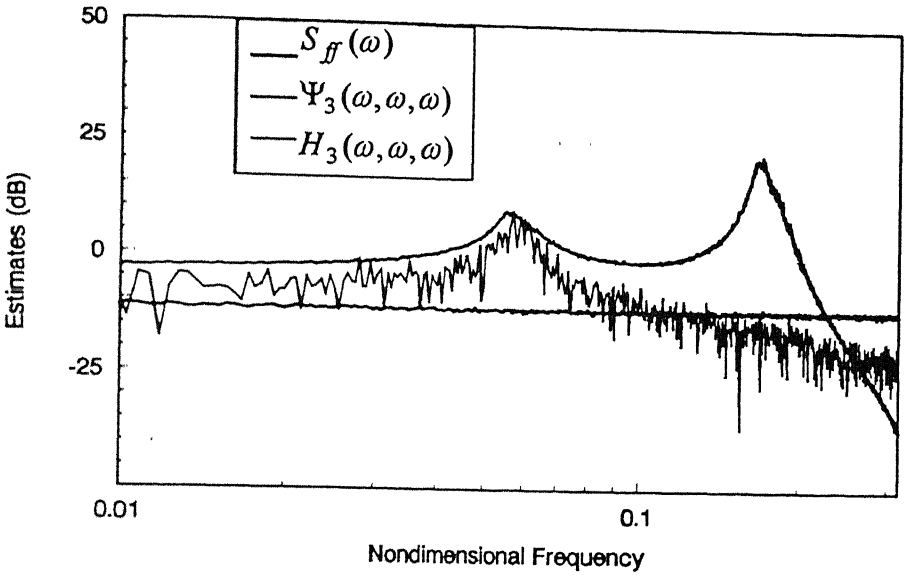

(a) Estimates with sample size = 500.

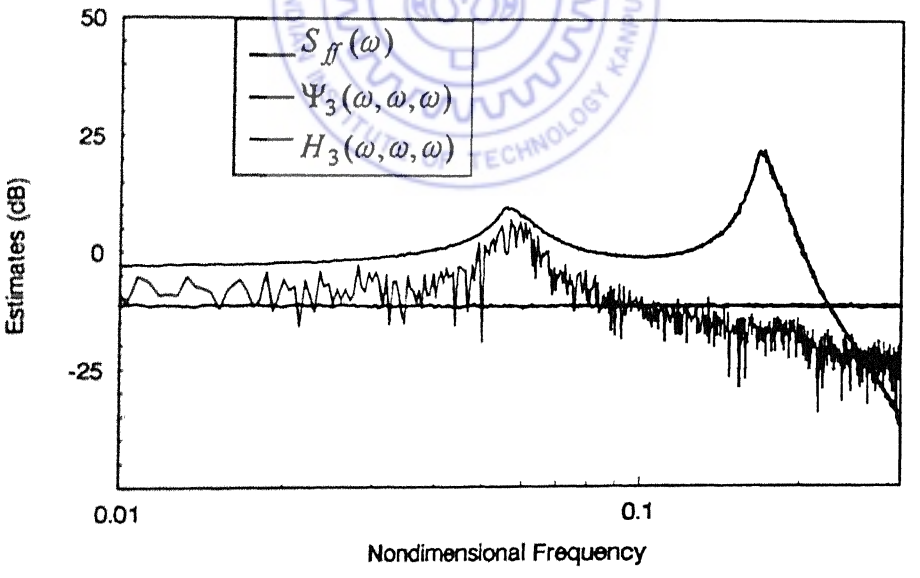

(b) Estimates with sample size = 1000.

Fig. 3.11 Influence of sample size on input auto-power spectrum and third order estimates (for simulation values of $\lambda = 0.10$; $\xi = 0.01$), Contd.

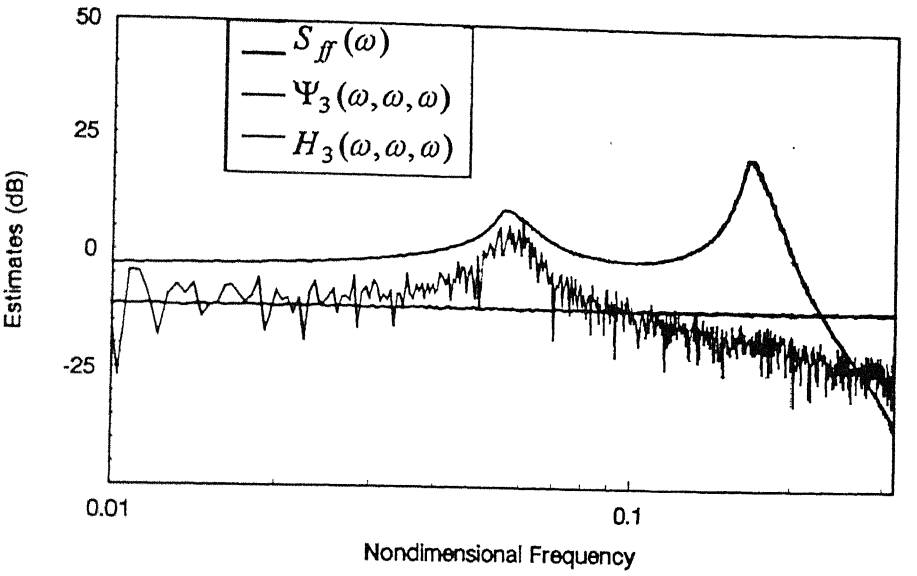

(c) Estimates with sample size = 1500.

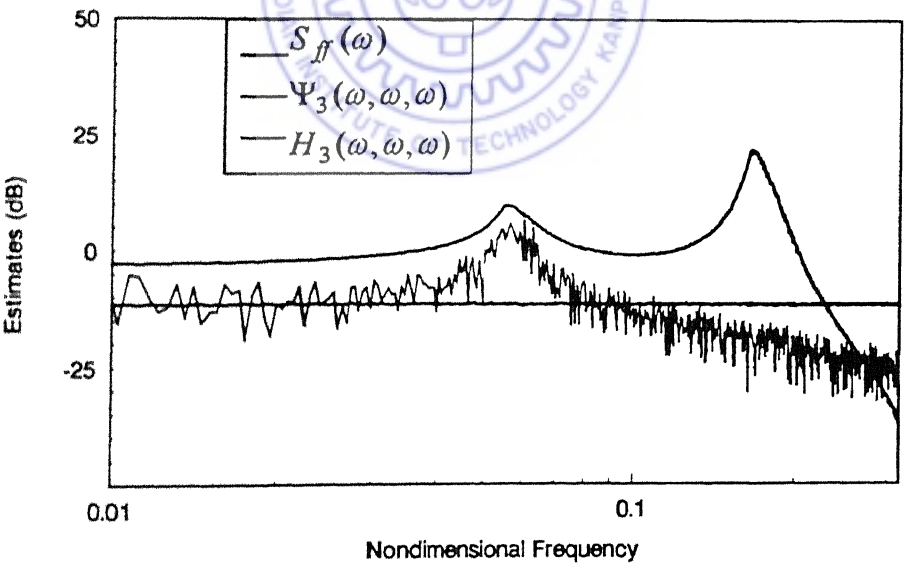

(d) Estimates with sample size = 2000.

Fig 3.11 Influence of sample size on input auto-power spectrum and third order estimates (for simulation values of $\lambda = 0.10$; $\xi = 0.01$).

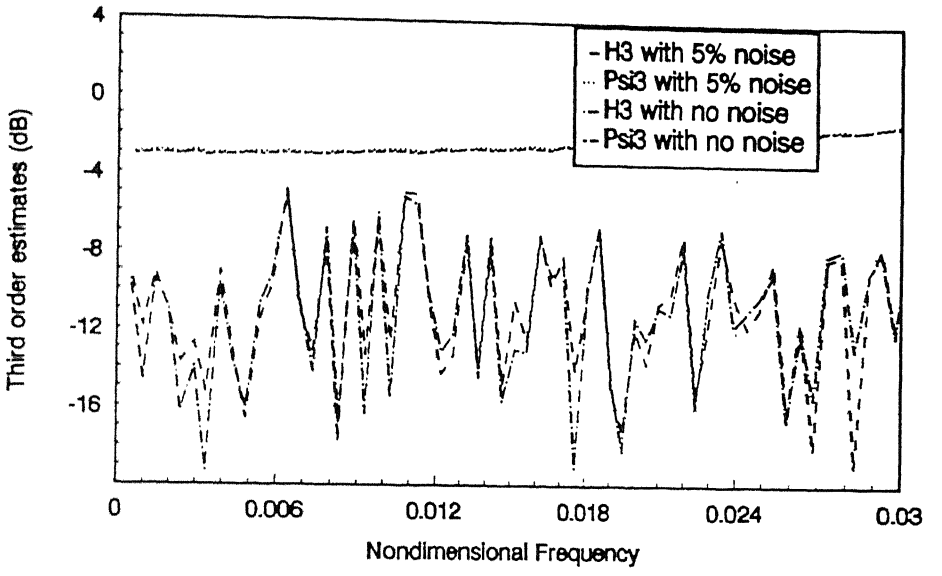

(a) $\Psi_3(\omega,\omega,\omega)$ and $H_3(\omega,\omega,\omega)$ in frequency range (0.0-0.03).

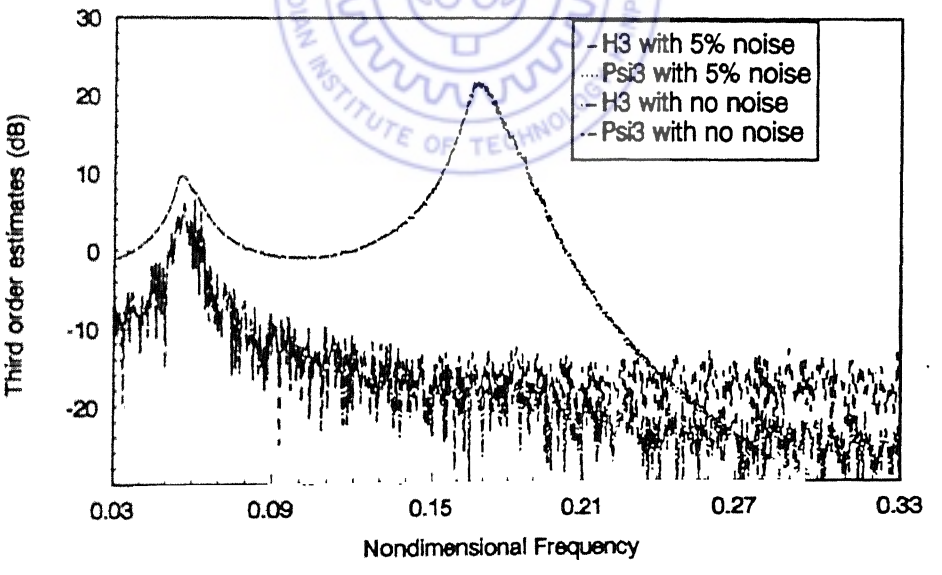

(b) $\Psi_3(\omega,\omega,\omega)$ and $H_3(\omega,\omega,\omega)$ in frequency range (0.03-0.33).

Fig. 3.12 Effect of measurement noise on third order estimates (for simulation values of $\lambda = 0.10$; $\xi = 0.01$).

3.6.5 Influence of Damping on the Accuracy of Nonlinear Estimates

Apart from the nonlinear parameter λ, the other nondimensional parameter contained by the governing equation (3.2) is the damping ratio ξ. Numerical simulation is carried out to check the accuracy of the estimation procedure and the response is simulated for two different damping values ξ = 0.01 and 0.001 (for λ = 1.0). Figs. 3.13(a,b)-3.14(a,b) show the estimates in the two cases. The estimates of λ (1.08 and 1.72, respectively) can be seen to be sensitive to damping being accurate for higher damping.

3.6.6 Identification of the Sign of Nonlinear Parameter

In the results depicted so far, nonlinear estimates have been arrived at by dividing (refer equation 3.44) the absolute value of the measured third order kernel transform, $H_3(\omega,\omega,\omega)$, by the absolute value of the third order kernel factor, $\Psi_3(\omega,\omega,\omega)$. Both these terms are, however, complex quantities and their absolute values have been considered while estimating the nonlinear parameter λ, solely for achieving better smoothening of data. This involves the loss of information on the sign (whether positive or negative) of λ. The nonlinear parameter λ being a real constant, information on its sign along with its magnitude, can be readily obtained if the real part of $H_3(\omega,\omega,\omega)$ were to be divided by the real part of $\Psi_3(\omega,\omega,\omega)$ (or the imaginary part of $H_3(\omega,\omega,\omega)$ were to be divided by the imaginary part of $\Psi_3(\omega,\omega,\omega)$). Consideration of equations (3.19) and (3.20) reveals that $\Psi_3(\omega,\omega,\omega)$, a term synthesised from the first order kernel transform is a function solely of the linear parameters ω_n and ξ. and will be the same whether the nonlinearity in system is ($+\lambda$) or ($-\lambda$). The information on the sign of λ is contained in $H_3(\omega,\omega,\omega)$, which shows a reversal of sign, with change in the sign of λ. This is illustrated in Figs. 3.15-3.17. The real and imaginary part of the synthesised third order kernel factor $\Psi_3(\omega,\omega,\omega)$ are shown Fig. 3.15(a), (b). The real and imaginary components of the measured third order Volterra kernel transform $H_3(\omega,\omega,\omega)$ for a positive nonlinearilty (i.e. $+\lambda$) are shown in Fig. 3.16(a), (b), while those for a negative nonlinearity (i.e. $-\lambda$) are given in Fig. 3.17(a), (b). The peaks, occurring at a frequency of 0.056 cycles / τ , can be seen to bear similar signs

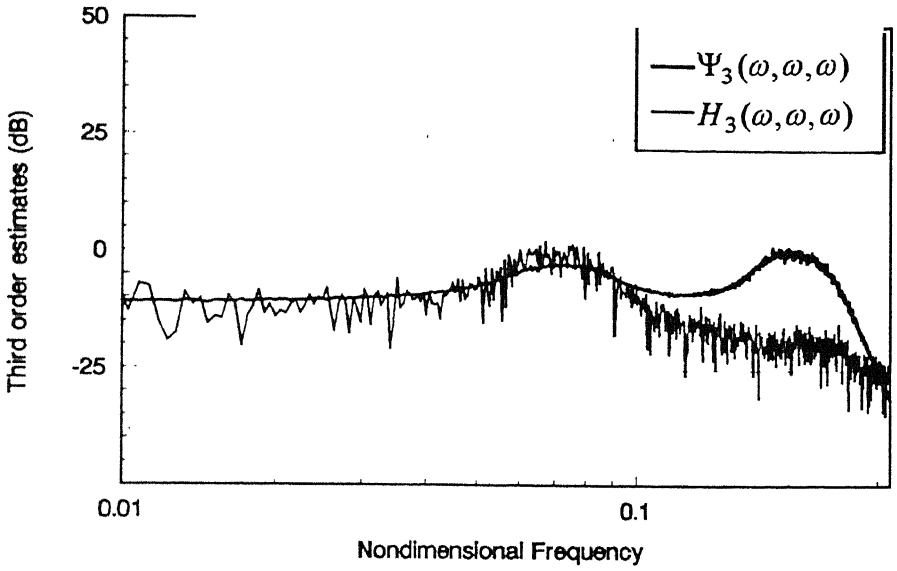

(a) Estimates of $\Psi_3(\omega,\omega,\omega)$ and $H_3(\omega,\omega,\omega)$.

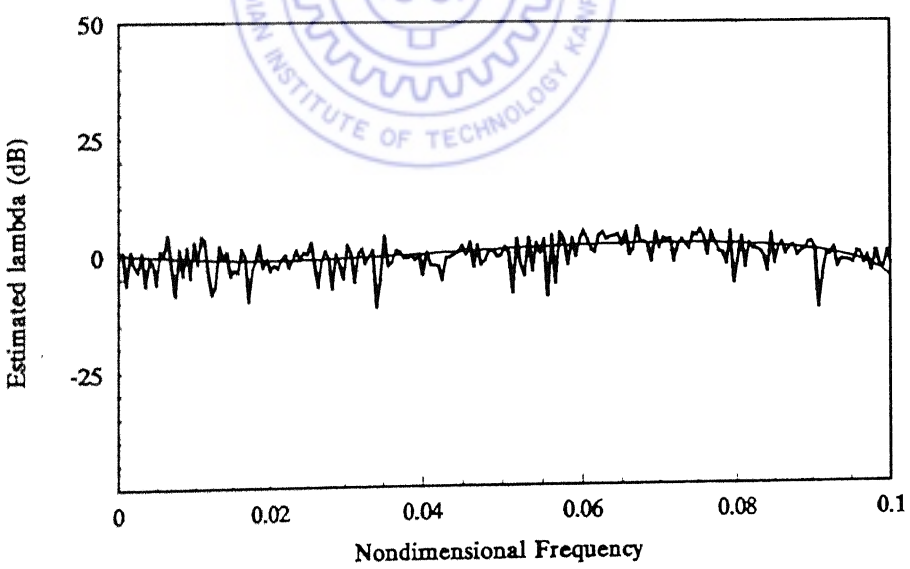

(b) Estimate of λ.

Fig. 3.13 Estimates of third order kernels and nonlinearity parameter λ (for simulation values of $\lambda = 1.00$; $\xi = 0.01$).

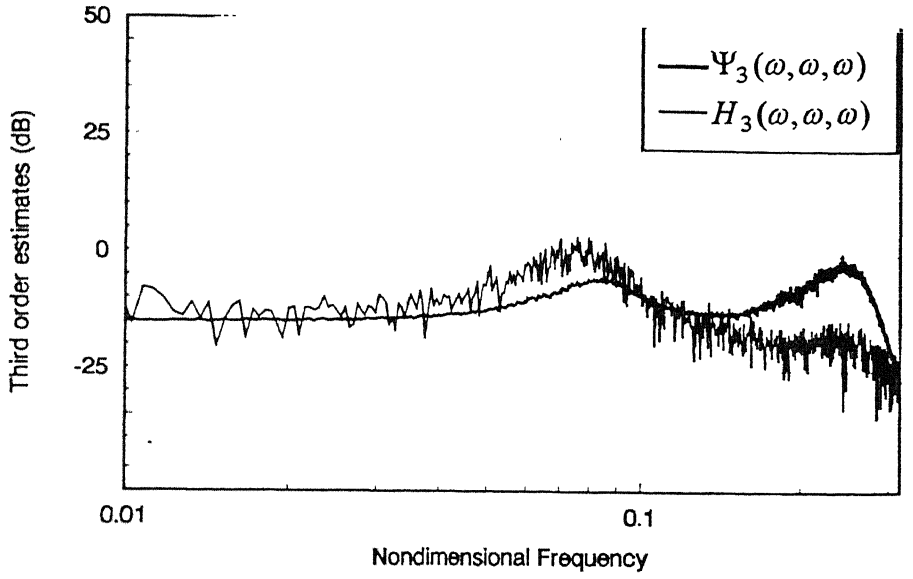

(a) Estimates of $\Psi_3(\omega,\omega,\omega)$ and $H_3(\omega,\omega,\omega)$.

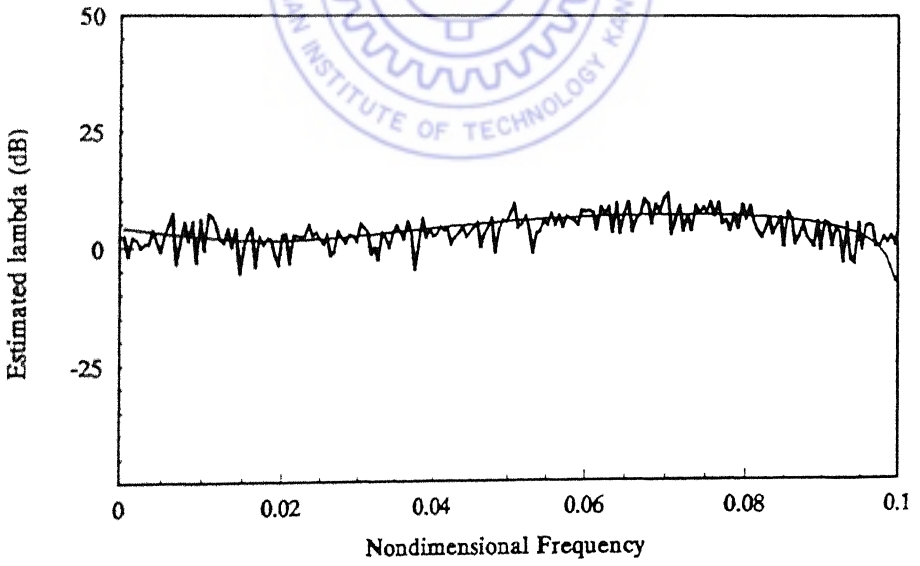

(b) Estimate of λ.

Fig. 3.14 Estimates of third order kernels and nonlinearity parameter λ (for simulation values of $\lambda = 1.00$; $\xi = 0.001$).

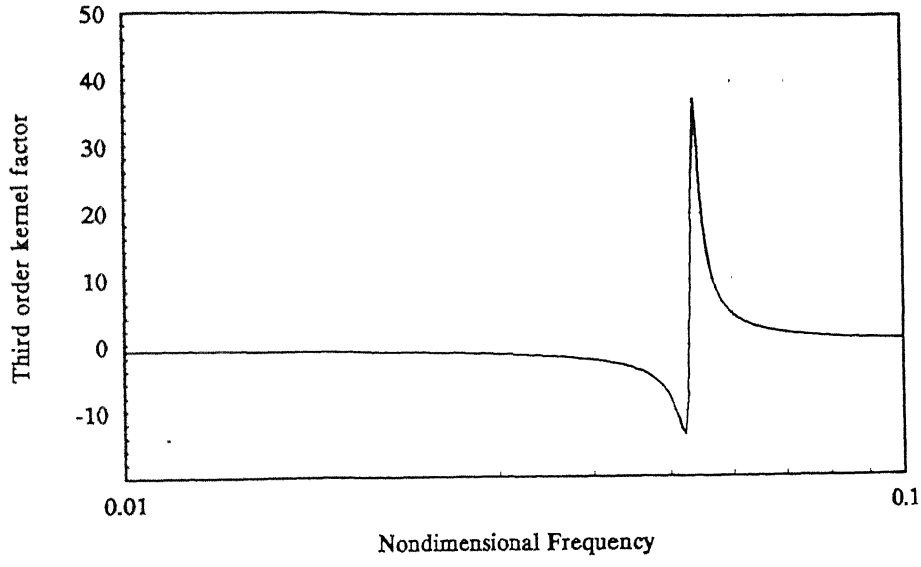

(a) Real component.

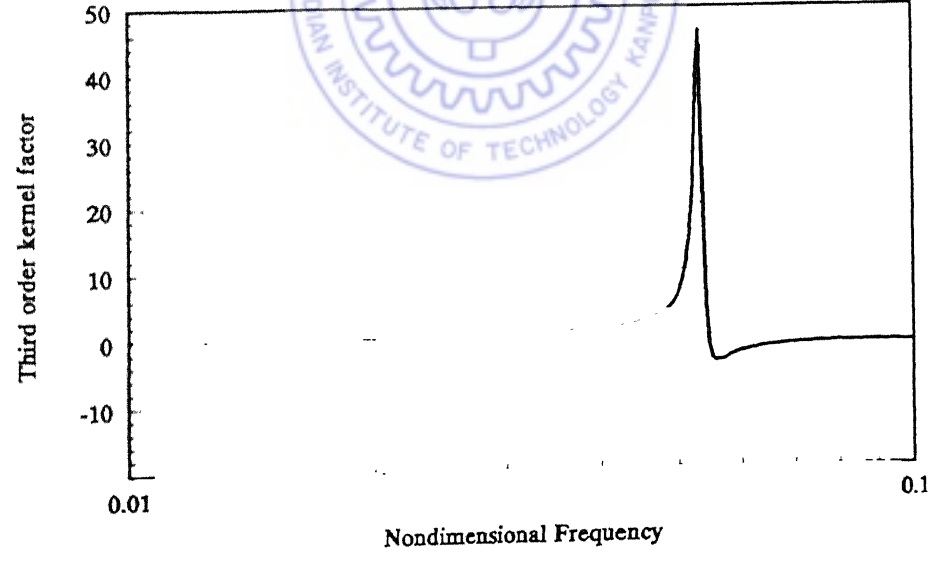

(b) Imaginary component.

Fig. 3.15 Third order kernel factor $\Psi_3(\omega,\omega,\omega)$ for Identification of sign of the nonlinear parameter.

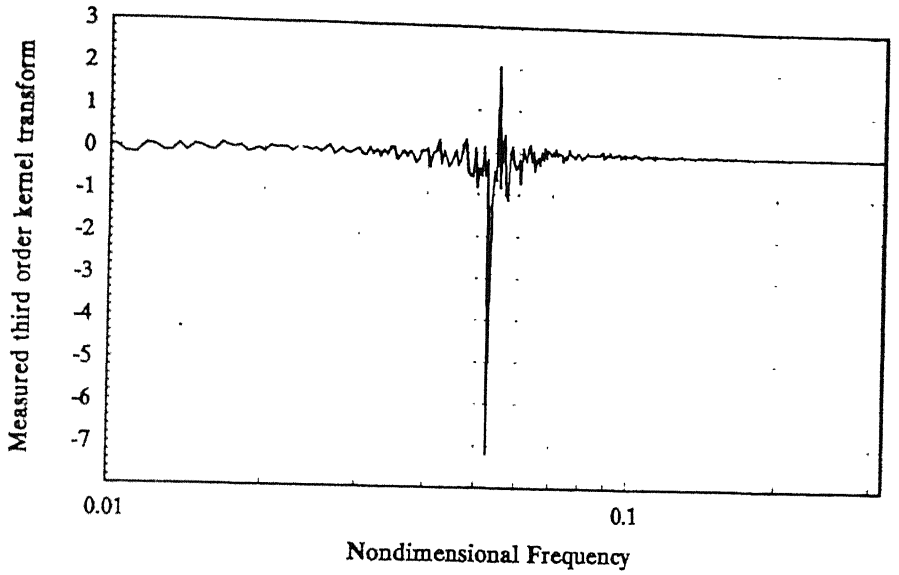

(a) Real component.

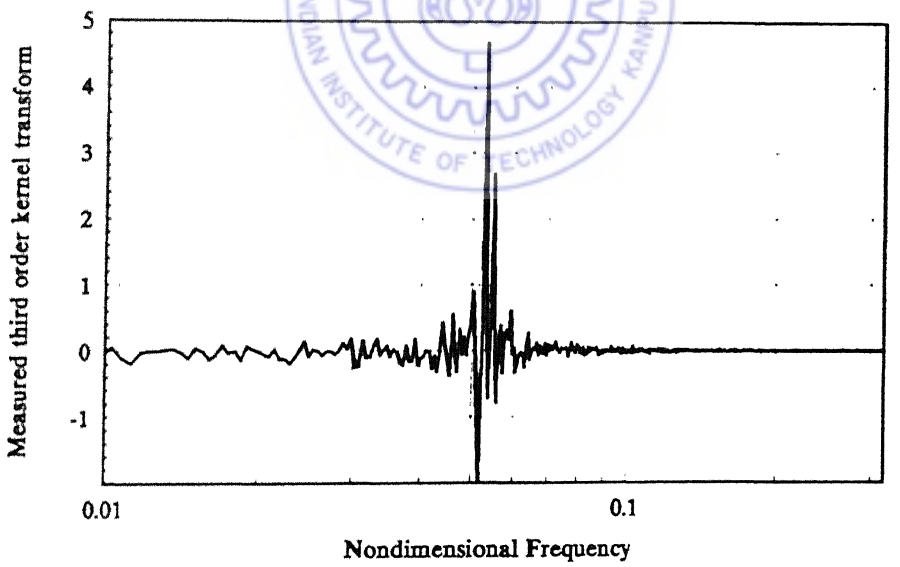

(b) Imaginary component.

Fig. 3.16 Third order measured kernel transform $H_3(\omega,\omega,\omega)$ for Identification of sign of the nonlinear parameter (for positive nonlinearity).

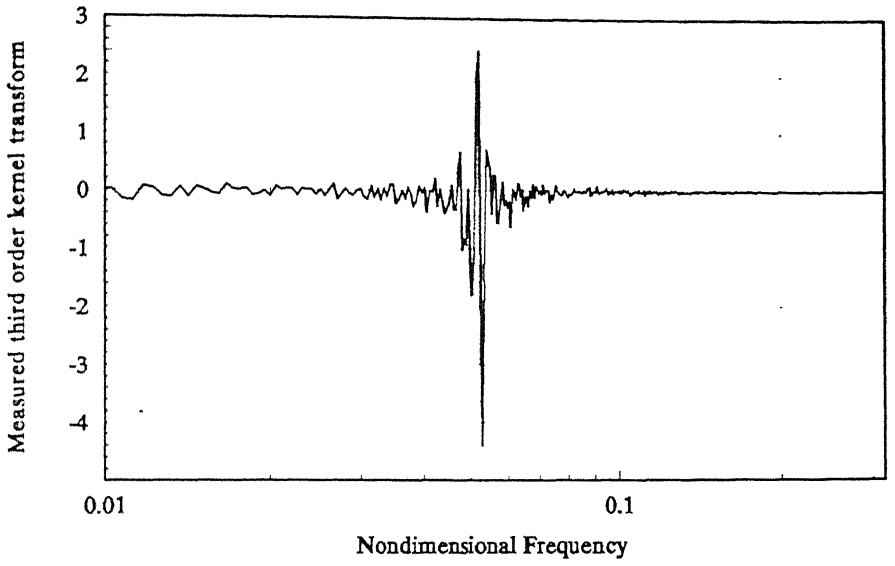

(a) Real component.

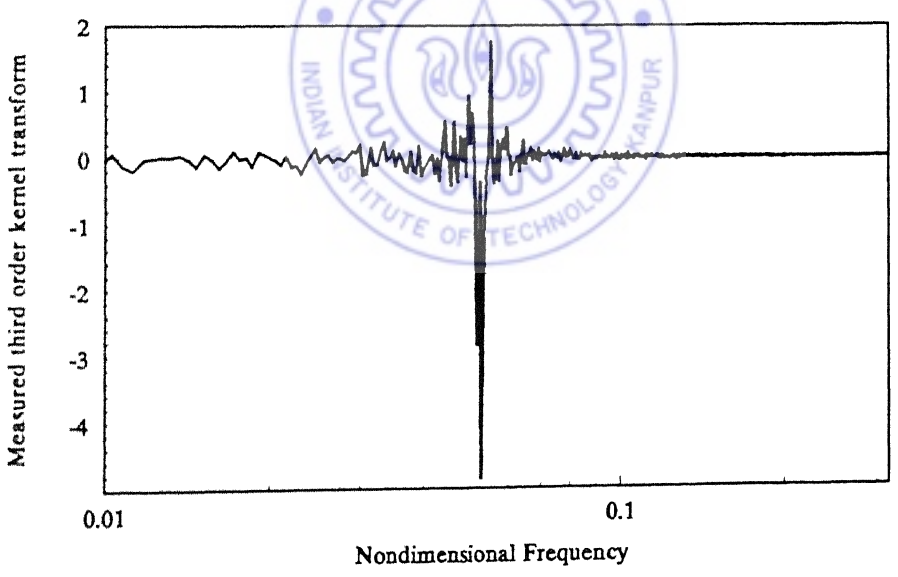

(b) Imaginary component.

Fig. 3.17 Third order measured kernel transform $H_3(\omega,\omega,\omega)$ for Identification of sign of the nonlinear parameter (for negative nonlinearity).

(Figs. 3.15, 3.16) for $\Psi_3(\omega,\omega,\omega)$ and $H_3(\omega,\omega,\omega)$, for positive nonlinearily. However, they bear opposite signs for negative nonlinearity, Figs. 3.15 and 3.17.

The results shown in Figs.3.15-3.17 pertain to nonlinearily λ equal to +0.01 and -0.01 and a value of damping parameter ξ equal to 0.01. Similar results are obtained for other values of the nonlinear parameter and damping ratios.

3.7 Remarks

The procedure developed gives good engineering estimates of the nonlinear parameter. The estimates are satisfactory for a range of system damping. It also appears to be robust to measurement noise. The analysis presented is in nondimensional form and can be suitably employed to design experiments. The accuracy of the estimates, shows improvement with the increase in the number of force and response samples, over which averaging is carried out. Extension of the present procedure to systems with more than one degree of freedom and involving coupling is explored in subsequent chapters.

CHAPTER 4

PARAMETER ESTIMATION IN RIGID ROTORS SUPPORTED IN BEARINGS WITH CROSS-COUPLING

The parameter estimation procedure, becomes more involved, if the cross-coupling effects in the bearings are taken into account. This may be the case for a rotor supported in fluid film bearings. In contrast to the no cross-coupling case, which could be treated as a single-degree-of-freedom system, bearings with cross-coupling pose a nonlinear two-degree-of-freedom problem. It is a system where an excitation, say, in the x-direction causes motion in the both the x and y-directions. Such a case, therefore would require cross-kernels to be defined, which can be convolved with the excitation for the response representation, in terms of Volterra or Wiener series.

Starting with the equations of motion, Laplace transforms are employed in this chapter, to derive expressions for the first and higher order direct and cross-kernel transforms. The algebra is kept simple by taking the damping to be linear and without cross-coupling. The nonlinearity is taken to be cubic and analysis is carried out in the frequency domain. First and the third order direct and cross-kernels are extracted from the measurements of the excitation force and response. Third order direct and cross-kernel factors are synthesised from the measured first order kernel transforms. These synthesised third order factors are then processed along with the measured third order kernel transforms for estimation of the nonlinear parameters. The procedure is illustrated through numerical simulation. The estimation is carried out for various values of the nondimensional nonlinearity parameter and damping ratio. Statistical considerations and effect of probable measurement noise are illustrated and discussed.

4.1 Governing Equations and Volterra Series Response Representation

The equations of motion for a two-degree-freedom idealisation of the rotor-bearing system shown in Fig. 4.1 are

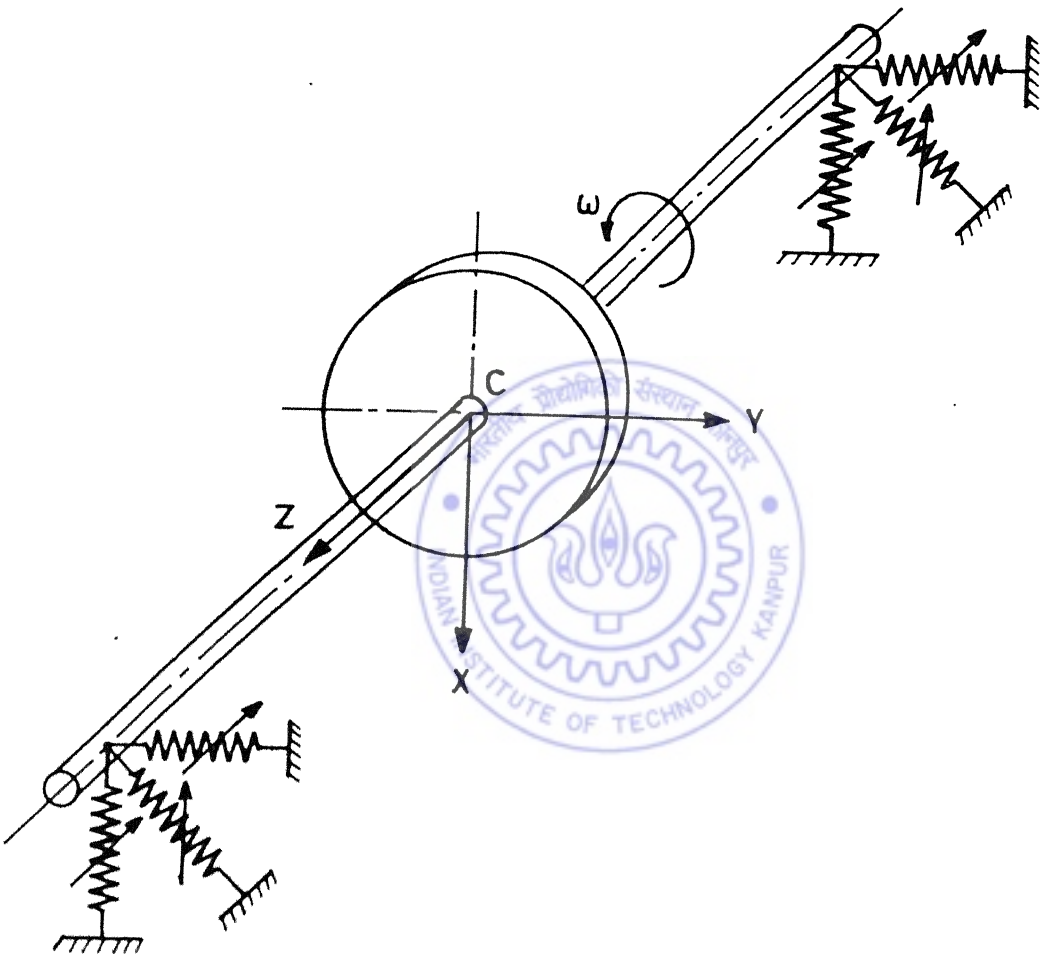

Figure 4.1 Rigid rotor in bearings with cross-coupling.

$$m\ddot{x} + c_{xx}\dot{x} + k_{xx}x + k_{xy}y + k_{xx}^{N}x^3 + k_{xy}^{N}y^3 = f_1(t)$$
$$m\ddot{y} + c_{yy}\dot{y} + k_{yy}y + k_{yx}x + k_{yy}^{N}y^3 + k_{yx}^{N}x^3 = f_2(t) \qquad (4.1)$$

In the above equations k_{xx}, k_{yy} are the direct linear stiffness terms, k_{xy}, k_{yx} are the cross-coupled stiffness terms, k_{xx}^{N}, k_{yy}^{N} are the direct nonlinear stiffness terms, while k_{xy}^{N}, k_{yx}^{N} represent the nonlinear cross-coupling terms. The damping is linear and comprising of direct terms c_{xx}, c_{yy} . The excitation forces in the x and y directions are $f_1(t), f_2(t)$ respectively.

Defining

$$\tau = p.t\,, \qquad p = \sqrt{k_{xx}/m}$$
$$^{x}\eta(\tau) = x/X_{st}\,, \qquad ^{y}\eta(\tau) = y/X_{st}\,; \qquad (4.2)$$
$$X_{st} = F_{\max_i}/k_{xx}\,, \qquad \bar{f}_i(\tau) = f_i(\tau)/F_{\max_i}\,; \qquad i = 1,2$$

and substituting in (4.1) the equations of motion can be written in nondimensional form as

$$^{x}\eta''(\tau) + 2\xi_{xx}\,^{x}\eta'(\tau) + ^{x}\eta(\tau) + \lambda_{xy}^{L}\,^{y}\eta(\tau) + \lambda_{xx}^{N}\,^{x}\eta^3(\tau) + \lambda_{xy}^{N}\,^{y}\eta^3(\tau) = \bar{f}_1(\tau)$$
$$^{y}\eta''(\tau) + 2\xi_{yy}\,^{y}\eta'(\tau) + \lambda_{yy}^{L}\,^{y}\eta(\tau) + \lambda_{yx}^{L}\,^{x}\eta(\tau) + \lambda_{yy}^{N}\,^{y}\eta^3(\tau) + \lambda_{yx}^{N}\,^{x}\eta^3(\tau) = \bar{f}_2(\tau) \qquad (4.3)$$

where

$$\xi_{ii} = \frac{c_{ii}}{2mp}, \qquad \lambda_{ij}^{L} = \frac{k_{ij}}{k_{xx}}, \qquad \lambda_{ij}^{N} = \frac{k_{ij}^{N}F_{\max}^{2}}{k_{xx}^{3}}; \qquad i = x,y\,;\ j = x,y \qquad (4.4)$$

The solution of equations (4.3) is represented in terms of Volterra operators as

$$^{x}\eta(\tau) = {}^{x}H\left[\bar{f}_1(\tau), \bar{f}_2(\tau)\right]$$
$$^{y}\eta(\tau) = {}^{y}H\left[\bar{f}_1(\tau), \bar{f}_2(\tau)\right] \qquad (4.5)$$

where, (with κ denoting x or y)

$$^{\kappa}H\left[\bar{f}_1(\tau), \bar{f}_2(\tau)\right] = {}^{\kappa}H_0 + \sum_{i=1,2} {}^{\kappa}H_1^{(i)}[\bar{f}_i(\tau)] + \sum_{i=1,2;j=1,2} {}^{\kappa}H_2^{(i,j)}[\bar{f}_i(\tau), \bar{f}_j(\tau)]$$
$$+ \sum_{i=1,2;j=1,2;k=1,2} {}^{\kappa}H_3^{(i,j,k)}[\bar{f}_i(\tau), \bar{f}_j(\tau), \bar{f}_k(\tau)] + \ldots\ldots\ldots \qquad (4.6)$$

The individual operators of equation (4.6) are given in kernel form by

$$ {}^{\kappa}H_1^{(i)}[\bar{f}_i(\tau)] = \int_{-\infty}^{\infty} {}^{\kappa}h_1^{(i)}(\tau)\bar{f}_i(\tau-\tau_1)d\tau_1 \qquad \text{for } i=1,2 $$

$$ {}^{\kappa}H_2^{(i,j)}[\bar{f}_i(\tau),\bar{f}_j(\tau)] = \int_{-\infty}^{\infty}\int_{-\infty}^{\infty} {}^{\kappa}h_2^{(i,j)}(\tau_1,\tau_2)\bar{f}_i(\tau-\tau_1)\bar{f}_j(\tau-\tau_2)d\tau_1 d\tau_2 \qquad (4.7) $$

$$ \text{for } i=1,2;\ j=1,2 $$

$$ {}^{\kappa}H_3^{(i,j,k)}[\bar{f}_i(\tau),\bar{f}_j(\tau),\bar{f}_k(\tau)] = \int_{-\infty}^{\infty}\int_{-\infty}^{\infty}\int_{-\infty}^{\infty} {}^{\kappa}h_3^{(i,j,k)}(\tau_1,\tau_2,\tau_3)\bar{f}_i(\tau-\tau_1)\bar{f}_j(\tau-\tau_2)\bar{f}_k(\tau-\tau_3) $$

$$ \text{x } d\tau_1\, d\tau_2 d\tau_3 \qquad \text{for } i=1,2;\ j=1,2;\ k=1,2 $$

with nth order Volterra kernel

$$ h_n(\tau_1,\ldots\ldots,\tau_n) = 0 \qquad \text{for } \tau_p < 0, \quad p = 1,2,3,\ldots\ldots n. \qquad (4.8) $$

For convenience, writing the Volterra operators as

$$ {}^{\kappa}\eta_1^{(i)} = {}^{\kappa}H_1^{(i)}\left[\bar{f}_i(\tau)\right] $$

$$ {}^{\kappa}\eta_2^{(i,j)} = {}^{\kappa}H_2^{(i,j)}\left[\bar{f}_i(\tau),\bar{f}_j(\tau)\right] \qquad (4.9) $$

$$ {}^{\kappa}\eta_3^{(i,j,k)} = {}^{\kappa}H_3^{(i,j,k)}\left[\bar{f}_i(\tau),\bar{f}_j(\tau),\bar{f}_k(\tau)\right] $$

the response of equation (4.5) can be written as

$$ {}^{x}\eta(\tau) = \sum_{i=1,2} {}^{x}\eta_1^{(i)} + \sum_{i=1,2;j=1,2} {}^{x}\eta_2^{(i,j)} + \sum_{i=1,2;j=1,2;k=1,2} {}^{x}\eta_3^{(i,j,k)} + \ldots\ldots $$

$$ {}^{y}\eta(\tau) = \sum_{i=1,2} {}^{y}\eta_1^{(i)} + \sum_{i=1,2;j=1,2} {}^{y}\eta_2^{(i,j)} + \sum_{i=1,2;j=1,2;k=1,2} {}^{y}\eta_3^{(i,j,k)} + \ldots\ldots \qquad (4.10) $$

4.2 Synthesis of Higher Order Volterra Kernel Factors

The Volterra operators are now determined as follows. The excitation forces $\bar{f}_1(\tau)$, $\bar{f}_2(\tau)$ are replaced by $c\bar{f}_1(\tau)$ and $c\bar{f}_2(\tau)$ respectively, c being a constant. Noting equations (4.7), the resulting response of the system, becomes

$$ {}^{x}\eta(\tau) = \sum_{i=1,2} c\,{}^{x}\eta_1^{(i)} + \sum_{i=1,2;j=1,2} c^2\,{}^{x}\eta_2^{(i,j)} + \sum_{i=1,2;j=1,2;k=1,2} c^3\,{}^{x}\eta_3^{(i,j,k)} + \ldots\ldots $$

$$ {}^{y}\eta(\tau) = \sum_{i=1,2} c\,{}^{y}\eta_1^{(i)} + \sum_{i=1,2;j=1,2} c^2\,{}^{y}\eta_2^{(i,j)} + \sum_{i=1,2;j=1,2;k=1,2} c^3\,{}^{y}\eta_3^{(i,j,k)} + \ldots\ldots \qquad (4.11) $$

Substituting equations (4.11) and the derivatives in equations (4.3) one gets

$$\left[\sum_{i=1,2} c^{\,x}\eta_1^{(i)''} + \sum_{i=1,2;j=1,2} c^{2\,x}\eta_2^{(i,j)''} + \sum_{i=1,2;j=1,2;k=1,2} c^{3\,x}\eta_3^{(i,j,k)''}\right]$$
$$+ 2\xi_{xx}\left[\sum_{i=1,2} c^{\,x}\eta_1^{(i)'} + \sum_{i=1,2;j=1,2} c^{2\,x}\eta_2^{(i,j)'} + \sum_{i=1,2;j=1,2;k=1,2} c^{3\,x}\eta_3^{(i,j,k)'}\right]$$
$$+\left[\sum_{i=1,2} c^{\,x}\eta_1^{(i)} + \sum_{i=1,2;j=1,2} c^{2\,x}\eta_2^{(i,j)} + \sum_{i=1,2;j=1,2;k=1,2} c^{3\,x}\eta_3^{(i,j,k)}\right]$$
$$+ \lambda_{xy}^{L}\left[\sum_{i=1,2} c^{\,y}\eta_1^{(i)} + \sum_{i=1,2;j=1,2} c^{2\,y}\eta_2^{(i,j)} + \sum_{i=1,2;j=1,2;k=1,2} c^{3\,y}\eta_3^{(i,j,k)}\right]$$
$$+ \lambda_{xx}^{N}\left[\sum_{i=1,2} c^{\,x}\eta_1^{(i)} + \sum_{i=1,2;j=1,2} c^{2\,x}\eta_2^{(i,j)} + \sum_{i=1,2;j=1,2;k=1,2} c^{3\,x}\eta_3^{(i,j,k)}\right]^3$$
$$+ \lambda_{xy}^{N}\left[\sum_{i=1,2} c^{\,y}\eta_1^{(i)} + \sum_{i=1,2;j=1,2} c^{2\,y}\eta_2^{(i,j)} + \sum_{i=1,2;j=1,2;k=1,2} c^{3\,y}\eta_3^{(i,j,k)}\right]^3 = c\bar{f}_1(\tau)$$

$$\left[\sum_{i=1,2} c^{\,y}\eta_1^{(i)''} + \sum_{i=1,2;j=1,2} c^{2\,y}\eta_2^{(i,j)''} + \sum_{i=1,2;j=1,2;k=1,2} c^{3\,y}\eta_3^{(i,j,k)''}\right]$$
$$+ 2\xi_{yy}\left[\sum_{i=1,2} c^{\,y}\eta_1^{(i)'} + \sum_{i=1,2;j=1,2} c^{2\,y}\eta_2^{(i,j)'} + \sum_{i=1,2;j=1,2;k=1,2} c^{3\,y}\eta_3^{(i,j,k)'}\right]$$
$$+ \lambda_{yy}^{L}\left[\sum_{i=1,2} c^{\,y}\eta_1^{(i)} + \sum_{i=1,2;j=1,2} c^{2\,y}\eta_2^{(i,j)} + \sum_{i=1,2;j=1,2;k=1,2} c^{3\,y}\eta_3^{(i,j,k)}\right]$$
$$+ \lambda_{yx}^{L}\left[\sum_{i=1,2} c^{\,x}\eta_1^{(i)} + \sum_{i=1,2;j=1,2} c^{2\,x}\eta_2^{(i,j)} + \sum_{i=1,2;j=1,2;k=1,2} c^{3\,x}\eta_3^{(i,j,k)}\right]$$
$$+ \lambda_{yy}^{N}\left[\sum_{i=1,2} c^{\,y}\eta_1^{(i)} + \sum_{i=1,2;j=1,2} c^{2\,y}\eta_2^{(i,j)} + \sum_{i=1,2;j=1,2;k=1,2} c^{3\,y}\eta_3^{(i,j,k)}\right]^3$$
$$+ \lambda_{yx}^{N}\left[\sum_{i=1,2} c^{\,x}\eta_1^{(i)} + \sum_{i=1,2;j=1,2} c^{2\,x}\eta_2^{(i,j)} + \sum_{i=1,2;j=1,2;k=1,2} c^{3\,x}\eta_3^{(i,j,k)}\right]^3 = c\bar{f}_2(\tau) \qquad (4.12)$$

Summing up the responses of equal order, one can write

I order response

$$ {}^{x}\eta_1 = \sum_{i=1,2} {}^{x}\eta_1^{(i)} $$

$$ {}^{y}\eta_1 = \sum_{i=1,2} {}^{y}\eta_1^{(i)} \qquad (4.13) $$

II order response

$$ {}^{x}\eta_2 = \sum_{i=1,2;j=1,2} {}^{x}\eta_2^{(i,j)} $$

$$ {}^{y}\eta_2 = \sum_{i=1,2;j=1,2} {}^{y}\eta_2^{(i,j)} \qquad (4.14) $$

III order response

$$ {}^{x}\eta_3 = \sum_{i=1,2;j=1,2;k=1,2} {}^{x}\eta_3^{(i,j,k)} $$

$$ {}^{y}\eta_3 = \sum_{i=1,2;j=1,2;k=1,2} {}^{y}\eta_3^{(i,j,k)} \qquad (4.15) $$

Noting the following symmetry of kernels (Schetzen, 1980)

$$ {}^{x}\eta_2^{(i,j)} = {}^{x}\eta_2^{(j,i)}; \qquad {}^{x}\eta_3^{(i,j,j)} = {}^{x}\eta_3^{(j,i,j)} = {}^{x}\eta_3^{(j,j,i)} \text{ ; etc.} $$

$$ {}^{y}\eta_2^{(i,j)} = {}^{y}\eta_2^{(j,i)}; \qquad {}^{y}\eta_3^{(i,j,j)} = {}^{y}\eta_3^{(j,i,j)} = {}^{y}\eta_3^{(j,j,i)} \qquad (4.16) $$

and using equations (4.13)-(4.16), equations (4.12) are written in condensed form as,

$$ \sum_{n=1}^{\infty} c^n \left[{}^{x}\eta_n'' + 2\xi_{xx}\, {}^{x}\eta_n' + {}^{x}\eta_n + \lambda_{xy}^{L}\, {}^{y}\eta_n \right] + \lambda_{xx}^{N} \left[\sum_{n=1}^{\infty} c^n\, {}^{x}\eta_n \right]^3 + \lambda_{xy}^{N} \left[\sum_{n=1}^{\infty} c^n\, {}^{y}\eta_n \right]^3 = c\bar{f}_1(\tau) $$

$$ \sum_{n=1}^{\infty} c^n \left[{}^{y}\eta_n'' + 2\xi_{yy}\, {}^{y}\eta_n' + \lambda_{yy}^{L}\, {}^{y}\eta_n + \lambda_{yx}^{L}\, {}^{x}\eta_n \right] + \lambda_{yy}^{N} \left[\sum_{n=1}^{\infty} c^n\, {}^{y}\eta_n \right]^3 + \lambda_{yx}^{N} \left[\sum_{n=1}^{\infty} c^n\, {}^{x}\eta_n \right]^3 = c\bar{f}_2(\tau) \qquad (4.17) $$

Equations (4.17) are power series in c with coefficients of c^n being ${}^{x}\eta_n$ or ${}^{y}\eta_n$. The responses, ${}^{x}\eta_n$ and ${}^{y}\eta_n$ are determined by equating the like powers of c as follows

c^1 terms :

$$
\begin{aligned}
&{}^{x}\eta_1'' + 2\xi_{xx}\,{}^{x}\eta_1' + {}^{x}\eta_1 + \lambda_{xy}^{L}\,{}^{y}\eta_1 = \bar{f}_1(\tau) \\
&{}^{y}\eta_1'' + 2\xi_{yy}\,{}^{y}\eta_1' + \lambda_{yy}^{L}\,{}^{y}\eta_1 + \lambda_{yx}^{L}\,{}^{x}\eta_1 = \bar{f}_2(\tau)
\end{aligned}
\tag{4.18}
$$

c^2 terms:

$$
\begin{aligned}
&{}^{x}\eta_2'' + 2\xi_{xx}\,{}^{x}\eta_2' + {}^{x}\eta_2 + \lambda_{xy}^{L}\,{}^{y}\eta_2 = 0 \\
&{}^{y}\eta_2'' + 2\xi_{yy}\,{}^{y}\eta_2' + \lambda_{yy}^{L}\,{}^{y}\eta_2 + \lambda_{yx}^{L}\,{}^{x}\eta_2 = 0
\end{aligned}
\tag{4.19}
$$

c^3 terms:

$$
\begin{aligned}
&{}^{x}\eta_3'' + 2\xi_{xx}\,{}^{x}\eta_3' + {}^{x}\eta_3 + \lambda_{xy}^{L}\,{}^{y}\eta_3 + \lambda_{xx}^{N}\,{}^{x}\eta_1^3 + \lambda_{xy}^{N}\,{}^{y}\eta_1^3 = 0 \\
&{}^{y}\eta_3'' + 2\xi_{yy}\,{}^{y}\eta_3' + \lambda_{yy}^{L}\,{}^{y}\eta_3 + \lambda_{yx}^{L}\,{}^{x}\eta_3 + \lambda_{yy}^{N}\,{}^{y}\eta_1^3 + \lambda_{yx}^{N}\,{}^{x}\eta_1^3 = 0
\end{aligned}
\tag{4.20}
$$

Equations (4.18)-(4.20) can be solved sequentially. Taking Laplace transforms of equations (4.18), for zero initial conditions, one obtains

$$
\begin{aligned}
&\left[s^2\,{}^{x}\eta_1(s) + 2\xi_{xx}s\,{}^{x}\eta_1(s) + {}^{x}\eta_1(s) + \lambda_{xy}^{L}\,{}^{y}\eta_1(s)\right] = F_1(s) \\
&\left[s^2\,{}^{y}\eta_1(s) + 2\xi_{yy}s\,{}^{y}\eta_1(s) + \lambda_{yy}^{L}\,{}^{y}\eta_1(s) + \lambda_{yx}^{L}\,{}^{x}\eta_1(s)\right] = F_2(s)
\end{aligned}
\tag{4.21}
$$

Solving the above two simultaneous equations, the solutions for ${}^{x}\eta_1(s)$ and ${}^{y}\eta_1(s)$ are

$$
\begin{aligned}
{}^{x}\eta_1(s) &= \frac{(s^2 + 2\xi_{yy}s + \lambda_{yy}^{L})F_1(s) - \lambda_{xy}^{L}F_2(s)}{(s^2 + 2\xi_{xx}s + 1)(s^2 + .2\xi_{yy}s + \lambda_{yy}^{L}) - (\lambda_{xy}^{L}\lambda_{yx}^{L})} \\
{}^{y}\eta_1(s) &= \frac{(s^2 + 2\xi_{yy}s + 1)F_2(s) - \lambda_{yx}^{L}F_1(s)}{(s^2 + 2\xi_{xx}s + 1)(s^2 + 2\xi_{yy}s + \lambda_{yy}^{L}) - (\lambda_{xy}^{L}\lambda_{yx}^{L})}
\end{aligned}
\tag{4.22}
$$

Referring to the notations (4.9) and (4.13), the individual Volterra operators, from the above, are

$$
{}^{x}H_1^{(1)}(s) = \frac{(s^2 + 2\xi_{yy}s + \lambda_{yy}^L)}{(s^2 + 2\xi_{xx}s + 1)(s^2 + 2\xi_{yy}s + \lambda_{yy}^L) - (\lambda_{xy}^L \lambda_{yx}^L)}
$$

$$
{}^{x}H_1^{(2)}(s) = \frac{-\lambda_{xy}^L}{(s^2 + 2\xi_{xx}s + 1)(s^2 + 2\xi_{yy}s + \lambda_{yy}^L) - (\lambda_{xy}^L \lambda_{yx}^L)}
$$

(4.23)

$$
{}^{y}H_1^{(1)}(s) = \frac{-\lambda_{yx}^L}{(s^2 + 2\xi_{xx}s + 1)(s^2 + 2\xi_{yy}s + \lambda_{yy}^L) - (\lambda_{xy}^L \lambda_{yx}^L)}
$$

$$
{}^{y}H_1^{(2)}(s) = \frac{(s^2 + 2\xi_{xx}s + 1)}{(s^2 + 2\xi_{xx}s + 1)(s^2 + 2\xi_{yy}s + \lambda_{yy}^L) - (\lambda_{xy}^L \lambda_{yx}^L)}
$$

For the second order kernels, the Laplace transforms of equations (4.19), similarly give

$$
\begin{aligned}
&\left[s^2\, {}^{x}\eta_2(s) + 2\xi_{xx}s\, {}^{x}\eta_2(s) + {}^{x}\eta_2(s) + \lambda_{yx}^L\, {}^{y}\eta_2(s)\right] = 0 \\
&\left[s^2\, {}^{y}\eta_2(s) + 2\xi_{yy}s\, {}^{y}\eta_2(s) + \lambda_{yy}^L\, {}^{y}\eta_2(s) + \lambda_{yx}^L\, {}^{x}\eta_2(s)\right] = 0
\end{aligned}
\qquad (4.24)
$$

which yield

$$
\begin{aligned}
&{}^{x}\eta_2(s) = 0 \\
&{}^{y}\eta_2(s) = 0
\end{aligned}
\qquad (4.25)
$$

that is, the second order kernel is identically zero -

$$
\begin{aligned}
&{}^{x}h_2(\tau_1, \tau_2) = 0 \\
&{}^{y}h_2(\tau_1, \tau_2) = 0
\end{aligned}
\qquad (4.26)
$$

In order to synthesise expressions for third order kernels, equations (4.20) can be written as

$$
\begin{aligned}
&{}^{x}\eta_3'' + 2\xi_{xx}\, {}^{x}\eta_3' + {}^{x}\eta_3 + \lambda_{xy}^L\, {}^{y}\eta_3 = q_1 \\
&{}^{y}\eta_3'' + 2\xi_{yy}\, {}^{y}\eta_3' + \lambda_{yy}^L\, {}^{y}\eta_3 + \lambda_{yx}^L\, {}^{x}\eta_3 = q_2
\end{aligned}
\qquad (4.27)
$$

where the following abbreviations have been used

$$
\begin{aligned}
&q_1 = -\lambda_{xx}^N\, {}^{x}\eta_1^3 - \lambda_{xy}^N\, {}^{y}\eta_1^3 \\
&q_2 = -\lambda_{yy}^N\, {}^{y}\eta_1^3 - \lambda_{yx}^N\, {}^{x}\eta_1^3
\end{aligned}
\qquad (4.28)
$$

Equations (4.27) are linear in η_3, similar to equations (4.18) and therefore the solution in terms of Volterra operators is

$$
\begin{aligned}
{}^{x}\eta_3 &= {}^{x}H_1[q_1, q_2] \\
{}^{y}\eta_3 &= {}^{y}H_1[q_1, q_2]
\end{aligned}
\tag{4.29}
$$

that is

$$
\begin{aligned}
{}^{x}H_3[\bar{f}_1(\tau), \bar{f}_2(\tau)] &= {}^{x}H_1[q_1, q_2] \\
{}^{y}H_3[\bar{f}_1(\tau), \bar{f}_2(\tau)] &= {}^{y}H_1[q_1, q_2]
\end{aligned}
\tag{4.30}
$$

However, since ${}^{x}H_1$ and ${}^{y}H_1$ are linear operators, one obtains

$$
\begin{aligned}
{}^{x}\eta_3 &= {}^{x}H_1[q_1, q_2] \\
&= {}^{x}H_1^{(1)}[q_1] + {}^{x}H_1^{(2)}[q_2] \\
{}^{y}\eta_3 &= {}^{y}H_1[q_1, q_2] \\
&= {}^{y}H_1^{(1)}[q_1] + {}^{y}H_1^{(2)}[q_2]
\end{aligned}
\tag{4.31}
$$

Noting the abbreviations (eqn. 4.31), the terms on the right hand sides of the above equations, are individually expanded as

$$
\begin{aligned}
{}^{x}H_1^{(1)}[q_1] &= {}^{x}H_1^{(1)}[(-\lambda_{xx}^{N}\ {}^{x}\eta_1^3 - \lambda_{xy}^{N}\ {}^{y}\eta_1^3)] \\
&= {}^{x}H_1^{(1)}[-\lambda_{xx}^{N}\ {}^{x}\eta_1^3] + {}^{x}H_1^{(1)}[-\lambda_{xy}^{N}\ {}^{y}\eta_1^3] \\
&= -\lambda_{xx}^{N}\ {}^{x}H_1^{(1)}[{}^{x}\eta_1^3] - \lambda_{xy}^{N}\ {}^{x}H_1^{(1)}[{}^{y}\eta_1^3]
\end{aligned}
\tag{4.32}
$$

In the above equations

$$
\begin{aligned}
{}^{x}\eta_1 &= {}^{x}\eta_1^{(1)} + {}^{x}\eta_1^{(2)} \\
&= {}^{x}H_1^{(1)}\left[\bar{f}_1(\tau)\right] + {}^{x}H_1^{(2)}\left[\bar{f}_2(\tau)\right] \\
{}^{y}\eta_1 &= {}^{y}\eta_1^{(1)} + {}^{y}\eta_1^{(2)} \\
&= {}^{y}H_1^{(1)}\left[\bar{f}_1(\tau)\right] + {}^{y}H_1^{(2)}\left[\bar{f}_2(\tau)\right]
\end{aligned}
\tag{4.33}
$$

Taking Laplace transforms of equations (4.32) gives

$$
\begin{aligned}
{}^{x}H_1^{(1)}[Q_1(s_1, s_2, s_3)] = \lambda_{xx}^{N}\ ({}^{xx}\Psi_3^{1-1,1,1} + 3\ {}^{xx}\Psi_3^{1-1,1,2} + 3\ {}^{xx}\Psi_3^{1-1,2,2} + {}^{xx}\Psi_3^{1-2,2,2}) \\
+ \lambda_{xy}^{N}\ ({}^{xy}\Psi_3^{1-1,1,1} + 3\ {}^{xy}\Psi_3^{1-1,1,2} + 3\ {}^{xy}\Psi_3^{1-1,2,2} + {}^{xy}\Psi_3^{1-2,2,2})
\end{aligned}
\tag{4.34}
$$

In equation (4.34), the terms ${}^{xx}\Psi_3^{(i-j,k,l)}(s_1,s_2,s_3)$ and ${}^{xy}\Psi_3^{(l-i,j,k)}(s_1,s_2,s_3)$ have been called in this work as third order kernel factors and are defined as

$$
\begin{aligned}
{}^{xx}\Psi_3^{(i-j,k,l)}(s_1,s_2,s_3) &= -\,{}^{x}H_1^{(i)}(s_1+s_2+s_3)\;{}^{x}H_1^{(j)}(s_1)\;{}^{x}H_1^{(k)}(s_2)\;{}^{x}H_1^{(l)}(s_3)\\
{}^{xy}\Psi_3^{(l-i,j,k)}(s_1,s_2,s_3) &= -\,{}^{x}H_1^{(l)}(s_1+s_2+s_3)\;{}^{y}H_1^{(i)}(s_1)\;{}^{y}H_1^{(j)}(s_2)\;{}^{y}H_1^{(k)}(s_3)\\
& \qquad i=1,2\,;\; j=1,2\,;\; k=1,2\,;\; l=1,2
\end{aligned}
\tag{4.35}
$$

The third order kernel factors above, can be readily constructed, using equations from the first order kernels ${}^{x}H_1^{(1)}(s)$, ${}^{x}H_1^{(2)}(s)$, ${}^{y}H_1^{(1)}(s)$, ${}^{y}H_1^{(2)}(s)$.

Similarly, the Laplace transforms of other terms on the right hand side of equations (4.31) can be worked out to be

$$
\begin{aligned}
{}^{x}H_1^{(2)}[Q_2(s_1,s_2,s_3)] &= \lambda_{yy}^{N}\,({}^{xy}\Psi_3^{2-1,1,1}+3\;{}^{xy}\Psi_3^{2-1,1,2}+3\;{}^{xy}\Psi_3^{2-1,2,2}+{}^{xy}\Psi_3^{2-2,2,2})\\
&\quad+\lambda_{yx}^{N}\,({}^{xx}\Psi_3^{2-1,1,1}+3\;{}^{xx}\Psi_3^{2-1,1,2}+3\;{}^{xx}\Psi_3^{2-1,2,2}+{}^{xx}\Psi_3^{2-2,2,2})
\end{aligned}
\tag{4.36}
$$

$$
\begin{aligned}
{}^{y}H_1^{(1)}[Q_1(s_1,s_2,s_3)] &= \lambda_{xx}^{N}\,({}^{yx}\Psi_3^{1-1,1,1}+3\;{}^{yx}\Psi_3^{1-1,1,2}+3\;{}^{yx}\Psi_3^{1-1,2,2}+{}^{yx}\Psi_3^{1-2,2,2})\\
&\quad+\lambda_{xy}^{N}\,({}^{yy}\Psi_3^{1-1,1,1}+3\;{}^{yy}\Psi_3^{1-1,1,2}+3\;{}^{yy}\Psi_3^{1-1,2,2}+{}^{yy}\Psi_3^{1-2,2,2})
\end{aligned}
\tag{4.37}
$$

$$
\begin{aligned}
{}^{y}H_1^{(2)}[Q_2(s_1,s_2,s_3)] &= \lambda_{yy}^{N}\,({}^{yy}\Psi_3^{2-1,1,1}+3\;{}^{yy}\Psi_3^{2-1,1,2}+3\;{}^{yy}\Psi_3^{2-1,2,2}+{}^{yy}\Psi_3^{2-2,2,2})\\
&\quad+\lambda_{yx}^{N}\,({}^{yx}\Psi_3^{2-1,1,1}+3\;{}^{yx}\Psi_3^{2-1,1,2}+3\;{}^{yx}\Psi_3^{2-1,2,2}+{}^{yx}\Psi_3^{2-2,2,2})
\end{aligned}
\tag{4.38}
$$

In equations (4.36)-(4.38), the following third order kernel factors have been used in addition to those defined in equation (4.35).

$$
\begin{aligned}
{}^{yy}\Psi_3^{(i-j,k,l)}(s_1,s_2,s_3) &= -\,{}^{y}H_1^{(i)}(s_1+s_2+s_3)\;{}^{y}H_1^{(j)}(s_1)\;{}^{y}H_1^{(k)}(s_2)\;{}^{y}H_1^{(l)}(s_3)\\
{}^{yx}\Psi_3^{(l-i,j,k)}(s_1,s_2,s_3) &= -\,{}^{y}H_1^{(l)}(s_1+s_2+s_3)\;{}^{x}H_1^{(i)}(s_1)\;{}^{x}H_1^{(j)}(s_2)\;{}^{x}H_1^{(k)}(s_3)\\
& \qquad i=1,2\,;\; j=1,2\,;\; k=1,2\,;\; l=1,2
\end{aligned}
\tag{4.39}
$$

The Laplace transforms of the third order kernels (equations (4.30)), can now be expressed as

$$
\begin{aligned}
{}^{x}H_3(s_1,s_2,s_3) &= \lambda_{xx}^{N}\,({}^{xx}\Psi_3^{1-1,1,1} + 3\,{}^{xx}\Psi_3^{1-1,1,2} + 3\,{}^{xx}\Psi_3^{1-1,2,2} + {}^{xx}\Psi_3^{1-2,2,2}) \\
&+ \lambda_{xy}^{N}\,({}^{xy}\Psi_3^{1-1,1,1} + 3\,{}^{xy}\Psi_3^{1-1,1,2} + 3\,{}^{xy}\Psi_3^{1-1,2,2} + {}^{xy}\Psi_3^{1-2,2,2}) \\
&+ \lambda_{yy}^{N}\,({}^{xy}\Psi_3^{2-1,1,1} + 3\,{}^{xy}\Psi_3^{2-1,1,2} + 3\,{}^{xy}\Psi_3^{2-1,2,2} + {}^{xy}\Psi_3^{2-2,2,2}) \\
&+ \lambda_{yx}^{N}\,({}^{xx}\Psi_3^{2-1,1,1} + 3\,{}^{xx}\Psi_3^{2-1,1,2} + 3\,{}^{xx}\Psi_3^{2-1,2,2} + {}^{xx}\Psi_3^{2-2,2,2}) \\
{}^{y}H_3(s_1,s_2,s_3) &= \lambda_{xx}^{N}\,({}^{yx}\Psi_3^{1-1,1,1} + 3\,{}^{yx}\Psi_3^{1-1,1,2} + 3\,{}^{yx}\Psi_3^{1-1,2,2} + {}^{yx}\Psi_3^{1-2,2,2}) \\
&+ \lambda_{xy}^{N}\,({}^{yy}\Psi_3^{1-1,1,1} + 3\,{}^{yy}\Psi_3^{1-1,1,2} + 3\,{}^{yy}\Psi_3^{1-1,2,2} + {}^{yy}\Psi_3^{1-2,2,2}) \\
&+ \lambda_{yy}^{N}\,({}^{yy}\Psi_3^{2-1,1,1} + 3\,{}^{yy}\Psi_3^{2-1,1,2} + 3\,{}^{yy}\Psi_3^{2-1,2,2} + {}^{yy}\Psi_3^{2-2,2,2}) \\
&+ \lambda_{yx}^{N}\,({}^{yx}\Psi_3^{2-1,1,1} + 3\,{}^{yx}\Psi_3^{2-1,1,2} + 3\,{}^{yx}\Psi_3^{2-1,2,2} + {}^{yx}\Psi_3^{2-2,2,2})
\end{aligned}
\tag{4.40}
$$

4.3 Measurement of Wiener Kernels

As stated in Chapter 3, measurement of individual Volterra kernels is not possible, while equivalent Wiener kernels can be extracted from the measured response if the excitation to the system is white and Gaussian. These Wiener kernels can then be used to generate the Volterra kernels.

In the present case, the Wiener kernels of the nonlinear system are extracted by application of white Gaussian forces $\bar{f}_1(\tau)$ and $\bar{f}_2(\tau)$, one at a time, i.e. first a white Gaussian force $\bar{f}_1(\tau)$ with variance A_1, is applied in the x-direction, while keeping the y-direction force, $\bar{f}_2(\tau) = 0$. The resulting response (in both the x and y directions), is employed to extract the direct, x-direction, Wiener kernels and the cross (x-y) kernels. In the next instance, a white Gaussian force $\bar{f}_2(\tau)$ with variance A_2, is applied in the y-direction, while keeping the x-direction force, $\bar{f}_1(\tau) = 0$. The system response, in this instance, is employed to extract the direct y-direction Wiener kernels and the cross (y-x) kernels.

The system response, in terms of Wiener kernels, is now expressed, in the two individual cases as –

$\bar{f}_1(\tau)$ Gaussian white, with variance A_1 and $\bar{f}_2(\tau) = 0$:

$$
\begin{aligned}
{}^{x}\eta(\tau) &= {}^{x}W\left[\bar{f}_1(\tau),\ 0\right] = {}^{x}W\left[\bar{f}_1(\tau)\right] \\
{}^{y}\eta(\tau) &= {}^{y}W\left[\bar{f}_1(\tau),\ 0\right] = {}^{y}W\left[\bar{f}_1(\tau)\right]
\end{aligned}
\tag{4.41}
$$

$\bar{f}_2(\tau)$ Gaussian white, with variance A_2 and $\bar{f}_1(\tau) = 0$:

$$
\begin{aligned}
{}^{x}\eta(\tau) &= {}^{x}W\left[0,\ \bar{f}_2(\tau)\right] = {}^{x}W\left[\bar{f}_2(\tau)\right] \\
{}^{y}\eta(\tau) &= {}^{y}W\left[0,\ \bar{f}_2(\tau)\right] = {}^{y}W\left[\bar{f}_2(\tau)\right]
\end{aligned}
\tag{4.42}
$$

In the above equations

$$
{}^{\kappa}W\left[\bar{f}_i(\tau)\right] = {}^{\kappa}W_0 + {}^{\kappa}W_1^{(i)}[\bar{f}_i(\tau)] + {}^{\kappa}W_2^{(i)}[\bar{f}_i(\tau)] + {}^{\kappa}W_3^{(i)}[\bar{f}_i(\tau)] + \ldots\ldots\ldots \tag{4.43}
$$

(with κ denoting x or y) for $i = 1$ or 2

The individual operators of equation (4.43) being given in kernel form by

$$
\begin{aligned}
{}^{\kappa}W_1^{(i)}[\bar{f}_i(\tau)] &= \int_{-\infty}^{\infty} {}^{\kappa}w_1^{(i)}(\tau_1)\bar{f}_i(\tau-\tau_1)d\tau_1 \\
{}^{\kappa}W_2^{(i)}[\bar{f}_i(\tau)] &= \int_{-\infty}^{\infty}\int_{-\infty}^{\infty} {}^{\kappa}w_2^{(i)}(\tau_1,\tau_2)\bar{f}_i(\tau-\tau_1)\bar{f}_i(\tau-\tau_2)d\tau_1 d\tau_2 - A_i\int_{-\infty}^{\infty} {}^{\kappa}w_2^{(i)}(\tau_2,\tau_2)d\tau_2 \\
{}^{\kappa}W_3^{(i)}[\bar{f}_i(\tau)] &= \int_{-\infty}^{\infty}\int_{-\infty}^{\infty}\int_{-\infty}^{\infty} {}^{\kappa}w_3^{(i)}(\tau_1,\tau_2,\tau_3)\bar{f}_i(\tau-\tau_1)\bar{f}_i(\tau-\tau_2)\bar{f}_i(\tau-\tau_3)\ d\tau_1\, d\tau_2 d\tau_3 \\
&\quad - 3A_i\int_{-\infty}^{\infty}\int_{-\infty}^{\infty} {}^{\kappa}w_3^{(i)}(\tau_1,\tau_2,\tau_2)\bar{f}_i(\tau-\tau_1)\,d\tau_1\,d\tau_2
\end{aligned}
\tag{4.44}
$$

The relationship between the Volterra kernels of equations (4.7) and the Wiener kernels above, as in the previous chapter can be shown to be (for a third order response representation)

$$
\begin{aligned}
{}^{\kappa}h_3^{(i)}(\tau_1,\tau_2,\tau_3) &= {}^{\kappa}w_3^{(i)}(\tau_1,\tau_2,\tau_3)\\
{}^{\kappa}h_2^{(i)}(\tau_1,\tau_2) &= {}^{\kappa}w_2^{(i)}(\tau_1,\tau_2)\\
{}^{\kappa}h_1^{(i)}(\tau_1) &= {}^{\kappa}w_1^{(i)}(\tau_1) + {}^{\kappa}w_{1(3)}^{(i)}(\tau_1)\\
{}^{\kappa}h_0 &= {}^{\kappa}w_0 + {}^{\kappa}w_{0(2)}
\end{aligned}
\qquad (4.45)
$$

with

$$
{}^{\kappa}w_{1(3)}^{(i)}(\tau_1) = -3A_i \int_{-\infty}^{\infty} {}^{\kappa}w_3^{(i)}(\tau_1,\tau_2,\tau_2)d\tau_2
$$

$$
{}^{\kappa}w_{0(2)}^{(i)} = -A_i \int_{-\infty}^{\infty} {}^{\kappa}w_2^{(i)}(\tau_1,\tau_1)d\tau_1
$$

Employing the following Fourier transforms,

$$
\begin{aligned}
\bar{f}_i(\tau) &= \int_{-\infty}^{\infty} \bar{F}_i(\omega)e^{j\omega\tau}d\omega\\
{}^{\kappa}\eta(\tau) &= \int_{-\infty}^{\infty} {}^{\kappa}\eta(\omega)e^{j\omega\tau_1}d\omega\\
{}^{\kappa}w_1^{(i)}(\tau) &= \int_{-\infty}^{\infty} {}^{\kappa}W_1^{(i)}(\omega_1)e^{j\omega_1\tau}d\omega_1\\
{}^{\kappa}w_2^{(i)}(\tau_1,\tau_2) &= \int_{-\infty}^{\infty}\int_{-\infty}^{\infty} {}^{\kappa}W_2^{(i)}(\omega_1,\omega_2)e^{j(\omega_1\tau_1+\omega_2\tau_2)}d\omega_1 d\omega_2\\
{}^{\kappa}w_3^{(i)}(\tau_1,\tau_2,\tau_3) &= \int_{-\infty}^{\infty}\int_{-\infty}^{\infty}\int_{-\infty}^{\infty} {}^{\kappa}W_3^{(i)}(\omega_1,\omega_2,\omega_3)e^{j(\omega_1\tau_1+\omega_2\tau_2+\omega_3\tau_3)}d\omega_1 d\omega_2 d\omega_3
\end{aligned}
\qquad (4.46)
$$

and using the relationship

$$
\int_{-\infty}^{\infty} e^{j\omega\tau}d\tau = \delta(\omega)\text{, the Dirac Delta function,} \qquad (4.47)
$$

the responses (4.41) and (4.42) can be expressed as

$$
\begin{aligned}
{}^{x}\eta(\tau) = {}^{x}W_0 &+ \int_{-\infty}^{\infty} {}^{x}W_1^{(i)}(\omega_1)F_i(\omega_1)e^{j\omega_1\tau}d\omega_1 \\
&+ \left[\int_{-\infty}^{\infty}\int_{-\infty}^{\infty} {}^{x}W_2^{(i)}(\omega_1,\omega_2)F_i(\omega_1)F_i(\omega_2)e^{j(\omega_1+\omega_2)\tau}d\omega_1 d\omega_2 - A_i\int_{-\infty}^{\infty} {}^{x}W_2^{(i)}(\omega_2,-\omega_2)d\omega_2\right] \\
&+ \int_{-\infty}^{\infty}\int_{-\infty}^{\infty}\int_{-\infty}^{\infty} {}^{x}W_3^{(i)}(\omega_1,\omega_2,\omega_3)F_i(\omega_1)\bar{F}_i(\omega_2)\bar{F}_i(\omega_3)e^{j(\omega_1+\omega_2+\omega_3)\tau}d\omega_1 d\omega_2 d\omega_3 \\
&- 3A_i\int_{-\infty}^{\infty}\int_{-\infty}^{\infty} {}^{x}W_3^{(i)}(\omega_1,\omega_2,-\omega_2)d\omega_1 d\omega_2\Bigg] \\
&+ \ldots\ldots\ldots\ldots\ldots\ldots\ldots\ldots
\end{aligned}
\tag{4.48}
$$

$$
\begin{aligned}
{}^{y}\eta(\tau) = {}^{y}W_0 &+ \int_{-\infty}^{\infty} {}^{y}W_1^{(i)}(\omega_1)F_i(\omega_1)e^{j\omega_1\tau}d\omega_1 \\
&+ \left[\int_{-\infty}^{\infty}\int_{-\infty}^{\infty} {}^{y}W_2^{(i)}(\omega_1,\omega_2)F_i(\omega_1)\bar{F}_i(\omega_2)e^{j(\omega_1+\omega_2)\tau}d\omega_1 d\omega_2 - A_i\int_{-\infty}^{\infty} {}^{y}W_2^{(i)}(\omega_2,-\omega_2)d\omega_2\right] \\
&+ \int_{-\infty}^{\infty}\int_{-\infty}^{\infty}\int_{-\infty}^{\infty} {}^{y}W_3^{(i)}(\omega_1,\omega_2,\omega_3)F_i(\omega_1)\bar{F}_i(\omega_2)\bar{F}_i(\omega_3)e^{j(\omega_1+\omega_2+\omega_3)\tau}d\omega_1 d\omega_2 d\omega_3 \\
&- 3A_i\int_{-\infty}^{\infty}\int_{-\infty}^{\infty} {}^{y}W_3^{(i)}(\omega_1,\omega_2,-\omega_2)d\omega_1 d\omega_2\Bigg] \\
&+ \ldots\ldots\ldots\ldots\ldots\ldots\ldots\ldots
\end{aligned}
\tag{4.49}
$$

A complex exponential filter, similar to the one described in Chapter 3, has been used for measurement of the individual Wiener kernel transforms. Referring to Fig.4.2, the output of the filter is

$$
\begin{aligned}
z^{(i)}(\tau) &= \int_{-\infty}^{\infty} e^{j\omega\tau_1} f_i(\tau-\tau_1)d\tau_1 \\
&= F_i^{*}(\omega)e^{-j\omega\tau_1}
\end{aligned}
\tag{4.50}
$$

and the ensemble averages of the outputs of the circuit are,

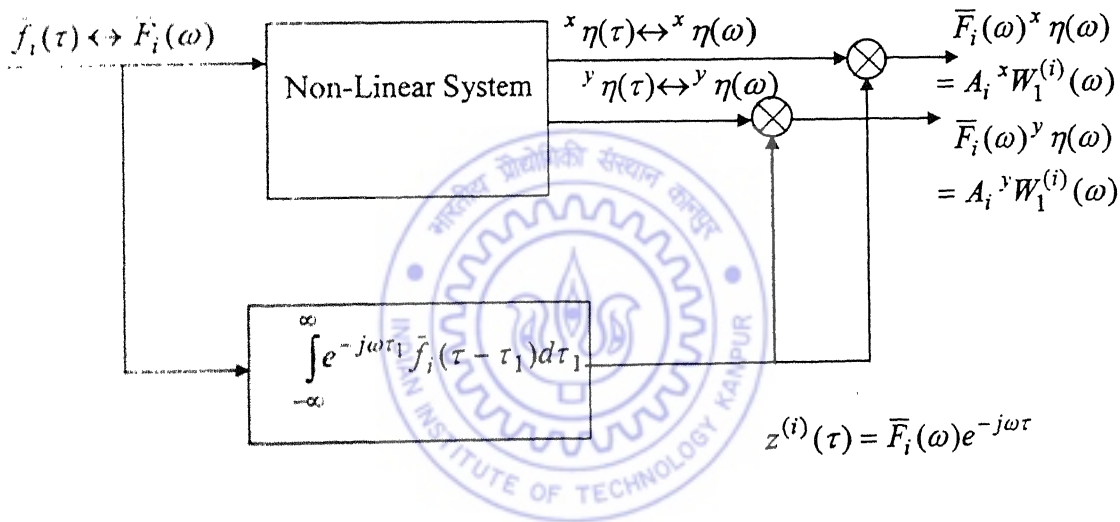

Fig. 4.2 Scheme for evaluating the first order direct and cross Wiener kernel transforms, $W_1^{(i)}(\omega)$.

$$
\begin{aligned}
{}^{x}\eta(\tau)z^{(i)}(\tau) \;=\; & {}^{x}W_0'\left\langle \bar{F}_i^{*}(\omega)\right\rangle e^{-j\omega\tau} + \int_{-\infty}^{\infty} {}^{x}W_1^{(i)}(\omega_1)\left\langle \bar{F}_i(\omega_1)\bar{F}_i^{*}(\omega)\right\rangle e^{-j\tau(\omega_1-\omega)}d\omega_1 \\
& + \Bigg[\int_{-\infty}^{\infty}\int_{-\infty}^{\infty} {}^{x}W_2^{(i)}(\omega_1,\omega_2)\left\langle \bar{F}_i(\omega_1)\bar{F}_i(\omega_2)\bar{F}_i^{*}(\omega)\right\rangle e^{-j\tau(\omega_1+\omega_2-\omega)}d\omega_1 d\omega_2 \\
& \quad - A_i\left\langle F_i^{*}(\omega)\right\rangle e^{-j\omega_1\tau}\int_{-\infty}^{\infty} {}^{x}W_2^{(i)}(\omega_2,-\omega_2)d\omega_2 \Bigg] \\
& + \Bigg[\int_{-\infty}^{\infty}\int_{-\infty}^{\infty}\int_{-\infty}^{\infty} {}^{x}W_3^{(i)}(\omega_1,\omega_2,\omega_3)\left\langle \bar{F}_i(\omega_1)\bar{F}_i(\omega_2)\bar{F}_i(\omega_3)\bar{F}_i^{*}(\omega)\right\rangle \\
& \qquad \times e^{-j\tau(\omega_1+\omega_2+\omega_3-\omega)}\,d\omega_1 d\omega_2 d\omega_3 \\
& \quad -3A_i\int_{-\infty}^{\infty}\int_{-\infty}^{\infty} {}^{x}W_3^{(i)}(\omega_1,\omega_2,-\omega_2)\left\langle \bar{F}_i(\omega_1)\bar{F}_i^{*}(\omega)\right\rangle e^{-j\tau(\omega_1-\omega)}d\omega_1 d\omega_2 \Bigg] \\
& + \ldots\ldots\ldots\ldots
\end{aligned}
\tag{4.51}
$$

$$
\begin{aligned}
\left\langle {}^{y}\eta(\tau)z^{(i)}(\tau)\right\rangle = & \left\langle F_i^{*}(\omega)\right\rangle e^{-j\omega\tau}\;{}^{y}W_0 + \int_{-\infty}^{\infty} {}^{y}W_1^{(i)}(\omega_1)\left\langle \bar{F}_i(\omega_1)\bar{F}_i^{*}(\omega)\right\rangle e^{-j\tau(\omega_1-\omega)}d\omega_1 \\
& + \Bigg[\int_{-\infty}^{\infty}\int_{-\infty}^{\infty} {}^{y}W_2^{(i)}(\omega_1,\omega_2)\left\langle \bar{F}_i(\omega_1)\bar{F}_i(\omega_2)\bar{F}_i^{*}(\omega)\right\rangle e^{-j\tau(\omega_1+\omega_2-\omega)}d\omega_1 d\omega_2 \\
& \quad - A_i\left\langle F_i^{*}(\omega)\right\rangle e^{-j\omega_1\tau}\int_{-\infty}^{\infty} {}^{y}W_2^{(i)}(\omega_2,-\omega_2)d\omega_2 \Bigg] \\
& + \Bigg[\int_{-\infty}^{\infty}\int_{-\infty}^{\infty}\int_{-\infty}^{\infty} {}^{y}W_3^{(i)}(\omega_1,\omega_2,\omega_3)\left\langle \bar{F}_i(\omega_1)\bar{F}_i(\omega_2)\bar{F}_i(\omega_3)\bar{F}_i^{*}(\omega)\right\rangle \\
& \qquad \times e^{-j\tau(\omega_1+\omega_2+\omega_3-\omega)}\,d\omega_1 d\omega_2 d\omega_3 \\
& \quad -3A_i\int_{-\infty}^{\infty}\int_{-\infty}^{\infty} {}^{y}W_3^{(i)}(\omega_1,\omega_2,-\omega_2)\left\langle \bar{F}_i(\omega_1)\bar{F}_i^{*}(\omega)\right\rangle e^{-j\tau(\omega_1-\omega)}d\omega_1 d\omega_2 \Bigg] \\
& + \ldots\ldots\ldots\ldots
\end{aligned}
\tag{4.52}
$$

Since $\bar{f}_i(\tau)$ is stationary Gaussian white noise with zero mean and variance A_i, the Fourier transform, $\bar{F}_i(\omega)$, is also a stationary Gaussian white noise process and employing equations (3.30) from the previous chapter for ensemble averages of the products transformed functions, equations (4.51) and (4.52) can be reduced, after some algebra to

$$\left\langle {}^{x}\eta(\tau)z^{(i)}(\tau)\right\rangle = A_i\, {}^{x}W_1^{(i)}(\omega) \tag{4.53}$$

$$\left\langle {}^{y}\eta(\tau)z^{(i)}(\tau)\right\rangle = A_i\, {}^{y}W_1^{(i)}(\omega) \tag{4.54}$$

However, due to the equivalence of time and ensemble averages, the ensemble average $\left\langle {}^{x}\eta(\tau)z^{(i)}(\tau)\right\rangle$ can also be written as,

$$\left\langle {}^{x}\eta(\tau)z^{(i)}(\tau)\right\rangle = \lim_{T\to\infty}\frac{1}{T}\int_{-T/2}^{T/2} {}^{x}\eta(\tau)z^{(i)}(\tau)d\tau$$

$$= \bar{F}_i^{*}(\omega)\ {}^{x}\eta(\omega) \tag{4.55}$$

Equations (4.53) and (4.55) give

$$A_i\, {}^{x}W_1^{(i)}(\omega) = \bar{F}_i^{*}(\omega)\ {}^{x}\eta(\omega) \tag{4.56}$$

from which the expression for the first order Wiener kernel transform is obtained as

$${}^{x}W_1^{(i)}(\omega) = \bar{F}_i^{*}(\omega)\ {}^{x}\eta(\omega)\Big/A_i \tag{4.57}$$

Similarly,

$${}^{y}W_1^{(i)}(\omega) = \bar{F}_i^{*}(\omega)\ {}^{y}\eta(\omega)/A_i \tag{4.58}$$

Since i takes values 1 and 2 the direct kernels ${}^{x}W_1^{(1)}(\omega)$, ${}^{y}W_1^{(2)}(\omega)$ and the cross kernels ${}^{x}W_1^{(2)}(\omega)$, ${}^{y}W_1^{(1)}(\omega)$ can be extracted from the measured responses ${}^{x}\eta(\omega)$, ${}^{y}\eta(\omega)$ and the applied force ($\bar{F}_1(\omega)$ and its variance A_1 or $\bar{F}_2(\omega)$ and its variance A_2) , through equations (4.57) and (4.58).

For measurement of the third order kernel transform, a circuit involving three exponential delay filters, as shown in Fig. 4.3, is considered. The output, $z^{(i)}(\tau)$, from the exponential filters is

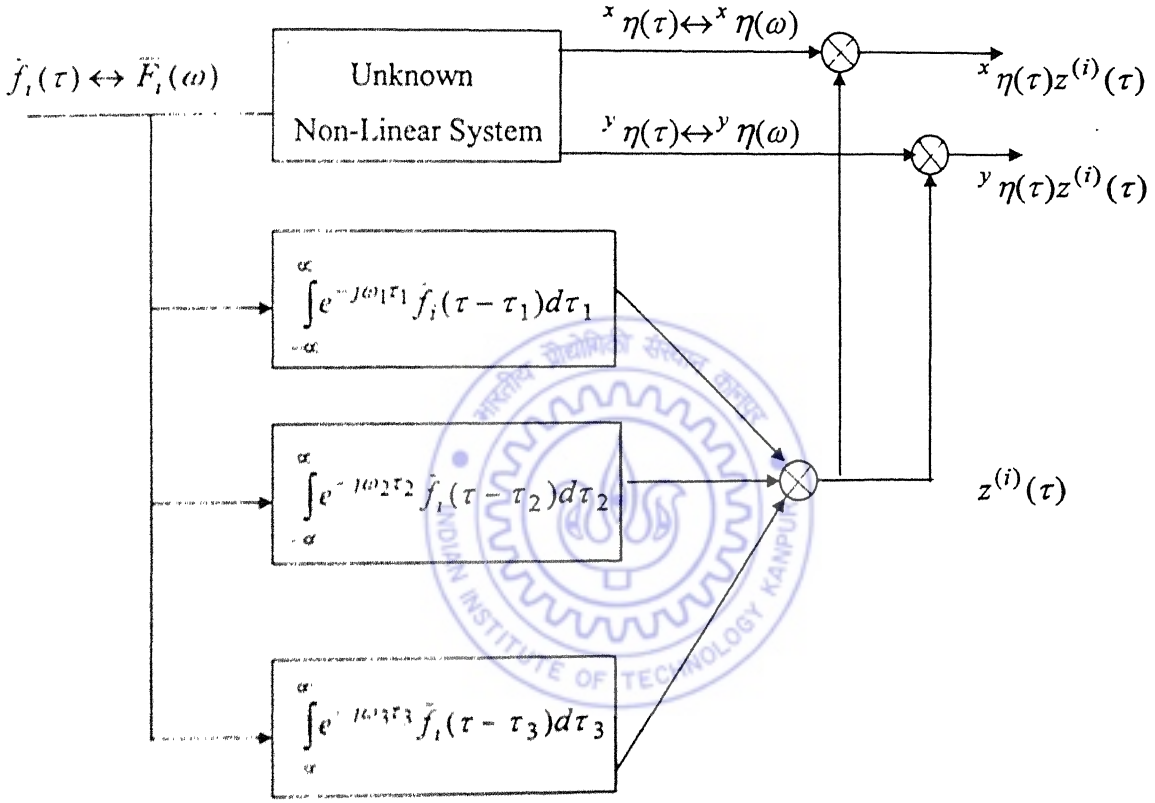

Fig. 4.3 Scheme for evaluating the third order direct and cross Wiener kernel transforms, $W_3^{(i)}(\omega,\omega,\omega)$.

$$z^{(i)}(\tau) = \int_{-\infty}^{\infty} e^{-j\omega_1\tau_1} \bar{f}_i(\tau-\tau_1)d\tau_1 \int_{-\infty}^{\infty} e^{-j\omega_2\tau_2} \bar{f}_i(\tau-\tau_2)d\tau_2 \int_{-\infty}^{\infty} e^{-j\omega_3\tau_3} \bar{f}_i(\tau-\tau_3)d\tau_3$$
$$= \bar{F}_i(-\omega_1)\bar{F}_i(-\omega_2)\bar{F}_i(-\omega_3)e^{-j(\omega_1+\omega_2+\omega_3)\tau} \tag{4.59}$$

and the ensemble averages of the outputs of the circuit are

$$\left\langle {}^{x}\eta(\tau)z^{(i)}(\tau)\right\rangle = \Big[A_i^2 [\, {}^{x}W_1^{(i)}(\omega_1)\delta(-\omega_2-\omega_3)e^{j(-\omega_2-\omega_3)\tau}$$
$$+ {}^{x}W_1^{(i)}(\omega_2)\delta(-\omega_1-\omega_3)e^{j(-\omega_1-\omega_3)\tau}$$
$$+ {}^{x}W_1^{(i)}(\omega_3)\delta(-\omega_1-\omega_2)e^{j(-\omega_1-\omega_2)\tau}\,]\Big] \tag{4.60}$$
$$+\Big[6A_i^3 W_3^{(i)}(\omega_1,\omega_2,\omega_3)\Big]$$

However, the equivalence of time and ensemble averages gives

$$\left\langle {}^{x}\eta(\tau)z^{(i)}(\tau)\right\rangle = \lim_{T\to\infty}\frac{1}{T}\int_{-T/2}^{T/2} {}^{x}\eta(\tau)z^{(i)}(\tau)d\tau_i$$
$$= \bar{F}_i(-\omega_1)\bar{F}_i(-\omega_2)\bar{F}_i(-\omega_3)\ {}^{x}\eta(\omega_1+\omega_2+\omega_3) \tag{4.61}$$

Equations (4.60) and (4.61) give the expression for the measurement of the third order Wiener kernel transform as

$${}^{x}W_3^{(i)}(\omega_1,\omega_2,\omega_3) = \frac{1}{6A_i^3}\Big[\bar{F}_i^{*}(\omega_1)\bar{F}_i^{*}(\omega_2)\bar{F}_i^{*}(\omega_3)\ {}^{x}\eta(\omega_1+\omega_2+\omega_3)\Big]$$
$$-\frac{1}{6A_i}\Big[{}^{x}W_1^{(i)}(\omega_1)\delta(\omega_1+\omega_3)+{}^{x}W_1^{(i)}(\omega_2)\delta(\omega_1+\omega_3)+{}^{x}W_1^{(i)}(\omega_3)\delta(\omega_1+\omega_2)\Big] \tag{4.62}$$

similarly we can have,

$${}^{y}W_3^{(i)}(\omega_1,\omega_2,\omega_3) = \frac{1}{6A_i^3}\Big[\bar{F}_i^{*}(\omega_1)\bar{F}_i^{*}(\omega_2)\bar{F}_i^{*}(\omega_3)\ {}^{y}\eta(\omega_1+\omega_2+\omega_3)\Big]$$
$$-\frac{1}{6A_i}\Big[{}^{y}W_1^{(i)}(\omega_1)\delta(\omega_1+\omega_3)+{}^{y}W_1^{(i)}(\omega_2)\delta(\omega_1+\omega_3)+{}^{y}W_1^{(i)}(\omega_3)\delta(\omega_1+\omega_2)\Big] \tag{4.63}$$

The third order kernel transforms, ${}^{x}W_3^{(i)}(\omega_1,\omega_2,\omega_3)$, ${}^{y}W_3^{(i)}(\omega_1,\omega_2,\omega_3)$ form multi-dimensional surfaces on the $(\omega_1,\omega_2,\omega_3)$ axes. Measurements are made for special trispectral kernels with $\omega_1=\omega_2=\omega_3=\omega$. As stated in the earlier chapter, these kernels are functions of only one variable ω and are much easier to compute and interpret. For such trispectral kernel transforms the expressions (4.62) and (4.63), for their measurement, reduce to

$$
\begin{aligned}
{}^{x}W_3^{(i)}(\omega,\omega,\omega) &= \frac{1}{6A_i^3}\left[\left\{\bar{F}_i^{*}(\omega)\right\}^3 {}^{x}\eta(3\omega)\right] - \frac{1}{6A_i}\left[{}^{x}W_1^{(i)}(\omega)\delta(\omega)+{}^{x}W_1^{(i)}(\omega)\delta(\omega)+{}^{x}W_1^{(i)}(\omega)\delta(\omega)\right] \\
{}^{y}W_3^{(i)}(\omega,\omega,\omega) &= \frac{1}{6A_i^3}\left[\left\{\bar{F}_i^{*}(\omega)\right\}^3 {}^{y}\eta(3\omega)\right] - \frac{1}{6A_i}\left[{}^{y}W_1^{(i)}(\omega)\delta(\omega)+{}^{y}W_1^{(i)}(\omega)\delta(\omega)+{}^{y}W_1^{(i)}(\omega)\delta(\omega)\right]
\end{aligned}
\qquad (4.64)
$$

4.4 Parameter Estimation

The third order Special Trispectral direct Wiener kernel transforms ${}^{x}W_3^{(1)}(\omega,\omega,\omega)$, ${}^{y}W_3^{(2)}(\omega,\omega,\omega)$ and the cross-kernel transforms ${}^{x}W_3^{(2)}(\omega,\omega,\omega)$, ${}^{y}W_3^{(1)}(\omega,\omega,\omega)$ are extracted from the measurements of the responses ${}^{x}\eta(3\omega)$, ${}^{y}\eta(3\omega)$ and the applied force ($\bar{F}_1(\omega)$ and its variance A_1 or $\bar{F}_2(\omega)$ and its variance A_2). Subsequently, for a third order representation of the system response, noting the equivalence between the Volterra and Wiener kernels (equations 4.45), the third order Special Trispectral Volterra kernel transforms can be computed as –

direct-kernels:

$$
\begin{aligned}
{}^{x}H_3^{(1)}(\omega,\omega,\omega) &= {}^{x}W_3^{(1)}(\omega,\omega,\omega) \\
&= \frac{1}{6A_1^3}\left[\left\{\bar{F}_1^{*}(\omega)\right\}^3 {}^{x}\eta(3\omega)\right] - \frac{1}{6A_1}\left[{}^{x}W_1^{(1)}(\omega)\delta(\omega)+{}^{x}W_1^{(1)}(\omega)\delta(\omega)+{}^{x}W_1^{(1)}(\omega)\delta(\omega)\right] \\
{}^{y}H_3^{(2)}(\omega,\omega,\omega) &= {}^{y}W_3^{(2)}(\omega,\omega,\omega) \\
&= \frac{1}{6A_2^3}\left[\left\{\bar{F}_2^{*}(\omega)\right\}^3 {}^{y}\eta(3\omega)\right] - \frac{1}{6A_2}\left[{}^{y}W_1^{(2)}(\omega)\delta(\omega)+{}^{y}W_1^{(2)}(\omega)\delta(\omega)+{}^{y}W_1^{(2)}(\omega)\delta(\omega)\right]
\end{aligned}
$$

cross-kernels:

$$
\begin{aligned}
{}^{x}H_3^{(2)}(\omega,\omega,\omega) &= {}^{x}W_3^{(2)}(\omega,\omega,\omega) \\
&= \frac{1}{6A_2^3}\left[\left\{F_2^{*}(\omega)\right\}^3 {}^{x}\eta(3\omega)\right] - \frac{1}{6A_2}\left[{}^{x}W_1^{(2)}(\omega)\delta(\omega) + {}^{x}W_1^{(2)}(\omega)\delta(\omega) + {}^{x}W_1^{(2)}(\omega)\delta(\omega)\right] \\
{}^{y}H_3^{(1)}(\omega,\omega,\omega) &= {}^{y}W_3^{(1)}(\omega,\omega,\omega) \\
&= \frac{1}{6A_1^3}\left[\left\{F_1^{*}(\omega)\right\}^3 {}^{y}\eta(3\omega)\right] - \frac{1}{6A_1}\left[{}^{y}W_1^{(1)}(\omega)\delta(\omega) + {}^{y}W_1^{(1)}(\omega)\delta(\omega) + {}^{y}W_1^{(1)}(\omega)\delta(\omega)\right]
\end{aligned}
\tag{4.65}
$$

Similarly from equations (4.45), the expressions for the first order Volterra kernel transforms, in terms of the extracted Wiener kernel transforms become

direct-kernels:

$$
{}^{x}H_1^{(1)}(\omega) = {}^{x}W_1^{(1)}(\omega) + {}^{x}W_{1(3)}^{(1)}(\omega)
$$

$$
{}^{y}H_1^{(2)}(\omega) = {}^{y}W_1^{(2)}(\omega) + {}^{y}W_{1(3)}^{(2)}(\omega)
$$

cross-kernels:

$$
{}^{x}H_1^{(2)}(\omega) = {}^{x}W_1^{(2)}(\omega) + {}^{x}W_{1(3)}^{(2)}(\omega)
$$

$$
{}^{y}H_1^{(1)}(\omega) = {}^{y}W_1^{(1)}(\omega) + {}^{y}W_{1(3)}^{(1)}(\omega)
\tag{4.66}
$$

where ${}^{x}W_{1(3)}^{(i)}(\omega)$ and ${}^{y}W_{1(3)}^{(i)}(\omega)$, with i taking a value 1 or 2, are kernels derived from the third order kernels through the following expressions.

$$
\begin{aligned}
{}^{x}W_{1(3)}^{(i)}(\omega) &= \int_{-\infty}^{\infty} {}^{x}W_3^{(i)}(\omega,\omega_2,-\omega_2)d\omega_2 \\
{}^{y}W_{1(3)}^{(i)}(\omega) &= \int_{-\infty}^{\infty} {}^{y}W_3^{(i)}(\omega,\omega_2,-\omega_2)d\omega_2
\end{aligned}
\tag{4.67}
$$

The linear parameters can be obtained from the above estimates of the first order Volterra kernel transforms, ${}^{x}H_1^{(1)}(\omega)$, ${}^{y}H_1^{(1)}(\omega)$, ${}^{x}H_1^{(2)}(\omega)$, ${}^{y}H_1^{(2)}(\omega)$. Noting the algebraic

expressions of these kernel transforms in equations (4.23), the ratios of the estimated kernel transforms can be expressed in terms of the linear parameters as follows

$$
\begin{aligned}
{}^{x}H_1^{(1)}(\omega) / {}^{y}H_1^{(1)}(\omega) &= (-\omega^2 + 2j\xi_{yy}\omega + \lambda_{yy}^{L})/(-\lambda_{yx}^{L}) \\
{}^{y}H_1^{(2)}(\omega) / {}^{x}H_1^{(2)}(\omega) &= (-\omega^2 + 2j\xi_{xx}\omega + 1)/(-\lambda_{yx}^{L})
\end{aligned}
\tag{4.68}
$$

The parameters λ_{yy}^{L}, λ_{yx}^{L}, λ_{xy}^{L}, ξ_{yy} and ξ_{xx} are estimated through application of a curve fitting routine.

Nonlinear parameters are computed from the estimates of the Special Trispectral Volterra Kernels, ${}^{x}H_3^{(1)}(\omega,\omega,\omega)$, ${}^{x}H_3^{(2)}(\omega,\omega,\omega)$, ${}^{y}H_3^{(1)}(\omega,\omega,\omega)$, ${}^{y}H_3^{(2)}(\omega,\omega,\omega)$. Noting that these kernel transforms are estimated by application of a single white Gaussian force at a time, the expressions (4.40), for the third order Volterra kernel transforms, synthesised in Section 4.2, also get reduced, in the two individual cases, to

$f_1(\tau)$ Gaussian white, with variance A_1 and $f_2(\tau) = 0$:

$$
\begin{aligned}
{}^{x}H_3^{(1)}(\omega,\omega,\omega) &= \lambda_{xx}^{N}\,({}^{xx}\Psi_3^{1-1,1,1}) + \lambda_{xy}^{N}({}^{xy}\Psi_3^{1-1,1,1}) + \lambda_{yy}^{N}\,({}^{xy}\Psi_3^{2-1,1,1}) + \lambda_{yx}^{N}({}^{xx}\Psi_3^{2-1,1,1}) \\
{}^{y}H_3^{(1)}(\omega,\omega,\omega) &= \lambda_{xx}^{N}\,({}^{yx}\Psi_3^{1-1,1,1}) + \lambda_{xy}^{N}({}^{yy}\Psi_3^{1-1,1,1}) + \lambda_{yy}^{N}\,({}^{yy}\Psi_3^{2-1,1,1}) + \lambda_{yx}^{N}({}^{yx}\Psi_3^{2-1,1,1})
\end{aligned}
$$

$f_2(\tau)$ Gaussian white, with variance A_2 and $f_1(\tau) = 0$:

$$
\begin{aligned}
{}^{x}H_3^{(2)}(\omega,\omega,\omega) &= \lambda_{xx}^{N}\,({}^{xx}\Psi_3^{1-2,2,2}) + \lambda_{xy}^{N}({}^{xy}\Psi_3^{1-2,2,2}) + \lambda_{yy}^{N}\,({}^{xy}\Psi_3^{2-2,2,2}) + \lambda_{yx}^{N}({}^{xx}\Psi_3^{2-2,2,2}) \\
{}^{y}H_3^{(2)}(\omega,\omega,\omega) &= \lambda_{xx}^{N}\,({}^{yx}\Psi_3^{1-2,2,2}) + \lambda_{xy}^{N}({}^{yy}\Psi_3^{1-2,2,2}) + \lambda_{yy}^{N}\,({}^{yy}\Psi_3^{2-2,2,2}) + \lambda_{yx}^{N}({}^{yx}\Psi_3^{2-2,2,2})
\end{aligned}
$$

(4.69)

Substitution of the estimated third order kernel transforms on the left-hand side of the above, gives four equations,

$$\frac{1}{6A_1^3}\left[\left\{\bar{F}_1^*(\omega)\right\}^3 {}^x\eta(3\omega)\right]-\frac{1}{2A_1}\left[{}^xW_1^{(1)}(\omega)\delta(\omega)\right]=\lambda_{xx}^N({}^{xx}\Psi_3^{1-1,1,1})+\lambda_{xy}^N({}^{xy}\Psi_3^{1-1,1,1})$$

$$+\lambda_{yy}^N({}^{xy}\Psi_3^{2-1,1,1})+\lambda_{yx}^N({}^{xx}\Psi_3^{2-1,1,1})$$

$$\frac{1}{6A_2^3}\left[\left\{\bar{F}_2^*(\omega)\right\}^3 {}^x\eta(3\omega)\right]-\frac{1}{2A_2}\left[{}^yW_1^{(2)}(\omega)\delta(\omega)\right]=\lambda_{xx}^N({}^{yx}\Psi_3^{1-2,2,2})+\lambda_{xy}^N({}^{yy}\Psi_3^{1-2,2,2})$$

$$+\lambda_{yy}^N({}^{yy}\Psi_3^{2-2,2,2})+\lambda_{yx}^N({}^{yx}\Psi_3^{2-2,2,2})$$

$$\frac{1}{6A_2^3}\left[\left\{\bar{F}_2^*(\omega)\right\}^3 {}^x\eta(3\omega)\right]-\frac{1}{2A_2}\left[{}^xW_1^{(2)}(\omega)\delta(\omega)\right]=\lambda_{xx}^N({}^{xx}\Psi_3^{1-2,2,2})+\lambda_{xy}^N({}^{xy}\Psi_3^{1-2,2,2})$$

$$+\lambda_{yy}^N({}^{xy}\Psi_3^{2-2,2,2})+\lambda_{yx}^N({}^{xx}\Psi_3^{2-2,2,2})$$

$$\frac{1}{6A_1^3}\left[\left\{\bar{F}_1^*(\omega)\right\}^3 {}^x\eta(3\omega)\right]-\frac{1}{2A_1}\left[{}^yW_1^{(1)}(\omega)\delta(\omega)\right]=\lambda_{xx}^N({}^{yx}\Psi_3^{1-1,1,1})+\lambda_{xy}^N({}^{yy}\Psi_3^{1-1,1,1})$$

$$+\lambda_{yy}^N({}^{yy}\Psi_3^{2-1,1,1}+\lambda_{yx}^N({}^{yx}\Psi_3^{2-1,1,1})$$

(4.70)

which can be solved simultaneously for the four unknowns, namely the nonlinear parameters, λ_{xx}^N, λ_{xy}^N, λ_{yy}^N, λ_{yx}^N.

4.5 Computer Simulation

The procedure is illustrated through numerical simulation of the response for the nondimensional coupled equations (4.3). The forcing functions in the equations are normalised, zero mean random forces, $\bar{f}_1(\tau)$ and $\bar{f}_2(\tau)$. The excitation forces are simulated through random number generating subroutines and are normalised with respect to the maximum value of $f_1(t)$. A typical sample of such excitation is shown in Fig. 4.4(a). Fig. 4.4(b) shows the corresponding power-spectrum of the excitation force averaged over 2000 samples.

Owing to the statistical nature of the problem, the procedure is illustrated for various sets of linear and nonlinear stiffness parameters and damping factors. Various case studies have

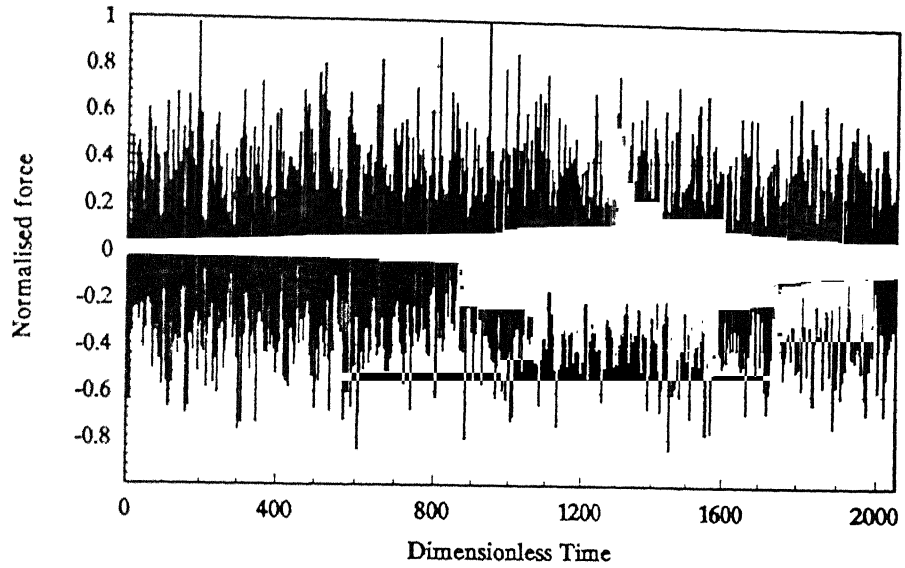

Fig. 4.4(a) Typical sample of input force.

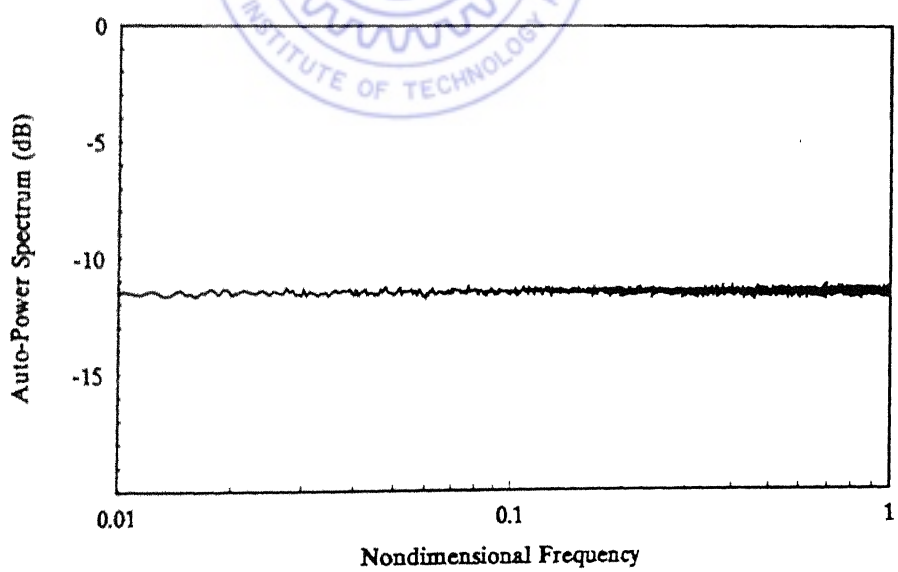

Fig. 4.4(b) Power-spectrum of the input force (averaged over 2000 samples).

been designed to study the influence of these parameters and the errors involved. The following scheme is adopted.

- Keeping the linear parameters, $\lambda^L_{xx}, \lambda^L_{yy}, \lambda^L_{xy}$ (with $\lambda^L_{yx} = \lambda^L_{xy}$), fixed, the relative values of the nonlinear parameters λ^N_{xx} and λ^N_{yy} are varied.
- Keeping the nonlinear parameters, λ^N_{xx} and λ^N_{yy}, fixed, the relative values of the linear parameters $\lambda^L_{xx}, \lambda^L_{yy}, \lambda^L_{xy}$ (with $\lambda^L_{yx} = \lambda^L_{xy}$) are varied.
- For computational ease the nonlinear parameters λ^N_{xy} and λ^N_{yx} are taken as zero.
- Damping is fixed and taken to be identical in the two directions, i.e. $\xi_{xx} = \xi_{yy} = 0.01$. (The variation in the values of damping is taken up later)

The response is computationally simulated by solving the governing equations through a standard fourth-order Runge-Kutta subroutine. These responses are fed as inputs to the parameter estimation algorithm. The estimated parameters are compared with those originally used for the simulation of response.

4.5.1 Case Study 1 (a)

In the first instance, the nonlinear parameters are taken to be numerically equal, for response simulation. The direct linear parameters are also taken to be identical. The linear cross-coupled parameters are taken as half of the direct linear terms. The numerical values are given below

$\bar{f}_1(\tau)$ = normalised Gaussian white, as shown in Fig.4.4(a); $\bar{f}_2(\tau) = 0$;

$\lambda^N_{xx} = \lambda^N_{yy} = 0.10$

$\lambda^N_{xy} = \lambda^N_{yx} = 0.0$

$\lambda^L_{xx} = \lambda^L_{yy} = 1.00$

$\lambda^L_{xy} = \lambda^L_{yx} = 0.50$

$\xi_{xx} = \xi_{yy} = 0.01$

With the above values, the simulated nondimensional responses, ${}^{x}\eta(\tau)$, and ${}^{y}\eta(\tau)$ are typically shown in Figs. 4.5 (a) and 4.5 (b). These responses have been numerically generated for 4096 number of instances in the nondimensional time (τ) range 0-2048. 2000 number of such samples of response are obtained from 2000 different samples of the simulated random force. (The influence of the number of samples in the ensemble is discussed later) Ensemble average of the power spectrum of the responses can be seen in Fig. 4.6 (a) and 4.6 (b).

These spectra are fed as inputs to the parameter estimation algorithm.

Estimates of Linear Parameters

The first order direct Volterra kernel transform, ${}^{x}H_1^{(1)}(\omega)$ and the first order cross Volterra kernel transform, ${}^{y}H_1^{(1)}(\omega)$, Figs. 4.7 (a) and 4.7 (b) respectively, are computed, using equations (4.66). These kernel transforms exhibit peak responses at frequencies equal to 0.112 and 0.195, which correspond to two critical frequencies (refer the denominators of equations (4.23)).

$$\omega_{n_{1,2}} = [1/2((\lambda^{L}_{yy} + 1) \pm ((\lambda^{L}_{yy} + 1)^2 + 4(\lambda^{L^2}_{xy} - \lambda^{L}_{yy}))^{1/2})]^{1/2} \qquad (4.71)$$

The linear parameters λ^{L}_{yy}, λ^{L}_{yx}, λ^{L}_{xy}, ξ_{yy} and ξ_{xx} are computed from these direct and cross kernel transforms, as explained in equation (4.68), through routine modal analysis procedures (Ewins, 1984). The linear parameters, thus estimated are

$\lambda^{L}_{xx} = \lambda^{L}_{yy} = 0.1598$ (cycles / τ)

$= 1.0046$ (rad / τ)

$\lambda^{L}_{xy} = \lambda^{L}_{yx} = 0.0799$ (cycles / τ)

$= 0.5025$ (rad / τ)

$\xi_{xx} = \xi_{yy} = 0.015$.

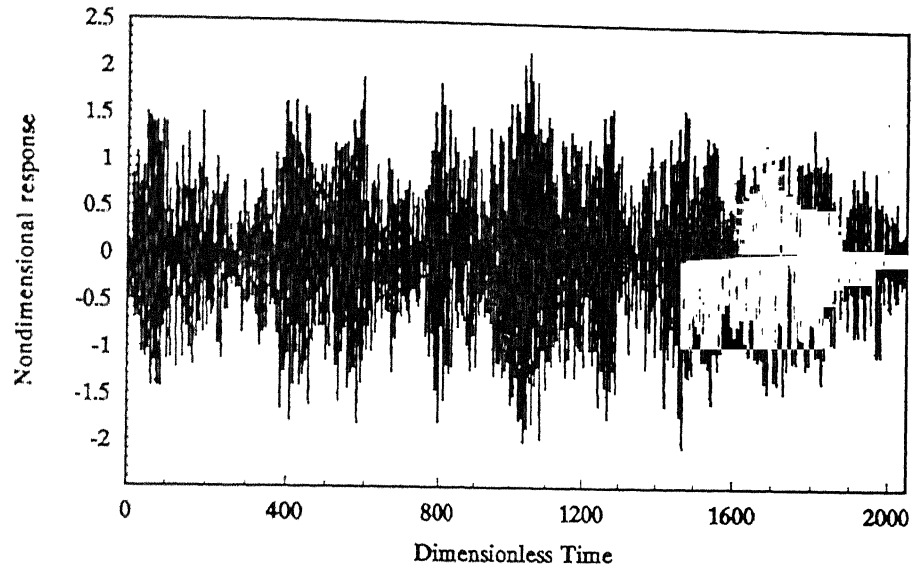

Fig. 4.5(a) Typical sample of the response in x-direction: Case 1(a).

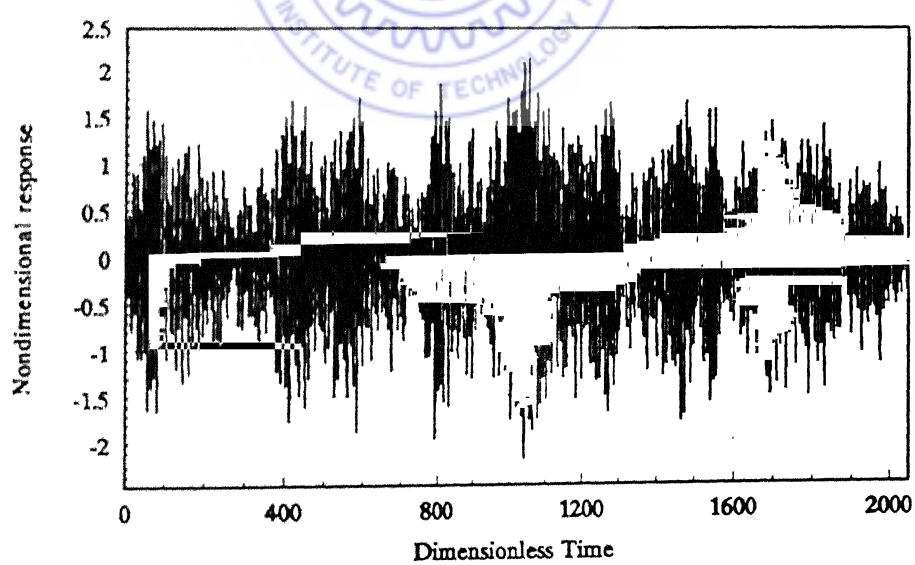

Fig. 4.5(b) Typical sample of the response in y-direction: Case 1(a).

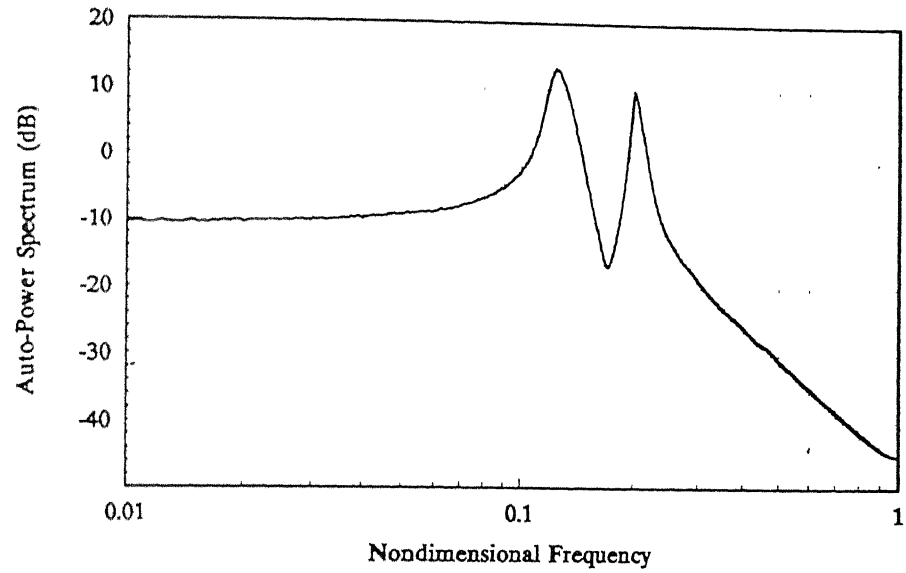

Fig. 4.6(a) Power-spectrum of response in x-direction (averaged over 2000 samples): Case 1(a).

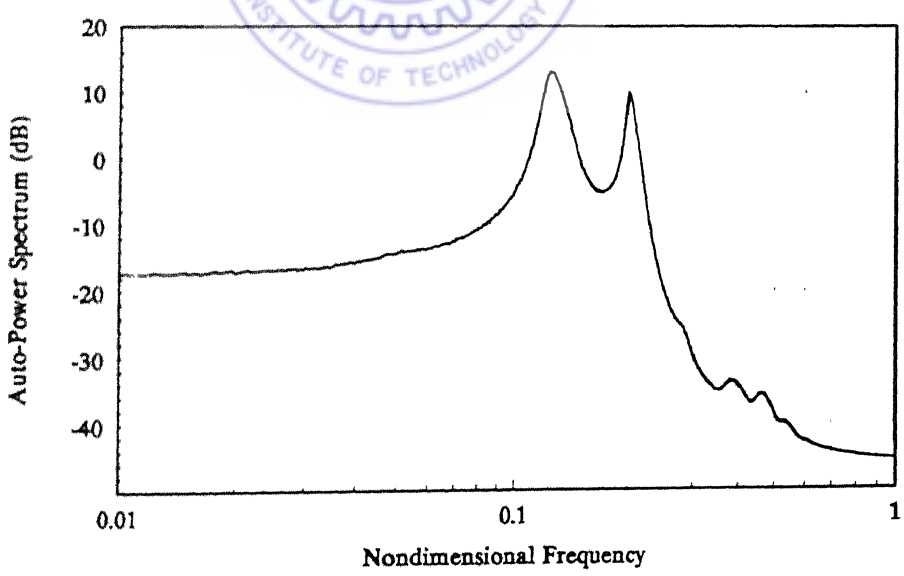

Fig. 4.6(b) Power-spectrum of response in y-direction (averaged over 2000 samples): Case 1(a).

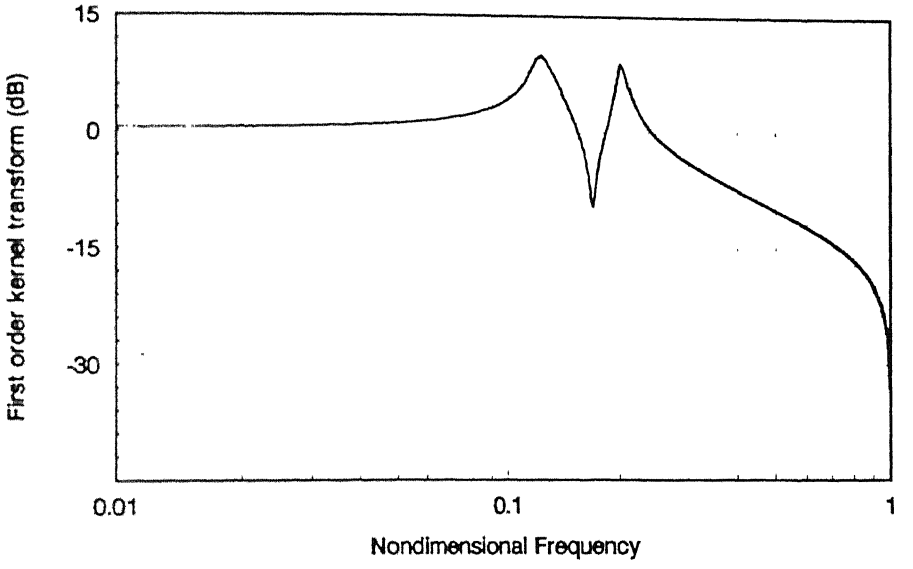

Fig. 4.7(a) Estimate of the first order direct Volterra kernel transform, ${}^{x}H_1^{(1)}(\omega)$: Case 1(a).

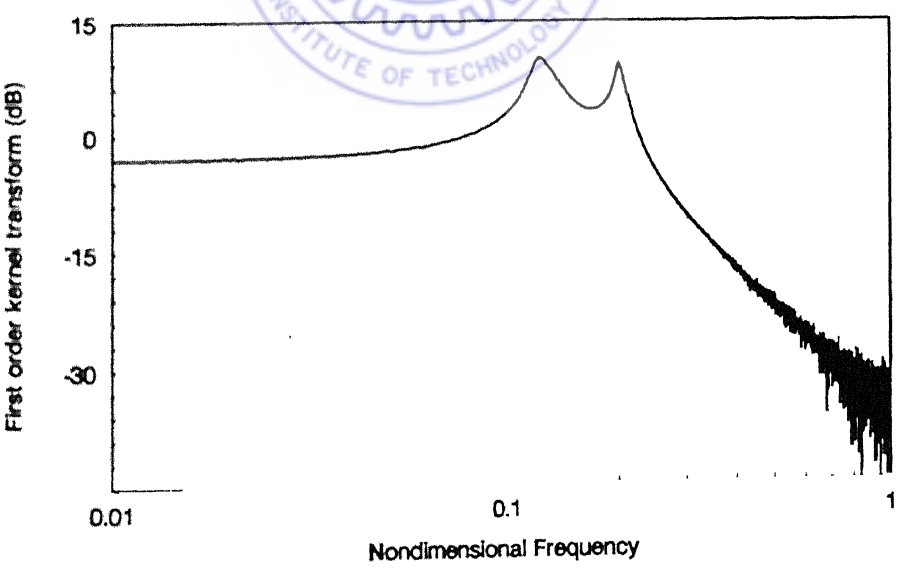

Fig. 4.7(b) Estimate of the first order cross Volterra kernel transform, ${}^{y}H_1^{(1)}(\omega)$: Case 1(a).

The exact values of the above parameters are those used as input for numerical simulation of the response. While, linear stiffness parameters can be seen to be estimated with a good degree of accuracy, the error in the damping estimates is higher. Damping has been estimated by applying the standard half-power method on the first order kernels. The curves of Figs. 4.8 (a) and 4.8 (b) show the errors incurred in the estimate of ${}^{x}H_1^{(1)}(\omega)$ and ${}^{y}H_1^{(1)}(\omega)$ due to the statistical nature of the Fast Fourier Transform computational procedure and the finite length of samples (4096 in the present case). (The exact values of these kernels are those obtained from the expressions (4.23), after direct substitution of the numerical values of the linear parameters employed for the simulation of the responses). The normalised random error, as known, can be seen to be the maximum in the vicinity of the peak responses at critical frequencies $\omega_{n_{1,2}}$. Since the numerical error is higher in the vicinity of the peaks, the error in damping estimates, obtained by application of half-power method about the peaks, will be higher than those in the stiffness estimates.

The first order kernel transforms ${}^{x}H_1^{(2)}(\omega)$ and ${}^{y}H_1^{(2)}(\omega)$, estimated by applying white Gaussian excitation in the *y*-direction, while keeping that in *x*-direction as zero, are shown in Figs. 4.9(a), (b) respectively.

Estimates of Nonlinear Parameters

As observed from Figs. 4.8 (a) and 4.8 (b), the statistical errors in the estimate of ${}^{x}H_1^{(1)}(\omega)$ and ${}^{y}H_1^{(1)}(\omega)$, the error is less than 6%, in the frequency range 0.0 - 0.10 , for the ensemble size of 2000. It can be readily inferred that the normalised error for the higher order kernels would show a similar trend and the error, in the estimate of the nonlinear parameters λ_{xx}^{N} and λ_{yy}^{N}, can be expected to be less in the frequency zone 0.0 - 0.10.

The third order kernel factors, ${}^{xx}\Psi_3^{1-1,1,1}(\omega,\omega,\omega)$, ${}^{xy}\Psi_3^{2-1,1,1}(\omega,\omega,\omega)$, ${}^{yx}\Psi_3^{1-1,1,1}(\omega,\omega,\omega)$, ${}^{yy}\Psi_3^{2-1,1,1}(\omega,\omega,\omega)$, synthesised from first order kernel transforms in accordance with equations (4.35) and (4.39) are shown in Figs. 4.10 (a)-(d).

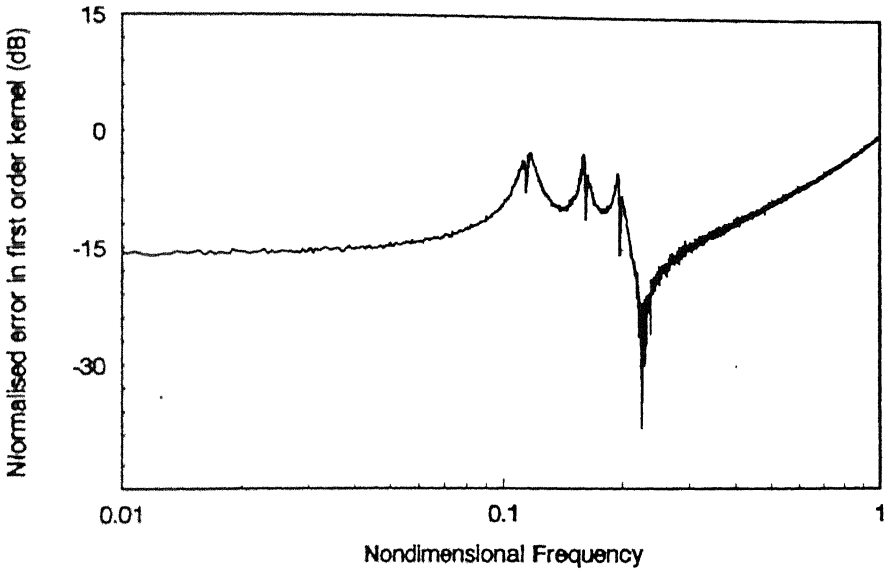

Fig. 4.8(a) Error in the estimate of first order direct kernel transform, ${}^{x}H_1^{(1)}(\omega)$.

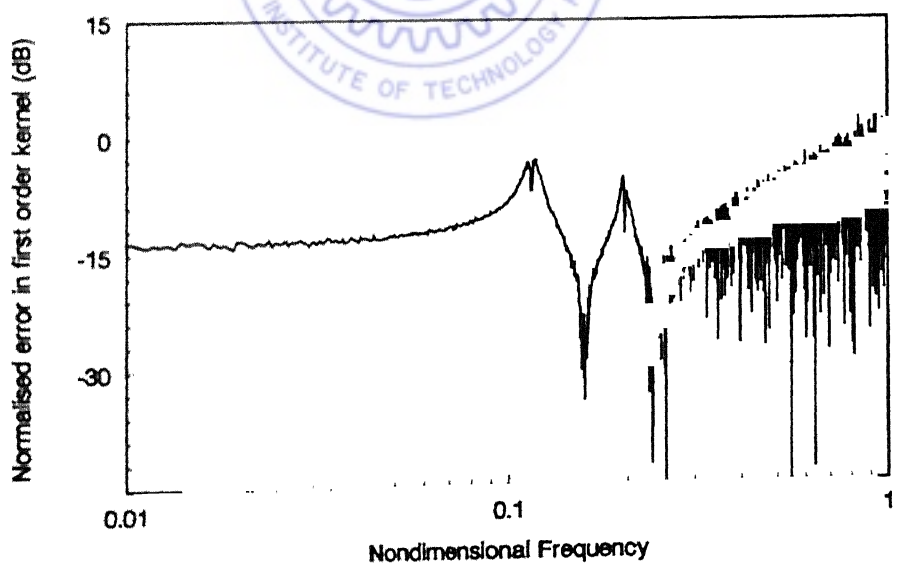

Fig. 4.8(b) Error in the estimate of first order cross-kernel transform, ${}^{y}H_1^{(1)}(\omega)$.

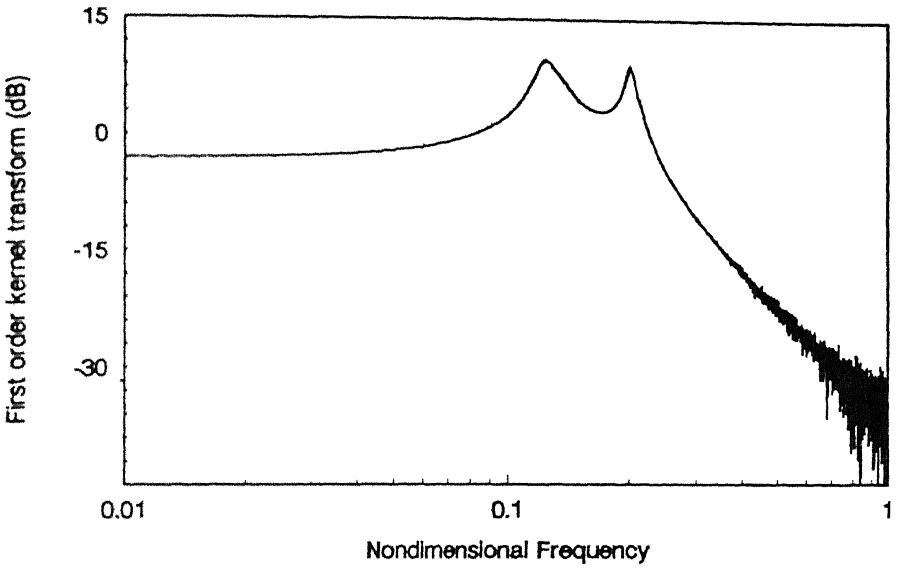

Fig. 4.9(a) Estimate of the first order cross Volterra kernel transform, ${}^{x}H_1^{(2)}(\omega)$: Case 1(a).

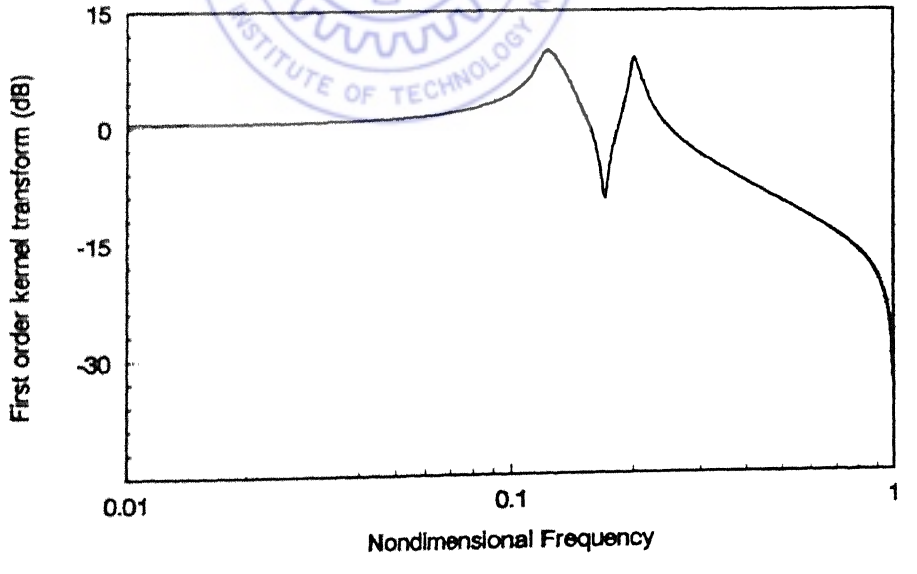

Fig. 4.9(b) Estimate of the first order direct Volterra kernel transform, ${}^{y}H_1^{(2)}(\omega)$: Case 1(a).

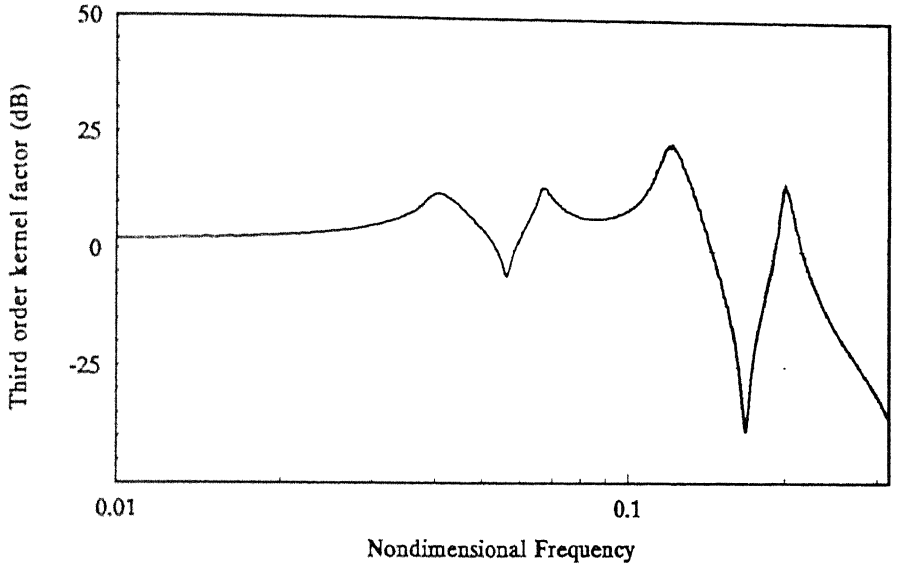

(a) Estimate of ${}^{xx}\Psi_3^{1-1,1,1}(\omega,\omega,\omega)$.

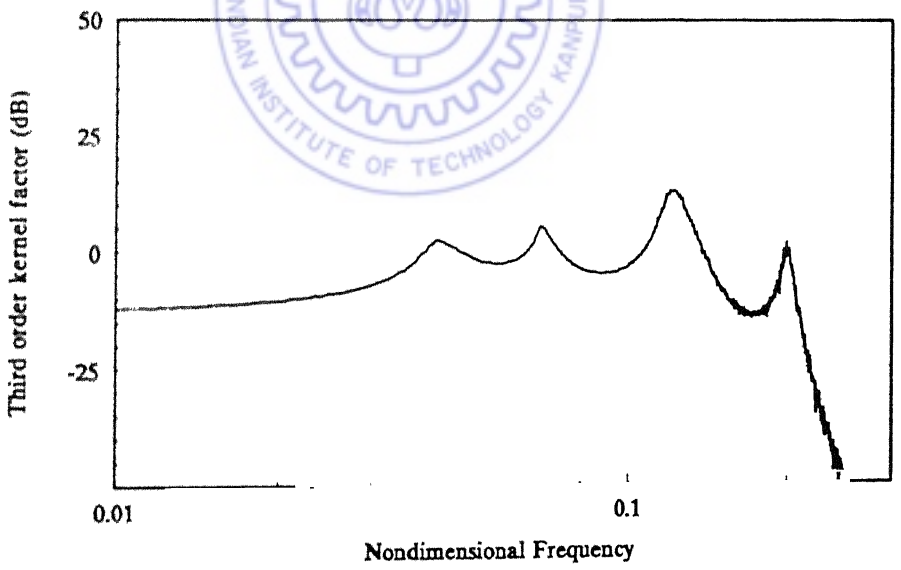

(b) Estimate of ${}^{xy}\Psi_3^{2-1,1,1}(\omega,\omega,\omega)$.

Fig. 4.10 Third order kernel factors: Case 1(a) (Contd.)

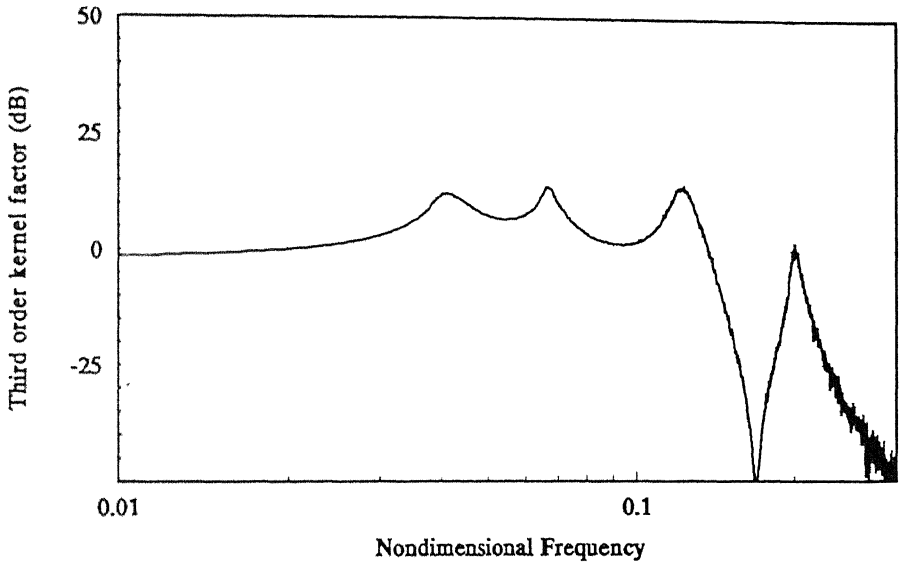

(c) Estimate of ${}^{yx}\Psi_3^{1-1,1,1}(\omega,\omega,\omega)$.

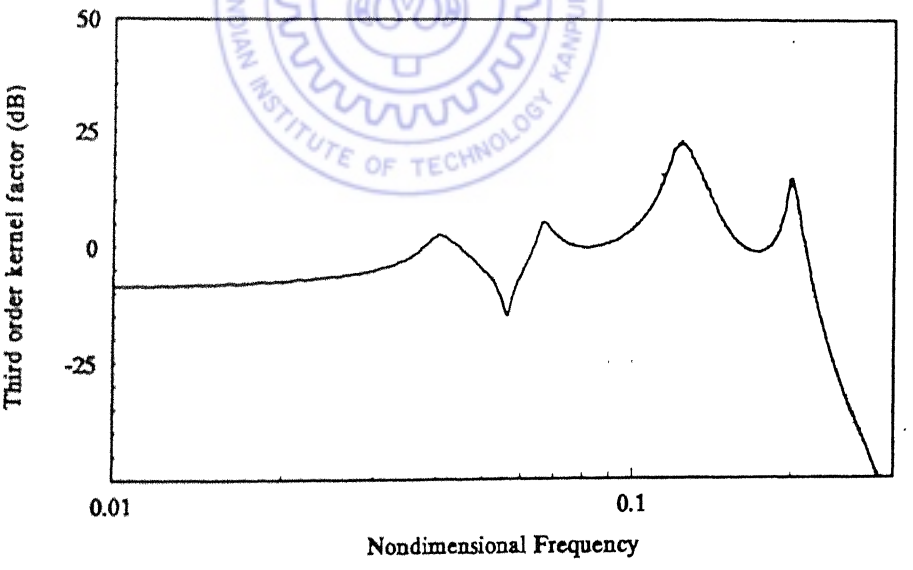

(d) Estimate of ${}^{yy}\Psi_3^{2-1,1,1}(\omega,\omega,\omega)$.

Fig. 4.10 Third order kernel factors: Case 1(a).

The system response is then processed to extract the set of third order measured kernel transforms ${}^{x}H_3^{(1)}(\omega,\omega,\omega)$, ${}^{y}H_3^{(1)}(\omega,\omega,\omega)$ (with $\bar{f}_1(\tau)\neq 0$ and $\bar{f}_2(\tau)=0$) and ${}^{x}H_3^{(2)}(\omega,\omega,\omega)$, ${}^{y}H_3^{(2)}(\omega,\omega,\omega)$ (with $\bar{f}_2(\tau)\neq 0$ and $\bar{f}_1(\tau)=0$).

However, since the nonlinear cross-coupling terms, λ_{xy}^{N}, λ_{yx}^{N} are taken to be zero, only one of the above sets, of third order kernel transforms, is sufficient for parameter estimation (refer equations 4.70). Presently, the first set ${}^{x}H_3^{(1)}(\omega,\omega,\omega)$, ${}^{y}H_3^{(1)}(\omega,\omega,\omega)$, as shown in Figs. 4.11 (a) and 4.11 (b), is extracted for use in parameter estimation. While the first order kernels are estimated in the entire available frequency range 0.0 - 1.0, the third order kernels, involving a 3ω factor, have to be restricted to one-third of this frequency zone (i.e. 0.0 - 0.33), as mentioned in the previous chapter. It can be observed, from the figures, that while the measured third order kernel transform ${}^{y}H_3^{(1)}(\omega,\omega,\omega)$ is reasonably accurate in showing the harmonic at $\omega_{n_{1,2}}/3$ (at nondimensional frequencies = 0.037 and 0.067), the identification of the harmonic at $\omega_{n_{1,2}}$ (at nondimensional frequencies = 0.112 and 0.195) is weak, due to higher statistical errors, mentioned earlier. The estimation of nonlinear parameters λ_{xx}^{N} and λ_{yy}^{N}, from these kernel transforms, is therefore restricted to the frequency zone of 0.0 - 0.10.

The estimates of the nonlinear parameter λ_{xx}^{N} and λ_{yy}^{N}, obtained in accordance with the relationship (4.70), are shown in Figs. 4.12 (a) and 4.12 (b). A fourth order polynomial curve regressed through the estimates of these nonlinear parameters , over the frequency range, is also shown in these figures. The mean values of the estimates are found to be

$\lambda_{xx}^{N} = 0.098$

$\lambda_{yy}^{N} = 0.112$

The exact values of the above nonlinear parameters are those chosen for response simulation, that is, $\lambda_{xx}^{N} = \lambda_{yy}^{N} = 0.10$. The nonlinear parameters can be seen to be estimated within the

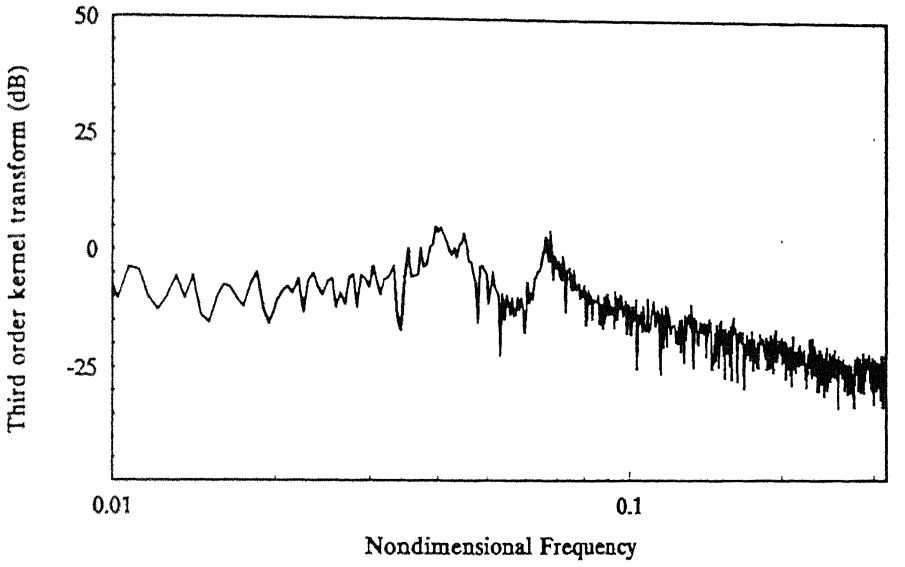

Fig. 4.11(a) Third order measured kernel transform, ${}^{x}H_3^{(1)}(\omega,\omega,\omega)$: Case 1(a) .

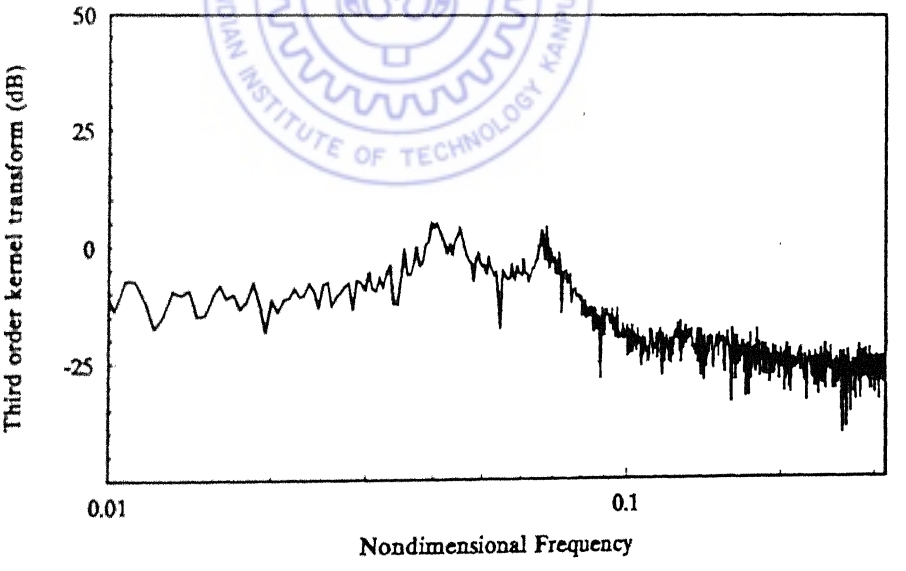

Fig. 4.11(b) Third order measured kernel transform ${}^{y}H_3^{(1)}(\omega,\omega,\omega)$: Case 1(a).

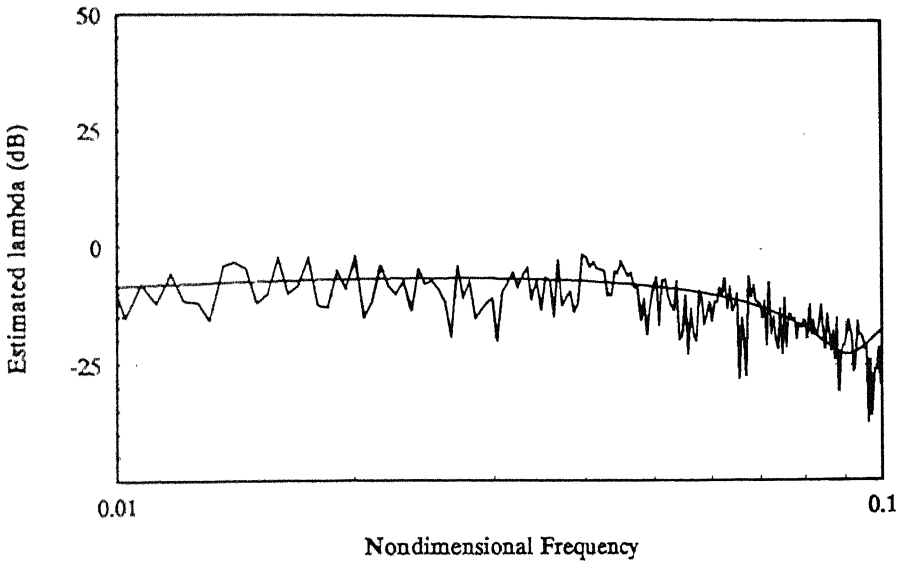

Fig. 4.12(a) Estimate of the nonlinear parameter, λ^{N}_{xx} : Case 1(a).

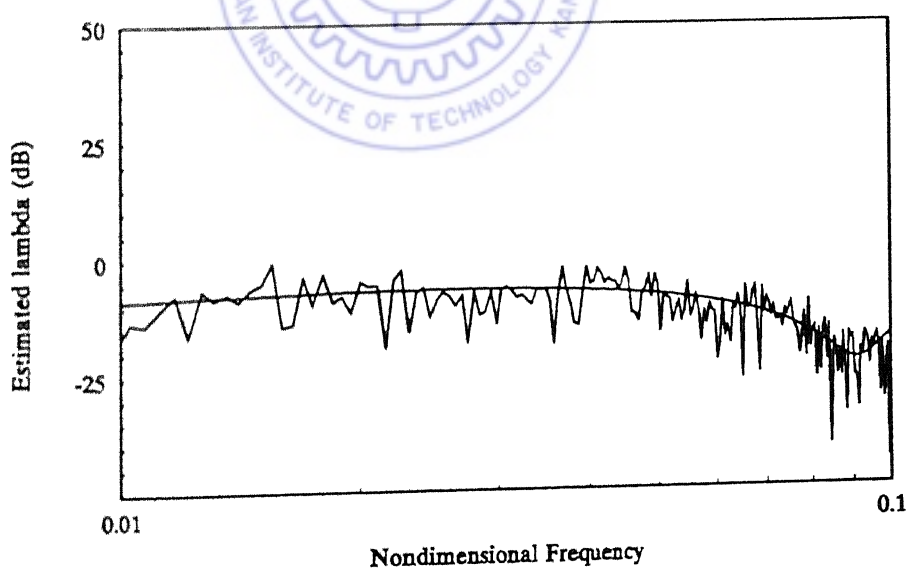

Fig. 4.12(b) Estimate of the nonlinear parameter, λ^{N}_{yy} : Case 1(a).

correct decimal orders, with the errors being 2% and 12%. The primary source of error is the restriction of response representation to third order kernels only. This has been done to keep the computations to a manageable level. Inclusion of higher order kernels (5^{th}., 7^{th} order) in the response representation can be expected to improve the accuracy of the estimates at increased computational effort. Another source of inaccuracy in the estimates is the finite length of samples and the ensemble size. The nondimensional time interval for sampling has been taken as 0.5 and 4096 samples are collected for an ensemble, for this numerical simulation which give a frequency bandwidth of $\pm$ 1.0 cycles / τ and a frequency resolution of 0.488×10^{-3} cycles / τ. Increased sample size and/or increased ensemble size can be expected to yield more accurate estimates.

4.5.2 Case Studies 1 (b) and 1 (c)

In the case study 1 (a), the values of the nonlinear parameters, λ^N_{xx}, λ^N_{yy} were kept identical (= 0.1), in response simulation. As the next cases, dissimilar values of these parameters are chosen for response simulation and their subsequent estimation from the simulated response.

Case 1 (b): $\lambda^N_{xx} = 0.1$; $\lambda^N_{yy} = 1.0$

Case 1 (c): $\lambda^N_{xx} = 0.1$; $\lambda^N_{yy} = 0.01$

The remaining parameters remain the same as in Case 1(a).

The results obtained are shown in the figures listed in Table 4.1

Table 4.1 Figures of Cases 1 (b) and 1 (c)

Parameters	Case 1 (b)	Case 1 (c)
${}^{x}H_1^{(1)}(\omega)$, ${}^{y}H_1^{(1)}(\omega)$ ${}^{x}H_1^{(2)}(\omega)$, ${}^{y}H_1^{(2)}(\omega)$	Figs. 4.13 (a)-(d)	Figs. 4.17 (a)-(d)
${}^{xx}\Psi_3^{1-1,1,1}(\omega,\omega,\omega)$, ${}^{xy}\Psi_3^{2-1,1,1}(\omega,\omega,\omega)$, ${}^{yx}\Psi_3^{1-1,1,1}(\omega,\omega,\omega)$, ${}^{yy}\Psi_3^{2-1,1,1}(\omega,\omega,\omega)$	Figs. 4.14 (a)-(d)	Figs. 4.18 (a)-(d)
${}^{x}H_3^{(1)}(\omega,\omega,\omega)$, ${}^{y}H_3^{(1)}(\omega,\omega,\omega)$	Figs. 4.15 (a), (b)	Figs. 4.19 (a), (b)
λ^N_{xx}, λ^N_{yy}	Figs. 4.16 (a), (b)	Figs. 4.20 (a), (b)

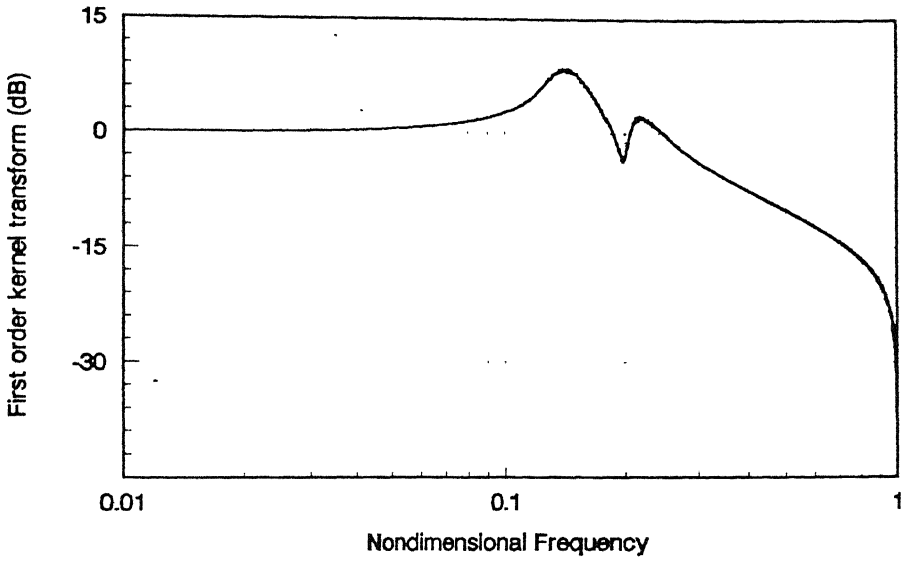

(a) First order direct kernel transform, ${}^{x}H_1^{(1)}(\omega)$.

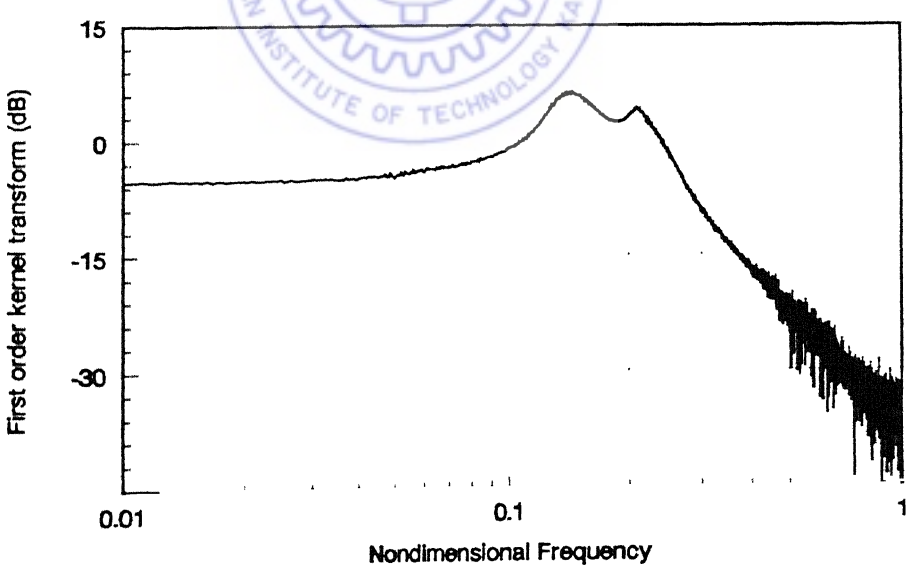

(b) First order cross-kernel transform, ${}^{x}H_1^{(2)}(\omega)$.

Fig. 4.13 Estimates of the first order direct and cross-kernel transforms: Case 1(b) (Contd.)

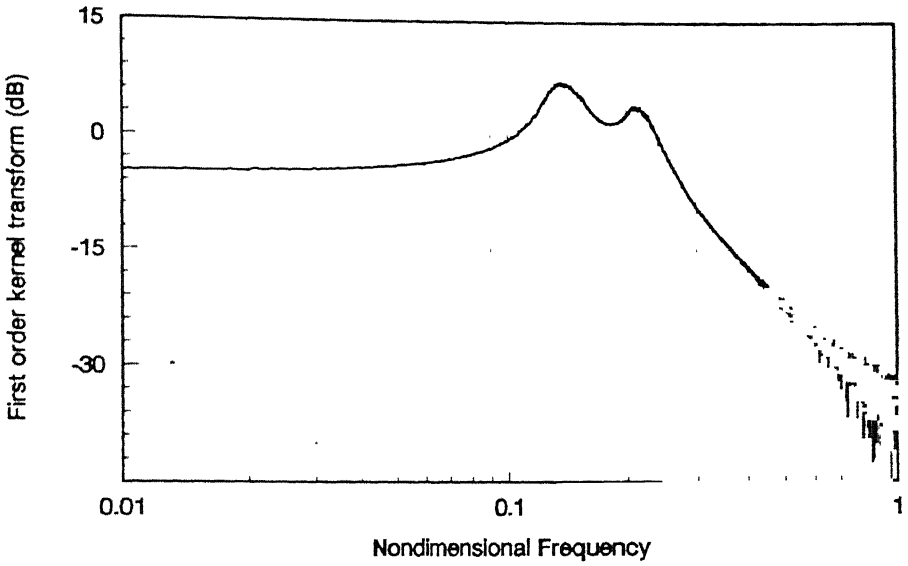

(c) First order cross-kernel transform, ${}^{y}H_1^{(1)}(\omega)$.

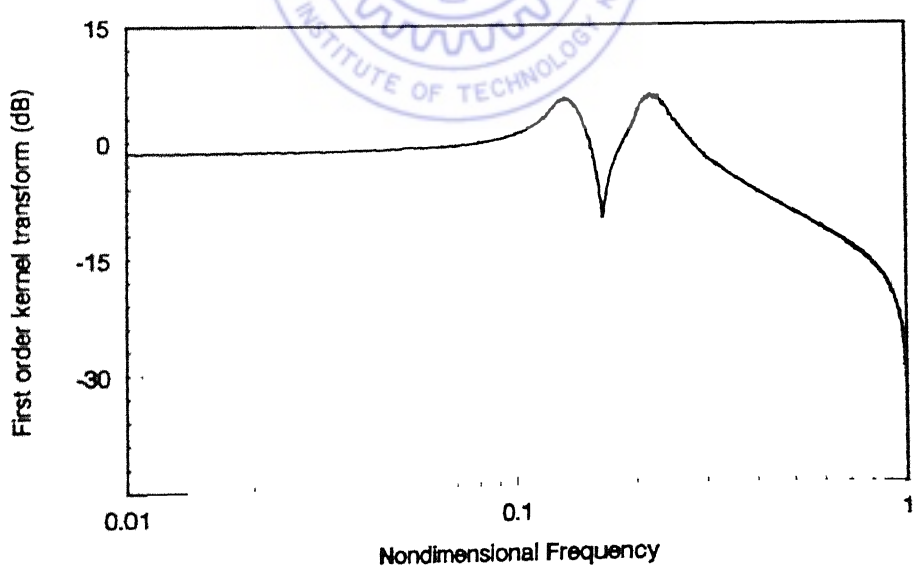

(d) First order direct kernel transform, ${}^{y}H_1^{(2)}(\omega)$.

Fig. 4.13 Estimates of the first order direct and cross-kernel transforms: Case 1(b)

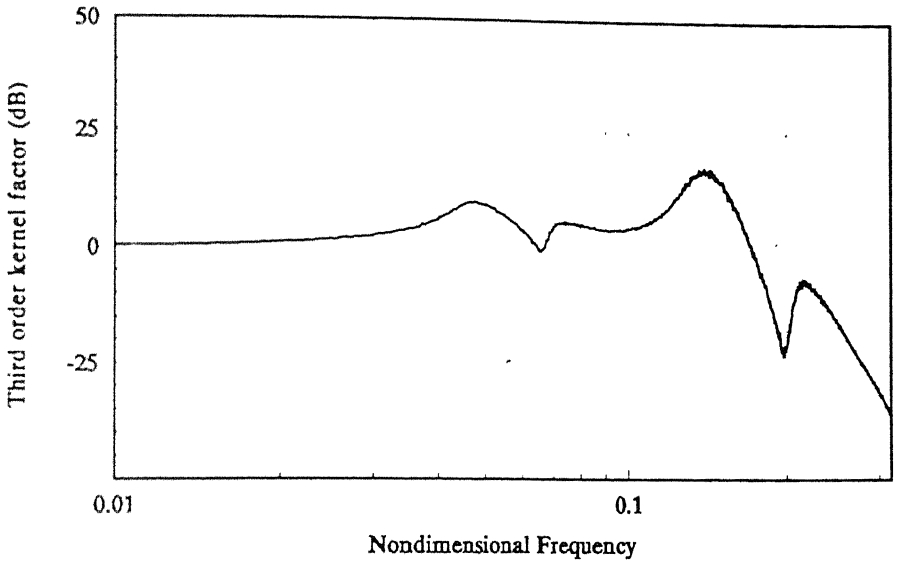

(a) Estimate of ${}^{xx}\Psi_3^{1-1,1,1}(\omega,\omega,\omega)$.

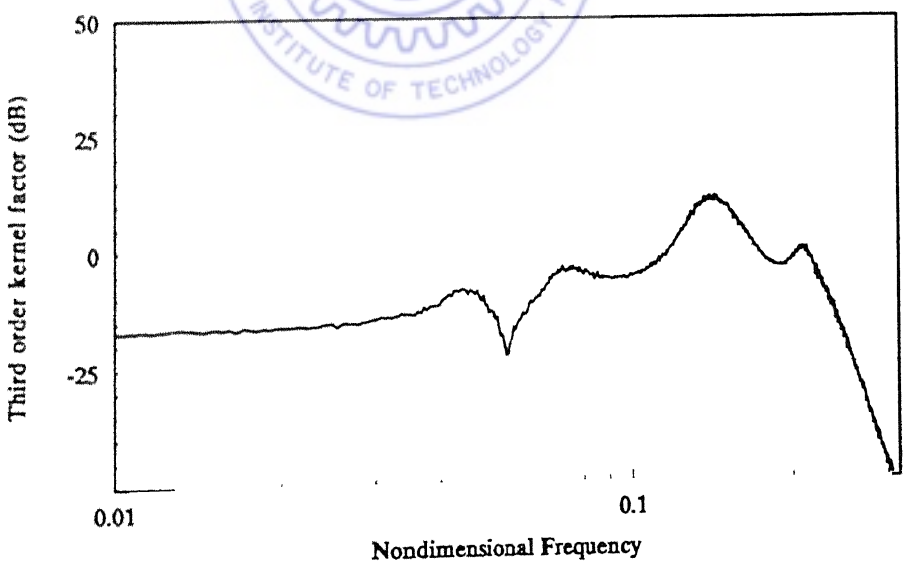

(b) Estimate of ${}^{xy}\Psi_3^{2-1,1,1}(\omega,\omega,\omega)$.

Fig. 4.14 Third order kernel factors: Case 1(b) (Contd.)

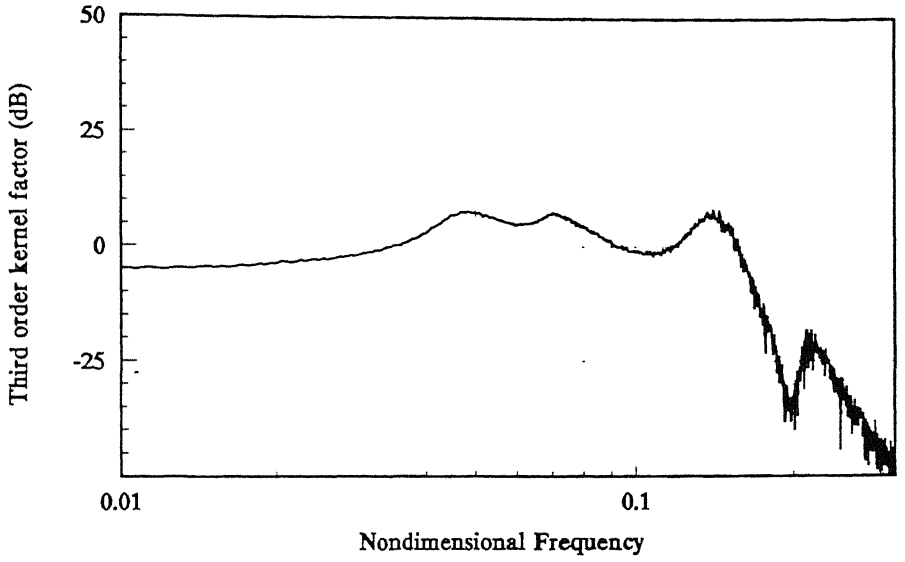

(c) Estimate of $\Psi_3^{1-1,1,1}(\omega,\omega,\omega)$.

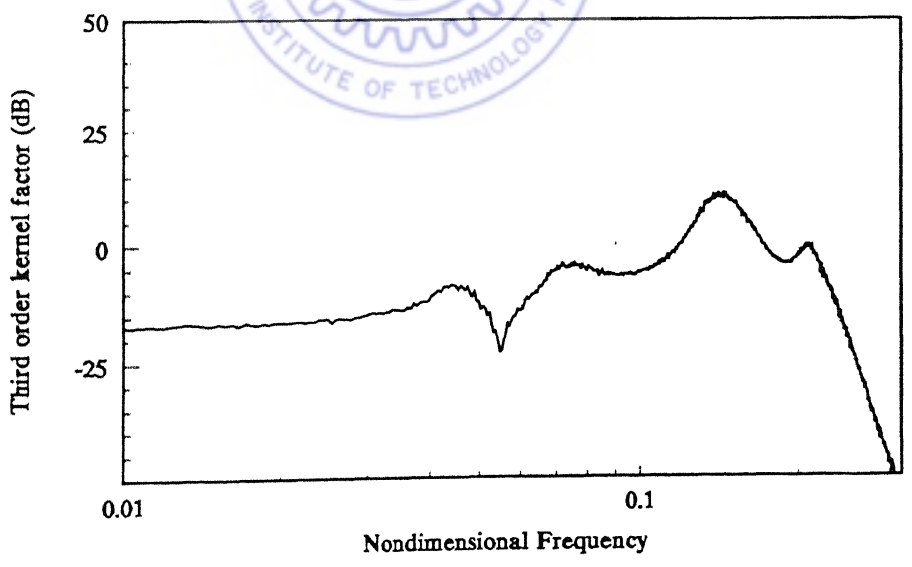

(d) Estimate of $\Psi_3^{2-1,1,1}(\omega,\omega,\omega)$.

Fig. 4.14 Third order kernel factors: Case 1(b).

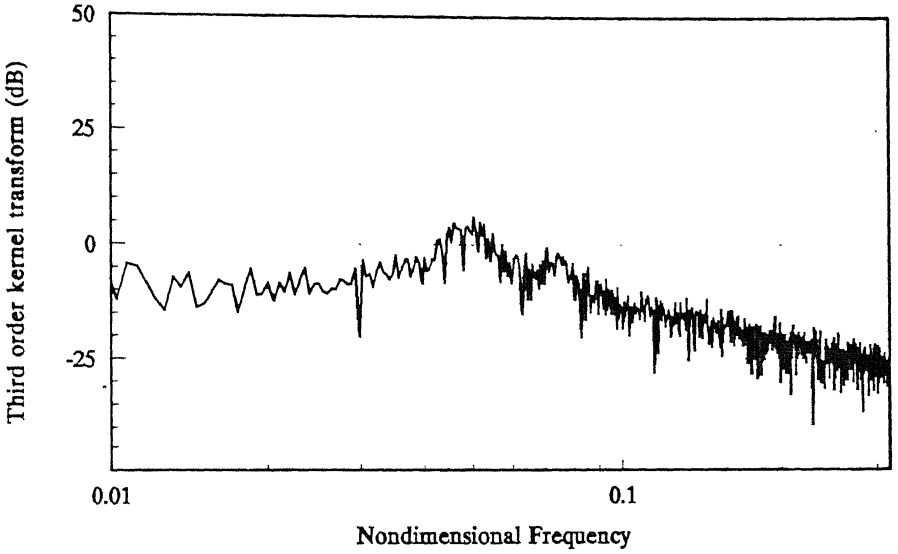

(a) Estimate of ${}^{x}H_3^{(1)}(\omega,\omega,\omega)$.

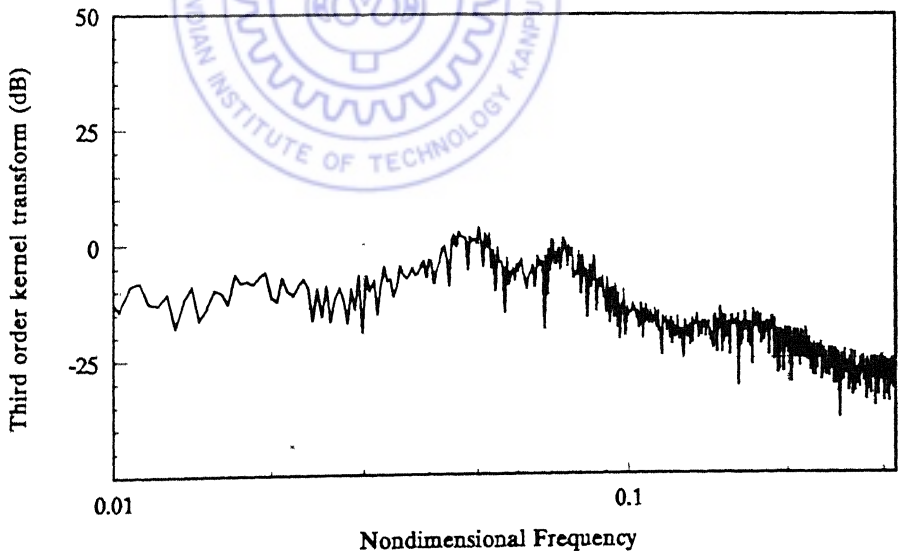

(b) Estimate of ${}^{y}H_3^{(1)}(\omega,\omega,\omega)$.

Fig. 4.15 Third order measured kernel transforms: Case 1(b).

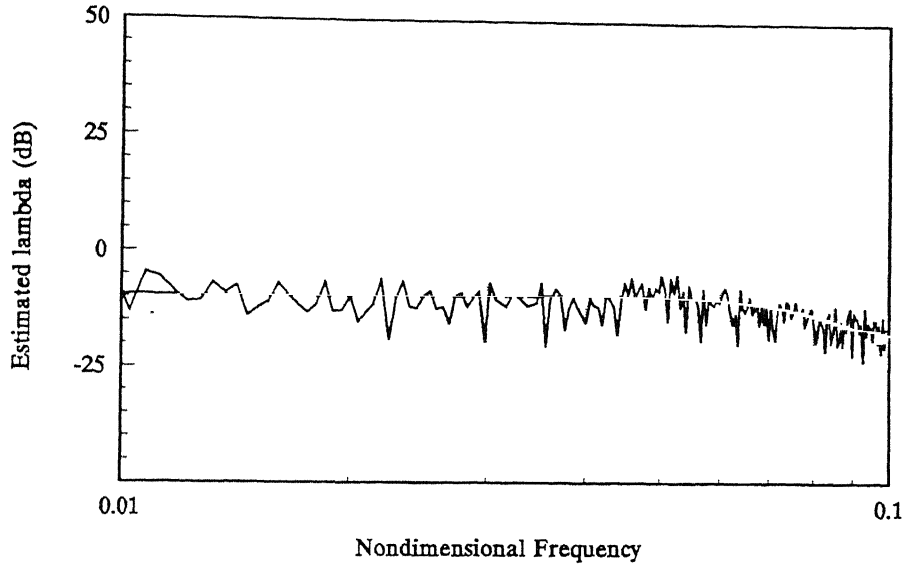

Fig. 4.16(a) Estimate of the nonlinear parameter, λ_{xx}^{N}: Case 1(b).

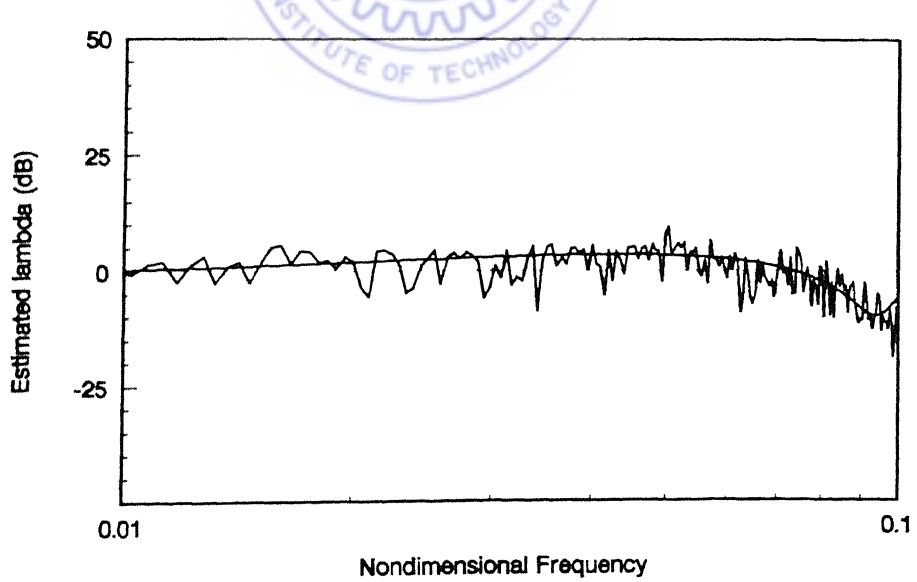

Fig. 4.16(b) Estimate of the nonlinear parameter, λ_{yy}^{N}: Case 1(b).

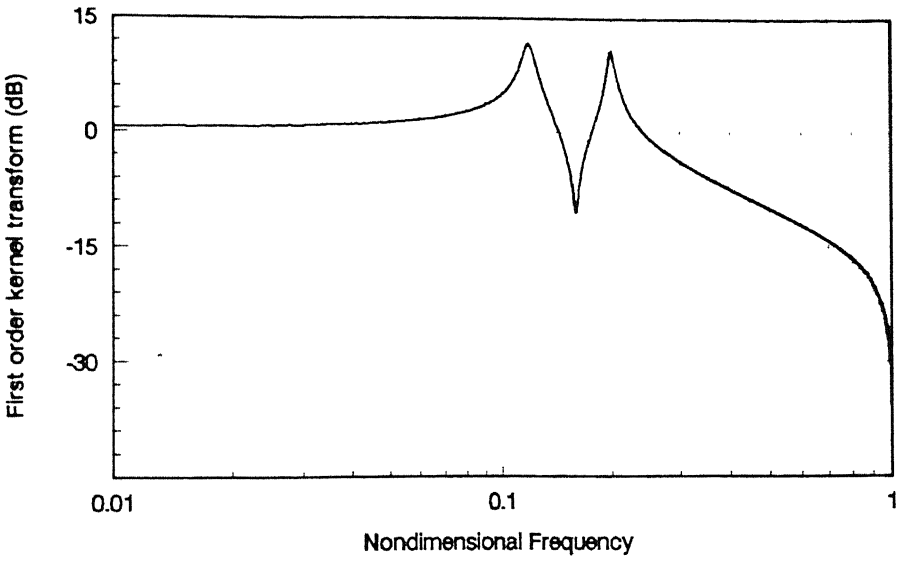

(a) First order direct kernel transform, ${}^{x}H_1^{(1)}(\omega)$.

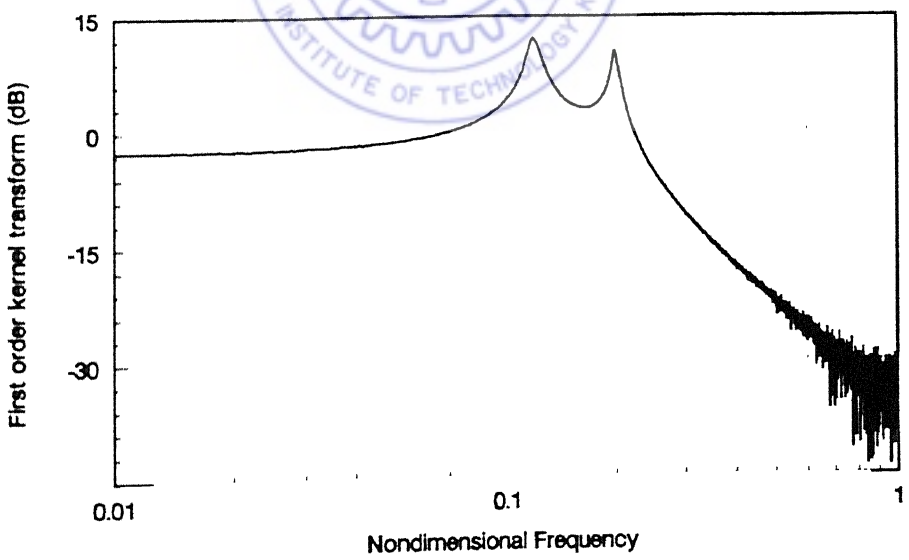

(b) First order cross-kernel transform, ${}^{x}H_1^{(2)}(\omega)$.

Fig. 4.17 Estimates of the first order direct and cross-kernel transforms: Case 1(c) (Contd.)

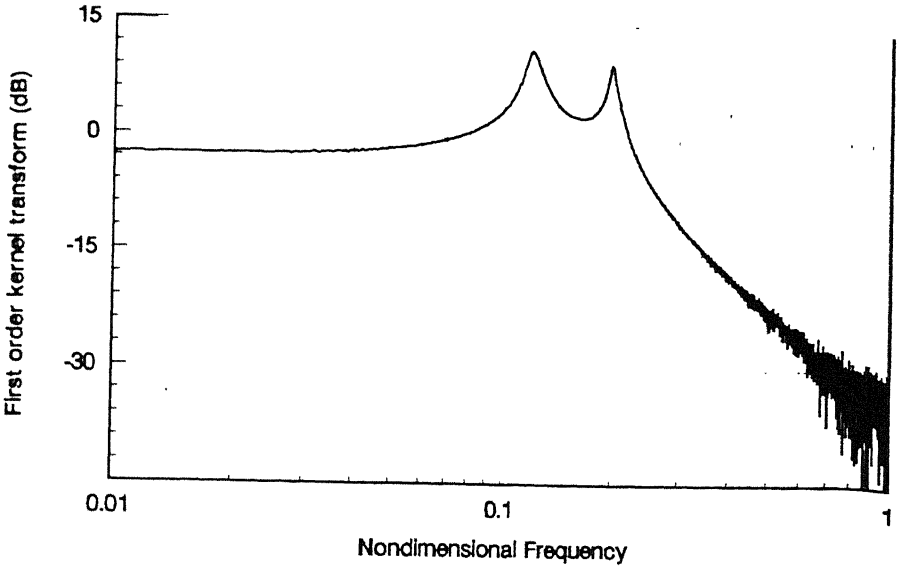

(c) First order cross-kernel transform, ${}^{y}H_1^{(1)}(\omega)$.

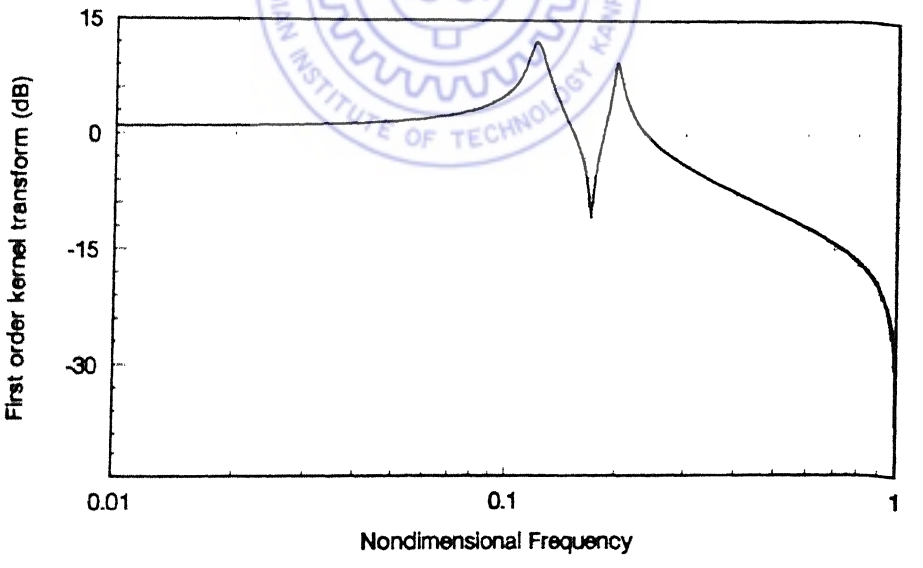

(d) First order direct kernel transform, ${}^{y}H_1^{(2)}(\omega)$.

Fig. 4.17 Estimates of the first order direct and cross-kernel transforms: Case 1(c).

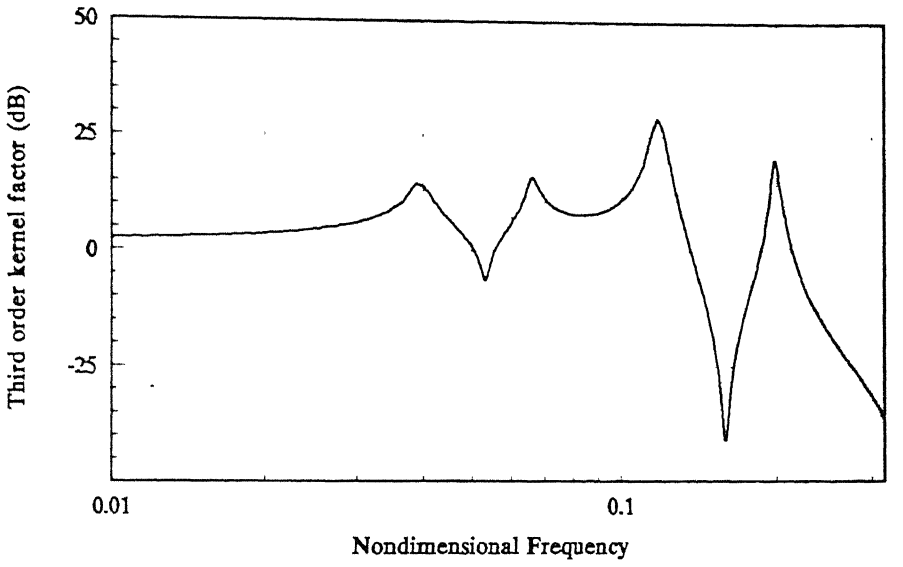

(a) Estimate of ${}^{xx}\Psi_3^{1-1,1,1}(\omega,\omega,\omega)$.

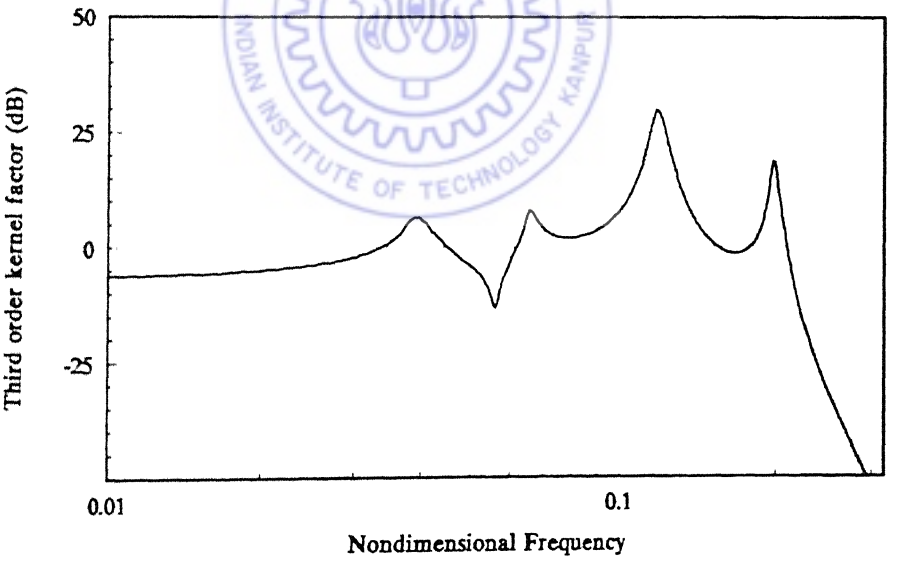

(b) Estimate of ${}^{xy}\Psi_3^{2-1,1,1}(\omega,\omega,\omega)$.

Fig. 4.18 Third order kernel factors: Case 1(c) (Contd.)

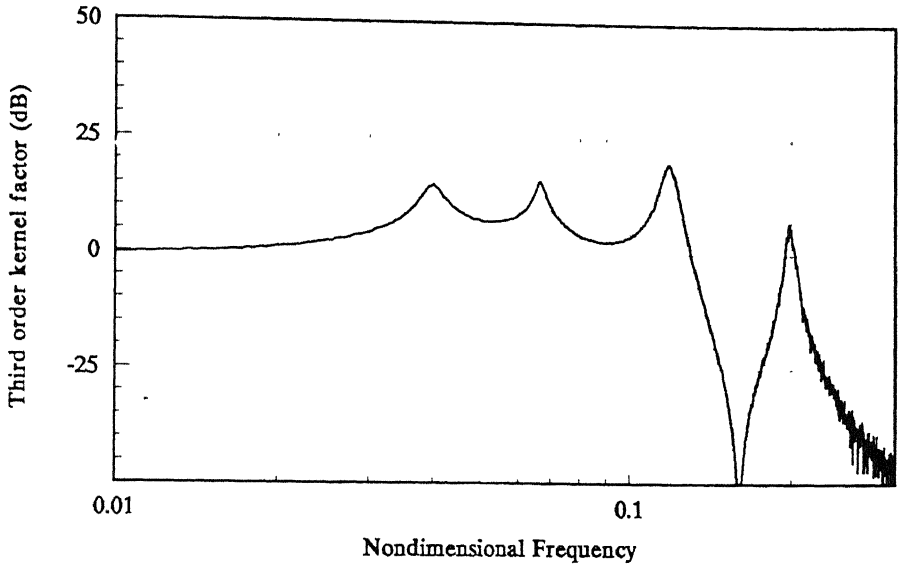

(c) Estimate of ${}^{yx}\Psi_3^{1-1,1,1}(\omega,\omega,\omega)$.

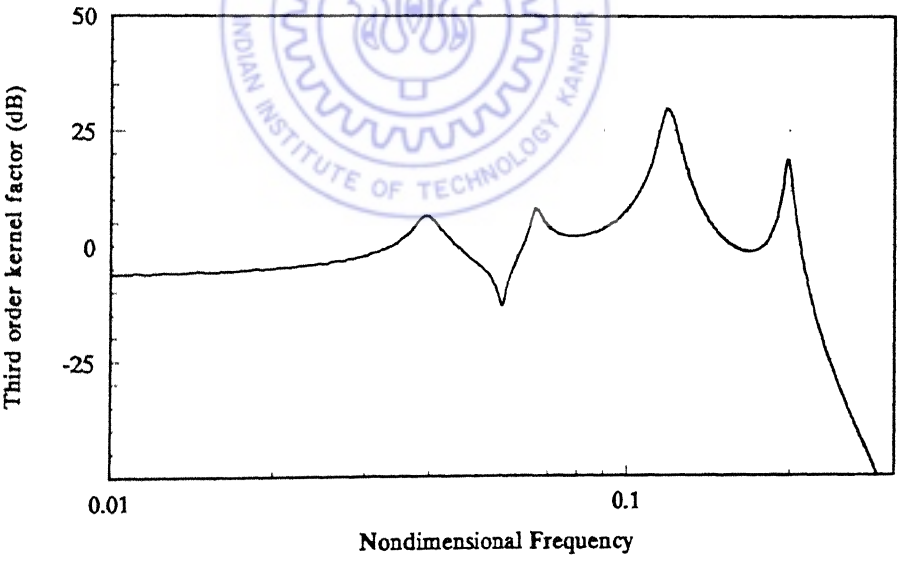

(d) Estimate of ${}^{yy}\Psi_3^{2-1,1,1}(\omega,\omega,\omega)$.

Fig. 4.18 Third order kernel factors: Case 1(c).

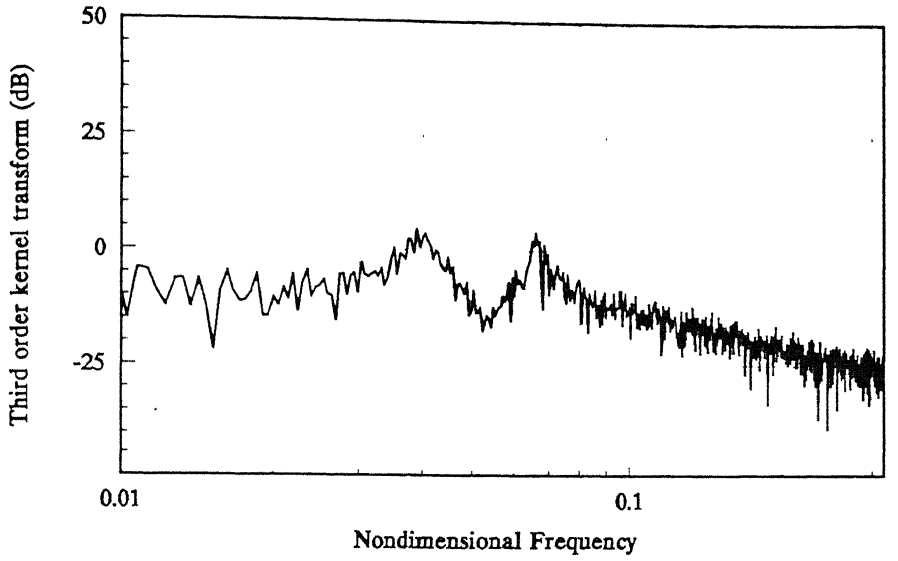

(a) Estimate of ${}^{x}H_3^{(1)}(\omega,\omega,\omega)$.

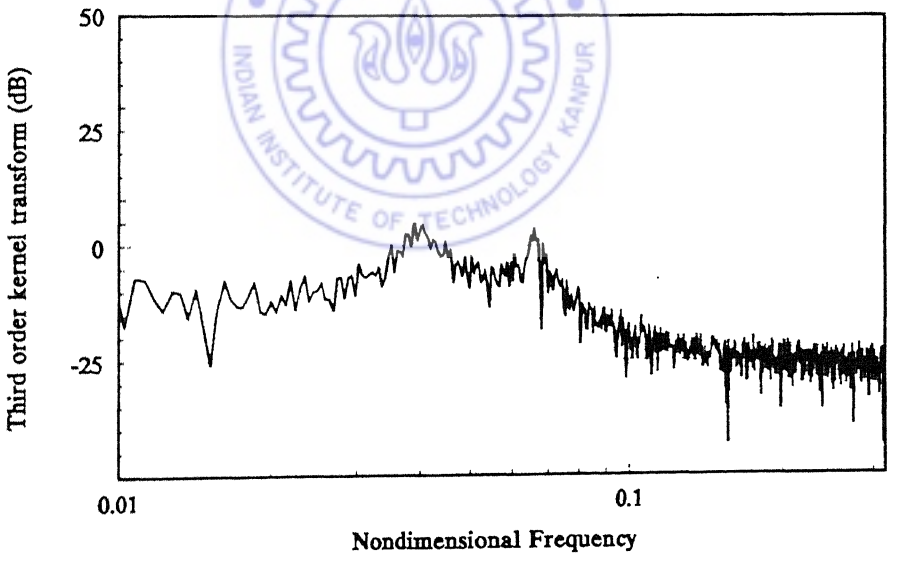

(b) Estimate of ${}^{y}H_3^{(1)}(\omega,\omega,\omega)$.

Fig. 4.19 Third order measured kernel transforms: Case 1(c).

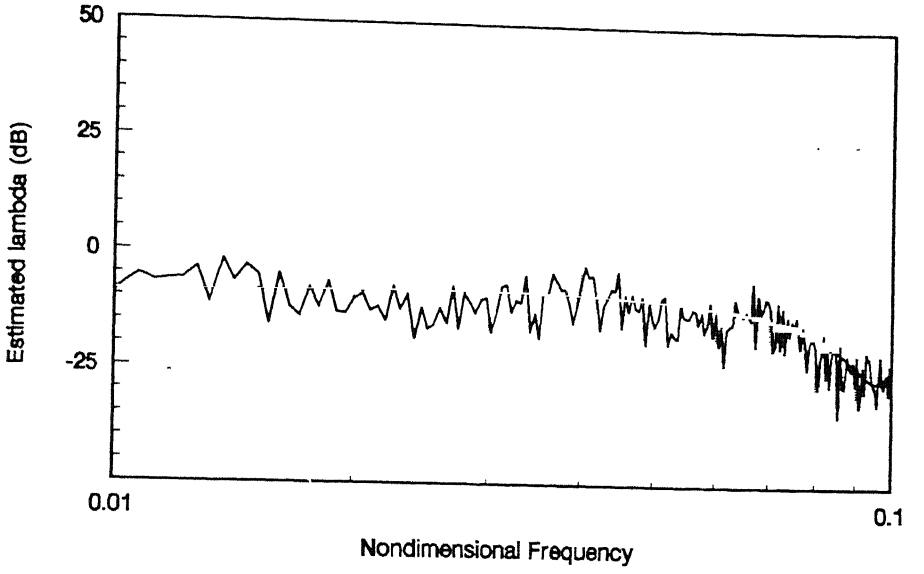

Fig. 4.20(a) Estimate of the nonlinear parameter, λ_{xx}^{N}: Case 1(c).

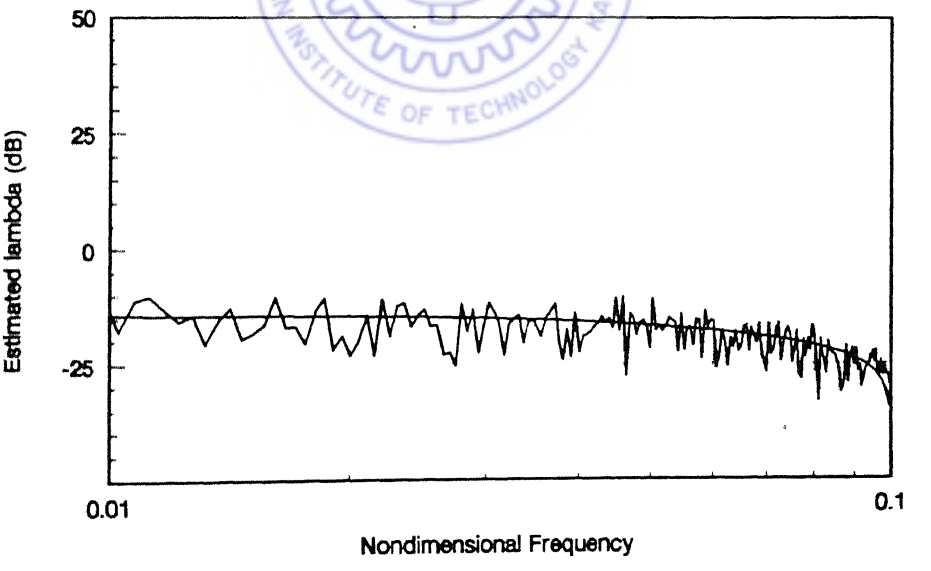

Fig. 4.20(b) Estimate of the nonlinear parameter, λ_{yy}^{N}: Case 1(c).

The parameter estimates are given in Table 4.2

Table 4.2 Parameter estimates in Cases 1 (b) and 1 (c)

Parameters	Case 1 (b)	Case 1 (c)
$\lambda^L_{xx} (= \lambda^L_{yy})$	1.109	1.005
$\lambda^L_{xy} (= \lambda^L_{yx})$	0.499	0.503
$\xi_{xx} (= \xi_{yy})$	0.016	0.011
λ^N_{xx}	0.089	0.088
λ^N_{yy}	1.18	0.012

In these cases too, the linear stiffness parameters are estimated accurately. Damping estimates involve higher errors, due to reasons cited earlier. The estimates of the nonlinear parameters show an error between 11-20%.

4.5.3 Case Study 2

For the next set of illustrations, the nonlinear parameters λ^N_{xx} and λ^N_{yy} are kept fixed at 0.1, as in Case Study 1 (a), and the linear parameters are varied. In all the Cases 1, the direct linear stiffness parameters were chosen to be identical (= 1.0) and the cross-coupled stiffness parameters were taken as half of the direct ones (= 0.5).

In Case 2 (a) the following sets of values are now chosen for response simulation and their subsequent estimation from the response.

$$\lambda^L_{xx} = 1.0; \qquad \lambda^L_{yy} = 2.0; \qquad \lambda^L_{xy} = \lambda^L_{yx} = 1.0$$

In Case 2 (b), the negative cross-coupling effect has been incorporated, with

$$\lambda^L_{xx} = \lambda^L_{yy} = 1.0; \qquad \lambda^L_{xy} = \lambda^L_{yx} = -0.50$$

The figures for these two cases are listed in Table 4.3.

Table 4.3 Figures of Cases 2 (a) and 2 (b)

Parameters	Case 2 (a)	Case 2 (b)
${}^{x}H_1^{(1)}(\omega)$, ${}^{y}H_1^{(1)}(\omega)$ ${}^{x}H_1^{(2)}(\omega)$, ${}^{y}H_1^{(2)}(\omega)$	Figs. 4.21 (a)-(d)	Figs. 4.25 (a)-(d)
${}^{xx}\Psi_3^{1-1,1,1}(\omega,\omega,\omega)$, ${}^{xy}\Psi_3^{2-1,1,1}(\omega,\omega,\omega)$, ${}^{yx}\Psi_3^{1-1,1,1}(\omega,\omega,\omega)$, ${}^{yy}\Psi_3^{2-1,1,1}(\omega,\omega,\omega)$	Figs. 4.22 (a)-(d)	Figs. 4.26 (a)-(d)
${}^{x}H_3^{(1)}(\omega,\omega,\omega)$, ${}^{y}H_3^{(1)}(\omega,\omega,\omega)$	Figs. 4.23 (a), (b)	Figs. 4.27 (a), (b)
λ_{xx}^{N}, λ_{yy}^{N}	Figs. 4.24 (a), (b)	Figs. 4.28 (a), (b)

The estimates are given in Table 4.4.

Table 4.4 Parameter estimates in Cases 2 (a) and 2 (b)

Parameters	Case 2 (a)	Case 2 (b)
λ_{xx}^{L}	1.01	1.03
λ_{yy}^{L}	2.03	1.07
$\lambda_{xy}^{L}(=\lambda_{yx}^{L})$	0.992	- 0.495
$\xi_{xx}(=\xi_{yy})$	0.013	0.012
λ_{xx}^{N}	0.078	0.108
λ_{yy}^{N}	0.107	0.111

The estimate of the direct linear term λ_{xx}^{L} has been made by replacing term 1 on the r.h.s of equations (4.68) by λ_{xx}^{L} itself. It can be seen from Table 4.4 that, in Cases 2 (a) and (b), where the direct linear stiffness terms are dissimilar (unlike Case 1 (a)), the pattern and accuracy of estimates is similar to the previous cases. It can also be noted, in Case 2 (b), that negative cross- coupling effect has been correctly identified.

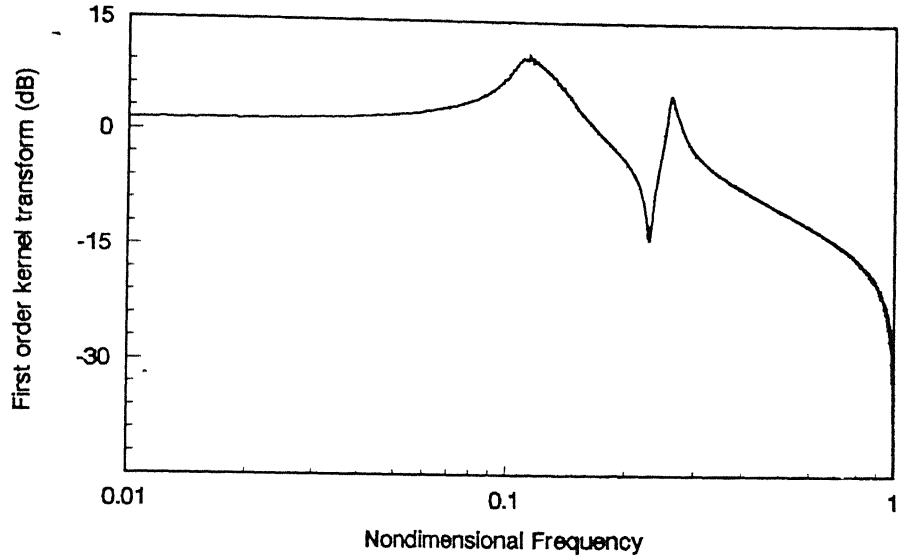

(a) First order direct kernel transform, ${}^{x}H_1^{(1)}(\omega)$.

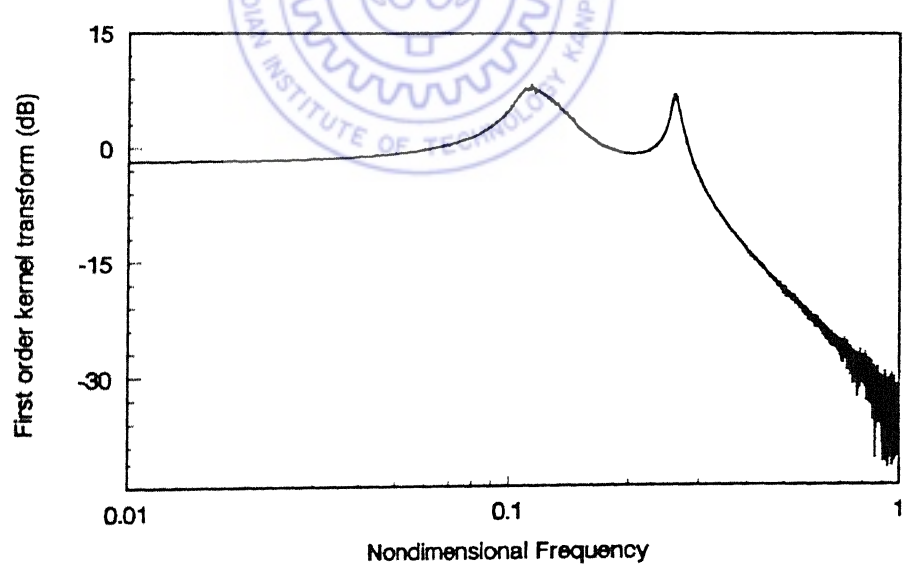

(b) First order cross-kernel transform, ${}^{x}H_1^{(2)}(\omega)$.

Fig. 4.21 Estimates of the first order direct and cross-kernel transforms: Case 2(a) (Contd.)

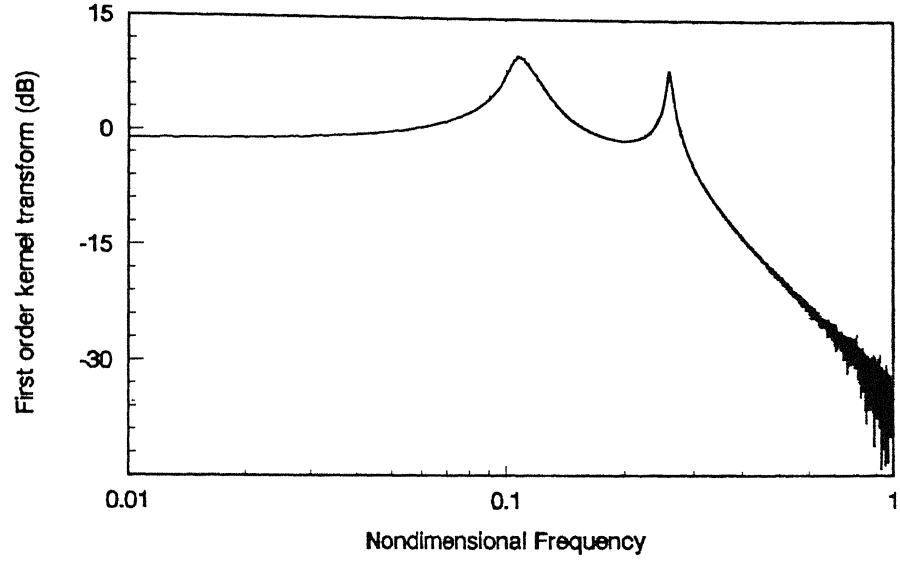

(c) First order cross-kernel transform, ${}^{y}H_1^{(1)}(\omega)$.

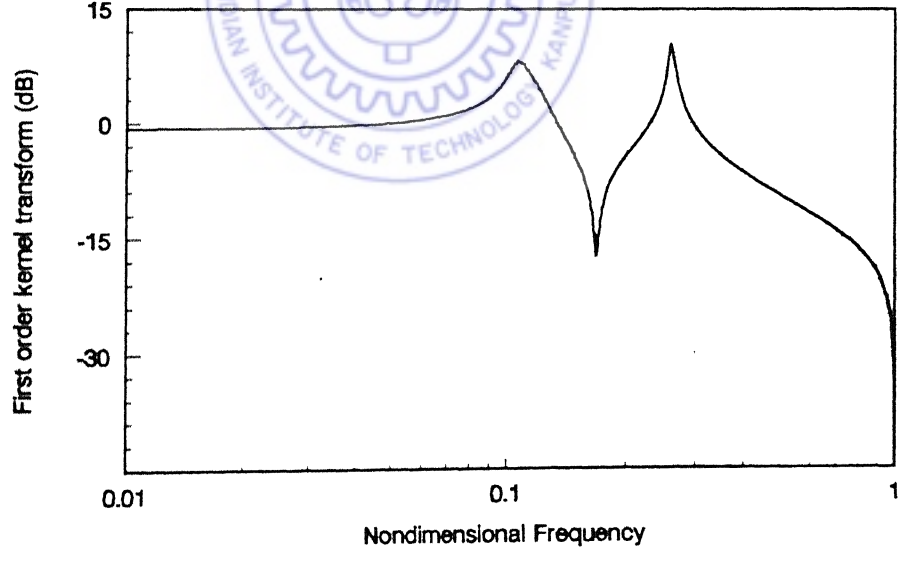

(d) First order direct kernel transform, ${}^{y}H_1^{(2)}(\omega)$.

Fig. 4.21 Estimates of the first order direct and cross-kernel transforms: Case 2(a).

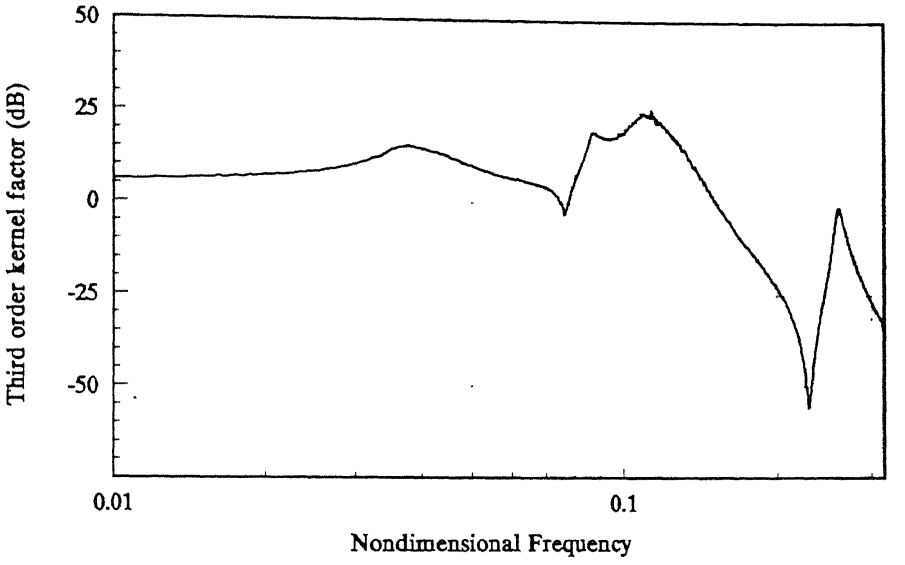

(a) Estimate of ${}^{xx}\Psi_3^{1-1,1,1}(\omega,\omega,\omega)$.

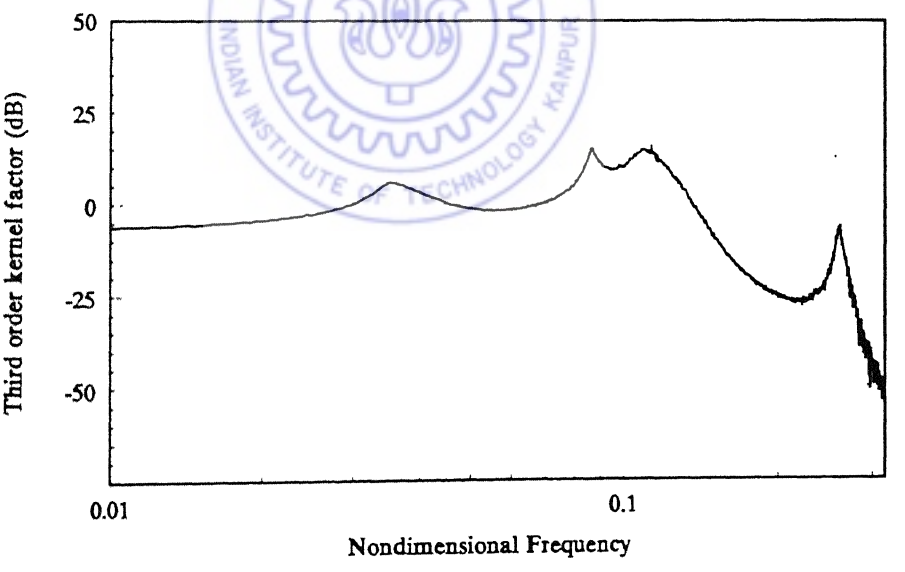

(b) Estimate of ${}^{xy}\Psi_3^{2-1,1,1}(\omega,\omega,\omega)$.

Fig. 4.22 Third order kernel factors: Case 2(a) (Contd.)

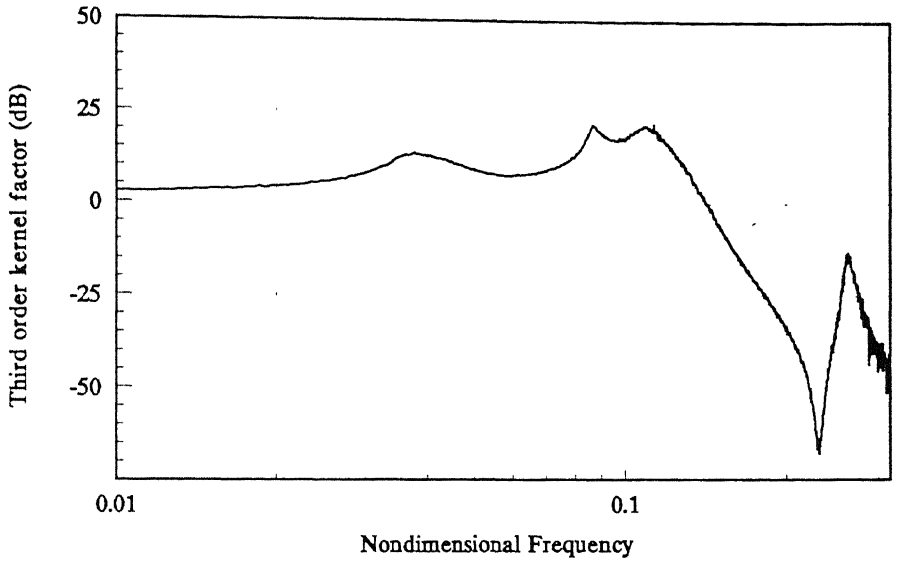

(c) Estimate of ${}^{yx}\Psi_3^{1-1,1,1}(\omega,\omega,\omega)$.

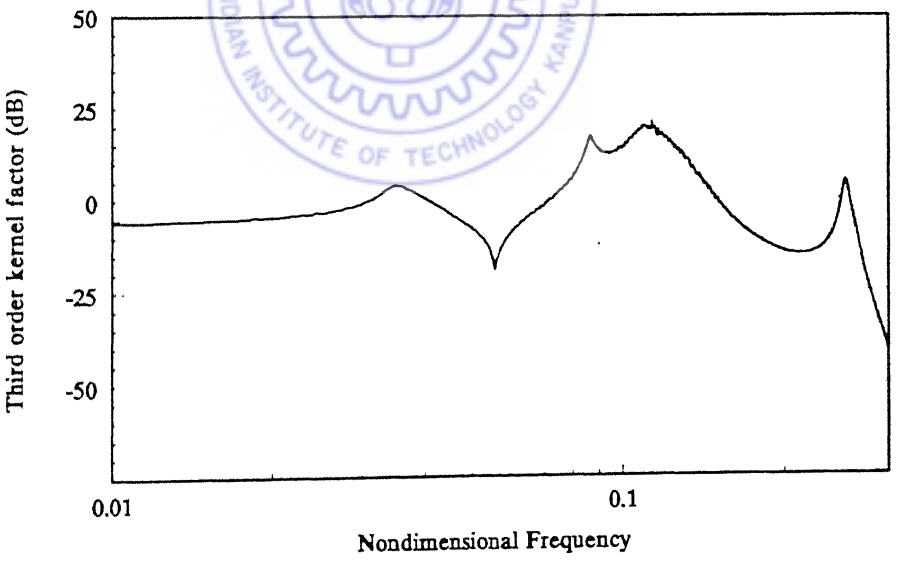

(d) Estimate of ${}^{yy}\Psi_3^{2-1,1,1}(\omega,\omega,\omega)$.

Fig. 4.22 Third order kernel factors: Case 2(a).

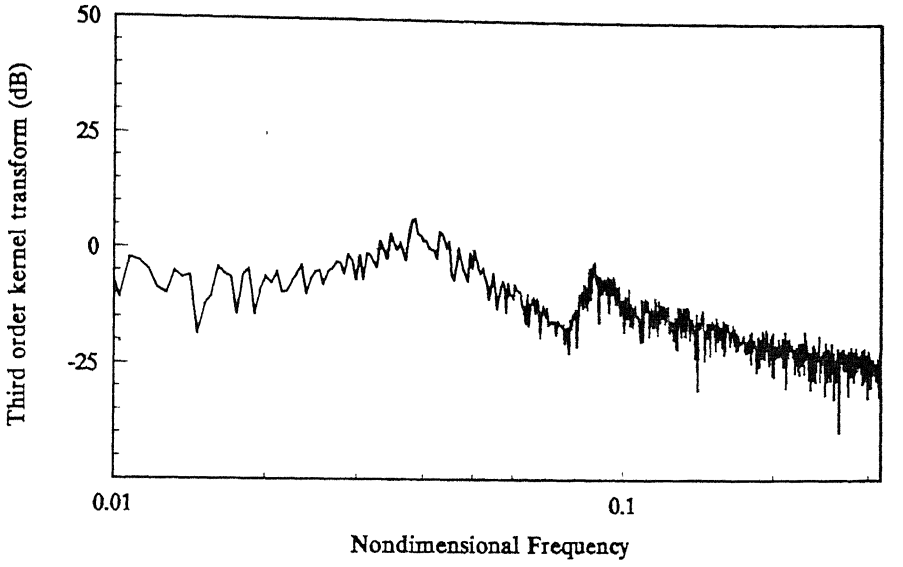

(a) Estimate of ${}^{x}H_3^{(1)}(\omega,\omega,\omega)$.

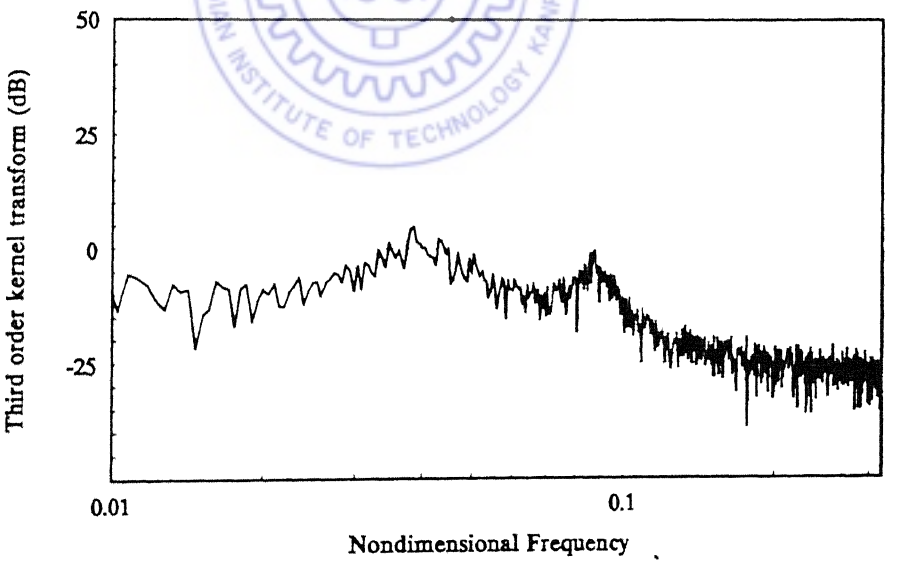

(b) Estimate of ${}^{y}H_3^{(1)}(\omega,\omega,\omega)$.

Fig. 4.23 Third order measured kernel transforms: Case 2(a).

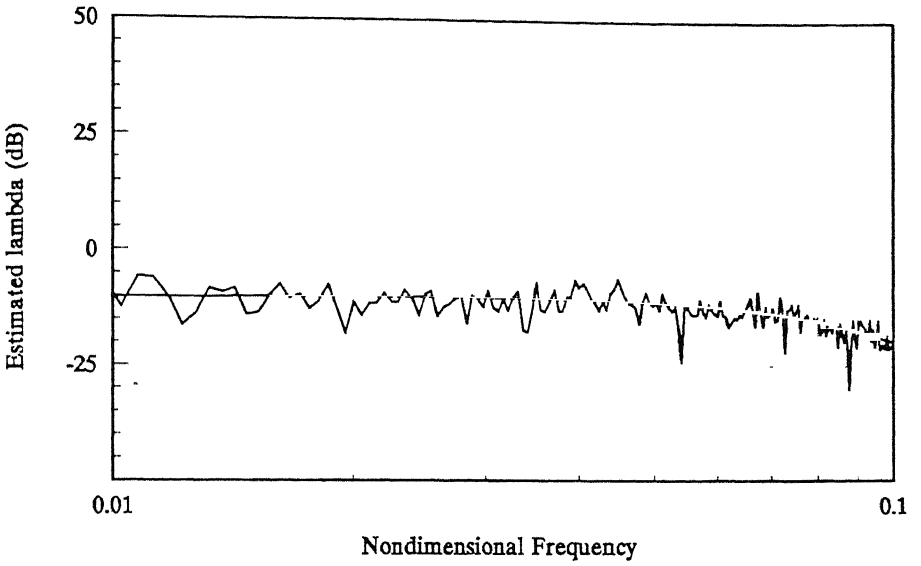

Fig. 4.24(a) Estimate of the nonlinear parameter, λ_{xx}^{N}: Case 2(a).

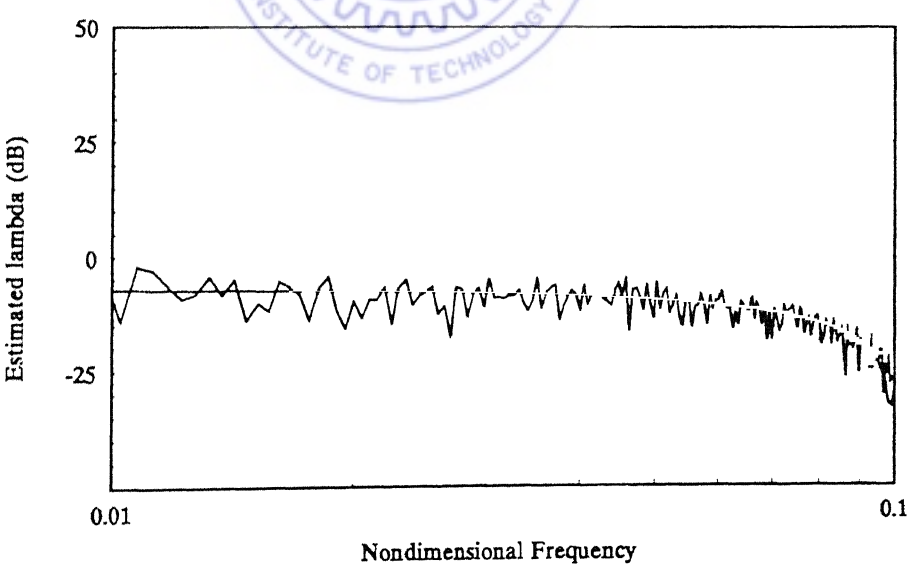

Fig. 4.24(b) Estimate of the nonlinear parameter, λ_{yy}^{N}: Case 2(a).

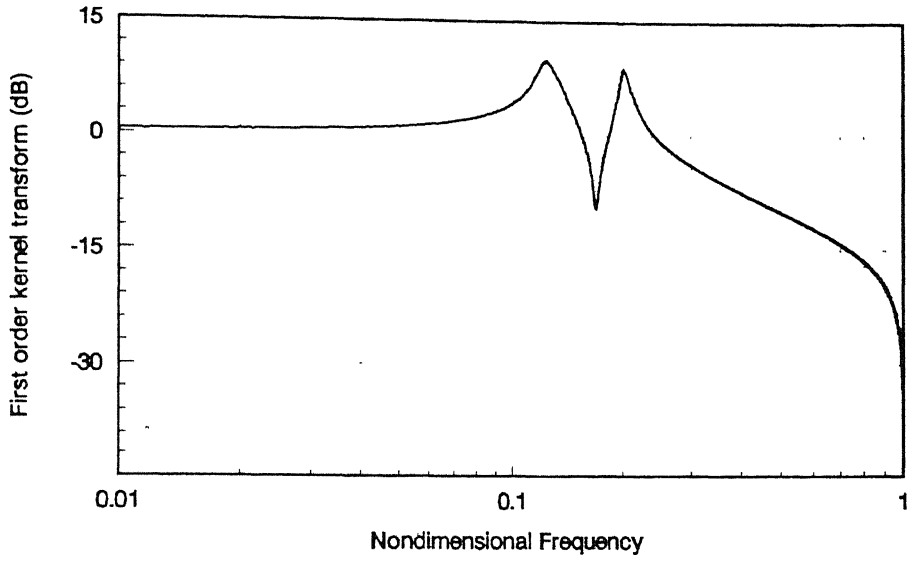

(a) First order direct kernel transform, ${}^{x}H_1^{(1)}(\omega)$.

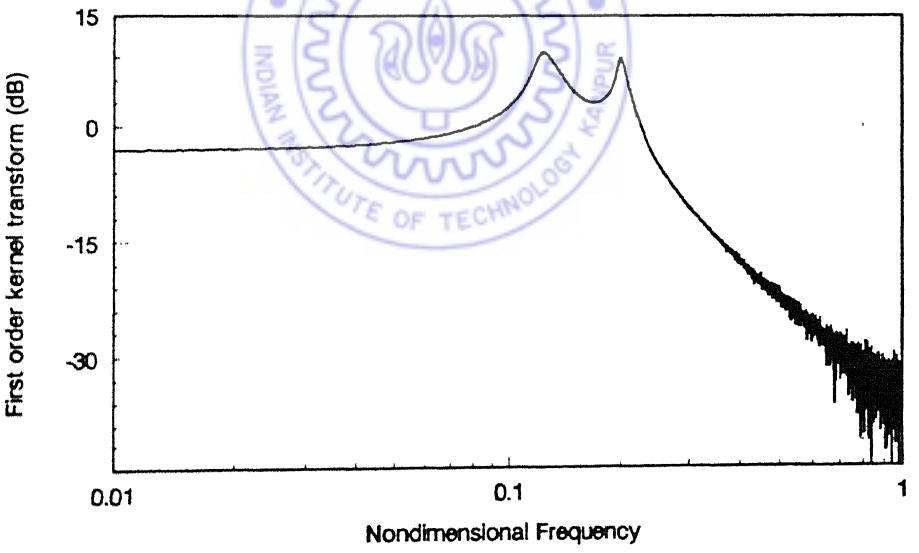

(b) First order cross-kernel transform, ${}^{x}H_1^{(2)}(\omega)$.

Fig. 4.25 Estimates of the first order direct and cross-kernel transforms: Case 2(b) (Contd.)

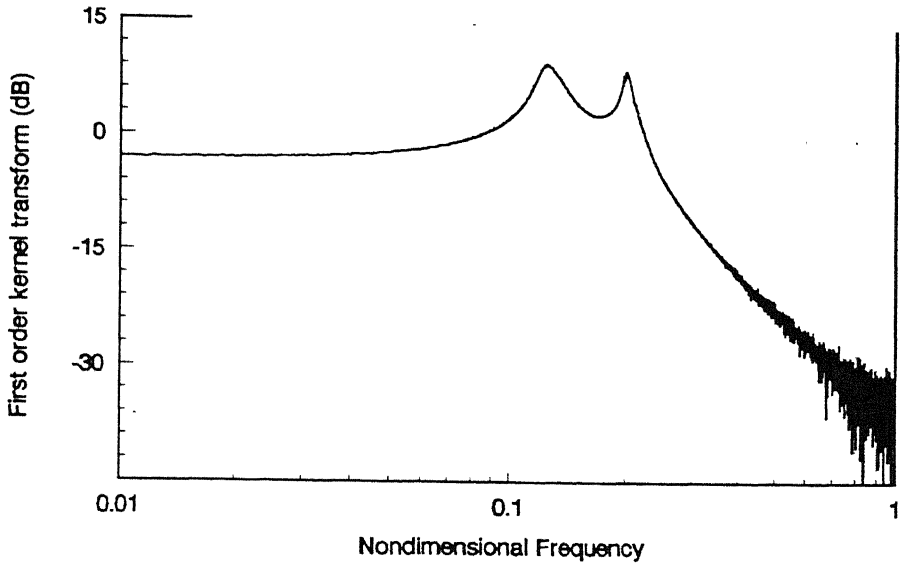

(c) First order cross-kernel transform, ${}^{y}H_1^{(1)}(\omega)$.

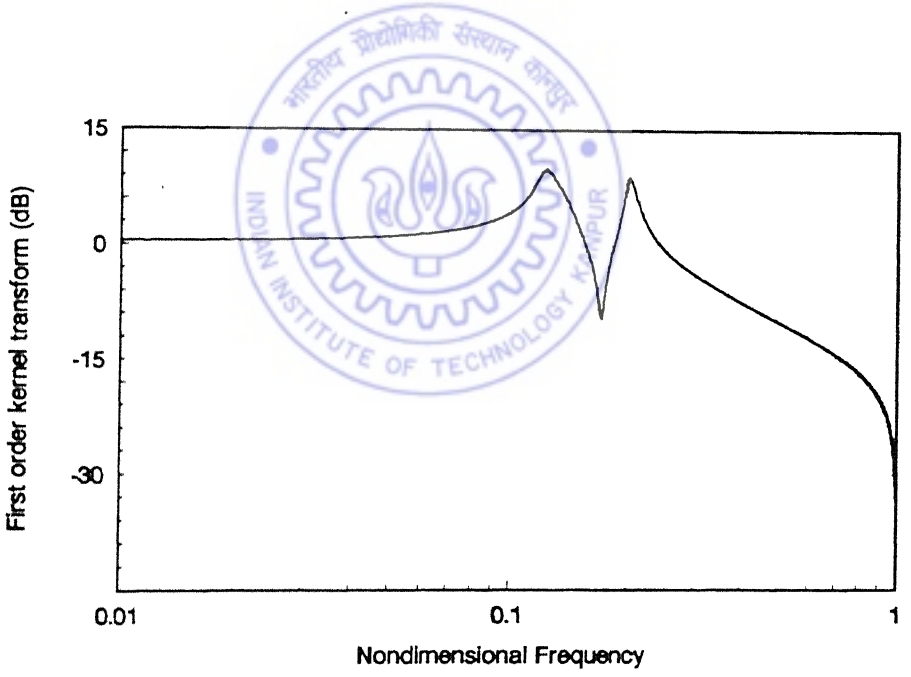

(d) First order direct kernel transform, ${}^{y}H_1^{(2)}(\omega)$.

Fig. 4.25 Estimates of the first order direct and cross-kernel transforms: Case 2(b).

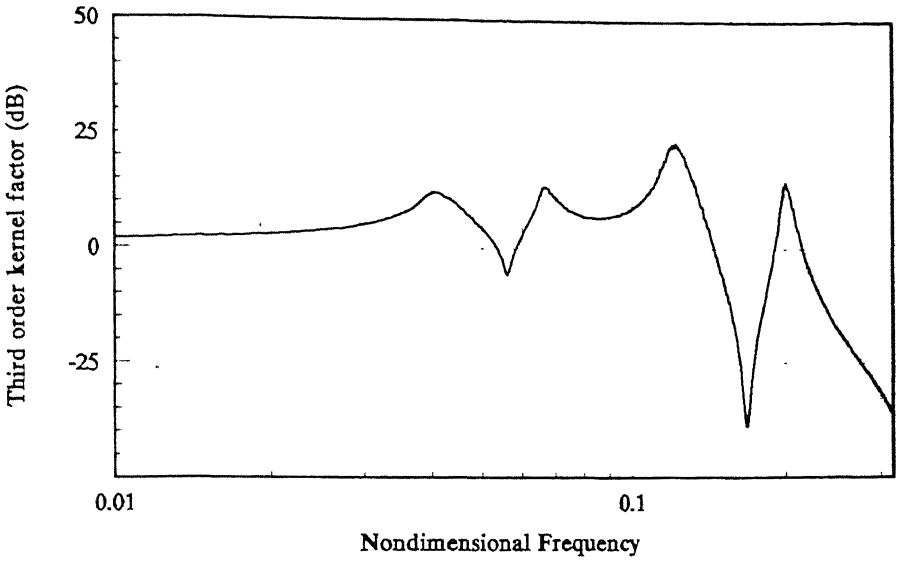

(a) Estimate of ${}^{xx}\Psi_3^{1-1,1,1}(\omega,\omega,\omega)$.

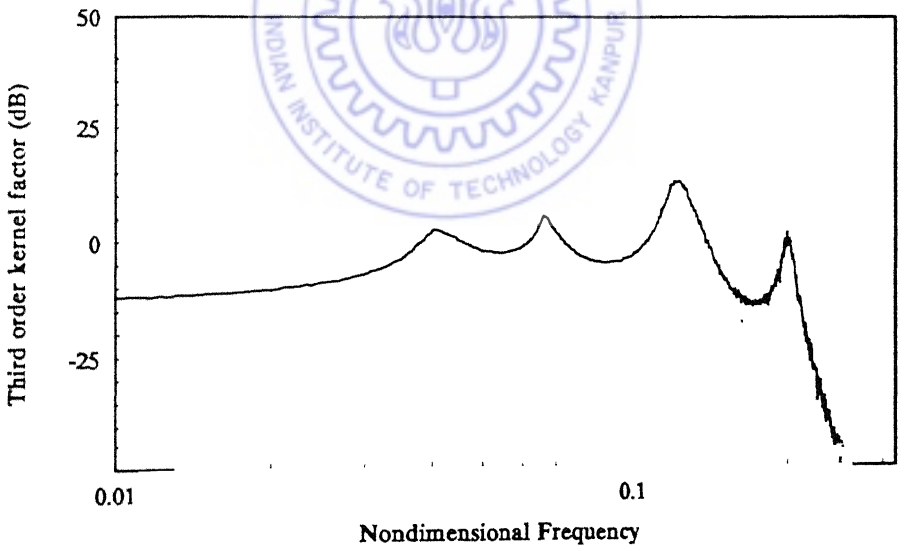

(b) Estimate of ${}^{xy}\Psi_3^{2-1,1,1}(\omega,\omega,\omega)$.

Fig. 4.26 Third order kernel factors: Case 2(b) (Contd.)

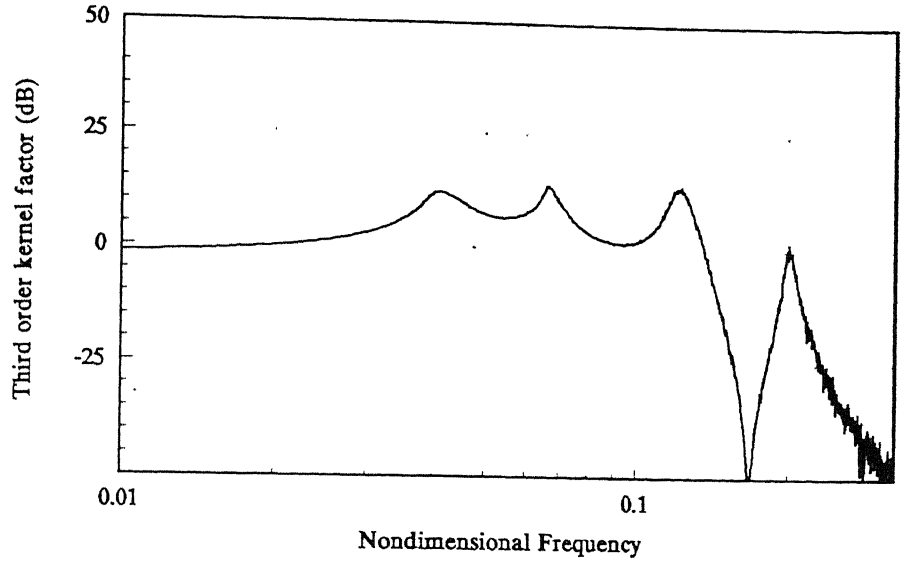

(c) Estimate of ${}^{yx}\Psi_3^{1-1,1,1}(\omega,\omega,\omega)$.

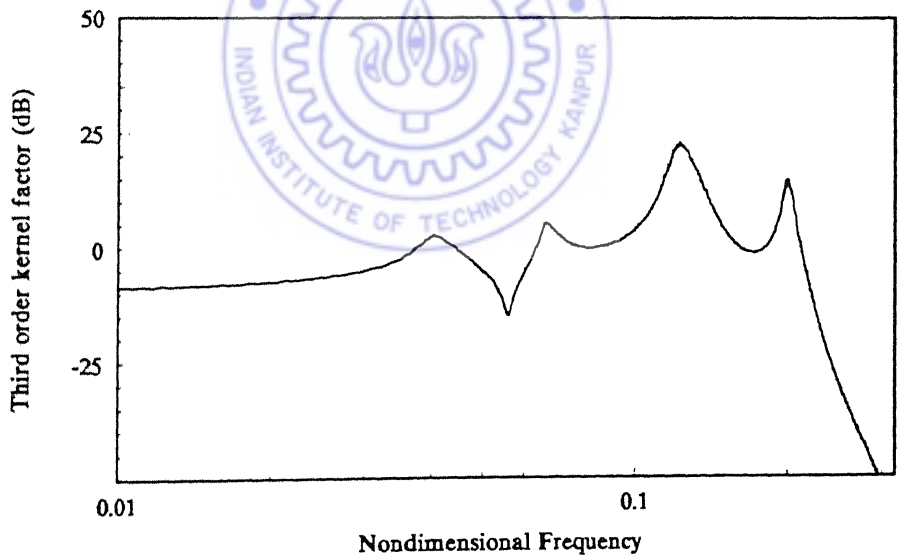

(d) Estimate of ${}^{yy}\Psi_3^{2-1,1,1}(\omega,\omega,\omega)$.

Fig. 4.26 Third order kernel factors: Case 2(b).

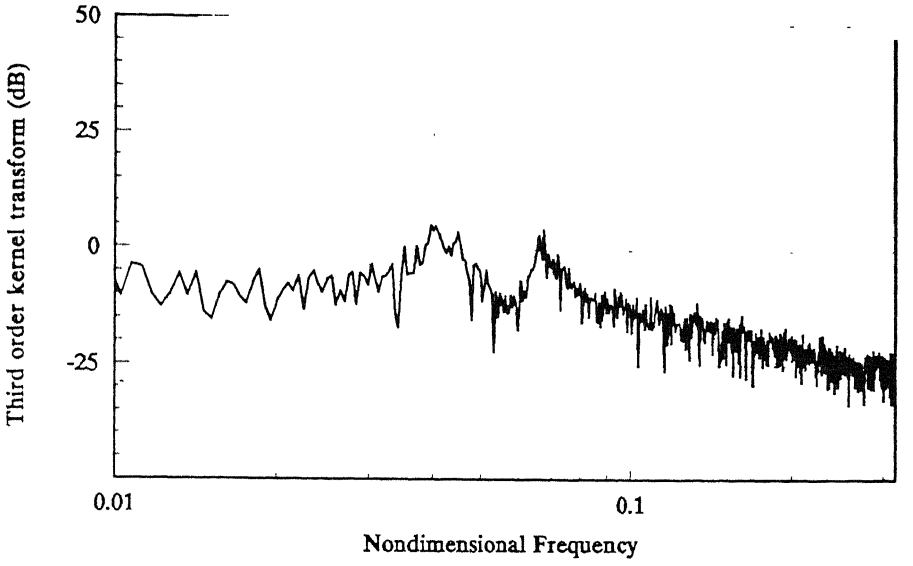

(a) Estimate of ${}^{x}H_3^{(1)}(\omega,\omega,\omega)$.

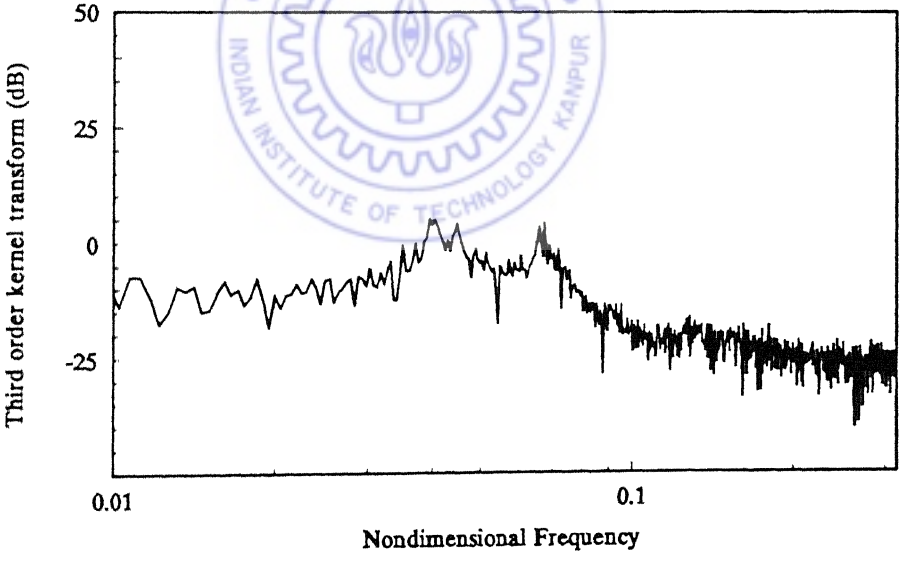

(b) Estimate of ${}^{y}H_3^{(1)}(\omega,\omega,\omega)$.

Fig. 4.27 Third order measured kernel transforms: Case 2(b).

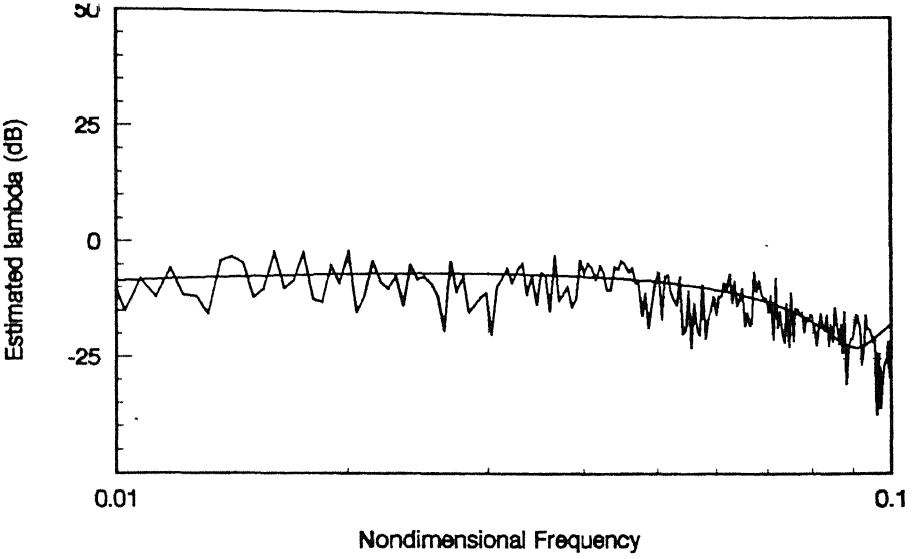

Fig. 4.28(a) Estimate of the nonlinear parameter, λ_{xx}^{N}: Case 2(b).

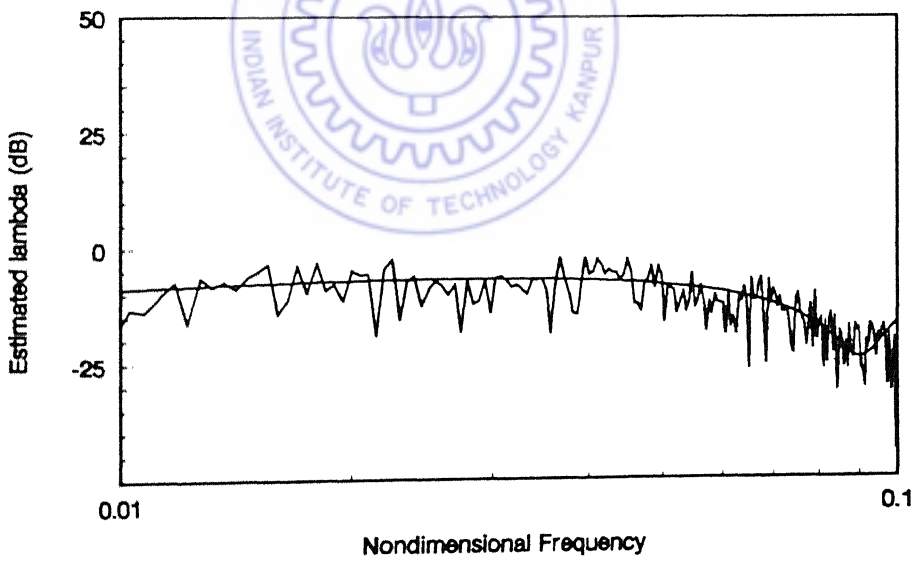

Fig. 4.28(b) Estimate of the nonlinear parameter, λ_{yy}^{N}: Case 2(b).

Apart from the linear and nonlinear stiffness parameters, other nondimensional parameters contained by the governing equation (4.3) are the damping ratios. All the previous case studies have been carried out for 1% damping ($\xi_{xx}=\xi_{yy}=0.01$). Numerical simulation is carried out to further, investigate the estimation procedure for a lower damping, with $\xi_{xx}=\xi_{yy}=0.001$ (keeping the values of the remaining parameters the same as those in Case 1 (a)). The parameters and the corresponding figures are given below

${}^{x}H_1^{(1)}(\omega)$, ${}^{y}H_1^{(1)}(\omega)$ ${}^{x}H_1^{(2)}(\omega)$, ${}^{y}H_1^{(2)}(\omega)$	Figs. 4.29 (a)-(d)
${}^{xx}\Psi_3^{1-1,1,1}(\omega,\omega,\omega)$, ${}^{xy}\Psi_3^{2-1,1,1}(\omega,\omega,\omega)$ ${}^{yx}\Psi_3^{1-1,1,1}(\omega,\omega,\omega)$, ${}^{yy}\Psi_3^{2-1,1,1}(\omega,\omega,\omega)$	Figs. 4.30 (a)-(d)
${}^{x}H_3^{(1)}(\omega,\omega,\omega)$, ${}^{y}H_3^{(1)}(\omega,\omega,\omega)$	Figs. 4.31 (a), (b)
λ_{xx}^{N}, λ_{yy}^{N}	Figs. 4.32 (a), (b)

The estimates are:

$\lambda_{xx}^{L}=\lambda_{yy}^{L}$	1.07
$\lambda_{xy}^{L}(=\lambda_{yx}^{L})$	0.488
$\xi_{xx}(=\xi_{yy})$	0.002
λ_{xx}^{N}	0.150
λ_{yy}^{N}	0.170

The estimates can be seen to be sensitive to damping and comparison with the results of Case 1 (a) shows that, the results are less accurate in the present case, with lower damping. Averaging over increased sample and ensemble sizes can be expected to reduce the statistical errors in the extracted kernels and improve the accuracy of the estimates.

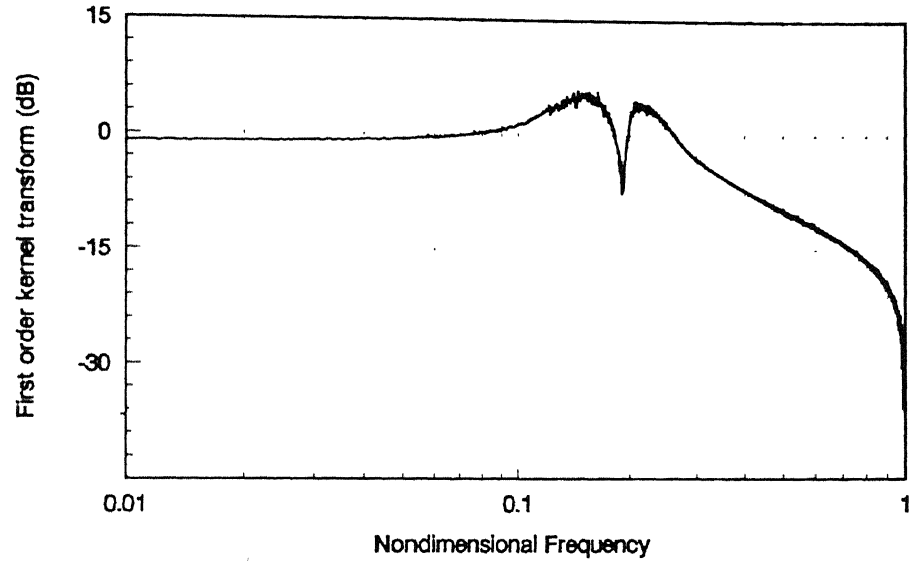

(a) First order direct kernel transform, ${}^{x}H_1^{(1)}(\omega)$.

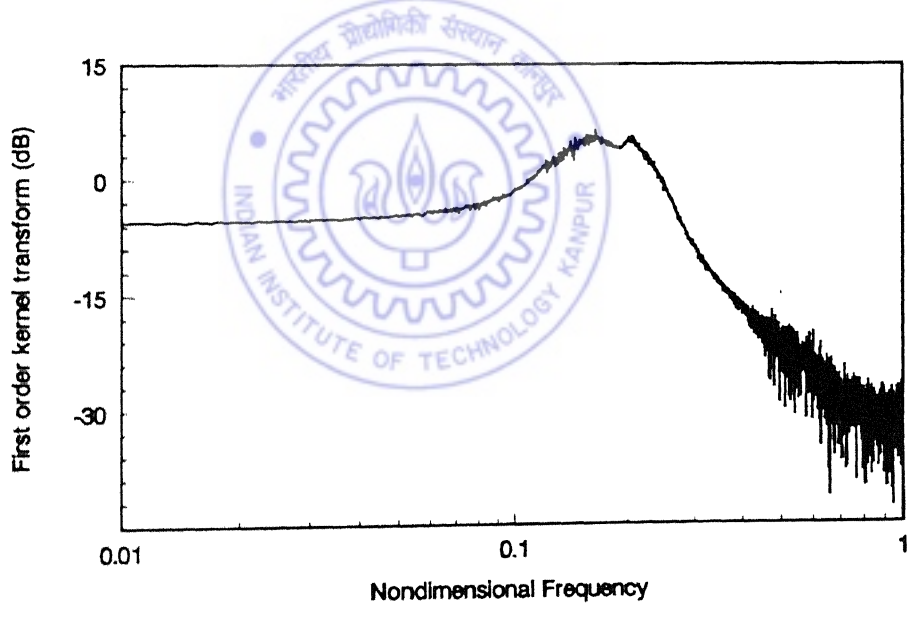

(b) First order cross-kernel transform, ${}^{x}H_1^{(2)}(\omega)$.

Fig. 4.29 Estimates of the first order direct and cross-kernel transforms: Case 3 (Contd.)

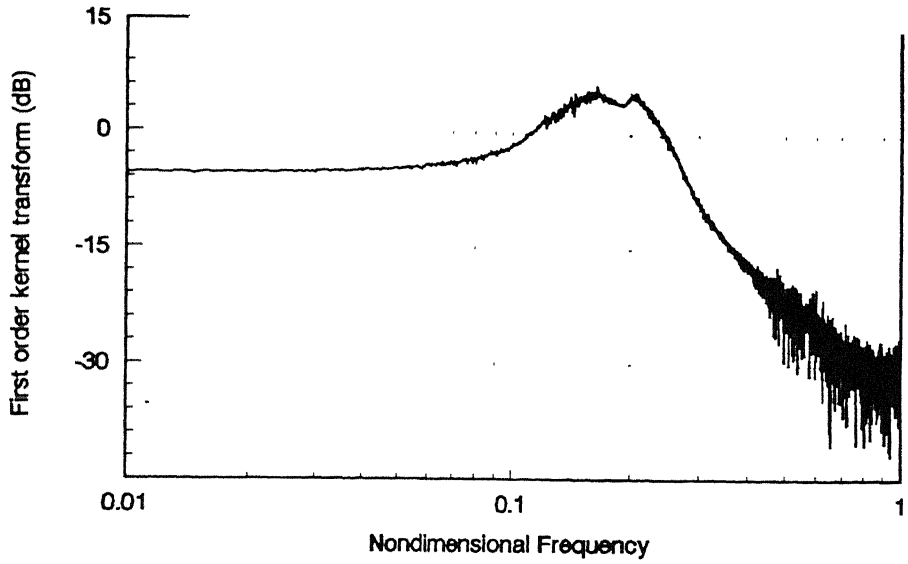

(c) First order cross-kernel transform, ${}^{y}H_1^{(1)}(\omega)$.

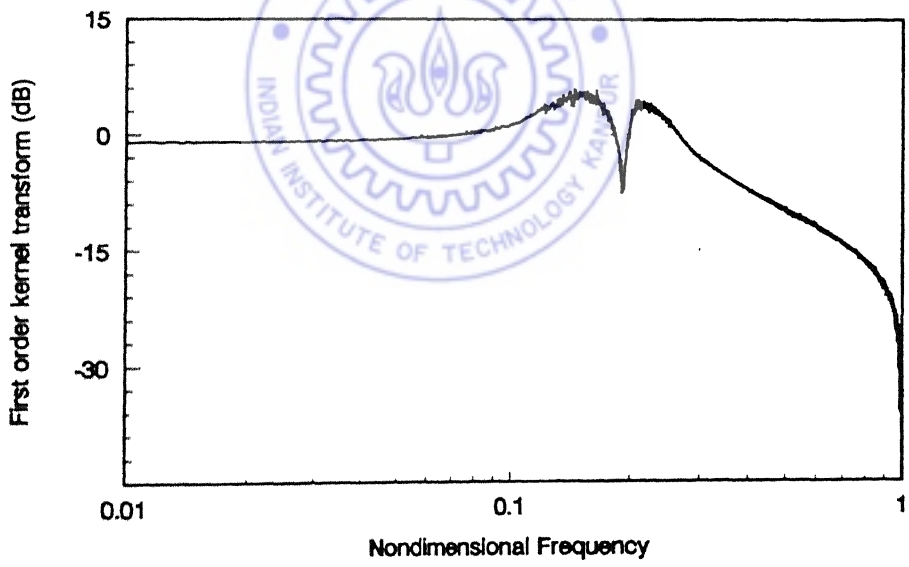

(d) First order direct kernel transform, ${}^{y}H_1^{(2)}(\omega)$.

Fig. 4.29 Estimates of the first order direct and cross-kernel transforms: Case 3.

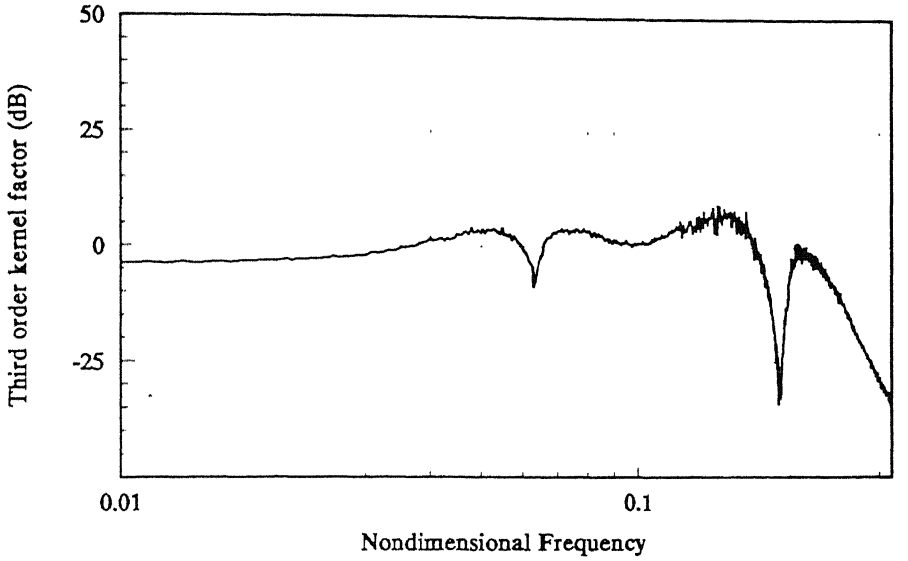

(a) Estimate of ${}^{xx}\Psi_3^{1-1,1,1}(\omega,\omega,\omega)$.

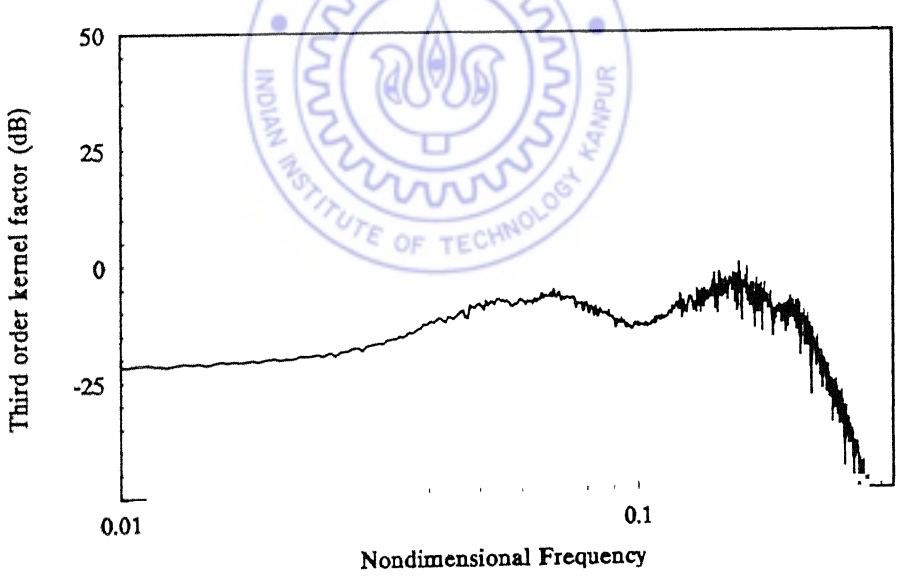

(b) Estimate of ${}^{xy}\Psi_3^{2-1,1,1}(\omega,\omega,\omega)$.

Fig. 4.30 Third order kernel factors: Case 3 (Contd.)

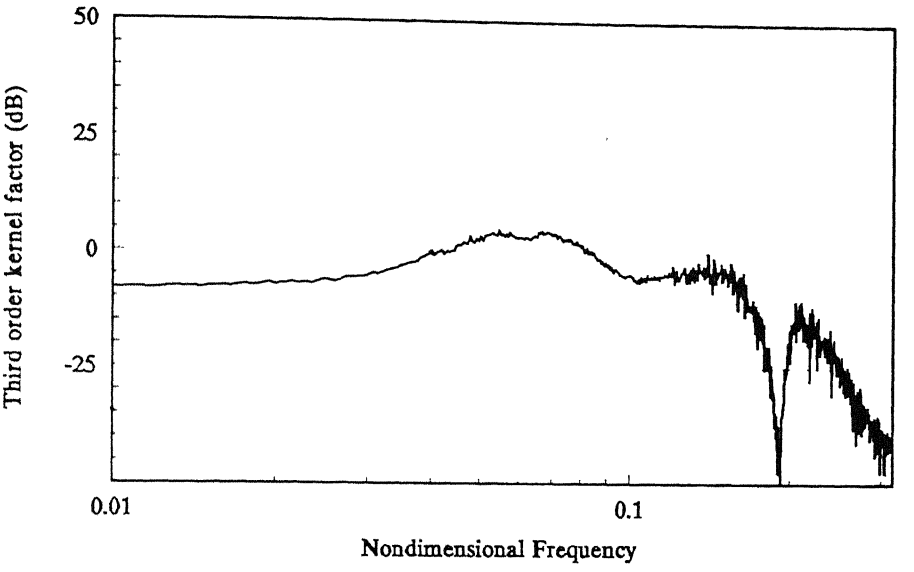

(c) Estimate of ${}^{yx}\Psi_3^{1-1,1,1}(\omega,\omega,\omega)$.

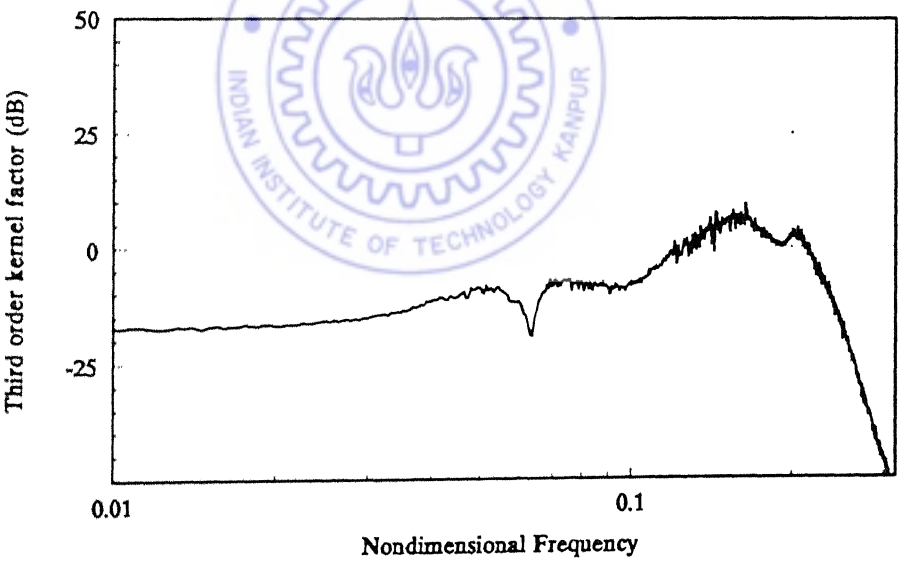

(d) Estimate of ${}^{yy}\Psi_3^{2-1,1,1}(\omega,\omega,\omega)$.

Fig. 4.30 Third order kernel factors: Case 3.

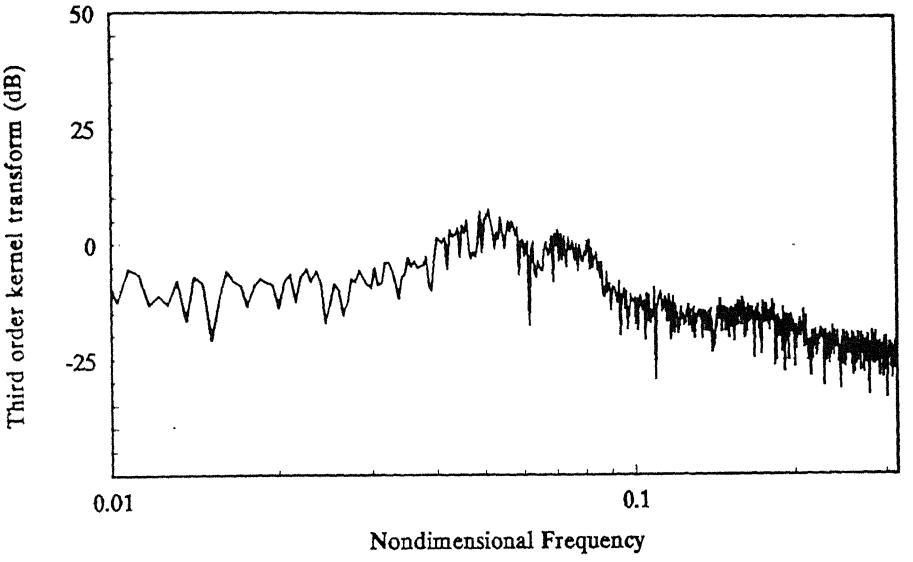

(a) Estimate of ${}^{x}H_3^{(1)}(\omega,\omega,\omega)$.

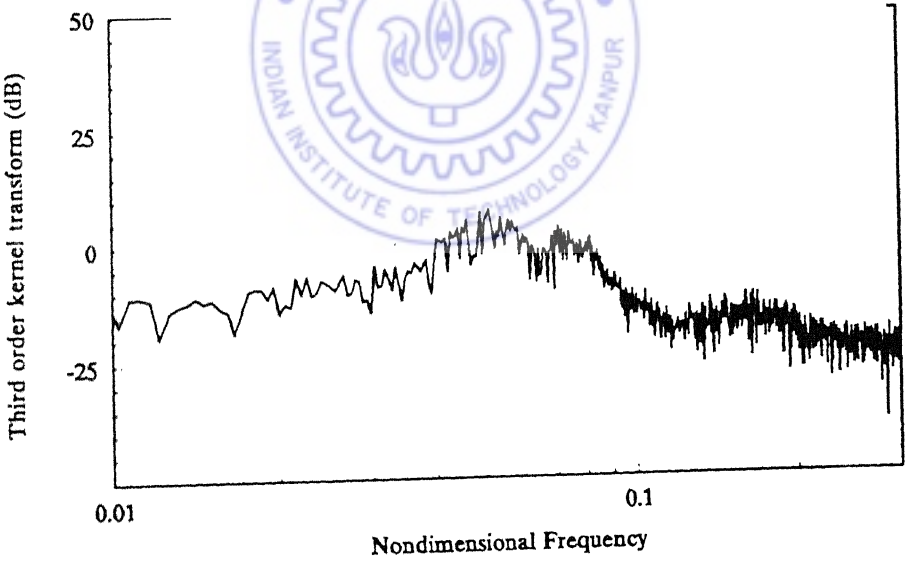

(b) Estimate of ${}^{y}H_3^{(1)}(\omega,\omega,\omega)$.

Fig. 4.31 Third order measured kernel transforms: Case 3.

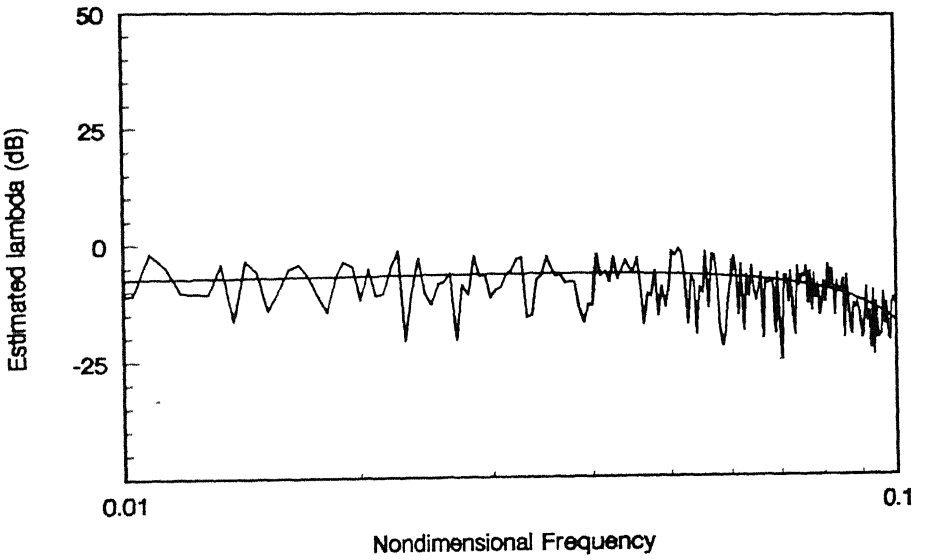

Fig. 4.32(a) Estimate of the nonlinear parameter, λ_{xx}^{N}: Case 3.

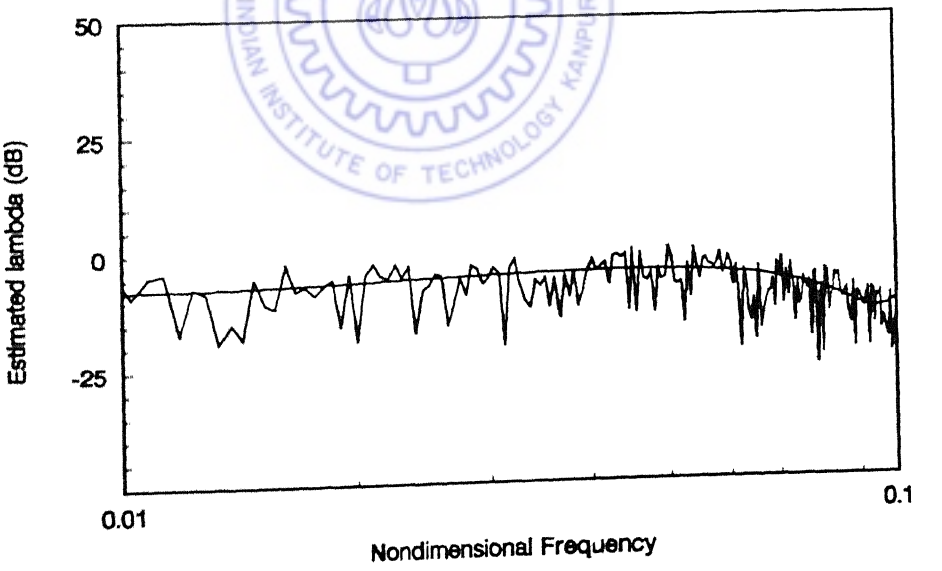

Fig. 4.32(b) Estimate of the nonlinear parameter, λ_{yy}^{N}: Case 3.

4.5.5 Influence of Ensemble Size

It was observed that increasing the ensemble size beyond 500 has insignificant influence on the first order estimates, the influence on the third order estimates is investigated for ensemble sizes 500, 1000, 1500 and 2000. The parameters are kept the same as in Case 1 (a) and the results are arranged, for clarity, as given below

	Ensemble Size			
	500	1000	1500	2000
${}^{xx}\Psi_3^{1-1,1,1}(\omega,\omega,\omega)$, ${}^{xy}\Psi_3^{2-1,1,1}(\omega,\omega,\omega)$ ${}^{x}H_3^{(1)}(\omega,\omega,\omega)$	Fig. 4.33(a)	Fig. 4.34(a)	Fig. 4.35(a)	Fig. 4.36(a)
${}^{yx}\Psi_3^{1-1,1,1}(\omega,\omega,\omega)$, ${}^{yy}\Psi_3^{2-1,1,1}(\omega,\omega,\omega)$, ${}^{y}H_1^{(1)}(\omega,\omega,\omega)$	Fig. 4.33(b)	Fig. 4.34(b)	Fig. 4.35(b)	Fig. 4.36(b)

It can be seen from the above figures that the third order Wiener kernel transforms, ${}^{x}H_3^{(1)}(\omega,\omega,\omega)$ and ${}^{y}H_3^{(1)}(\omega,\omega,\omega)$ get refined with increasing number of samples in the ensemble. However, the refinement in the kernel factors, ${}^{xx}\Psi_3^{1-1,1,1}(\omega,\omega,\omega)$ etc., which are synthesised from first order kernel transforms, is marginal. The ensemble size was not increased beyond 2000, in the present study, due to data storage limitations of the computer.

4.5.6 Influence of Measurement Noise

The influence of measurement noise, which can be expected during an experiment, in the measurement of the excitation force and the response signals, is studied by contaminating the simulated force and response signals with 5% simulated random noise. The parameter estimation algorithm was found to be robust in the presence of this noise and the change in the estimates is marginal. For illustration, only the third order kernel factors, ${}^{yx}\Psi_3^{1-1,1,1}(\omega,\omega,\omega)$, ${}^{yy}\Psi_3^{2-1,1,1}(\omega,\omega,\omega)$ and the third order Wiener kernel transform, ${}^{y}H_3^{(1)}(\omega,\omega,\omega)$, are shown in Figs. 4.37 (a) and 4.37 (b). The data corresponds to

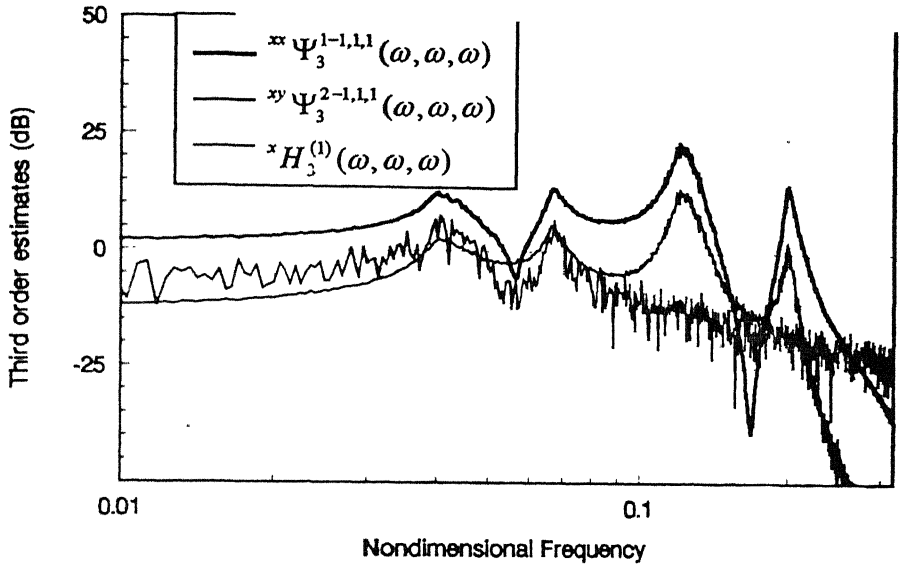

(a) Estimates of $^{xx}\Psi_3^{1-1,1,1}(\omega,\omega,\omega)$, $^{xy}\Psi_3^{2-1,1,1}(\omega,\omega,\omega)$ and $^{x}H_3^{(1)}(\omega,\omega,\omega)$.

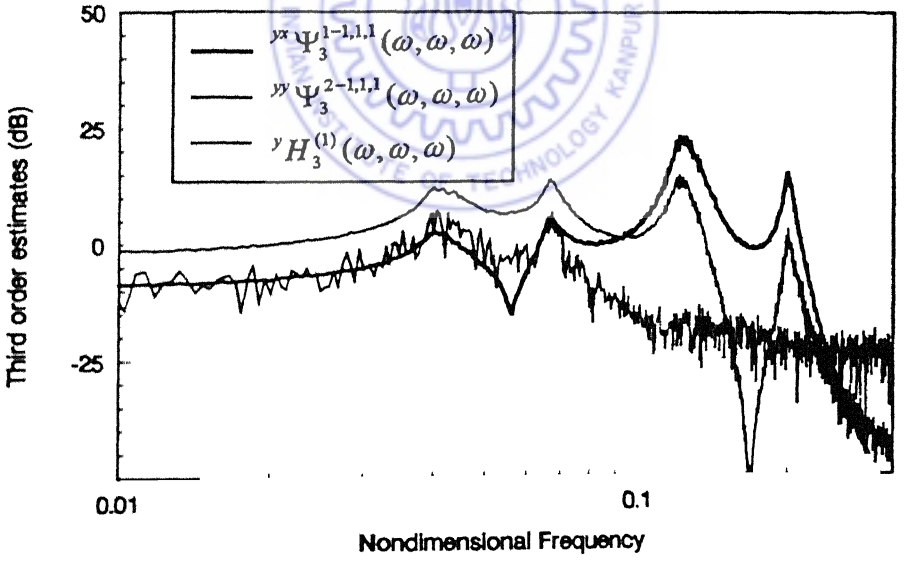

(b) Estimates of $^{yx}\Psi_3^{1-1,1,1}(\omega,\omega,\omega)$, $^{yy}\Psi_3^{2-1,1,1}(\omega,\omega,\omega)$ and $^{y}H_3^{(1)}(\omega,\omega,\omega)$.

Fig. 4.33 Influence of sample size on third order estimates: Case 1(a) (sample size = 500).

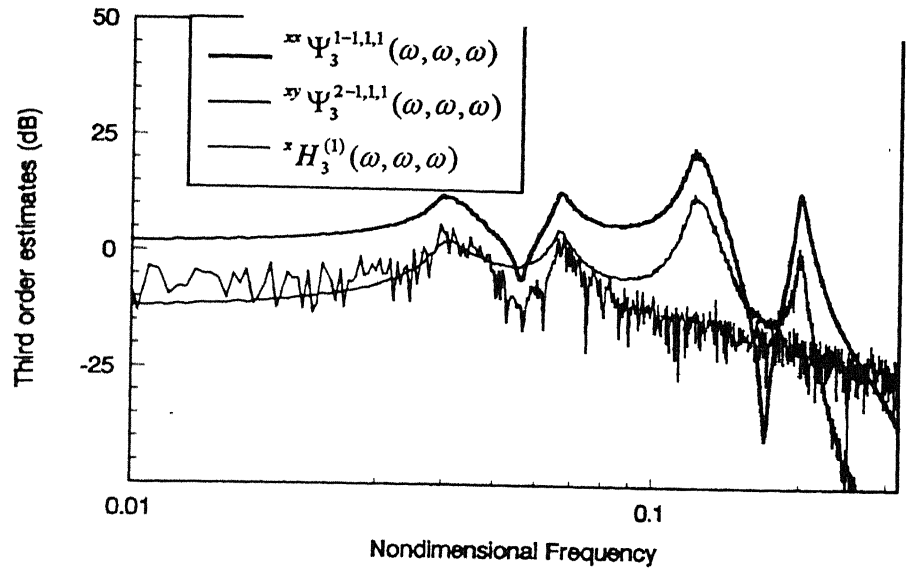

(a) Estimates of $^{xx}\Psi_3^{1-1,1,1}(\omega,\omega,\omega)$, $^{xy}\Psi_3^{2-1,1,1}(\omega,\omega,\omega)$ and $^{x}H_3^{(1)}(\omega,\omega,\omega)$.

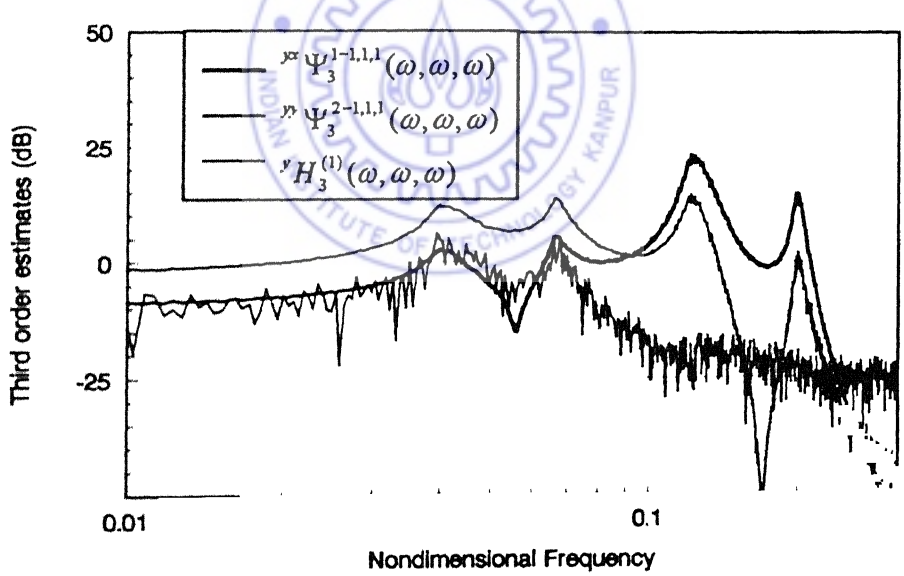

(b) Estimates of $^{yx}\Psi_3^{1-1,1,1}(\omega,\omega,\omega)$, $^{yy}\Psi_3^{2-1,1,1}(\omega,\omega,\omega)$ and $^{y}H_3^{(1)}(\omega,\omega,\omega)$.

Fig. 4.34 Influence of sample size on third order estimates: Case 1(a) (sample size = 1000).

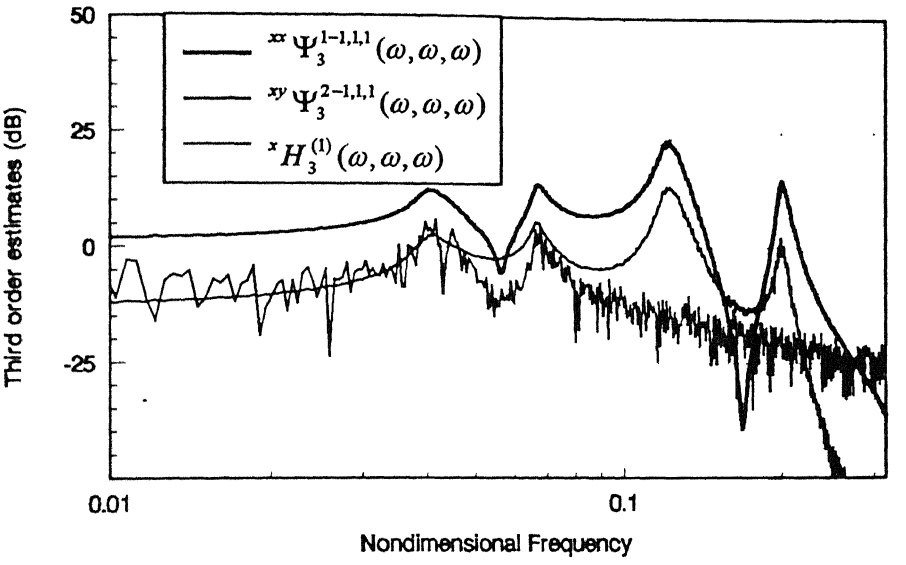

(a) Estimates of $^{xx}\Psi_3^{1-1,1,1}(\omega,\omega,\omega)$, $^{xy}\Psi_3^{2-1,1,1}(\omega,\omega,\omega)$ and $^{x}H_3^{(1)}(\omega,\omega,\omega)$.

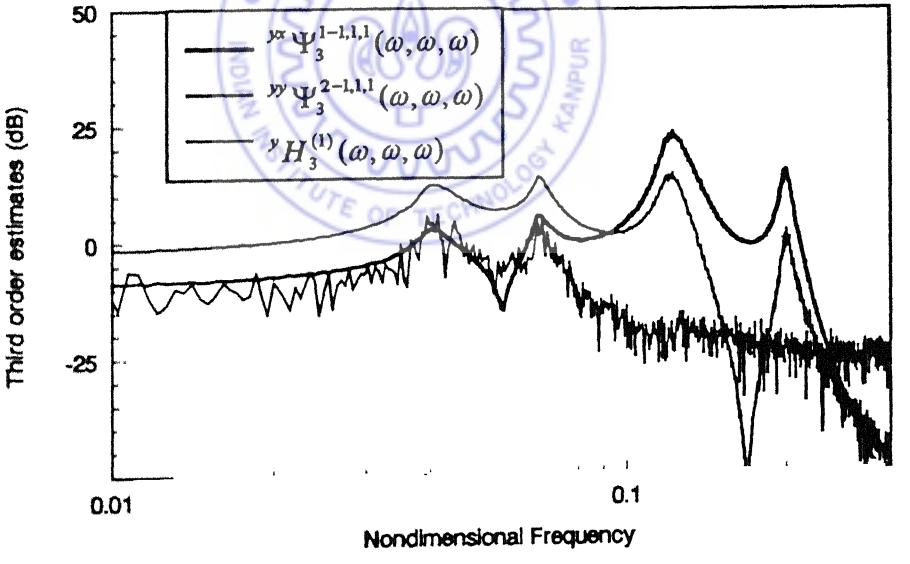

(b) Estimates of $^{yx}\Psi_3^{1-1,1,1}(\omega,\omega,\omega)$, $^{yy}\Psi_3^{2-1,1,1}(\omega,\omega,\omega)$ and $^{y}H_3^{(1)}(\omega,\omega,\omega)$.

Fig. 4.35 Influence of sample size on third order estimates: Case 1(a) (sample size = 1500).

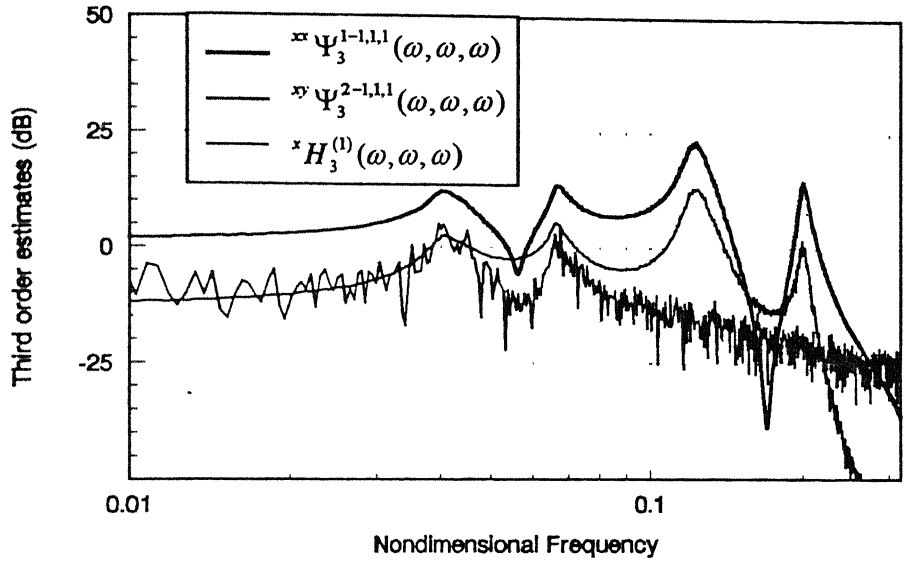

(a) Estimates of $^{xx}\Psi_3^{1-1,1,1}(\omega,\omega,\omega)$, $^{xy}\Psi_3^{2-1,1,1}(\omega,\omega,\omega)$ and $^{x}H_3^{(1)}(\omega,\omega,\omega)$.

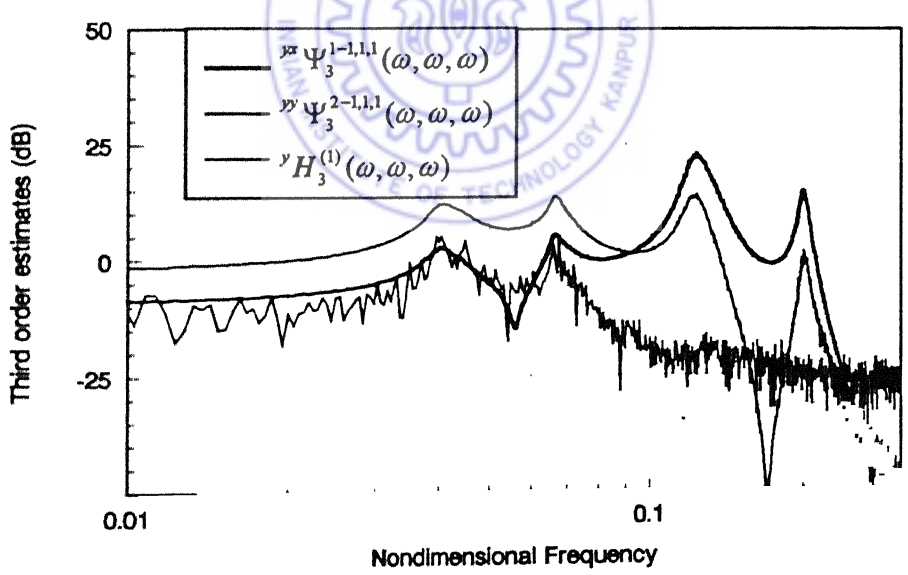

(b) Estimates of $^{yx}\Psi_3^{1-1,1,1}(\omega,\omega,\omega)$, $^{yy}\Psi_3^{2-1,1,1}(\omega,\omega,\omega)$ and $^{y}H_3^{(1)}(\omega,\omega,\omega)$.

Fig. 4.36 Influence of sample size on third order estimates: Case 1(a) (sample size = 2000).

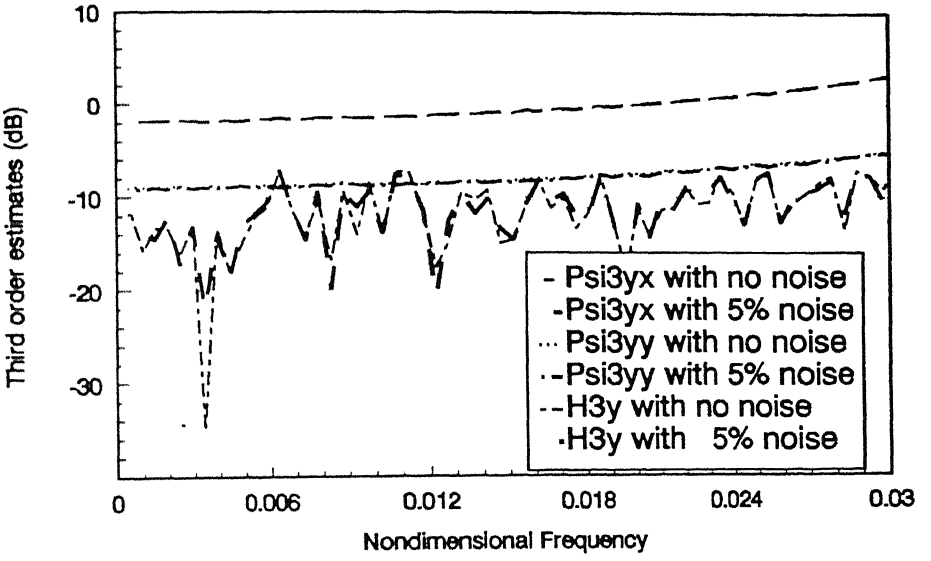

(a) ${}^{yx}\Psi_3^{1-1,1,1}(\omega,\omega,\omega)$, ${}^{yy}\Psi_3^{2-1,1,1}(\omega,\omega,\omega)$, ${}^{y}H_3^{(1)}(\omega,\omega,\omega)$ in the frequency range (0.0-0.03).

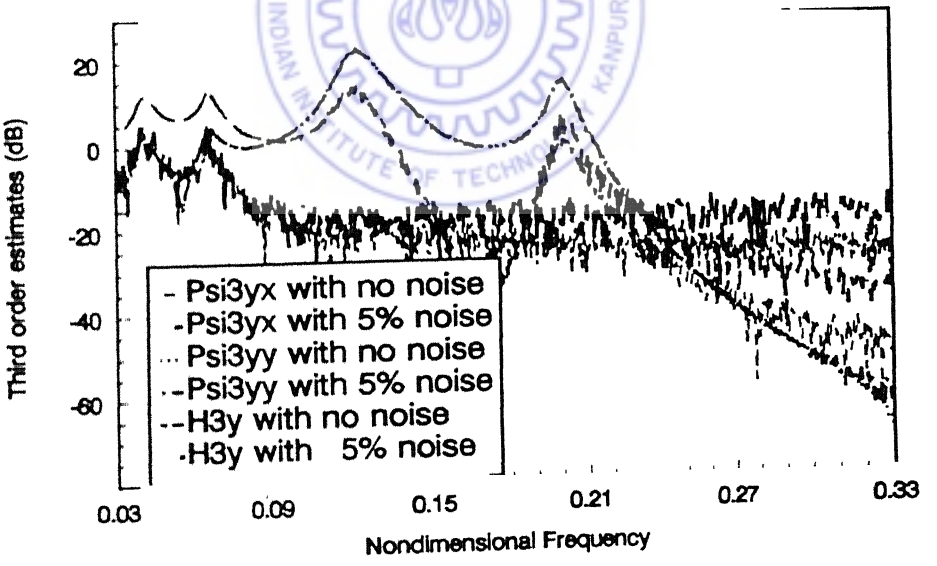

(b) ${}^{yx}\Psi_3^{1-1,1,1}(\omega,\omega,\omega)$, ${}^{yy}\Psi_3^{2-1,1,1}(\omega,\omega,\omega)$, ${}^{y}H_3^{(1)}(\omega,\omega,\omega)$ in the frequency range (0.03-0.33).

Fig. 4.37 Effect of measurement noise on third order estimates: Case 1(a).

Case 1 (a). The figures show the results for two different situations - (a) no measurement noise and (b) 5% random noise in both i. e. input as well as response. (The noise signals are uncorrelated random signals with rms values equal to 5% of the rms values of the excitation force and the response) . In Figures 4.37 (a) and 4.37 (b), the frequency range has been split into two. Fig. 4.37 (a) corresponds to the frequency zone, of interest for parameter estimation, 0.00-0.03 cycles / τ , on a magnified scale. The remaining portions of the curves are shown in Fig. 4.37 (b).

4.6 Remarks

The salient features of the parameter estimation procedure for a rotor-bearing system, with cross-coupling effects in the bearings, are the definitions of cross-kernels, which upon convolution with the excitation represent the response in terms of Volterra or Wiener series. For the nonlinear two-degree-of-freedom problem, Laplace transforms are employed to derive expressions for the first and higher order direct and cross-kernel transforms. The numerical illustration reveals satisfactory performance of the procedure for various nondimensional parameters of the governing equations. Such a study can be usefully employed for design of experiments. The rotor has been treated as a rigid body in this chapter. The case of flexible rotors is discussed next.

CHAPTER 5

PARAMETER ESTIMATION IN FLEXIBLE ROTORS

The case of parameter estimation in flexible rotors is considered in this chapter. In the analysis so far, the rotor is treated as a rigid body and the shaft flexibility is not accounted for. The treatment in this chapter incorporates the influence of shaft flexibility. An attempt has been made to reduce the algebraic complexities by adopting the same rotor-bearing configuration as in Chapters 3 and 4. However, in order that there is no loss of the generality of approach, equations have been written in matrix form. The shaft flexibility has been included in the analysis through influence coefficients concepts. The shaft stiffness is taken to be purely linear with nonlinearity present in the bearing stiffness terms. Bearing cross-coupling effects which have already been discussed in the Chapter 4 has not been included in the analysis. Similarly, damping is treated to be linear with no cross-effects. The parameter estimation procedure follows previously described route of deriving expressions for the first and higher order direct and cross-kernels. These are to be extracted from the excitation force and response measurements. Third order kernel factors synthesised from measured first order kernel transforms are processed along with the measured third order kernel transforms for nonlinear parameter estimation. The procedure is illustrated through numerical simulation.

5.1 Governing Equations And Response

The equations of motion for a balanced rotor with a centrally located disc on a massless flexible shaft supported in bearings, shown in Fig. 5.1 are written as

$$\begin{bmatrix} m_1 & 0 & 0 \\ 0 & m_2 & 0 \\ 0 & 0 & m_3 \end{bmatrix} \begin{Bmatrix} \ddot{x}_1 \\ \ddot{x}_2 \\ \ddot{x}_3 \end{Bmatrix} + \begin{bmatrix} c_{11} & c_{12} & c_{13} \\ c_{21} & c_{22} & c_{23} \\ c_{31} & c_{32} & c_{33} \end{bmatrix} \begin{Bmatrix} \dot{x}_1 \\ \dot{x}_2 \\ \dot{x}_3 \end{Bmatrix} + \begin{bmatrix} k_{11} + k_{b_1}^{L} & k_{12} & k_{13} \\ k_{21} & k_{22} + k_{b_2}^{L} & k_{23} \\ k_{31} & k_{32} & k_{33} \end{bmatrix} \begin{Bmatrix} x_1 \\ x_2 \\ x_3 \end{Bmatrix}$$
$$+ \begin{bmatrix} k_{b_1}^{N} & 0 & 0 \\ 0 & k_{b_2}^{N} & 0 \\ 0 & 0 & 0 \end{bmatrix} \begin{Bmatrix} x_1^3 \\ x_2^3 \\ x_3^3 \end{Bmatrix} = \begin{Bmatrix} f_1(t) \\ f_2(t) \\ 0 \end{Bmatrix} \tag{5.1}$$

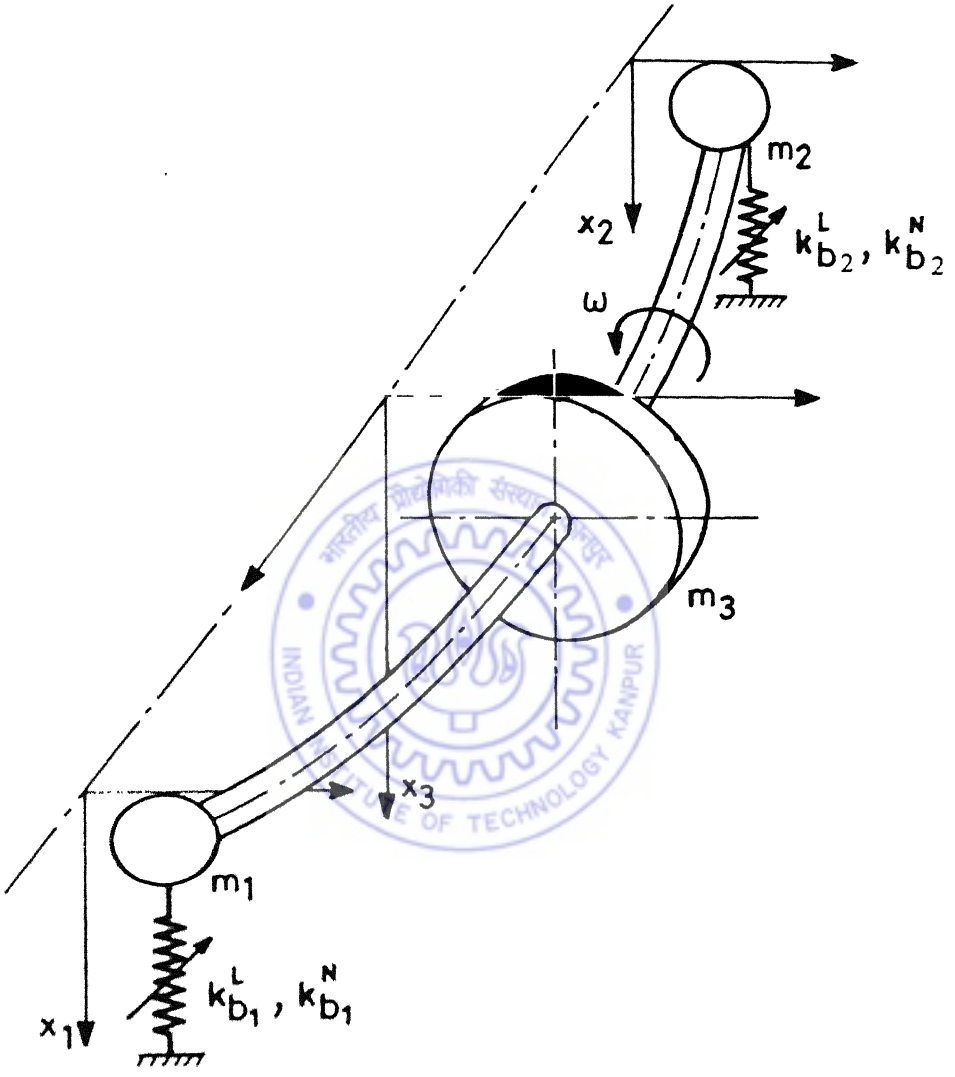

Figure 5.1 Flexible rotor in bearings.

In equation (5.1) m_1, m_2, m_3 are the system masses at stations 1, 2, and 3 respectively. The external white noise excitation provided at the stations 1 and 2 are $f_1(t)$, $f_2(t)$. $k_{b_1}^L$, $k_{b_2}^L$ are the unknown linear stiffness terms of the two bearings and $k_{b_1}^N$ and $k_{b_2}^N$ are their unknown nonlinear stiffness terms. The shaft stiffness parameters are represented by k_{ij} terms, which are defined as the resistive force at the *i*th station corresponding to a unit deflection at the *j*th station, with all other deflections held to zero. The values of the k_{ij} terms can be obtained from the Strength of Materials formulae. c_{11}, c_{12}, c_{13} etc. are linear damping terms .

Defining

$$\tau = pt, \qquad p = \sqrt{k_{33}/m_3};$$

$$^{x_i}\eta(\tau) = x_i / {}^{i}X_{st}, \qquad {}^{i}X_{st} = F_{\max_i}/m_i p^2 \quad ;$$

$$\xi_{ij} = c_{ij}/2m_i p, \qquad \lambda_{ij} = k_{ij}/m_i p^2; \qquad i, j = 1, 2, 3$$

and (5.2)

$$\bar{f}_i(\tau) = f_i(\tau)/F_{\max_i}, \qquad \lambda_{b_i}^L = k_{b_i}^L/m_i p^2, \qquad \lambda_{b_i}^N = k_{b_i}^N F_{\max}^2/m_i^3 p^6;$$

for i=1, 2

and considering only the direct damping terms, in order to keep the algebra simple equation (5.1) reduces to

$$\begin{Bmatrix} {}^{x_1}\eta'' \\ {}^{x_2}\eta'' \\ {}^{x_3}\eta'' \end{Bmatrix} + 2\begin{bmatrix} \xi_{11} & 0 & 0 \\ 0 & \xi_{22} & 0 \\ 0 & 0 & \xi_{33} \end{bmatrix}\begin{Bmatrix} {}^{x_1}\eta' \\ {}^{x_2}\eta' \\ {}^{x_3}\eta' \end{Bmatrix} + \begin{bmatrix} \lambda_{11}+\lambda_{b_1}^L & \lambda_{12} & \lambda_{13} \\ \lambda_{21} & \lambda_{22}+\lambda_{b_2}^L & \lambda_{23} \\ \lambda_{31} & \lambda_{32} & \lambda_{33} \end{bmatrix}\begin{Bmatrix} {}^{x_1}\eta \\ {}^{x_2}\eta \\ {}^{x_3}\eta \end{Bmatrix} + \begin{bmatrix} \lambda_{b_1}^N & 0 & 0 \\ 0 & \lambda_{b_2}^N & 0 \\ 0 & 0 & 0 \end{bmatrix}\begin{Bmatrix} {}^{x_1}\eta^3 \\ {}^{x_2}\eta^3 \\ {}^{x_3}\eta^3 \end{Bmatrix} = \begin{Bmatrix} \bar{f}_1(\tau) \\ \bar{f}_2(\tau) \\ 0 \end{Bmatrix} \tag{5.3}$$

The solution of the equation (5.3) is represented in terms of Volterra operators as

$$^{\kappa}\eta(\tau) = {}^{\kappa}H\left[\bar{f}_1(\tau), \bar{f}_2(\tau)\right] = \sum_{n=1}^{\infty} {}^{\kappa}H_n\left[\bar{f}_1(\tau), \bar{f}_2(\tau)\right] \tag{5.4}$$

with κ denoting x_1, x_2 or x_3.

Further,

$$ {}^{\kappa}H\left[\bar{f}_1(\tau),\bar{f}_2(\tau)\right]={}^{\kappa}H_0+\sum_{i=1,2}{}^{\kappa}H_1^{(i)}[\bar{f}_i(\tau)]+\sum_{i=1,2;j=1,2}{}^{\kappa}H_2^{(i,j)}[\bar{f}_i(\tau),\bar{f}_j(\tau)] + \sum_{i=1,2;j=1,2;k=1,2}{}^{\kappa}H_3^{(i,j,k)}[\bar{f}_i(\tau),\bar{f}_j(\tau)\bar{f}_k(\tau)]+..... \tag{5.5} $$

and the individual operators are given in kernel form by

$$ {}^{\kappa}H_1^{(i)}[\bar{f}_i(\tau)]=\int_{-\infty}^{\infty}{}^{\kappa}h_1^{(i)}(\tau)\bar{f}_i(\tau-\tau_1)d\tau_1 \qquad \text{for } i=1,2 $$

$$ {}^{\kappa}H_2^{(i,j)}[\bar{f}_i(\tau),\bar{f}_j(\tau)]=\int_{-\infty}^{\infty}\int_{-\infty}^{\infty}{}^{\kappa}h_2^{(i,j)}(\tau_1,\tau_2)\bar{f}_i(\tau-\tau_1)\bar{f}_j(\tau-\tau_2)d\tau_1 d\tau_2 \tag{5.6} $$

$$ \text{for } i=1,2;\ j=1,2 $$

$$ {}^{\kappa}H_3^{(i,j,k)}[\bar{f}_i(\tau),\bar{f}_j(\tau),\bar{f}_k(\tau)]=\int_{-\infty}^{\infty}\int_{-\infty}^{\infty}\int_{-\infty}^{\infty}{}^{\kappa}h_3^{(i,j,k)}(\tau_1,\tau_2,\tau_3)\bar{f}_i(\tau-\tau_1)\bar{f}_j(\tau-\tau_2)\bar{f}_k(\tau-\tau_3) $$

$$ \text{x } d\tau_1\, d\tau_2 d\tau_3 \qquad \text{for } i=1,2;\ j=1,2;\ k=1,2 $$

For convenience, writing the Volterra operators as

$$ {}^{\kappa}\eta_1^{(i)}={}^{\kappa}H_1^{(i)}\left[\bar{f}_i(\tau)\right] $$

$$ {}^{\kappa}\eta_2^{(i,j)}={}^{\kappa}H_2^{(i,j)}\left[\bar{f}_i(\tau),\bar{f}_j(\tau)\right] \tag{5.7} $$

$$ {}^{\kappa}\eta_3^{(i,j,k)}={}^{\kappa}H_3^{(i,j,k)}\left[\bar{f}_i(\tau),\bar{f}_j(\tau),\bar{f}_k(\tau)\right] $$

the response of equation (5.3) can be written as

$$ {}^{\kappa}\eta(\tau)=\sum_{i=1,2}{}^{\kappa}\eta_1^{(i)}+\sum_{i=1,2,j=1,2}{}^{\kappa}\eta_2^{(i,j)}+\sum_{i=1,2;j=1,2;k=1,2}{}^{\kappa}\eta_3^{(i,j,k)}+..... \tag{5.8} $$

5.2 Synthesis of Higher Order Volterra Kernel Factors

The Volterra operators are now determined on the same lines as in the previous chapters. The excitation forces $\bar{f}_1(\tau)$, $\bar{f}_2(\tau)$ are replaced by $c\bar{f}_1(\tau)$ and $c\bar{f}_2(\tau)$ respectively, c being a constant. Noting equations (5.6), the resulting response of the system, becomes

$$ {}^{\kappa}\eta(\tau)=\sum_{i=1,2}c\,{}^{\kappa}\eta_1^{(i)}+\sum_{i=1,2;j=1,2}c^2\,{}^{\kappa}\eta_2^{(i,j)}+\sum_{i=1,2;j=1,2;k=1,2}c^3\,{}^{\kappa}\eta_3^{(i,j,k)}+..... \tag{5.9} $$

Substituting equations (5.9) and derivatives in equations (5.3), one gets

$$\begin{Bmatrix}\left[\sum_{i=1,2} c^{\,x_1}\eta_1^{(i)''}+\sum_{i=1,2;j=1,2} c^{2\,x_1}\eta_2^{(i,j)''}+\sum_{i=1,2;j=1,2;k=1,2} c^{3\,x_1}\eta_3^{(i,j,k)''}\right]\\ \left[\sum_{i=1,2} c^{\,x_2}\eta_1^{(i)''}+\sum_{i=1,2;j=1,2} c^{2\,x_2}\eta_2^{(i,j)''}+\sum_{i=1,2;j=1,2;k=1,2} c^{3\,x_2}\eta_3^{(i,j,k)''}\right]\\ \left[\sum_{i=1,2} c^{\,x3}\eta_1^{(i)''}+\sum_{i=1,2;j=1,2} c^{2\,x_3}\eta_2^{(i,j)''}+\sum_{i=1,2;j=1,2;k=1,2} c^{3\,x_3}\eta_3^{(i,j,k)''}\right]\end{Bmatrix}$$

$$+2\begin{bmatrix}\xi_{11}&0&0\\0&\xi_{22}&0\\0&0&\xi_{33}\end{bmatrix}\begin{Bmatrix}\left[\sum_{i=1,2} c^{\,x_1}\eta_1^{(i)'}+\sum_{i=1,2;j=1,2} c^{2\,x_1}\eta_2^{(i,j)'}+\sum_{i=1,2;j=1,2;k=1,2} c^{3\,x_1}\eta_3^{(i,j,k)'}\right]\\ \left[\sum_{i=1,2} c^{\,x_2}\eta_1^{(i)'}+\sum_{i=1,2;j=1,2} c^{2\,x_2}\eta_2^{(i,j)'}+\sum_{i=1,2;j=1,2;k=1,2} c^{3\,x_2}\eta_3^{(i,j,k)'}\right]\\ \left[\sum_{i=1,2} c^{\,x3}\eta_1^{(i)'}+\sum_{i=1,2;j=1,2} c^{2\,x_3}\eta_2^{(i,j)'}+\sum_{i=1,2;j=1,2;k=1,2} c^{3\,x_3}\eta_3^{(i,j,k)'}\right]\end{Bmatrix}$$

$$+\begin{bmatrix}\lambda_{11}+\lambda_{b_1}^{L}&\lambda_{12}&\lambda_{13}\\\lambda_{21}&\lambda_{22}+\lambda_{b_2}^{L}&\lambda_{23}\\\lambda_{31}&\lambda_{32}&\lambda_{33}\end{bmatrix}\begin{Bmatrix}\left[\sum_{i=1,2} c^{\,x_1}\eta_1^{(i)}+\sum_{i=1,2;j=1,2} c^{2\,x_1}\eta_2^{(i,j)}+\sum_{i=1,2;j=1,2;k=1,2} c^{3\,x_1}\eta_3^{(i,j,k)}\right]\\ \left[\sum_{i=1,2} c^{\,x_2}\eta_1^{(i)}+\sum_{i=1,2;j=1,2} c^{2\,x_2}\eta_2^{(i,j)}+\sum_{i=1,2;j=1,2;k=1,2} c^{3\,x_2}\eta_3^{(i,j,k)}\right]\\ \left[\sum_{i=1,2} c^{\,x3}\eta_1^{(i)}+\sum_{i=1,2;j=1,2} c^{2\,x_3}\eta_2^{(i,j)}+\sum_{i=1,2;j=1,2;k=1,2} c^{3\,x_3}\eta_3^{(i,j,k)}\right]\end{Bmatrix}$$

$$+\begin{bmatrix}\lambda_{b_1}^{N}&0&0\\0&\lambda_{b_2}^{N}&0\\0&0&0\end{bmatrix}\begin{Bmatrix}\left[\sum_{i=1,2} c^{\,x_1}\eta_1^{(i)}+\sum_{i=1,2;j=1,2} c^{2\,x_1}\eta_2^{(i,j)}+\sum_{i=1,2;j=1,2;k=1,2} c^{3\,x_1}\eta_3^{(i,j,k)}\right]^3\\ \left[\sum_{i=1,2} c^{\,x_2}\eta_1^{(i)}+\sum_{i=1,2;j=1,2} c^{2\,x_2}\eta_2^{(i,j)}+\sum_{i=1,2;j=1,2;k=1,2} c^{3\,x_2}\eta_3^{(i,j,k)}\right]^3\\ \left[\sum_{i=1,2} c^{\,x3}\eta_1^{(i)}+\sum_{i=1,2;j=1,2} c^{2\,x_3}\eta_2^{(i,j)}+\sum_{i=1,2;j=1,2;k=1,2} c^{3\,x_3}\eta_3^{(i,j,k)}\right]^3\end{Bmatrix}=c\begin{Bmatrix}\bar{f}_1(\tau)\\\bar{f}_2(\tau)\\0\end{Bmatrix} \tag{5.10}$$

Summing up the responses of equal order, as follows

I order response $\quad {}^{\kappa}\eta_1 = \sum_{i=1,2} {}^{\kappa}\eta_1^{(i)}$

II order response $\quad {}^{\kappa}\eta_2 = \sum_{i=1,2;j=1,2} {}^{\kappa}\eta_2^{(i,j)}$

III order response $\quad {}^{\kappa}\eta_3 = \sum_{i=1,2;j=1,2;k=1,2} {}^{\kappa}\eta_3^{(i,j,k)}$; $\quad \kappa$ being x_1, x_2, x_3 (5.11)

Noting the following symmetry of kernels (Schetzen, 1980)

$${}^{\kappa}\eta_2^{(i,j)} = {}^{\kappa}\eta_2^{(j,i)}; \quad {}^{\kappa}\eta_3^{(i,j,j)} = {}^{\kappa}\eta_3^{(j,i,j)} = {}^{\kappa}\eta_3^{(j,j,i)} \text{ ; etc.} \tag{5.12}$$

and using equations (5.11)-(5.12), equations (5.10) are written in condensed form as,

$$\begin{Bmatrix} \left[c^{\,x_1}\eta_1'' + c^2\,{}^{x_1}\eta_2'' + c^3\,{}^{x_1}\eta_3''\right] \\ \left[c^{\,x_2}\eta_1'' + c^2\,{}^{x_2}\eta_2'' + c^3\,{}^{x_2}\eta_3''\right] \\ \left[c^{\,x_3}\eta_1'' + c^2\,{}^{x_3}\eta_2'' + c^3\,{}^{x_3}\eta_3''\right] \end{Bmatrix} + 2\begin{bmatrix} \xi_{11} & 0 & 0 \\ 0 & \xi_{22} & 0 \\ 0 & 0 & \xi_{33} \end{bmatrix} \begin{Bmatrix} \left[c^{\,x_1}\eta_1' + c^2\,{}^{x_1}\eta_2' + c^3\,{}^{x_1}\eta_3'\right] \\ \left[c^{\,x_2}\eta_1' + c^2\,{}^{x_2}\eta_2' + c^3\,{}^{x_2}\eta_3'\right] \\ \left[c^{\,x_3}\eta_1' + c^2\,{}^{x_3}\eta_2' + c^3\,{}^{x_3}\eta_3'\right] \end{Bmatrix}$$

$$+ \begin{bmatrix} \lambda_{11} + \lambda_{b_1}^L & \lambda_{12} & \lambda_{13} \\ \lambda_{21} & \lambda_{22} + \lambda_{b_2}^L & \lambda_{23} \\ \lambda_{31} & \lambda_{32} & \lambda_{33} \end{bmatrix} \begin{Bmatrix} \left[c^{\,x_1}\eta_1 + c^2\,{}^{x_1}\eta_2 + c^3\,{}^{x_1}\eta_3\right] \\ \left[c^{\,x_2}\eta_1 + c^2\,{}^{x_2}\eta_2 + c^3\,{}^{x_2}\eta_3\right] \\ \left[c^{\,x_3}\eta_1 + c^2\,{}^{x_3}\eta_2 + c^3\,{}^{x_3}\eta_3\right] \end{Bmatrix}$$

$$+ \begin{bmatrix} \lambda_{b_1}^N & 0 & 0 \\ 0 & \lambda_{b_2}^N & 0 \\ 0 & 0 & 0 \end{bmatrix} \begin{Bmatrix} \left[c^{\,x_1}\eta_1 + c^2\,{}^{x_1}\eta_2 + c^3\,{}^{x_1}\eta_3\right]^3 \\ \left[c^{\,x_2}\eta_1 + c^2\,{}^{x_2}\eta_2 + c^3\,{}^{x_2}\eta_3\right]^3 \\ \left[c^{\,x_3}\eta_1 + c^2\,{}^{x_3}\eta_2 + c^3\,{}^{x_3}\eta_3\right]^3 \end{Bmatrix} = c\begin{Bmatrix} \bar{f}_1(\tau) \\ \bar{f}_2(\tau) \\ 0 \end{Bmatrix} \tag{5.13}$$

Equations (5.13) are power series in c with coefficients of c^n being ${}^{x_1}\eta_n$, ${}^{x_2}\eta_n$ or ${}^{x_3}\eta_n$ (n = 1,2,3). The responses, ${}^{x_1}\eta_n$, ${}^{x_2}\eta_n$ and ${}^{x_3}\eta_n$ are determined by equating the like powers of c as follows

c^i terms:

$$\begin{Bmatrix} {}^{x_1}\eta_1'' \\ {}^{x_2}\eta_1'' \\ {}^{x_3}\eta_1'' \end{Bmatrix} + 2\begin{bmatrix} \xi_{11} & 0 & 0 \\ 0 & \xi_{22} & 0 \\ 0 & 0 & \xi_{33} \end{bmatrix} \begin{Bmatrix} {}^{x_1}\eta_1' \\ {}^{x_2}\eta_1' \\ {}^{x_3}\eta_1' \end{Bmatrix} + \begin{bmatrix} \lambda_{11} + \lambda_{b_1}^L & \lambda_{12} & \lambda_{13} \\ \lambda_{21} & \lambda_{22} + \lambda_{b_2}^L & \lambda_{23} \\ \lambda_{31} & \lambda_{32} & \lambda_{33} \end{bmatrix} \begin{Bmatrix} {}^{x_1}\eta_1 \\ {}^{x_2}\eta_1 \\ {}^{x_3}\eta_1 \end{Bmatrix} = \begin{Bmatrix} \bar{f}_1(\tau) \\ \bar{f}_2(\tau) \\ 0 \end{Bmatrix} \tag{5.14}$$

c^2 terms:

$$\begin{Bmatrix} {}^{x_1}\eta_2'' \\ {}^{x_2}\eta_2'' \\ {}^{x_3}\eta_2'' \end{Bmatrix} + 2\begin{bmatrix} \xi_{11} & 0 & 0 \\ 0 & \xi_{22} & 0 \\ 0 & 0 & \xi_{33} \end{bmatrix}\begin{Bmatrix} {}^{x_1}\eta_2' \\ {}^{x_2}\eta_2' \\ {}^{x_3}\eta_2' \end{Bmatrix} + \begin{bmatrix} \lambda_{11}+\lambda_{b_1}^L & \lambda_{12} & \lambda_{13} \\ \lambda_{21} & \lambda_{22}+\lambda_{b_2}^L & \lambda_{23} \\ \lambda_{31} & \lambda_{32} & \lambda_{33} \end{bmatrix}\begin{Bmatrix} {}^{x_1}\eta_2 \\ {}^{x_2}\eta_2 \\ {}^{x_3}\eta_2 \end{Bmatrix} = \begin{Bmatrix} 0 \\ 0 \\ 0 \end{Bmatrix} \tag{5.15}$$

c^3 terms:

$$\begin{Bmatrix} {}^{x_1}\eta_3'' \\ {}^{x_2}\eta_3'' \\ {}^{x_3}\eta_3'' \end{Bmatrix} + 2\begin{bmatrix} \xi_{11} & 0 & 0 \\ 0 & \xi_{22} & 0 \\ 0 & 0 & \xi_{33} \end{bmatrix}\begin{Bmatrix} {}^{x_1}\eta_3' \\ {}^{x_2}\eta_3' \\ {}^{x_3}\eta_3' \end{Bmatrix} + \begin{bmatrix} \lambda_{11}+\lambda_{b_1}^L & \lambda_{12} & \lambda_{13} \\ \lambda_{21} & \lambda_{22}+\lambda_{b_2}^L & \lambda_{23} \\ \lambda_{31} & \lambda_{32} & \lambda_{33} \end{bmatrix}\begin{Bmatrix} {}^{x_1}\eta_3 \\ {}^{x_2}\eta_3 \\ {}^{x_3}\eta_3 \end{Bmatrix} + \begin{bmatrix} \lambda_{b_1}^N & 0 & 0 \\ 0 & \lambda_{b_2}^N & 0 \\ 0 & 0 & 0 \end{bmatrix}\begin{Bmatrix} {}^{x_1}\eta_1^3 \\ {}^{x_2}\eta_1^3 \\ {}^{x_3}\eta_1^3 \end{Bmatrix} = \begin{Bmatrix} 0 \\ 0 \\ 0 \end{Bmatrix} \tag{5.16}$$

Equations (5.14)-(5.16) can be solved sequentially. Taking Laplace transforms of equations (5.14), for zero initial conditions, one obtains

$$[\mathrm{M}]\{\eta_1(s)\} = \{F(s)\}$$

with

$$[\mathrm{M}] = \begin{bmatrix} s^2+2\xi_{11}s+\lambda_{11}+\lambda_{b_1}^L & \lambda_{12} & \lambda_{13} \\ \lambda_{21} & s^2+2\xi_{22}s+\lambda_{22}+\lambda_{b_2}^L & \lambda_{23} \\ \lambda_{31} & \lambda_{32} & s^2+2\xi_{33}s+\lambda_{33} \end{bmatrix}$$

$$\{\eta_1(s)\} = \begin{Bmatrix} {}^{x_1}\eta_1(s) \\ {}^{x_2}\eta_1(s) \\ {}^{x_3}\eta_1(s) \end{Bmatrix} \quad \text{and} \quad \{\mathrm{F(s)}\} = \begin{Bmatrix} F_1(s) \\ F_2(s) \\ 0 \end{Bmatrix} \tag{5.17}$$

The solution for ${}^{x_1}\eta_1(s)$, ${}^{x_2}\eta_1(s)$ and ${}^{x_3}\eta_1(s)$, from the above is,

$$\{\eta_1(s)\} = [\mathrm{H}]\{F(s)\} \tag{5.18}$$

where, the kernel transform matrix

$$[\mathrm{H}] = [\mathrm{M}]^{-1} \tag{5.19}$$

whose individual elements can be worked out to be

$$[\mathrm{H}]=\begin{bmatrix} {}^{x_1}H_1^{(1)}(s) & {}^{x_1}H_1^{(2)}(s) & {}^{x_1}H_1^{(3)}(s) \\ {}^{x_2}H_1^{(1)}(s) & {}^{x_2}H_1^{(2)}(s) & {}^{x_2}H_1^{(3)}(s) \\ {}^{x_3}H_1^{(1)}(s) & {}^{x_3}H_1^{(2)}(s) & {}^{x_3}H_1^{(3)}(s) \end{bmatrix}$$

$$\begin{aligned}
{}^{x_1}H_1^{(1)}(s) &= (-\lambda_{23}\lambda_{32}+(s^2+2s\xi_{22}+\lambda_{22}+\lambda_{b_2}^L)(s^2+2s\xi_{33}+\lambda_{33}))/D \\
{}^{x_1}H_1^{(2)}(s) &= (\lambda_{13}\lambda_{32}-\lambda_{12}(s^2+2s\xi_{33}+\lambda_{33}))/D \\
{}^{x_1}H_1^{(3)}(s) &= (-\lambda_{13}(s^2+2s\xi_{22}+\lambda_{22}+\lambda_{b_2}^L)+\lambda_{12}\lambda_{23})/D \\
{}^{x_2}H_1^{(1)}(s) &= (\lambda_{23}\lambda_{31}-\lambda_{21}(s^2+2s\xi_{33}+\lambda_{33}))/D \\
{}^{x_2}H_1^{(2)}(s) &= (-\lambda_{13}\lambda_{31}+(s^2+2s\xi_{11}+\lambda_{11}+\lambda_{b_1}^L)(s^2+2s\xi_{33}+\lambda_{33}))/D \\
{}^{x_2}H_1^{(3)}(s) &= (\lambda_{13}\lambda_{21}-(s^2+2s\xi_{11}+\lambda_{11}+\lambda_{b_1}^L)\lambda_{23})/D \\
{}^{x_3}H_1^{(1)}(s) &= (-(s^2+2s\xi_{22}+\lambda_{22}+\lambda_{b_2}^L)\lambda_{31}+\lambda_{21}\lambda_{32})/D \\
{}^{x_3}H_1^{(2)}(s) &= (\lambda_{12}\lambda_{31}-(s^2+2s\xi_{11}+\lambda_{11}+\lambda_{b_1}^L)\lambda_{32})/D \\
{}^{x_3}H_1^{(3)}(s) &= (-\lambda_{12}\lambda_{21}+(s^2+2s\xi_{11}+\lambda_{11}+\lambda_{b_1}^L)(s^2+2s\xi_{22}+\lambda_{22}+\lambda_{b_2}^L))/D
\end{aligned} \tag{5.20}$$

with

$$\begin{aligned}
D = {} & (s^2+2s\xi_{11}+\lambda_{11}+\lambda_{b_1}^L)(s^2+2s\xi_{22}+\lambda_{22}+\lambda_{b_2}^L)(s^2+2s\xi_{33}+\lambda_{33}) \\
& -(s^2+2s\xi_{11}+\lambda_{11}+\lambda_{b_1}^L)\lambda_{23}\lambda_{32}-\lambda_{13}(s^2+2s\xi_{22}+\lambda_{22}+\lambda_{b_2}^L)\lambda_{31} \\
& -\lambda_{12}\lambda_{21}(s^2+2s\xi_{33}+\lambda_{33})+\lambda_{12}\lambda_{23}\lambda_{31}+\lambda_{13}\lambda_{21}\lambda_{32}
\end{aligned} \tag{5.21}$$

Taking Laplace transform of the equation (5.15), similarly give

$$\begin{bmatrix} s^2+2s\xi_{11}+\lambda_{11}+\lambda_{b_1}^L & \lambda_{12} & \lambda_{13} \\ \lambda_{21} & s^2+2s\xi_{22}+\lambda_{22}+\lambda_{b_2}^L & \lambda_{23} \\ \lambda_{31} & \lambda_{32} & s^2+2s\xi_{33}+\lambda_{33} \end{bmatrix} \begin{Bmatrix} {}^{x_1}\eta_2(s) \\ {}^{x_2}\eta_2(s) \\ {}^{x_3}\eta_2(s) \end{Bmatrix} = \begin{Bmatrix} 0 \\ 0 \\ 0 \end{Bmatrix} \tag{5.22}$$

which yield

$$\begin{aligned}
{}^{x_1}\eta_2(s) &= 0 \\
{}^{x_2}\eta_2(s) &= 0 \\
{}^{x_3}\eta_2(s) &= 0
\end{aligned} \tag{5.23}$$

which shows that the second order kernel is identically zero i.e.,

$${}^{x_1}h_2(\tau_1,\tau_2)={}^{x_2}h_2(\tau_1,\tau_2)={}^{x_3}h_2(\tau_1,\tau_2)=0 \tag{5.24}$$

In order to synthesise expressions for third order kernels, equations (5.16) can be written as

$$\begin{Bmatrix} {}^{x_1}\eta_3'' \\ {}^{x_2}\eta_3'' \\ {}^{x_3}\eta_3'' \end{Bmatrix} + 2\begin{bmatrix} \xi_{11} & 0 & 0 \\ 0 & \xi_{22} & 0 \\ 0 & 0 & \xi_{33} \end{bmatrix}\begin{Bmatrix} {}^{x_1}\eta_3' \\ {}^{x_2}\eta_3' \\ {}^{x_3}\eta_3' \end{Bmatrix} + \begin{bmatrix} \lambda_{11}+\lambda_{b_1}^L & \lambda_{12} & \lambda_{13} \\ \lambda_{21} & \lambda_{22}+\lambda_{b_2}^L & \lambda_{23} \\ \lambda_{31} & \lambda_{32} & \lambda_{33} \end{bmatrix}\begin{Bmatrix} {}^{x_1}\eta_3 \\ {}^{x_2}\eta_3 \\ {}^{x_3}\eta_3 \end{Bmatrix} = \begin{Bmatrix} q_1(\tau) \\ q_2(\tau) \\ 0 \end{Bmatrix} \tag{5.25}$$

where the following abbreviations have been used

$$\begin{aligned} q_1(\tau) &= -\lambda_{b_1}^N {}^{x_1}\eta_1^3(\tau) \\ q_2(\tau) &= -\lambda_{b_2}^N {}^{x_2}\eta_1^3(\tau) \end{aligned} \tag{5.26}$$

Equations (5.25) are linear in η_3 terms, similar to equations (5.14) and therefore the solution in terms of Volterra operators as

$$\begin{aligned} {}^{x_1}\eta_3(\tau) &= {}^{x_1}H_1[q_1, q_2] \\ {}^{x_2}\eta_3(\tau) &= {}^{x_2}H_1[q_1, q_2] \\ {}^{x_3}\eta_3(\tau) &= {}^{x_3}H_1[q_1, q_2] \end{aligned} \tag{5.27}$$

that is

$$\begin{aligned} {}^{x_1}H_3[\bar{f}_1(\tau), \bar{f}_2(\tau)] &= {}^{x_1}H_1[q_1, q_2] \\ {}^{x_2}H_3[\bar{f}_1(\tau), \bar{f}_2(\tau)] &= {}^{x_2}H_1[q_1, q_2] \\ {}^{x_3}H_3[\bar{f}_1(\tau), \bar{f}_2(\tau)] &= {}^{x_3}H_1[q_1, q_2] \end{aligned} \tag{5.28}$$

However, since ${}^{x_1}H_1$, ${}^{x_2}H_1$ and ${}^{x_3}H_1$ are linear operators, one obtains

$$\begin{aligned} {}^{x_1}\eta_3(\tau) &= {}^{x_1}H_1[q_1, q_2] \\ &= {}^{x_1}H_1^{(1)}[q_1] + {}^{x_1}H_1^{(2)}[q_2] \\ {}^{x_2}\eta_3(\tau) &= {}^{x_2}H_1[q_1, q_2] \\ &= {}^{x_2}H_1^{(1)}[q_1] + {}^{x_2}H_1^{(2)}[q_2] \\ {}^{x_3}\eta_3(\tau) &= {}^{x_3}H_1[q_1, q_2] \\ &= {}^{x_3}H_1^{(1)}[q_1] + {}^{x_3}H_1^{(2)}[q_2] \end{aligned} \tag{5.29}$$

Noting the abbreviations (5.26), the terms on the right hand side of the above equations, are individually expanded as

$$
\begin{aligned}
{}^{x_1}H_1^{(1)}[q_1] &= {}^{x_1}H_1^{(1)}[(-\lambda_{b_1}^N \; {}^{x_1}\eta_1^3)] \\
&= -\lambda_{b_1}^N \; {}^{x_1}H_1^{(1)}[{}^{x_1}\eta_1^3]
\end{aligned}
\qquad \text{etc.} \qquad (5.30)
$$

In the above equations

$$
\begin{aligned}
{}^{x_1}\eta_1 &= {}^{x_1}\eta_1^{(1)} + {}^{x_1}\eta_1^{(2)} \\
&= {}^{x_1}H_1^{(1)}\left[\bar{f}_1(\tau)\right] + {}^{x_1}H_1^{(2)}\left[\bar{f}_2(\tau)\right] \\
{}^{x_2}\eta_1 &= {}^{x_2}\eta_1^{(1)} + {}^{x_2}\eta_1^{(2)} \\
&= {}^{x_2}H_1^{(1)}\left[\bar{f}_1(\tau)\right] + {}^{x_2}H_1^{(2)}\left[\bar{f}_2(\tau)\right] \\
{}^{x_3}\eta_1 &= {}^{x_3}\eta_1^{(1)} + {}^{x_3}\eta_1^{(2)} \\
&= {}^{x_3}H_1^{(1)}\left[\bar{f}_1(\tau)\right] + {}^{x_3}H_1^{(2)}\left[\bar{f}_2(\tau)\right]
\end{aligned}
\qquad (5.31)
$$

Laplace transforms of equations (5.30) gives

$$
{}^{x_1}H_1^{(1)}[Q_1(s_1,s_2,s_3)] = \lambda_{b_1}^N \left({}^{x_1x_1}\Psi_3^{1-1,1,1} + 3\,{}^{x_1x_1}\Psi_3^{1-1,1,2} + 3\,{}^{x_1x_1}\Psi_3^{1-1,2,2} + {}^{x_1x_1}\Psi_3^{1-2,2,2}\right) \qquad (5.32)
$$

where, ${}^{x_1x_1}\Psi_3^{(i-j,k,l)}(s_1,s_2,s_3)$ is the third order kernel factor which has been defined as

$$
{}^{x_1x_1}\Psi_3^{(i-j,k,l)}(s_1,s_2,s_3) = -\,{}^{x_1}H_1^{(i)}(s_1+s_2+s_3)\,{}^{x_1}H_1^{(j)}(s_1)\;{}^{x_1}H_1^{(k)}(s_2)\;{}^{x_1}H_1^{(l)}(s_3)
$$

$$
i = 1,2\;;\; j = 1,2\;;\; k = 1,2\;;\; l = 1,2 \qquad (5.33)
$$

The third order kernel factors above, can be readily constructed, using equations from the first order kernels ${}^{x_1}H_1^{(1)}(s)$, ${}^{x_1}H_1^{(2)}(s)$, ${}^{x_2}H_1^{(1)}(s)$, ${}^{x_2}H_1^{(2)}(s)$, ${}^{x_3}H_1^{(1)}(s)$, ${}^{x_3}H_1^{(2)}(s)$.

Similarly, the Laplace transforms of other terms on the right hand side of equations (5.29) can be worked out to be

$$
{}^{x_1}H_1^{(2)}[Q_2(s_1,s_2,s_3)] = \lambda_{b_2}^N \left({}^{x_1x_2}\Psi_3^{2-1,1,1} + 3\,{}^{x_1x_2}\Psi_3^{2-1,1,2} + 3\,{}^{x_1x_2}\Psi_3^{2-1,2,2} + {}^{x_1x_2}\Psi_3^{2-2,2,2}\right)
$$

$$
{}^{x_2}H_1^{(1)}[Q_1(s_1,s_2,s_3)] = \lambda_{b_1}^N \left({}^{x_2x_1}\Psi_3^{1-1,1,1} + 3\,{}^{x_2x_1}\Psi_3^{1-1,1,2} + 3\,{}^{x_2x_1}\Psi_3^{1-1,2,2} + {}^{x_2x_1}\Psi_3^{1-2,2,2}\right)
$$

$$
{}^{x_2}H_1^{(2)}[Q_2(s_1,s_2,s_3)] = \lambda_{b_2}^N \left({}^{x_2x_2}\Psi_3^{2-1,1,1} + 3\,{}^{x_2x_2}\Psi_3^{2-1,1,2} + 3\,{}^{x_2x_2}\Psi_3^{2-1,2,2} + {}^{x_2x_2}\Psi_3^{2-2,2,2}\right)
$$

$$
{}^{x_3}H_1^{(1)}[Q_1(s_1,s_2,s_3)] = \lambda_{b_1}^N \left({}^{x_3x_1}\Psi_3^{1-1,1,1} + 3\ {}^{x_3x_1}\Psi_3^{1-1,1,2} + 3\ {}^{x_3x_1}\Psi_3^{1-1,2,2} + {}^{x_3x_1}\Psi_3^{1-2,2,2}\right)
$$

$$
{}^{x_3}H_1^{(2)}[Q_2(s_1,s_2,s_3)] = \lambda_{b_2}^N \left({}^{x_3x_2}\Psi_3^{2-1,1,1} + 3\ {}^{x_3x_2}\Psi_3^{2-1,1,2} + 3\ {}^{x_3x_2}\Psi_3^{2-1,2,2} + {}^{x_3x_2}\Psi_3^{2-2,2,2}\right)
\tag{5.34}
$$

In equations (5.34), the following third order kernel factors have been used in addition to those defined in equation (5.33).

$$
{}^{x_2x_2}\Psi_3^{(i-j,k,l)}(s_1,s_2,s_3) = -\ {}^{x_2}H_1^{(i)}(s_1+s_2+s_3)\,{}^{x_2}H_1^{(j)}(s_1)\ {}^{x_2}H_1^{(k)}(s_2)\ {}^{x_2}H_1^{(l)}(s_3)
$$

$$
{}^{x_2x_1}\Psi_3^{(l-i,j,k)}(s_1,s_2,s_3) = -\ {}^{x_2}H_1^{(l)}(s_1+s_2+s_3)\,{}^{x_1}H_1^{(i)}(s_1)\ {}^{x_1}H_1^{(j)}(s_2)\ {}^{x_1}H_1^{(k)}(s_3)
$$

$$
{}^{x_3x_1}\Psi_3^{(i-j,k,l)}(s_1,s_2,s_3) = -\ {}^{x_3}H_1^{(i)}(s_1+s_2+s_3)\,{}^{x_1}H_1^{(j)}(s_1)\ {}^{x_1}H_1^{(k)}(s_2)\ {}^{x_1}H_1^{(l)}(s_3)
$$

$$
{}^{x_3x_2}\Psi_3^{(l-i,j,k)}(s_1,s_2,s_3) = -\ {}^{x_3}H_1^{(l)}(s_1+s_2+s_3)\,{}^{x_2}H_1^{(i)}(s_1)\ {}^{x_2}H_1^{(j)}(s_2)\ {}^{x_2}H_1^{(k)}(s_3)
$$

$$
i = 1,2\ ;\ j = 1,2\ ;\ k = 1,2\ ;\ l = 1,2 \tag{5.35}
$$

The Laplace transforms of the third order kernels (equations (5.28)), can now be expressed as

$$
\begin{aligned}
{}^{x_1}H_3(s_1,s_2,s_3) &= \lambda_{b_1}^N \left({}^{x_1x_1}\Psi_3^{1-1,1,1} + 3\ {}^{x_1x_1}\Psi_3^{1-1,1,2} + 3\ {}^{x_1x_1}\Psi_3^{1-1,2,2} + {}^{x_1x_1}\Psi_3^{1-2,2,2}\right) \\
&\quad + \lambda_{b_2}^N \left({}^{x_1x_2}\Psi_3^{2-1,1,1} + 3\ {}^{x_1x_2}\Psi_3^{2-1,1,2} + 3\ {}^{x_1x_2}\Psi_3^{2-1,2,2} + {}^{x_1x_2}\Psi_3^{2-2,2,2}\right) \\
{}^{x_2}H_3(s_1,s_2,s_3) &= \lambda_{b_1}^N \left({}^{x_2x_1}\Psi_3^{1-1,1,1} + 3\ {}^{x_2x_1}\Psi_3^{1-1,1,2} + 3\ {}^{x_2x_1}\Psi_3^{1-1,2,2} + {}^{x_2x_1}\Psi_3^{1-2,2,2}\right) \\
&\quad + \lambda_{b_2}^N \left({}^{x_2x_2}\Psi_3^{2-1,1,1} + 3\ {}^{x_2x_2}\Psi_3^{2-1,1,2} + 3\ {}^{x_2x_2}\Psi_3^{2-1,2,2} + {}^{x_2x_2}\Psi_3^{2-2,2,2}\right) \\
{}^{x_3}H_3(s_1,s_2,s_3) &= \lambda_{b_1}^N \left({}^{x_3x_1}\Psi_3^{1-1,1,1} + 3\ {}^{x_3x_1}\Psi_3^{1-1,1,2} + 3\ {}^{x_3x_1}\Psi_3^{1-1,2,2} + {}^{x_3x_1}\Psi_3^{1-2,2,2}\right) \\
&\quad + \lambda_{b_2}^N \left({}^{x_3x_2}\Psi_3^{2-1,1,1} + 3\ {}^{x_3x_2}\Psi_3^{2-1,1,2} + 3\ {}^{x_3x_2}\Psi_3^{2-1,2,2} + {}^{x_3x_2}\Psi_3^{2-2,2,2}\right)
\end{aligned}
\tag{5.36}
$$

5.3 Measurement of Wiener Kernels

As stated in Chapters 3 and 4, measurement of individual Volterra kernels is not possible, while equivalent Wiener kernels can be extracted from the measured response if the excitation to the system is white and Gaussian. These Wiener kernels can then be used to generate the Volterra kernels.

In the present case, the Wiener kernels of the nonlinear system are extracted by application of white Gaussian forces $\bar{f}_1(\tau)$ and $\bar{f}_2(\tau)$, one at a time, i.e. first a white Gaussian force $\bar{f}_1(\tau)$ with variance A_1, is applied at station 1, while keeping the force at station 2, $\bar{f}_2(\tau) = 0$. The resulting responses ${}^{x_1}\eta$, ${}^{x_2}\eta$ and ${}^{x_3}\eta$ are employed to extract the direct, $x_1 - x_1$-(at station 1), Wiener kernels and the cross (x_1-x_2 and x_1-x_3) kernels. In the next instance, a white Gaussian force $\bar{f}_2(\tau)$ with variance A_2, is applied at station 2, while keeping the force, $\bar{f}_1(\tau) = 0$. The system responses, in this instance, are employed to extract the direct x_2-coordinate Wiener kernels and the cross (x_2-x_1, x_2-x_3) kernels.

The system response, in terms of Wiener kernels, is now expressed, in the two individual cases as -

$\bar{f}_1(\tau)$ Gaussian white, with variance A_1 and $\bar{f}_2(\tau) = 0$:

$$\begin{aligned} {}^{x_1}\eta(\tau) &= {}^{x_1}W\left[\bar{f}_1(\tau),\ 0\right] = {}^{x_1}W\left[\bar{f}_1(\tau)\right] \\ {}^{x_2}\eta(\tau) &= {}^{x_2}W\left[\bar{f}_1(\tau),\ 0\right] = {}^{x_2}W\left[\bar{f}_1(\tau)\right] \\ {}^{x_3}\eta(\tau) &= {}^{x_3}W\left[\bar{f}_1(\tau),\ 0\right] = {}^{x_3}W\left[\bar{f}_1(\tau)\right] \end{aligned} \tag{5.37}$$

$\bar{f}_2(\tau)$ Gaussian white, with variance A_2 and $\bar{f}_1(\tau) = 0$:

$$\begin{aligned} {}^{x_1}\eta(\tau) &= {}^{x_1}W\left[0,\ \bar{f}_2(\tau)\right] = {}^{x_1}W\left[\bar{f}_2(\tau)\right] \\ {}^{x_2}\eta(\tau) &= {}^{x_2}W\left[0,\ \bar{f}_2(\tau)\right] = {}^{x_2}W\left[\bar{f}_2(\tau)\right] \\ {}^{x_3}\eta(\tau) &= {}^{x_3}W\left[0,\ \bar{f}_2(\tau)\right] = {}^{x_3}W\left[\bar{f}_2(\tau)\right] \end{aligned} \tag{5.38}$$

In equations (5.37)-(5.38), the Wiener operators are

$${}^{\kappa}W\left[\bar{f}_i(\tau)\right] = {}^{\kappa}W_0 + {}^{\kappa}W_1^{(i)}[\bar{f}_i(\tau)] + {}^{\kappa}W_2^{(i)}[\bar{f}_i(\tau)] + {}^{\kappa}W_3^{(i)}[\bar{f}_i(\tau)] + \ldots\ldots\ldots \tag{5.39}$$

(with κ denoting x_1, x_2 or x_3 for $i = 1$ or 2)

and the individual operators are given in kernel form by

$$
\begin{aligned}
{}^{\kappa}W_1^{(i)}[\bar{f}_i(\tau)] &= \int_{-\infty}^{\infty} {}^{\kappa}w_1^{(i)}(\tau_1)\bar{f}_i(\tau-\tau_1)d\tau_1 \\
{}^{\kappa}W_2^{(i)}[\bar{f}_i(\tau)] &= \int_{-\infty}^{\infty}\int_{-\infty}^{\infty} {}^{\kappa}w_2^{(i)}(\tau_1,\tau_2)\bar{f}_i(\tau-\tau_1)\bar{f}_i(\tau-\tau_2)d\tau_1 d\tau_2 - A_i\int_{-\infty}^{\infty} {}^{\kappa}w_2^{(i)}(\tau_2,\tau_2)d\tau_2 \\
{}^{\kappa}W_3^{(i)}[\bar{f}_i(\tau)] &= \int_{-\infty}^{\infty}\int_{-\infty}^{\infty}\int_{-\infty}^{\infty} {}^{\kappa}w_3^{(i)}(\tau_1,\tau_2,\tau_3)\bar{f}_i(\tau-\tau_1)\bar{f}_i(\tau-\tau_2)\bar{f}_i(\tau-\tau_3)\ d\tau_1\, d\tau_2 d\tau_3 \\
&\quad -3A_i\int_{-\infty}^{\infty}\int_{-\infty}^{\infty} {}^{\kappa}w_3^{(i)}(\tau_1,\tau_2,\tau_2)\bar{f}_i(\tau-\tau_1)\,d\tau_1\, d\tau_2
\end{aligned}
\tag{5.40}
$$

The relationship between the Volterra kernels of equations (5.6) and the Wiener kernels above, is the same as written in the previous chapter (for a third order response representation). These relationships are reproduced below.

$$
\begin{aligned}
{}^{\kappa}h_3^{(i)}(\tau_1,\tau_2,\tau_3) &= {}^{\kappa}w_3^{(i)}(\tau_1,\tau_2,\tau_3) \\
{}^{\kappa}h_2^{(i)}(\tau_1,\tau_2) &= {}^{\kappa}w_2^{(i)}(\tau_1,\tau_2) \\
{}^{\kappa}h_1^{(i)}(\tau_1) &= {}^{\kappa}w_1^{(i)}(\tau_1) + {}^{\kappa}w_{1(3)}^{(i)}(\tau_1) \\
{}^{\kappa}h_0 &= {}^{\kappa}w_0 + {}^{\kappa}w_{0(2)}
\end{aligned}
\tag{5.41}
$$

with

$$
\begin{aligned}
{}^{\kappa}w_{1(3)}^{(i)}(\tau_1) &= -3A_i\int_{-\infty}^{\infty} {}^{\kappa}w_3^{(i)}(\tau_1,\tau_2,\tau_2)d\tau_2 \\
{}^{\kappa}w_{0(2)}^{(i)}(\tau_1) &= -A_i\int_{-\infty}^{\infty} {}^{\kappa}w_2^{(i)}(\tau_1,\tau_1)d\tau_1
\end{aligned}
\tag{5.42}
$$

Employing the Fourier transform relations and the property of the Dirac-Delta function, $\delta(\omega)$, given in the previous chapter by equations (4.46) and (4.47), the responses (5.37) or (5.38) can be expressed as

$$
\begin{aligned}
{}^{\kappa}\eta(\tau) = {}^{\kappa}W_0 &+ \int_{-\infty}^{\infty} {}^{\kappa}W_1^{(i)}(\omega_1)\bar{F}_i(\omega_1)e^{j\omega_1\tau}d\omega_1 \\
&+ \left[\int_{-\infty}^{\infty}\int_{-\infty}^{\infty} {}^{\kappa}W_2^{(i)}(\omega_1,\omega_2)\bar{F}_i(\omega_1)\bar{F}_i(\omega_2)e^{j(\omega_1+\omega_2)\tau}d\omega_1 d\omega_2 - A_i\int_{-\infty}^{\infty} {}^{\kappa}W_2^{(i)}(\omega_2,-\omega_2)d\omega_2\right] \\
&+ \int_{-\infty}^{\infty}\int_{-\infty}^{\infty}\int_{-\infty}^{\infty} {}^{\kappa}W_3^{(i)}(\omega_1,\omega_2,\omega_3)\bar{F}_i(\omega_1)\bar{F}_i(\omega_2)\bar{F}_i(\omega_3)e^{j(\omega_1+\omega_2+\omega_3)\tau}d\omega_1 d\omega_2 d\omega_3 \\
&- 3A_i\int_{-\infty}^{\infty}\int_{-\infty}^{\infty} {}^{\kappa}W_3^{(i)}(\omega_1,\omega_2,-\omega_2)d\omega_1 d\omega_2\Bigg] \\
&+ \ldots\ldots\ldots\ldots\ldots\ldots \qquad \kappa \text{ being } x_1, x_2 \text{ or } x_3 \text{ and } i = 1,2
\end{aligned}
\tag{5.43}
$$

A complex exponential filter, similar to the one described in previous chapters, has been used for measurement of the individual Wiener kernel transforms. Referring to Fig. 5.2, the output of the filter is

$$
\begin{aligned}
z^{(i)}(\tau) &= \int_{-\infty}^{\infty} e^{j\omega\tau_1}\bar{f}_i(\tau-\tau_1)d\tau_1 \\
&= \bar{F}_i^{*}(\omega)e^{-j\omega\tau_1}
\end{aligned}
\tag{5.44}
$$

and the ensemble averages of the outputs of the circuit, for κ equal to x_1, x_2 and x_3 are,

$$
\begin{aligned}
\left\langle {}^{\kappa}\eta(\tau)z^{(i)}(\tau)\right\rangle = {}^{\kappa}W_0\left\langle \bar{F}_i^{*}(\omega)\right\rangle e^{-j\omega\tau} &+ \int_{-\infty}^{\infty} {}^{\kappa}W_1^{(i)}(\omega_1)\left\langle \bar{F}_i(\omega_1)\bar{F}_i^{*}(\omega)\right\rangle e^{-j\tau(\omega_1-\omega)}d\omega_1 \\
&+ \left[\int_{-\infty}^{\infty}\int_{-\infty}^{\infty} {}^{\kappa}W_2^{(i)}(\omega_1,\omega_2)\left\langle \bar{F}_i(\omega_1)\bar{F}_i(\omega_2)\bar{F}_i^{*}(\omega)\right\rangle e^{-j\tau(\omega_1+\omega_2-\omega)}d\omega_1 d\omega_2\right. \\
&\quad \left. - A_i\left\langle F_i^{*}(\omega)\right\rangle e^{-j\omega_1\tau}\int_{-\infty}^{\infty} {}^{\kappa}W_2^{(i)}(\omega_2,-\omega_2)d\omega_2\right] \\
&+ \left[\int_{-\infty}^{\infty}\int_{-\infty}^{\infty}\int_{-\infty}^{\infty} {}^{\kappa}W_3^{(i)}(\omega_1,\omega_2,\omega_3)\left\langle \bar{F}_i(\omega_1)\bar{F}_i(\omega_2)\bar{F}_i(\omega_3)\bar{F}_i^{*}(\omega)\right\rangle\right. \\
&\quad \left. \times e^{-j\tau(\omega_1+\omega_2+\omega_3-\omega)}d\omega_1 d\omega_2 d\omega_3\right. \\
&\quad \left. - 3A_i\int_{-\infty}^{\infty}\int_{-\infty}^{\infty} {}^{\kappa}W_3^{(i)}(\omega_1,\omega_2,-\omega_2)\left\langle \bar{F}_i(\omega_1)\bar{F}_i^{*}(\omega)\right\rangle e^{-j\tau(\omega_1-\omega)}d\omega_1 d\omega_2\right] \\
&+ \ldots\ldots\ldots\ldots
\end{aligned}
\tag{5.45}
$$

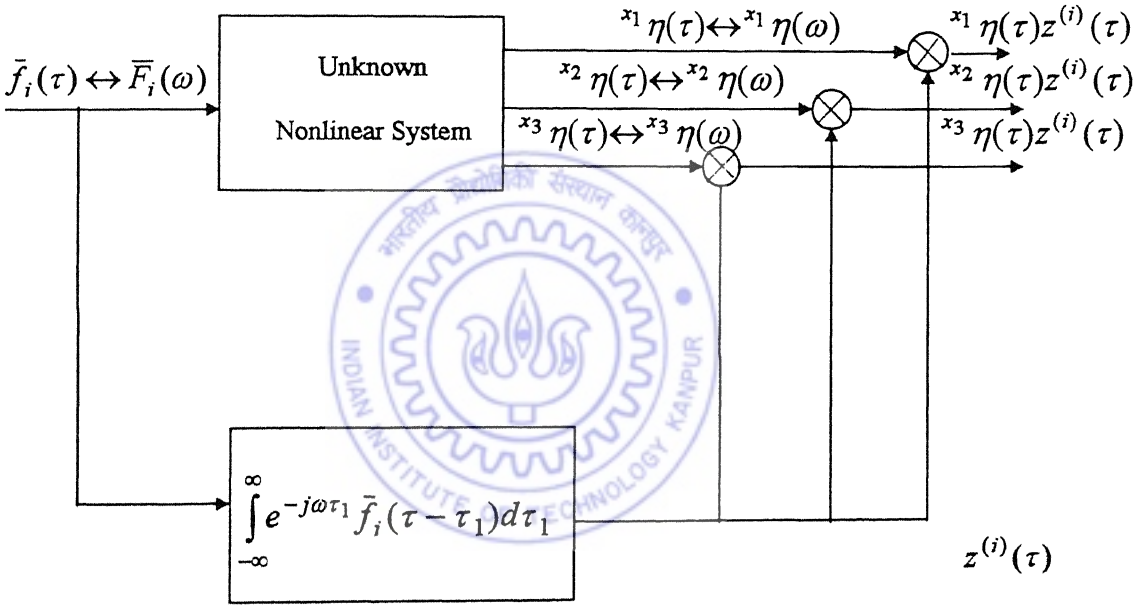

Fig. 5.2 Scheme for evaluation of the first order direct and cross Wiener kernel transforms, ${}^{x}W_1^{(i)}$.

Since $\bar{f}_i(\tau)$ is stationary Gaussian white noise with zero mean and variance A_i, the Fourier transform, $\bar{F}_i(\omega)$, is also a stationary Gaussian white noise process and employing the properties (ref. equation 3.30) of the ensemble averages of these products transformed functions, equations (5.45) get reduced, after some algebra, to

$$\left\langle {}^{\kappa}\eta(\tau)z^{(i)}(\tau)\right\rangle = A_i\, {}^{\kappa}W_1^{(i)}(\omega) \tag{5.46}$$

Due to the equivalence of time and ensemble averages, the ensemble average $\left\langle {}^{\kappa}\eta(\tau)z^{(i)}(\tau)\right\rangle$ can also be written as,

$$\left\langle {}^{\kappa}\eta(\tau)z^{(i)}(\tau)\right\rangle = \lim_{T\to\infty}\frac{1}{T}\int_{-T/2}^{T/2} {}^{\kappa}\eta(\tau)z^{(i)}(\tau)d\tau$$

$$= \bar{F}_i^{*}(\omega)\ {}^{\kappa}\eta(\omega) \tag{5.47}$$

Equation (5.46) and (5.47) give

$$A_i\, {}^{\kappa}W_1^{(i)}(\omega) = \bar{F}_i^{*}(\omega)\ {}^{\kappa}\eta(\omega) \tag{5.48}$$

from which the expression for the first order Wiener kernel transform is obtained as

$${}^{\kappa}W_1^{(i)}(\omega) = \bar{F}_i^{*}(\omega)\ {}^{\kappa}\eta(\omega)\Big/A_i \tag{5.49}$$

Since κ takes values x_1, x_2, x_3 and i takes values 1 and 2 the direct kernel transforms ${}^{x_1}W_1^{(1)}(\omega)$, ${}^{x_2}W_1^{(2)}(\omega)$ and the cross kernel transforms ${}^{x_1}W_1^{(2)}(\omega)$, ${}^{x_2}W_1^{(1)}(\omega)$, ${}^{x_3}W_1^{(1)}(\omega)$ ${}^{x_3}W_1^{(2)}(\omega)$, can be extracted from the measured responses ${}^{x_1}\eta(\omega)$, ${}^{x_2}\eta(\omega)$, ${}^{x_3}\eta(\omega)$ and the applied force ($\bar{F}_1(\omega)$ with variance A_1 or $\bar{F}_2(\omega)$ with variance A_2), through equation (5.49).

For measurement of the third order kernel transform, a circuit involving three exponential delay filters as shown in Fig. 5.3 is considered. The output, $z^{(i)}(\tau)$, of the exponential filters is

$$z^{(i)}(\tau) = \int_{-\infty}^{\infty} e^{-j\omega_1\tau_1}\bar{f}_i(\tau-\tau_1)d\tau_1 \int_{-\infty}^{\infty} e^{-j\omega_2\tau_2}\bar{f}_i(\tau-\tau_2)d\tau_2 \int_{-\infty}^{\infty} e^{-j\omega_3\tau_3}\bar{f}_i(\tau-\tau_3)d\tau_3$$

$$= \bar{F}_i(-\omega_1)\bar{F}_i(-\omega_2)\bar{F}_i(-\omega_3)e^{-j(\omega_1+\omega_2+\omega_3)\tau} \tag{5.50}$$

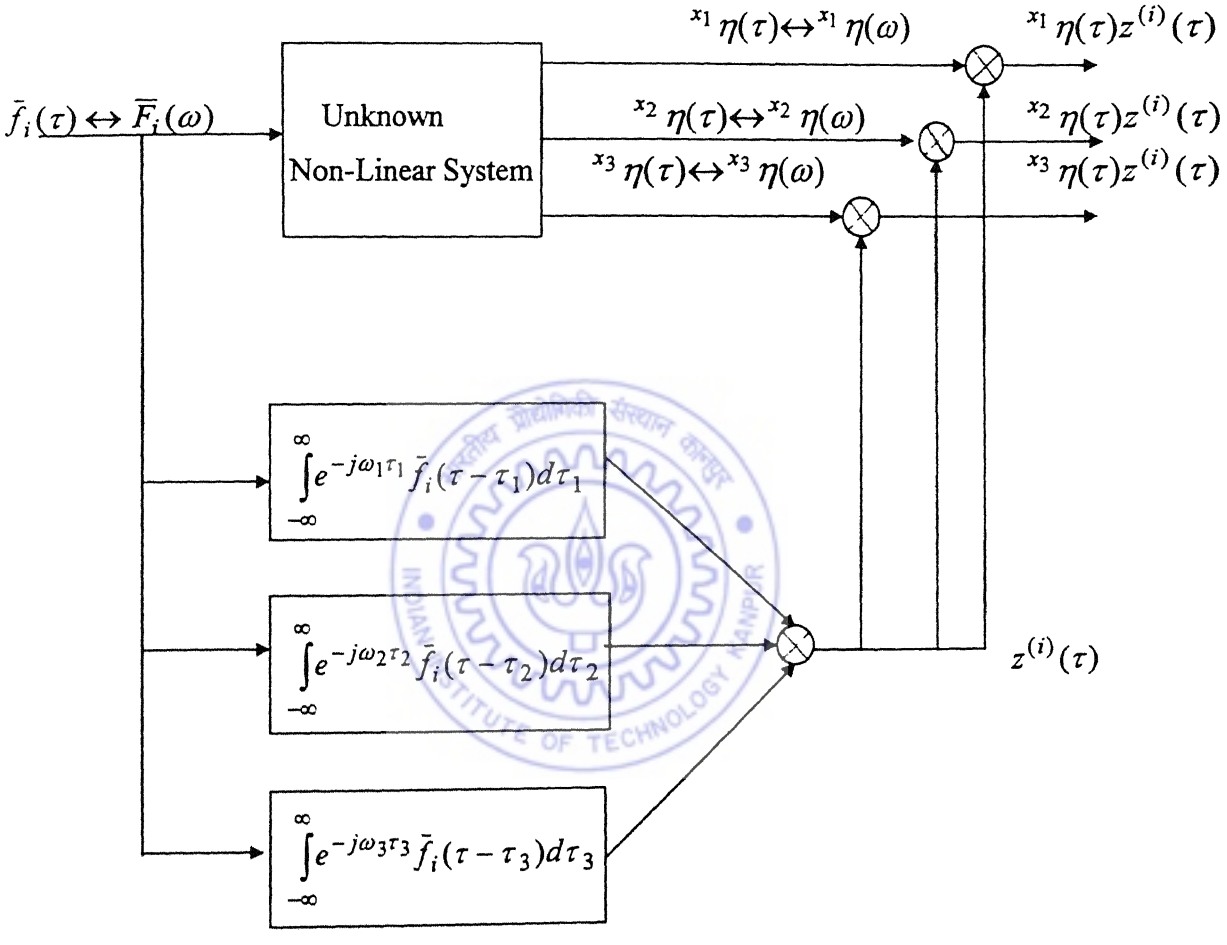

Fig. 5.3 Scheme for evaluation of the third order direct and cross Wiener kernel transforms, ${}^{x}W_3^{(i)}(\omega,\omega,\omega)$.

The ensemble averages of the outputs of the circuit (Fig. 5.3) are

$$\left\langle {}^{\kappa}\eta(\tau)z^{(i)}(\tau)\right\rangle = \left[A_i^2\left[{}^{\kappa}W_1^{(i)}(\omega_1)\delta(-\omega_2-\omega_3)e^{j(-\omega_2-\omega_3)\tau}+{}^{\kappa}W_1^{(i)}(\omega_2)\delta(-\omega_1-\omega_3)e^{j(-\omega_1-\omega_3)}\right.\right.$$
$$\left.\left.+{}^{\kappa}W_1^{(i)}(\omega_3)\delta(-\omega_1-\omega_2)e^{j(-\omega_1-\omega_2)\tau}\right]\right]+\left[6A_i^3\ {}^{\kappa}W_3^{(i)}(\omega_1,\omega_2,\omega_3)\right] \tag{5.51}$$

The equivalence of time and ensemble averages gives

$$\left\langle {}^{\kappa}\eta(\tau)z^{(i)}(\tau)\right\rangle = \lim_{T\to\infty}\frac{1}{T}\int_{-T/2}^{T/2}{}^{\kappa}\eta(\tau)z^{(i)}(\tau)d\tau_i$$

$$= \overline{F}_i(-\omega_1)\overline{F}_i(-\omega_2)\overline{F}_i(-\omega_3)\ {}^{\kappa}\eta(\omega_1+\omega_2+\omega_3) \tag{5.52}$$

Equations (5.51) and (5.52) give the expression for the measurement of the third order Wiener kernel transform as

$${}^{\kappa}W_3^{(i)}(\omega_1,\omega_2,\omega_3) = \frac{1}{6A_i^3}\left[\overline{F}_i^*(\omega_1)\overline{F}_i^*(\omega_2)\overline{F}_i^*(\omega_3)\ {}^{\kappa}\eta(\omega_1+\omega_2+\omega_3)\right]$$
$$-\frac{1}{6A_i}\left[\begin{array}{l}{}^{\kappa}W_1^{(i)}(\omega_1)\delta(\omega_1+\omega_3)+{}^{\kappa}W_1^{(i)}(\omega_2)\delta(\omega_1+\omega_3)\\+{}^{\kappa}W_1^{(i)}(\omega_3)\delta(\omega_1+\omega_2)\end{array}\right] \tag{5.53}$$

Measurements are made for special trispectral kernel transforms with $\omega_1=\omega_2=\omega_3=\omega$. As stated in earlier chapters, these transforms being functions of only one variable ω, are easier to compute and interpret. For such trispectral kernel transforms the expressions (5.53) reduce to

$${}^{x_1}W_3^{(i)}(\omega,\omega,\omega) = \frac{1}{6A_i^3}\left[\left\{\overline{F}_i^*(\omega)\right\}^{\beta\,x_1}\eta(3\omega)\right]-\frac{1}{6A_i}\left[{}^{x_1}W_1^{(i)}(\omega)+{}^{x_1}W_1^{(i)}(\omega)+{}^{x_1}W_1^{(i)}(\omega)\right]\delta(\omega)$$

$${}^{x_2}W_3^{(i)}(\omega,\omega,\omega) = \frac{1}{6A_i^3}\left[\left\{\overline{F}_i^*(\omega)\right\}^{\beta\,x_2}\eta(3\omega)\right]-\frac{1}{6A_i}\left[{}^{x_2}W_1^{(i)}(\omega)+{}^{x_2}W_1^{(i)}(\omega)+{}^{x_2}W_1^{(i)}(\omega)\right]\delta(\omega)$$

$${}^{x_3}W_3^{(i)}(\omega,\omega,\omega) = \frac{1}{6A_i^3}\left[\left\{\overline{F}_i^*(\omega)\right\}^{\beta\,x_3}\eta(3\omega)\right]-\frac{1}{6A_i}\left[{}^{x_3}W_1^{(i)}(\omega)+{}^{x_3}W_1^{(i)}(\omega)+{}^{x_3}W_1^{(i)}(\omega)\right]\delta(\omega)$$

(5.54)

5.4 Parameter Estimation

The first order direct and cross Wiener kernel transforms ${}^{\kappa}W_1^{(i)}(\omega)$ and the third order direct and cross Special Trispectral Wiener kernel transforms ${}^{\kappa}W_3^{(i)}(\omega,\omega,\omega)$ are estimated using equations (5.49) and (5.54) respectively, from the measurements of spectral component $\overline{F}(\omega)$ of the excitation force, its variance A_t and the spectral components ${}^{\kappa}\eta(\omega), {}^{\kappa}\eta(3\omega)$ of the corresponding response. Subsequently, for a third order representation of the system response, noting the equivalence between the Volterra and Wiener kernels (equations 5.41 and 5.42), the first order Volterra kernel transforms and the third order Special Trispectral Volterra kernel transforms can be computed as

$$\begin{aligned} {}^{\kappa}H_3^{(i)}(\omega,\omega,\omega) &= {}^{\kappa}W_3^{(i)}(\omega,\omega,\omega) \\ {}^{\kappa}H_1^{(i)}(\omega) &= {}^{\kappa}W_1^{(i)}(\omega) + {}^{\kappa}W_{1(3)}^{(i)}(\omega) \end{aligned} \tag{5.55}$$

where

$${}^{\kappa}W_{1(3)}^{(i)}(\omega) = \int_{-\infty}^{\infty} {}^{\kappa}W_3^{(i)}(\omega,\omega_2,-\omega_2)d\omega_2 \tag{5.56}$$

The linear parameters can be obtained from the above estimates of the first order Volterra kernels, ${}^{x_1}H_1^{(1)}(\omega)$, ${}^{x_2}H_1^{(1)}(\omega)$, ${}^{x_3}H_1^{(1)}(\omega)$ ${}^{x_1}H_1^{(2)}(\omega)$, ${}^{x_2}H_1^{(2)}(\omega)$, ${}^{x_3}H_1^{(2)}(\omega)$. Noting the algebraic expressions (eqns.5.20, 5.21) of these kernel transforms, the linear stiffness parameters of the bearings $\lambda_{b_1}^L, \lambda_{b_2}^L$ are estimated through a complex curve fitting routine (Levy, 1959). In addition to the bearing stiffnesses, the damping ratios ξ_{11}, ξ_{22}, ξ_{33} and the mass ratios μ_1, μ_2 are also obtained from the curve fit routine.

The nonlinear parameters are computed from the estimates of the Special Trispectral Volterra kernels ${}^{x_1}H_3^{(1)}(\omega,\omega,\omega)$, ${}^{x_1}H_3^{(2)}(\omega,\omega,\omega)$, ${}^{x_2}H_3^{(1)}(\omega,\omega,\omega)$, ${}^{x_2}H_3^{(2)}(\omega,\omega,\omega)$, ${}^{x_3}H_3^{(1)}(\omega,\omega,\omega)$, ${}^{x_3}H_3^{(2)}(\omega,\omega,\omega)$. Noting that these kernel transforms are estimated by application of a single white Gaussian force at a time, the synthesised

expressions (5.36), for the third order Volterra kernel transforms, also get reduced, in the two individual cases, to

$\bar{f}_1(\tau)$ Gaussian white, with variance A_1 and $\bar{f}_2(\tau) = 0$:

$$
\begin{aligned}
{}^{x_1}H_3(\omega,\omega,\omega) &= \lambda_{b_1}^N\,({}^{x_1x_1}\Psi_3^{1-1,1,1}) + \lambda_{b_2}^N\,({}^{x_1x_2}\Psi_3^{2-1,1,1}) \\
{}^{x_2}H_3(\omega,\omega,\omega) &= \lambda_{b_1}^N\,({}^{x_2x_1}\Psi_3^{1-1,1,1}) + \lambda_{b_2}^N\,({}^{x_2x_2}\Psi_3^{2-1,1,1}) \\
{}^{x_3}H_3(\omega,\omega,\omega) &= \lambda_{b_1}^N\,({}^{x_3x_1}\Psi_3^{1-1,1,1}) + \lambda_{b_2}^N\,({}^{x_3x_2}\Psi_3^{2-1,1,1})
\end{aligned}
\tag{5.57}
$$

$\bar{f}_2(\tau)$ Gaussian white, with variance A_2 and $\bar{f}_1(\tau) = 0$:

$$
\begin{aligned}
{}^{x_1}H_3(\omega,\omega,\omega) &= \lambda_{b_1}^N\,({}^{x_1x_1}\Psi_3^{1-2,2,2}) + \lambda_{b_2}^N\,({}^{x_1x_2}\Psi_3^{2-2,2,2}) \\
{}^{x_2}H_3(\omega,\omega,\omega) &= \lambda_{b_1}^N\,({}^{x_2x_1}\Psi_3^{1-2,2,2}) + \lambda_{b_2}^N\,({}^{x_2x_2}\Psi_3^{2-2,2,2}) \\
{}^{x_3}H_3(\omega,\omega,\omega) &= \lambda_{b_1}^N\,({}^{x_3x_1}\Psi_3^{1-2,2,2}) + \lambda_{b_2}^N\,({}^{x_3x_2}\Psi_3^{2-2,2,2})
\end{aligned}
\tag{5.58}
$$

It is to be noted here, that application of two forces (individually) is required for estimation of the linear cross-coupling terms. However, since no cross-coupling has been included in the nonlinear terms in the present analysis, only two equations out of the set of six expressions (5.57) and (5.58) are sufficient for the estimation of the two nonlinear unknown parameters $\lambda_{b_1}^N, \lambda_{b_2}^N$ (cross-coupled nonlinear parameters $\lambda_{12}^N, \lambda_{13}^N, \lambda_{23}^N$, being taken zero). Estimation of $\lambda_{b_1}^N, \lambda_{b_2}^N$ has been carried out here, using the first two equations from the set (5.57). For these two equations, using equations (5.55), we have

$$
\begin{aligned}
\frac{1}{6A_1^3}\left[\left\{\bar{F}_1^*(\omega)\right\}^3\,{}^{x_1}\eta(3\omega)\right] - \frac{1}{2A_1}\left[{}^{x_1}W_1^{(1)}(\omega)\delta(\omega)\right] &= \lambda_{b_1}^N\,({}^{x_1x_1}\Psi_3^{1-1,1,1}) \\
&\quad + \lambda_{b_2}^N\,({}^{x_1x_2}\Psi_3^{2-1,1,1})
\end{aligned}
\tag{5.59}
$$

$$
\begin{aligned}
\frac{1}{6A_1^3}\left[\left\{\bar{F}_1^*(\omega)\right\}^3\,{}^{x_2}\eta(3\omega)\right] - \frac{1}{2A_1}\left[{}^{x_2}W_1^{(1)}(\omega)\delta(\omega)\right] &= \lambda_{b_1}^N\,({}^{x_2x_1}\Psi_3^{1-1,1,1}) \\
&\quad + \lambda_{b_2}^N\,({}^{x_2x_2}\Psi_3^{2-1,1,1})
\end{aligned}
$$

The above equations are solved simultaneously for the nonlinear parameters $\lambda_{b_1}^N$ and $\lambda_{b_2}^N$.

5.5 Computer Simulation

The procedure is illustrated through numerical simulation of the response for the nondimensional equations (5.3). The excitation forces are simulated through random number generating subroutines and are normalised with respect to the maximum value of $f_1(t)$. A typical sample of the excitation is shown in Fig. 5.4 (a). The power spectrum of the input averaged over an ensemble of 2000 force samples is shown in Fig.5.4 (b)

The shaft stiffness matrix for the simply supported system, carrying a centrally located disc as (refer Fig. 5.1, for station numbering) is computed using Strength of Materials Formulae (Childs, 1990)

$$\begin{bmatrix} k_{11} & k_{12} & k_{13} \\ k_{21} & k_{22} & k_{23} \\ k_{31} & k_{32} & k_{33} \end{bmatrix} = \frac{12EI}{l^3} \begin{bmatrix} 1 & 0 & -1 \\ 0 & 1 & -1 \\ -1 & -1 & 2 \end{bmatrix} \tag{5.60}$$

which gives the nondimensionalised matrix as

$$\begin{bmatrix} \lambda_{11}+\lambda_{b_1}^L & \lambda_{12} & \lambda_{13} \\ \lambda_{21} & \lambda_{22}+\lambda_{b_2}^L & \lambda_{23} \\ \lambda_{31} & \lambda_{32} & \lambda_{33} \end{bmatrix} = \begin{bmatrix} (0.5+\lambda_{b_1}^L)/\mu_1 & 0 & -(0.5/\mu_1) \\ 0 & (0.5+\lambda_{b_2}^L)/\mu_2 & -(0.5/\mu_2) \\ -0.5 & -0.5 & 1 \end{bmatrix} \tag{5.61}$$

where μ_1, μ_2 are equal to the mass ratios m_1/m_3 and m_2/m_3 respectively. In the rotor configuration shown in Fig.5.1, m_1 and m_2 are the masses effectively seen by the sensors at the bearing ends and will be small in magnitude in comparison to m_3. However, for simplicity in numerical simulation the mass ratios m_1/m_3 and m_2/m_3 are chosen to be each equal to 1.0. The values, of the individual elements of the above lambda matrix, therefore become

$$\begin{aligned} &\lambda_{11} = \lambda_{22} = 0.5 \qquad \lambda_{33} = 1.0 \qquad \lambda_{12} = \lambda_{21} = 0 \\ &\lambda_{13} = \lambda_{23} = -0.5 \qquad \lambda_{31} = \lambda_{32} = -0.5 \end{aligned} \tag{5.62}$$

In order to illustrate the numerical results when shaft and bearing stiffness are both equally significant numerically, the values of the linear bearing stiffness parameters are taken as

$$\lambda_{b_1}^L = 0.5 \qquad \lambda_{b_2}^L = 1.0 \tag{5.63}$$

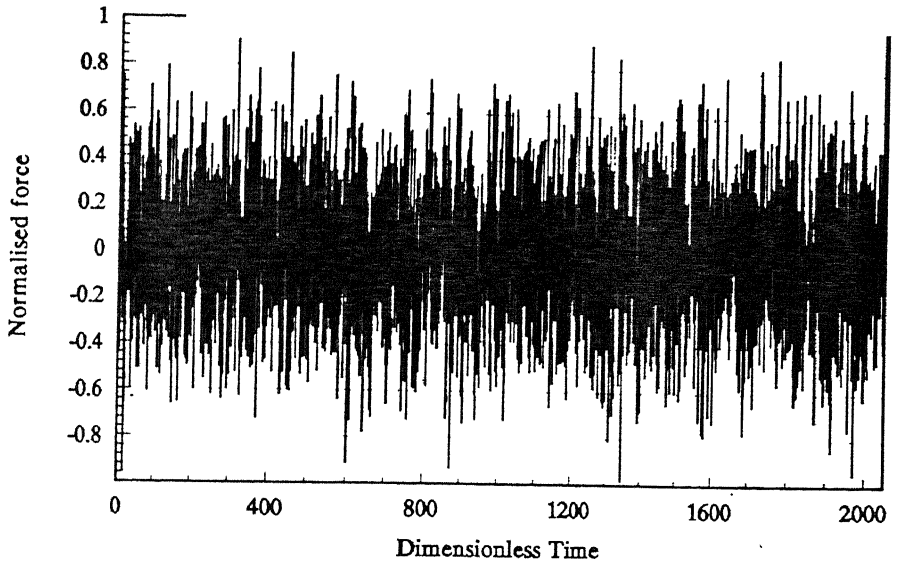

Fig. 5.4(a) Typical sample of input force.

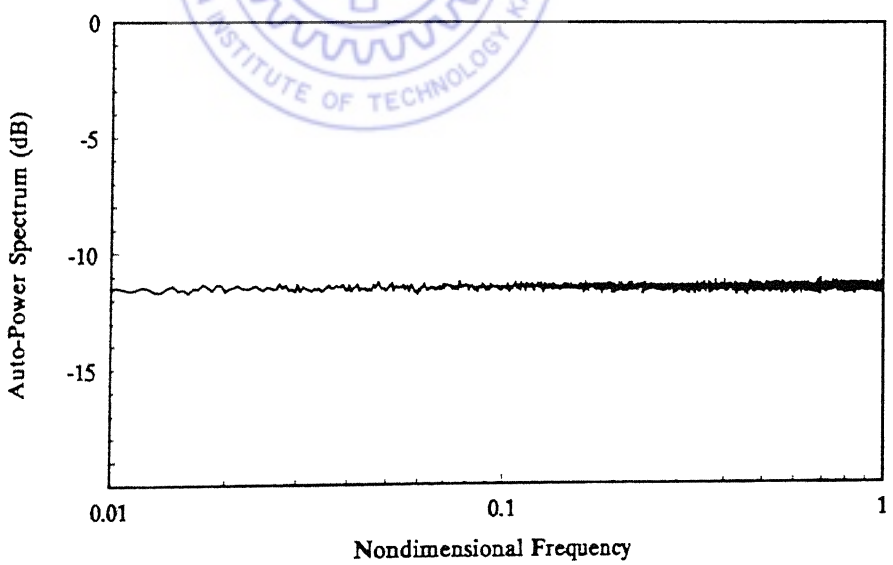

Fig. 5.4(b) Power-spectrum of the input force (averaged over 2000 samples).

For the above set of values of the linear parameters the estimation procedure is illustrated for the following sets of the nonlinear parameters -

Case 1: $\lambda_{b_1}^N = 0.1 \quad \lambda_{b_2}^N = 0.1$

Case 2: $\lambda_{b_1}^N = 0.1 \quad \lambda_{b_2}^N = 0.01$

Damping is chosen as $\xi_{11} = \xi_{22} = \xi_{33} = 0.01$ in both the cases. The same set of excitation as shown in Figs 5.4 (a), (b) is employed for the two cases. The governing equations are then numerically solved through a standard fourth-order Runge-Kutta subroutine, to obtain the responses ${}^{x_1}\eta$, ${}^{x_2}\eta$ and ${}^{x_3}\eta$. These responses are fed as inputs to the parameter estimation algorithm. The various first and higher order kernels are extracted from the responses and consequently parameter estimation is carried out. The output consists of the linear stiffness parameters $\lambda_{b_1}^L, \lambda_{b_2}^L$, the damping ratios $\xi_{11}, \xi_{22}, \xi_{33}$, the mass ratios μ_1, μ_2 and the nonlinear stiffness parameters $\lambda_{b_1}^N$, $\lambda_{b_2}^N$. The estimated parameters are compared with those originally used for the simulation of response.

Case1:

For the first set of values $\lambda_{b_1}^N = 0.10$, $\lambda_{b_2}^N = 0.10$, the nondimensional responses ${}^{x_1}\eta$, ${}^{x_2}\eta$ and ${}^{x_3}\eta$ numerically resulting from the force of Figs. 5.4 (a), (b), applied at station 1, are shown in Figs. 5.5 (a), (b) and (c). (No force is applied at station 2). Their corresponding power-spectra are shown in Figs.5.6 (a), (b) and (c). The critical frequencies of the system can be noticed from these figures to exist at 0.097, 0.175 and 0.219 (cycles/τ). These frequencies correspond to those obtained from the eigenvalue solution of the linear nondimensional stiffness matrix described in equations 5.61-5.63 and can be called $\omega_1, \omega_2, \omega_3$. It can also be noticed from the power-spectra of Figs. 5.6 (a),(b),(c) that the system nonlinearity is not apparently, equally displayed by responses ${}^{x_1}\eta$, ${}^{x_2}\eta$ and ${}^{x_3}\eta$. The plot of ${}^{x_2}\eta$ (Fig.5.6b) displays additional peaks at frequencies 0.263, 0.291, 0.341, 0.403, 0.491, 0.525 and 0.569 cycles/τ, which can be identified as $(2\omega_3 - \omega_2)$, $(3\omega_1)$, $(2\omega_3 - \omega_1)$, $(2\omega_1 + \omega_3)$, $(\omega_1 + \omega_2 + \omega_3)$, $(3\omega_2)$ and $(2\omega_2 + \omega_3)$

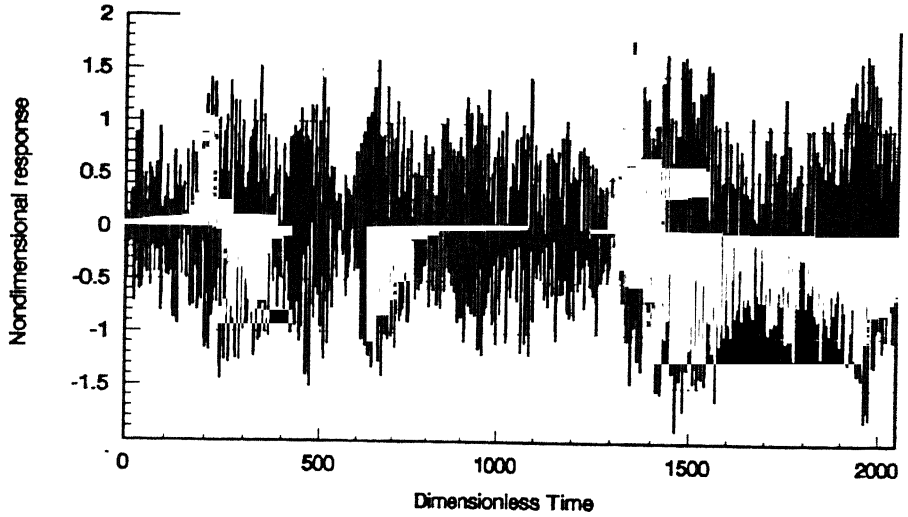

(a) Response, ${}^{x_1}\eta(\tau)$, at station 1.

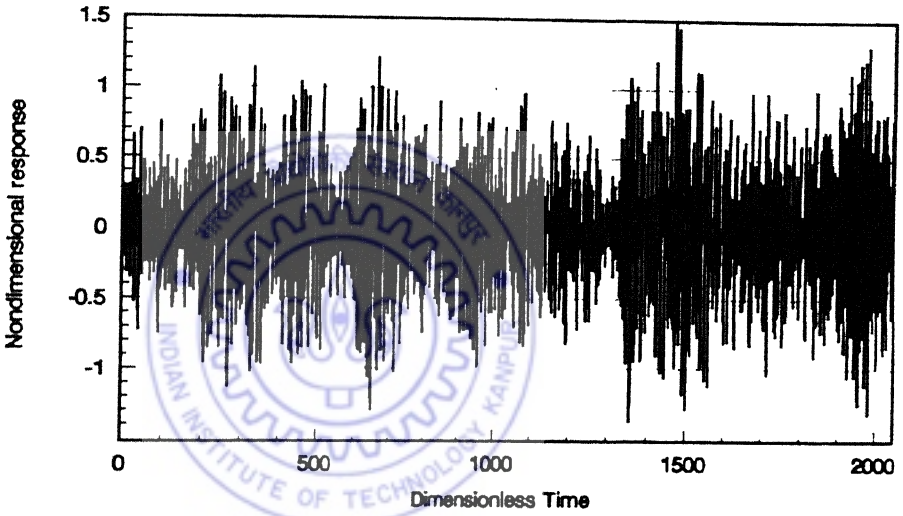

(b) Response, ${}^{x_2}\eta(\tau)$, at station 2.

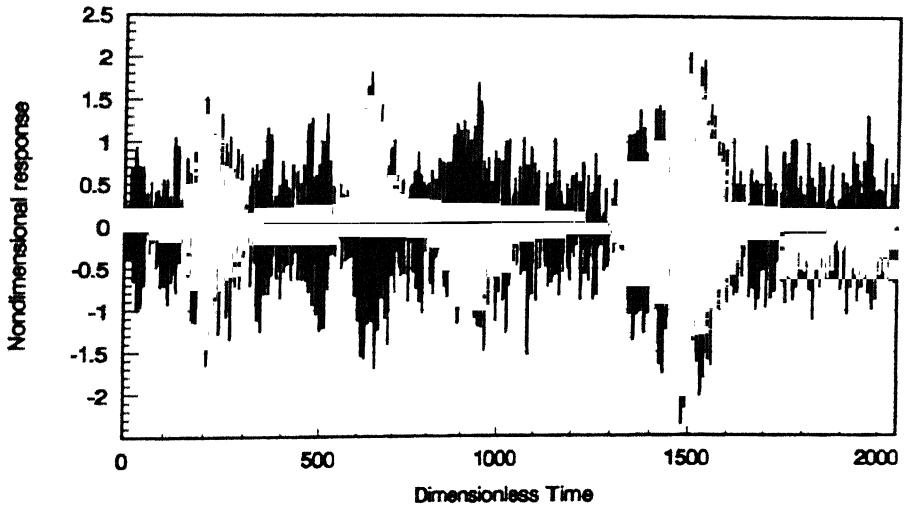

(c) Response, ${}^{x_3}\eta(\tau)$, at station 3.

Fig. 5.5 Typical response samples: Case 1.

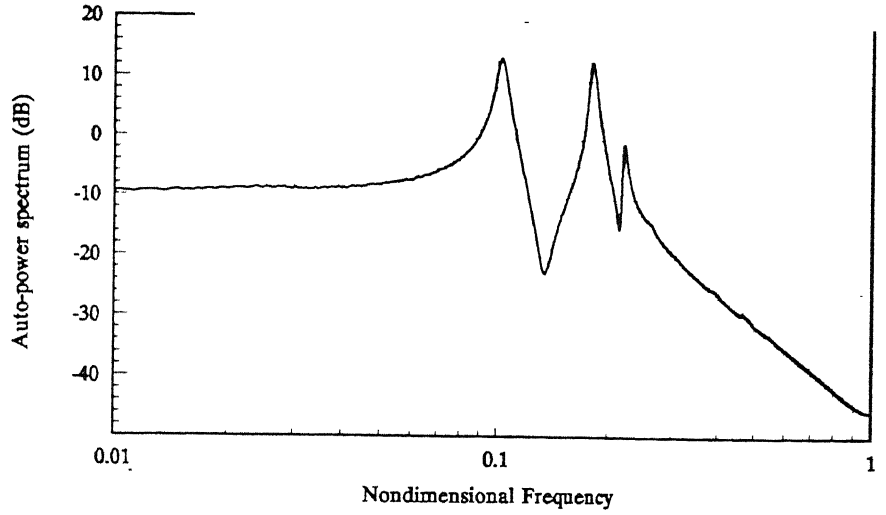

(a) Power-spectrum of ${}^{x_1}\eta(\tau)$.

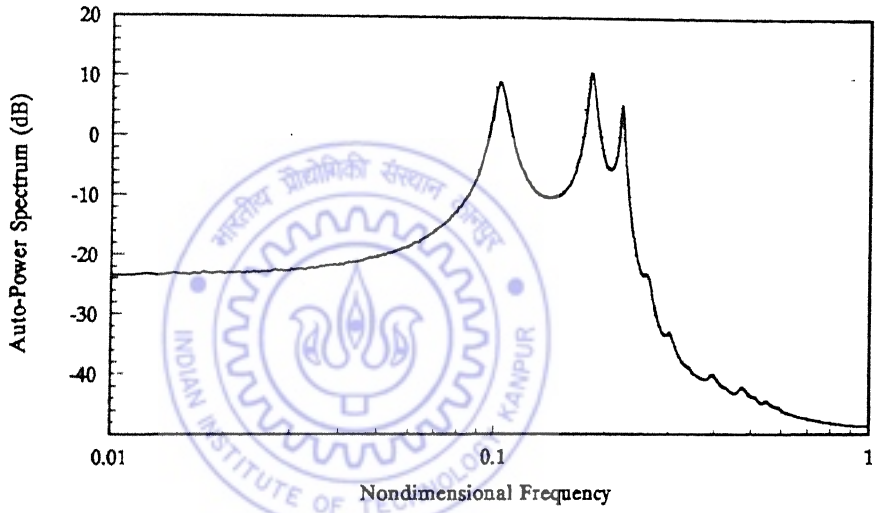

(b) Power-spectrum of ${}^{x_2}\eta(\tau)$.

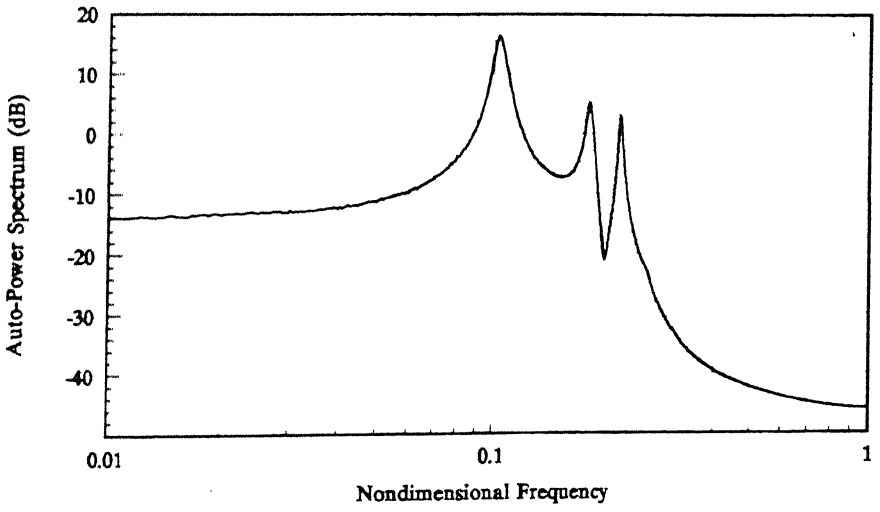

(c) Power-spectrum of ${}^{x_3}\eta(\tau)$.

Fig. 5.6 Power-spectra of the response (averaged over 2000 samples): Case 1

harmonics respectively. These harmonics are not distinctly, visible in the plots of ${}^{x_1}\eta$ (Fig. 5.6a) and ${}^{x_3}\eta$ (Fig. 5.6c). This is due to the fact that stations 1 and 3 being closer the station of force application (station 1), the linear response levels, are higher at these stations in comparison to that at station 2 and overlap the nonlinear contributions. Similar response plots can be obtained by application of the force at station 2, while keeping the force at station 1 equal to zero.

The applied force and resultant response at the three stations are employed in equations (5.49) and (5.55) to extract the first order Volterra kernel transforms, ${}^{\kappa}H_1^{(i)}(\omega)$ shown in Figs.5.7(a-f). These kernels show the three critical frequencies of the system, mentioned above. The errors in these estimated kernels are given in Figs. 5.8 (a)-(f). The errors are computed by comparing the estimated kernel transforms with those obtained from the exact analytical expressions (5.20). The errors are high in the vicinity of the fundamental frequencies, as in the cases of rotor configurations, discussed in the earlier chapters. However, the errors are within 10% zone upto a nondimensional frequency of 0.07 cycles/τ. Parameter estimation is therefore carried out in this frequency range.

The third order kernel factors ${}^{x_1x_1}\Psi_3^{1-1,1,1}(\omega,\omega,\omega)$, ${}^{x_1x_2}\Psi_3^{2-1,1,1}(\omega,\omega,\omega)$, ${}^{x_2x_1}\Psi_3^{1-1,1,1}(\omega,\omega,\omega)$, ${}^{x_2x_2}\Psi_3^{2-1,1,1}(\omega,\omega,\omega)$, ${}^{x_3x_1}\Psi_3^{1-1,1,1}(\omega,\omega,\omega)$ and ${}^{x_3x_2}\Psi_3^{2-1,1,1}(\omega,\omega,\omega)$ estimated from the first order kernel transforms, are shown in Figs.5.9 (a)-(f). However, in the present case, the last two factors, ${}^{x_3x_1}\Psi_3^{1-1,1,1}(\omega,\omega,\omega)$ and ${}^{x_3x_2}\Psi_3^{2-1,1,1}(\omega,\omega,\omega)$ are not required since the nonlinear parameter estimation can be carried out from the first two equations only, from the set of equations (5.57).

The third order measured kernel transforms ${}^{x_1}H_3^{(1)}(\omega,\omega,\omega)$, ${}^{x_2}H_3^{(1)}(\omega,\omega,\omega)$ and ${}^{x_3}H_3^{(1)}(\omega,\omega,\omega)$, extracted from the measurements of the force and response, in accordance with equations (5.54), are shown in Figs. 5.10 (a)-(c). As before, while the first order kernel transforms are estimated in the entire available frequency range 0.0 - 1.0, the third order kernel transforms, involving a 3ω factor, have to be restricted to one-

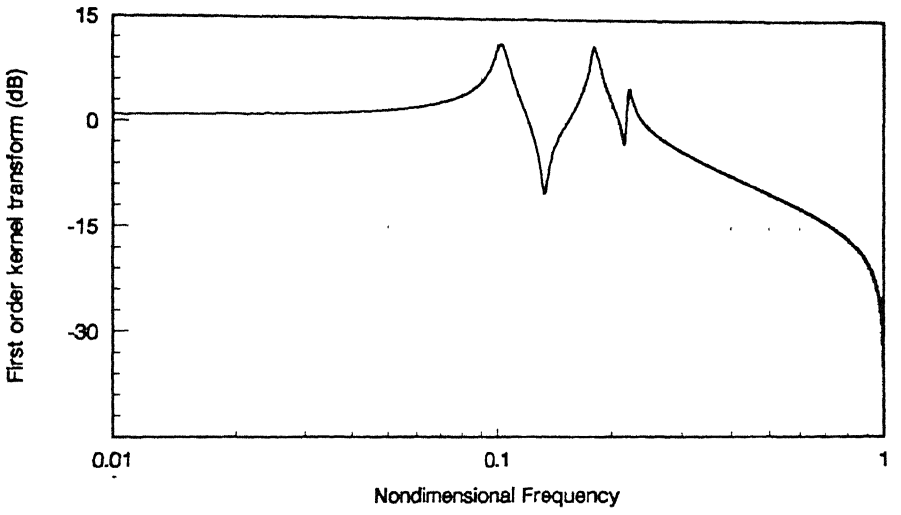

(a) Estimate of ${}^{x_1}H_1^{(1)}(\omega)$.

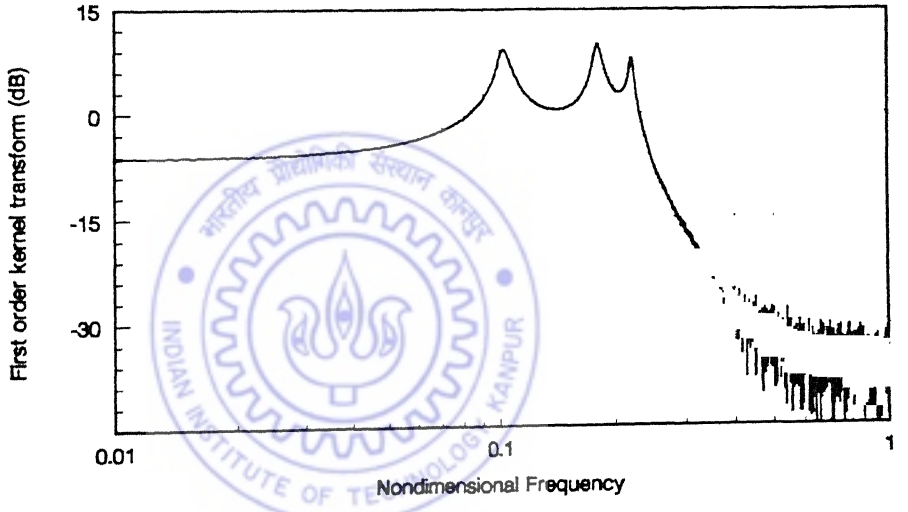

(b) Estimate of ${}^{x_2}H_1^{(1)}(\omega)$.

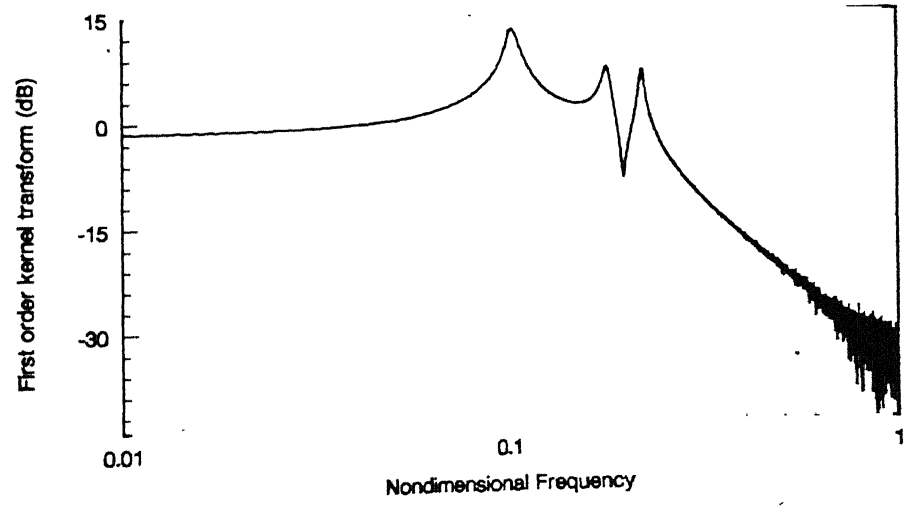

(c) Estimate of ${}^{x_3}H_1^{(1)}(\omega)$.

Fig. 5.7 Estimates of the first order kernel transforms: Case 1 (Contd.)

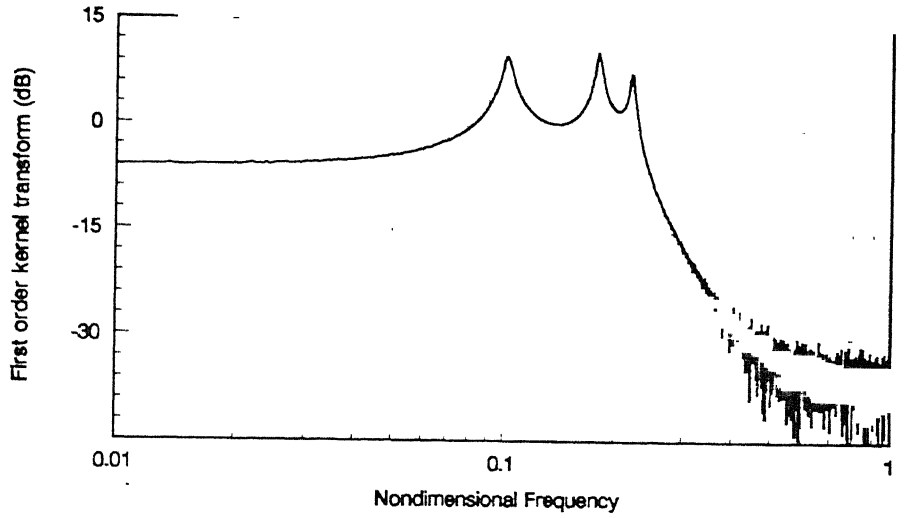

(d) Estimate of ${}^{x_1}H_1^{(2)}(\omega)$.

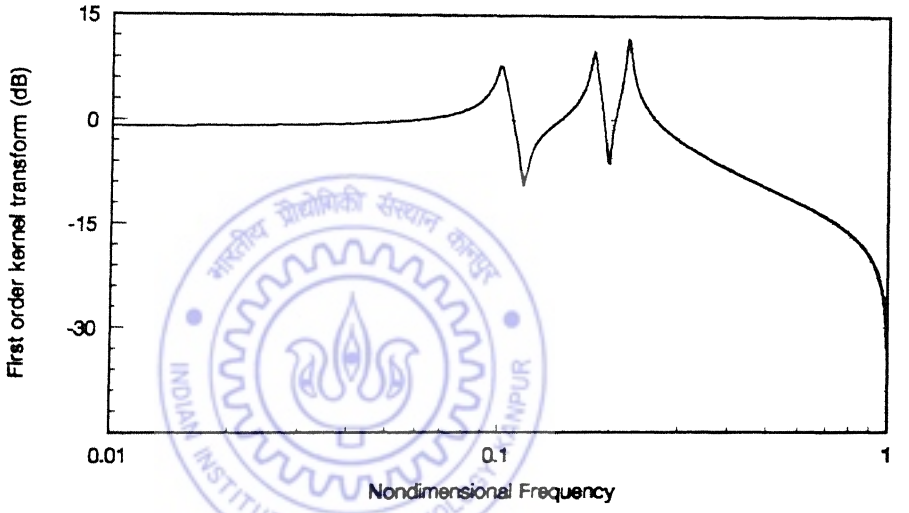

(e) Estimate of ${}^{x_2}H_1^{(2)}(\omega)$.

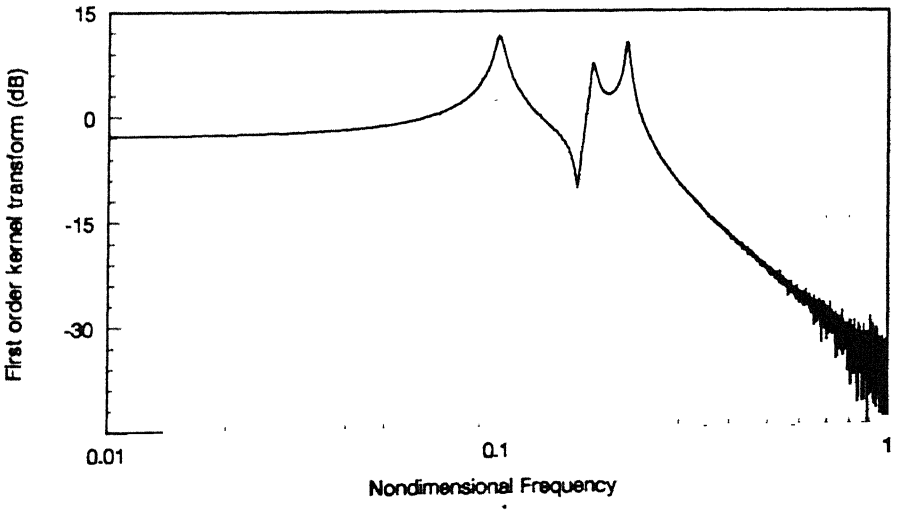

(f) Estimate of ${}^{x_3}H_1^{(2)}(\omega)$.

Fig. 5.7 Estimates of the first order kernel transforms: Case 1.

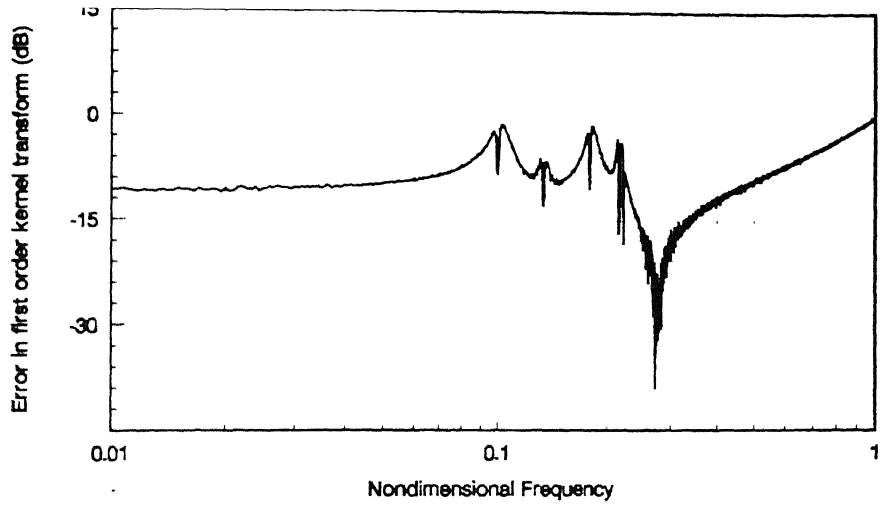

(a) Error in ${}^{x_1}H_1^{(1)}(\omega)$.

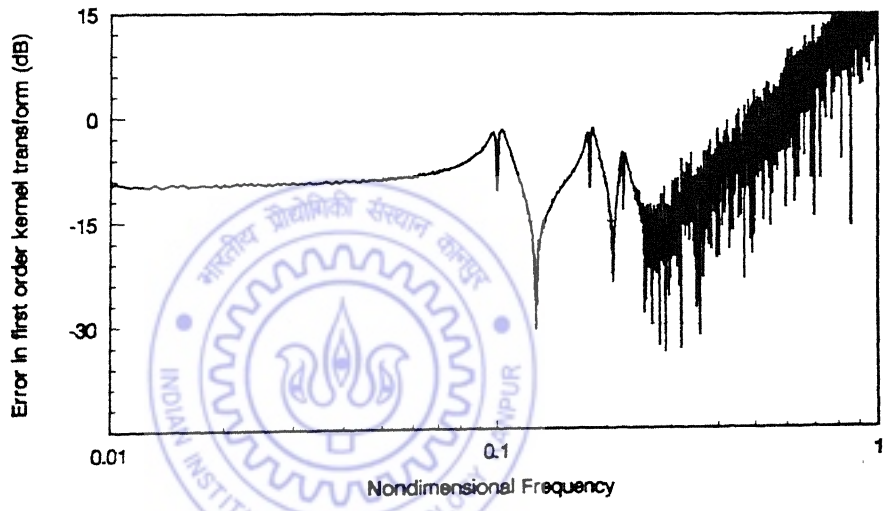

(b) Error in ${}^{x_2}H_1^{(1)}(\omega)$.

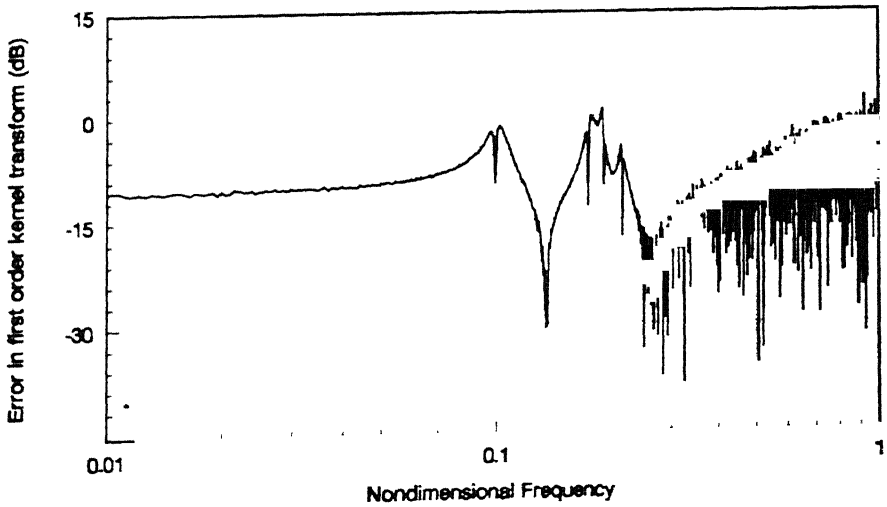

(c) Error in ${}^{x_3}H_1^{(1)}(\omega)$.

Fig. 5.8 Normalised error in the first order estimates: Case 1 (Contd.)

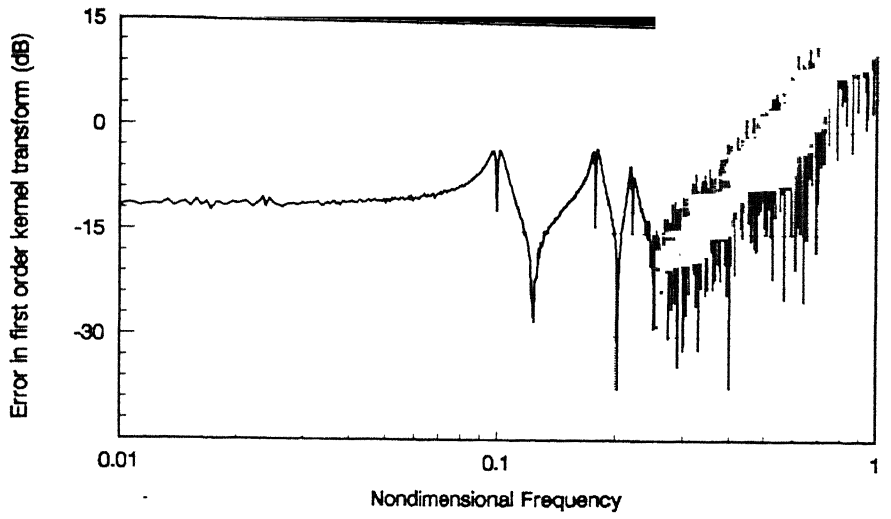

(d) Error in ${}^{x_1}H_1^{(2)}(\omega)$.

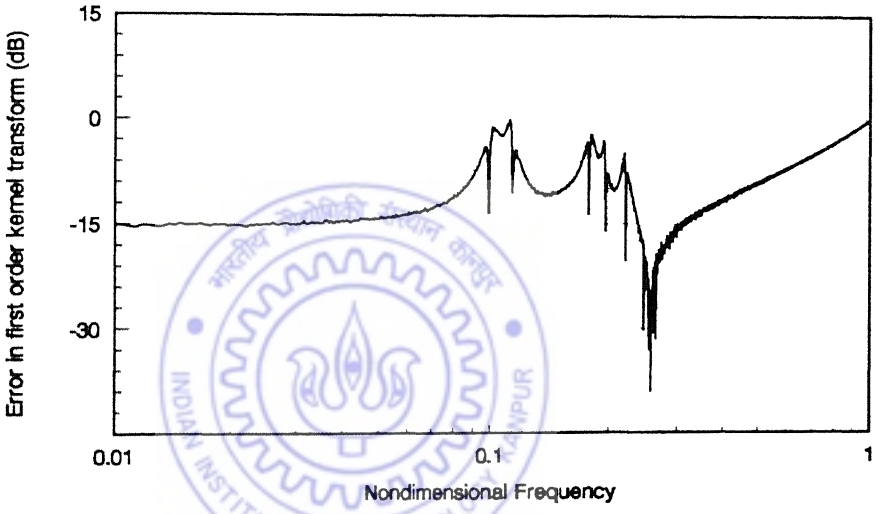

(e) Error in ${}^{x_2}H_1^{(2)}(\omega)$.

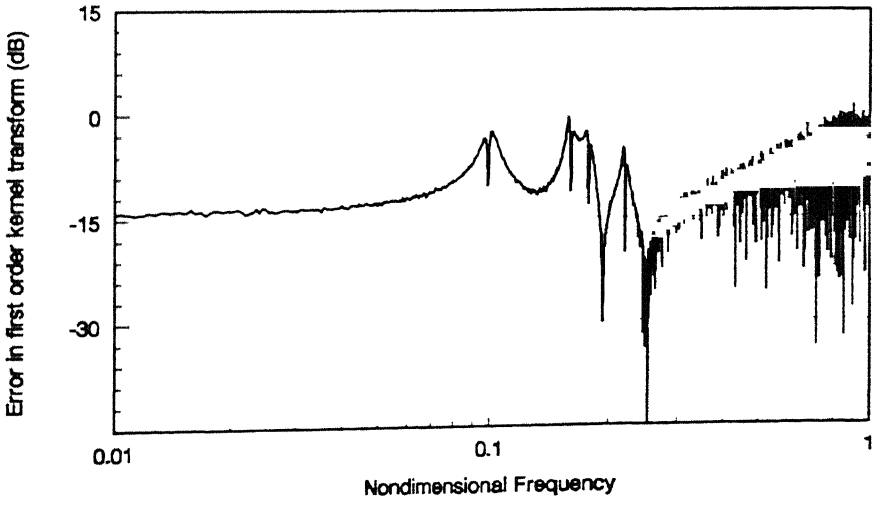

(f) Error in ${}^{x_3}H_1^{(2)}(\omega)$.

Fig. 5.8 Normalised error in the first order estimates: Case 1.

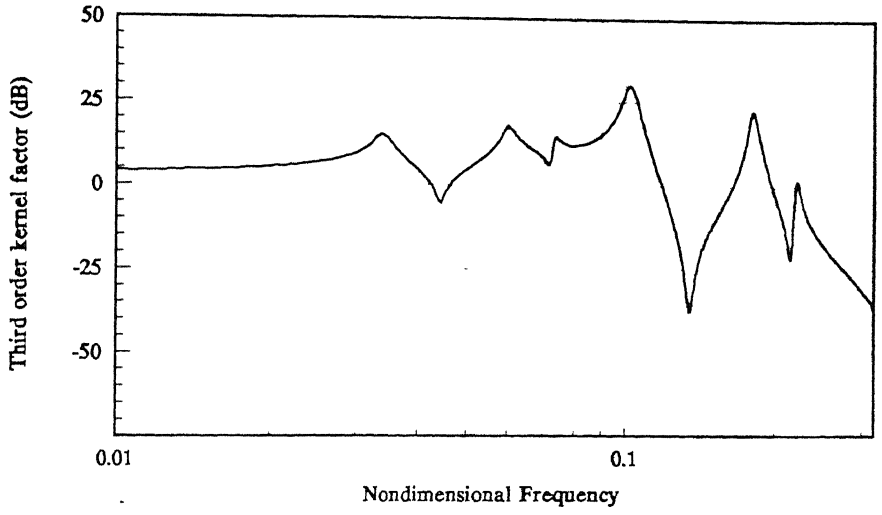

(a) Estimate of ${}^{x_1x_1}\Psi_3^{1-1,1,1}(\omega,\omega,\omega)$.

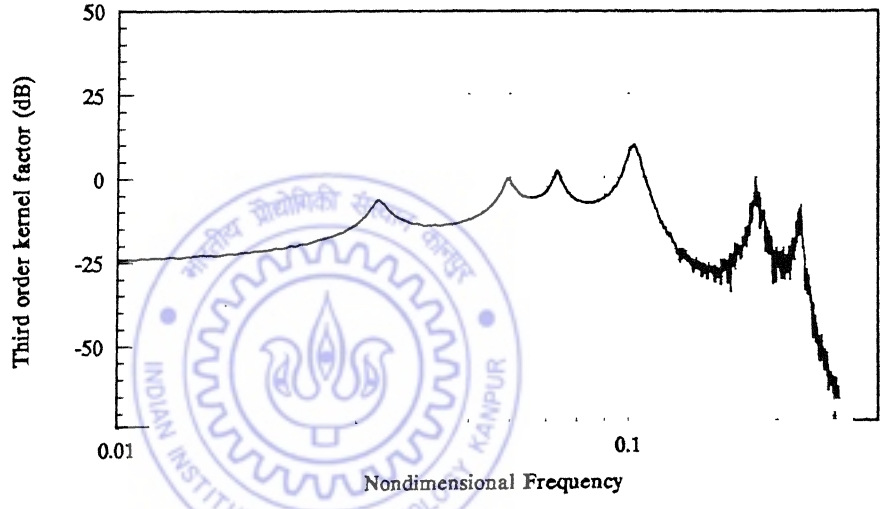

(b) Estimate of ${}^{x_1x_2}\Psi_3^{2-1,1,1}(\omega,\omega,\omega)$.

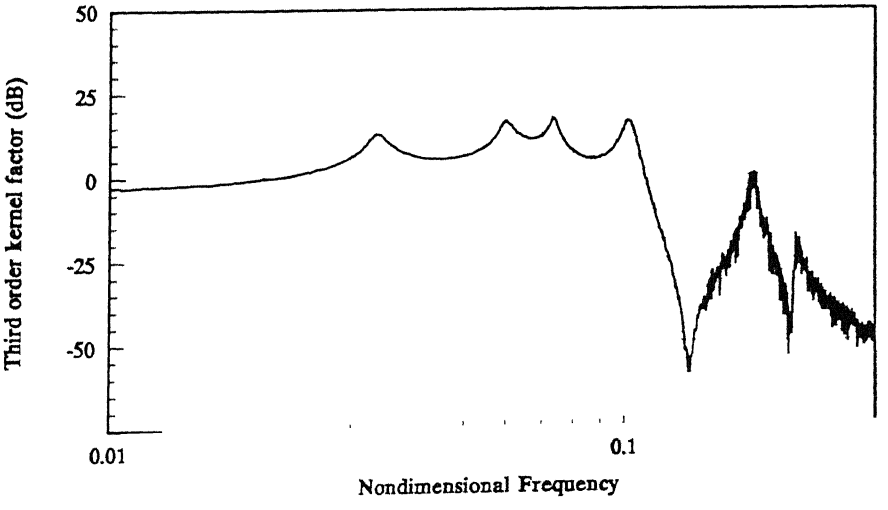

(c) Estimate of ${}^{x_2x_1}\Psi_3^{1-1,1,1}(\omega,\omega,\omega)$.

Fig. 5.9 Third order kernel factors: Case1 (Contd.)

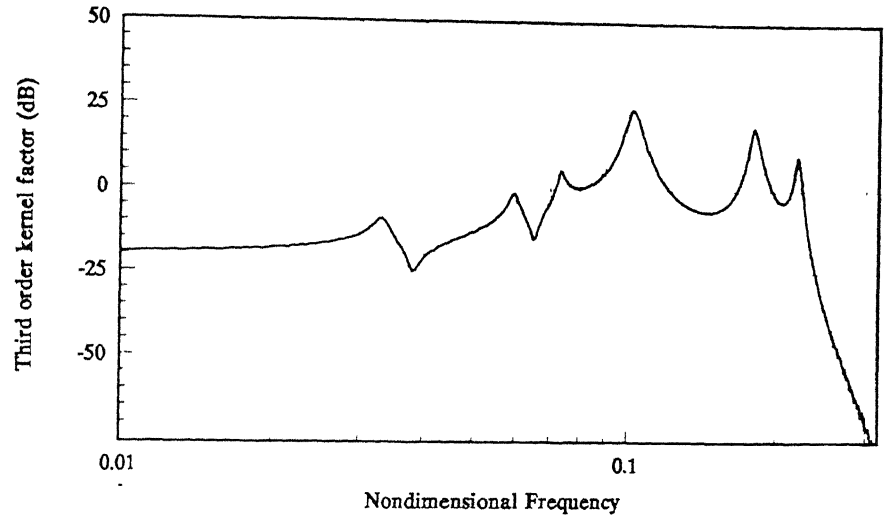

(d) Estimate of ${}^{x_2x_2}\Psi_3^{2-1,1,1}(\omega,\omega,\omega)$.

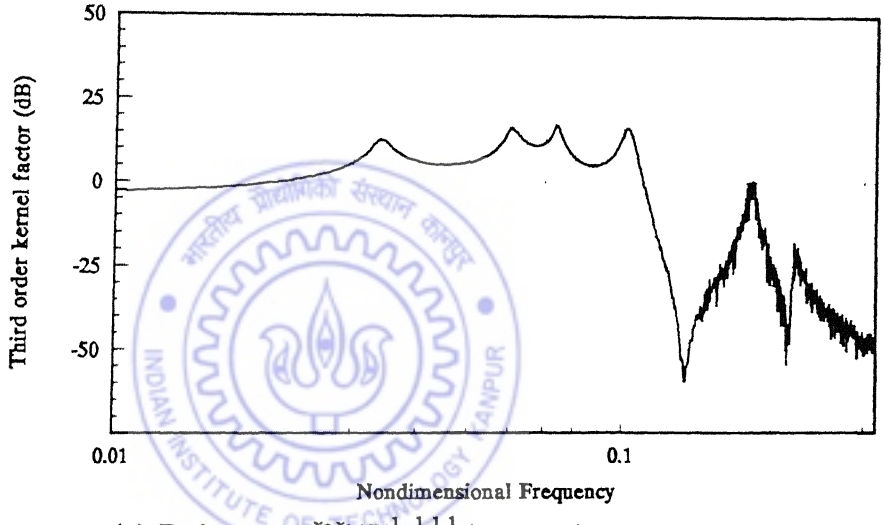

(e) Estimate of ${}^{x_3x_1}\Psi_3^{1-1,1,1}(\omega,\omega,\omega)$.

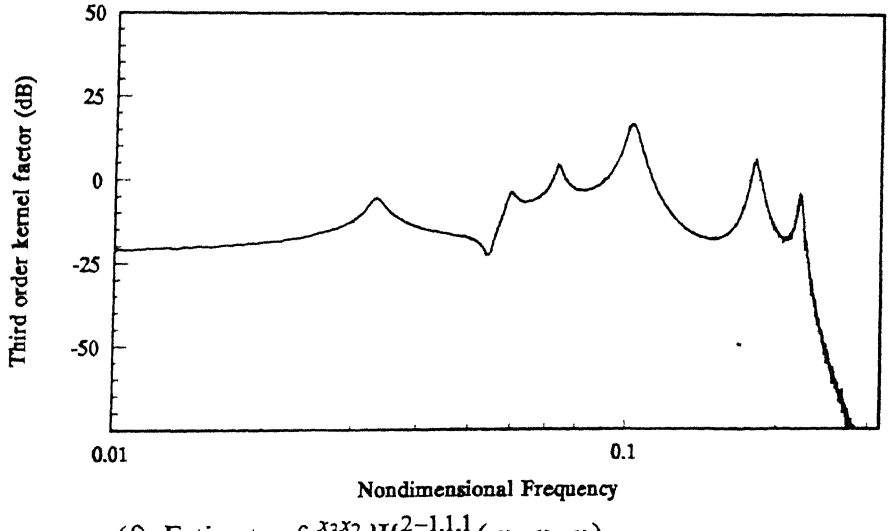

(f) Estimate of ${}^{x_3x_2}\Psi_3^{2-1,1,1}(\omega,\omega,\omega)$.

Fig. 5.9 Third order kernel factors: Case1.

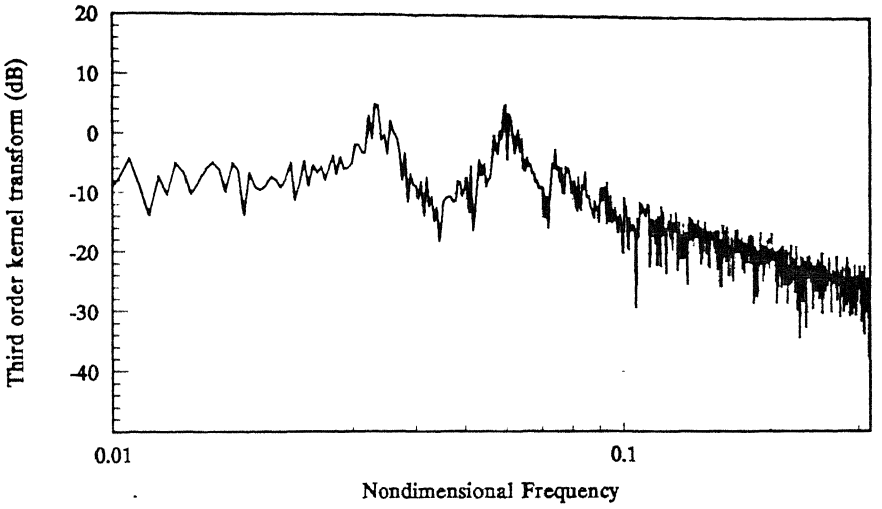

(a) Estimate of ${}^{x_1}H_3^{(1)}(\omega,\omega,\omega)$.

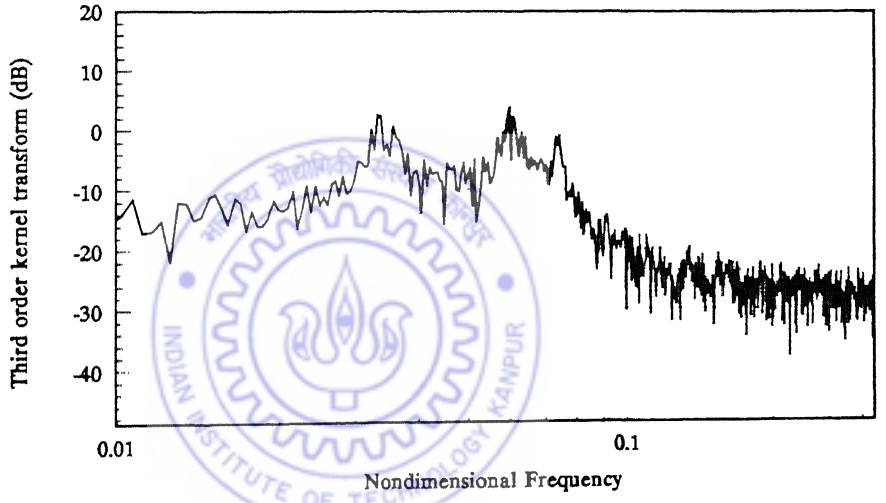

(b) Estimate of ${}^{x_2}H_3^{(1)}(\omega,\omega,\omega)$.

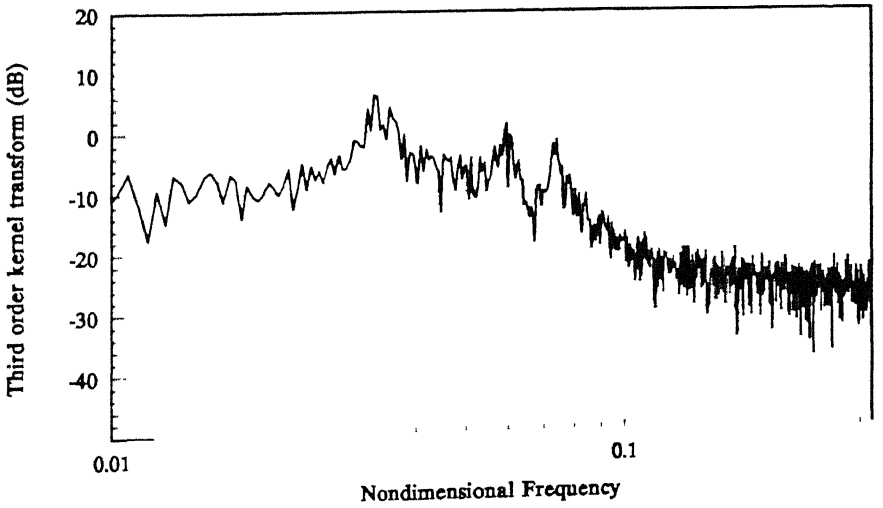

(c) Estimate of ${}^{x_3}H_3^{(1)}(\omega,\omega,\omega)$.

Fig. 5.10 Estimates of third order kernel transforms: Case 1.

third of this frequency zone (i.e. 0.0 - 0.33). It can be observed, from the figures, that while the measured third order kernel transforms are reasonably accurate in showing the harmonic at $\omega_{1,2,3}/3$ (at nondimensional frequencies = 0.032, 0.058 and 0.073 cycles/τ), the identification of the harmonic at $\omega_{1,2,3}$ (at nondimensional frequencies = 0.097, 0.175, 0.219 cycles/τ) is weak, due to higher statistical errors, mentioned earlier. The estimation of nonlinear parameters $\lambda_{b_1}^N$ and $\lambda_{b_2}^N$, from these kernel transforms, is therefore restricted to the frequency zone of 0.0 - 0.07.

The estimates of the nonlinear parameter $\lambda_{b_1}^N$ and $\lambda_{b_2}^N$, obtained in accordance with the relationships (5.59), are shown in Figs. 5.11 (a)-(b). A fourth order polynomial curve regressed through the estimates of these nonlinear parameters , over the frequency range, is also shown in these figures. The mean values of the estimates are found to be

$\lambda_{b_1}^N = 0.09$ and $\lambda_{b_2}^N = 0.12$

(The exact values of the above nonlinear parameters are those chosen for response simulation, that is, $\lambda_{b_1}^N = \lambda_{b_2}^N = 0.10$).

The linear parameters have been estimated from the first order kernel transforms of Figs.5.7 (a)-(f), using a complex curve fitting routine (Levy, 1959). The estimates are

$\mu_1 = 0.956 \qquad \mu_2 = 0.917$

$\lambda_{b_1} = 0.487 \qquad \lambda_{b_2} = 0.918$

$\xi_{11} = \xi_{22} = \xi_{33} = 0.011$

Case 2

In the case study 1, the values of the nonlinear parameters, $\lambda_{b_1}^N$, $\lambda_{b_2}^N$ were kept identical (=0.10), in response simulation. As the next case, dissimilar values $\lambda_{b_1}^N = 0.1$, $\lambda_{b_2}^N = 0.01$, of these parameters, are chosen for response simulation and their subsequent estimation from the simulated response. The linear parameters are the same as in Case 1 and the forcing function is the same as shown in Fig. 5.4 (a),(b). The results obtained are shown in the figures listed below.

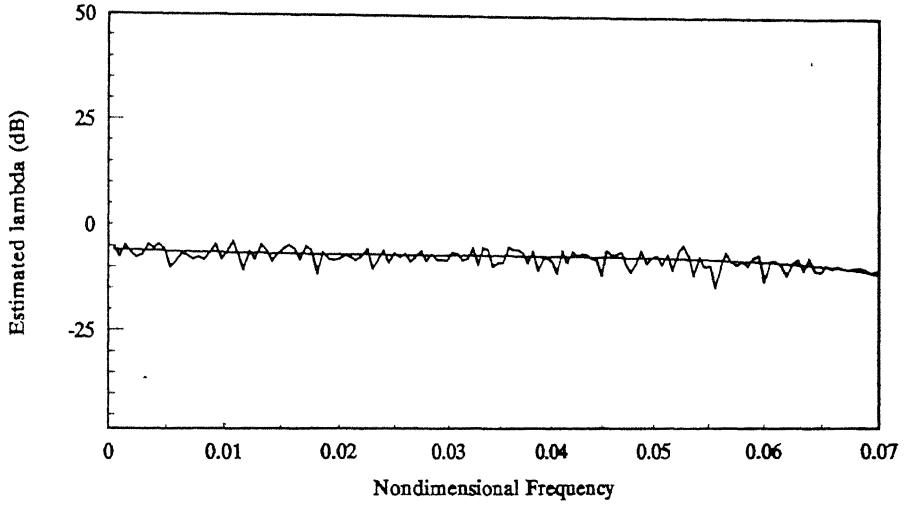

(a) Estimate of λ_{b1}^{N}.

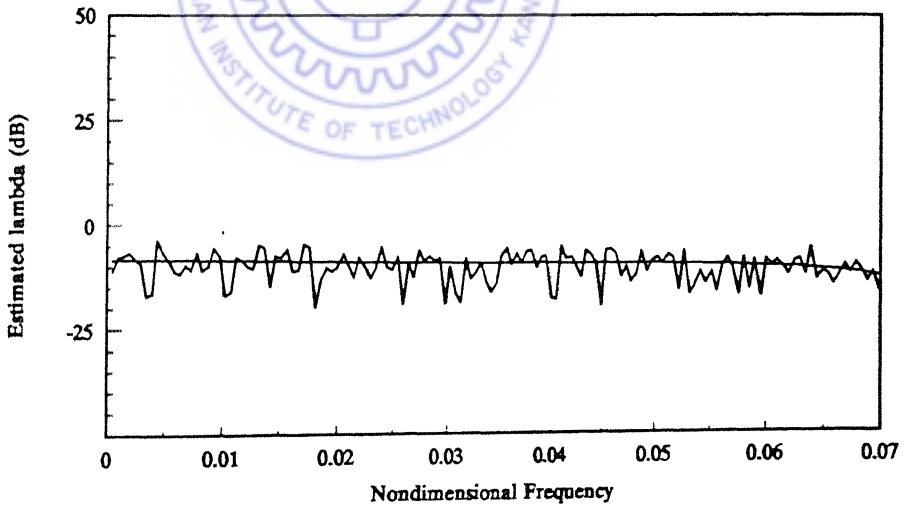

(b) Estimate of λ_{b2}^{N}.

Fig. 5.11 Estimates of the nonlinear parameters: Case 1.

nondimensional responses ${}^{x_1}\eta$, ${}^{x_2}\eta$, ${}^{x_3}\eta$	Figs. 5.12 (a),(b),(c)
power spectra of ${}^{x_1}\eta$, ${}^{x_2}\eta$, ${}^{x_3}\eta$	Figs. 5.13 (a),(b),(c)
first order Volterra kernel transforms, ${}^{\kappa}H_1^{(i)}(\omega)$	Figs. 5.14 (a-f)
third order kernel factors ${}^{x_1x_1}\Psi_3^{1-1,1,1}(\omega,\omega,\omega)$, ${}^{x_1x_2}\Psi_3^{2-1,1,1}(\omega,\omega,\omega)$, ${}^{x_2x_1}\Psi_3^{1-1,1,1}(\omega,\omega,\omega)$, ${}^{x_2x_2}\Psi_3^{2-1,1,1}(\omega,\omega,\omega)$, ${}^{x_3x_1}\Psi_3^{1-1,1,1}(\omega,\omega,\omega)$, ${}^{x_3x_2}\Psi_3^{2-1,1,1}(\omega,\omega,\omega)$	Figs. 5.15 (a-f)
third order measured kernel transforms ${}^{x_1}H_3^{(1)}(\omega,\omega,\omega)$, ${}^{x_2}H_3^{(1)}(\omega,\omega,\omega)$, ${}^{x_3}H_3^{(1)}(\omega,\omega,\omega)$	Figs. 5.16 (a-c)
nonlinear parameters $\lambda_{b_1}^N$, $\lambda_{b_2}^N$	Figs. 5.17 (a),(b)

The estimates computed in this case are

$\lambda_{b_1}^N = 0.106$ $\lambda_{b_2}^N = 0.04$

and

$\mu_1 = 0.99$ $\mu_2 = 0.95$

$\lambda_{b_1} = 0.49$ $\lambda_{b_2} = 0.95$

$\xi_{11} = \xi_{22} = \xi_{33} = 0.013$

Reasonably good estimates can be seen to be obtained, in both the numerical cases illustrated above. The accuracy lies within the 20% zone for the nonlinear parameters, except $\lambda_{b_2}^N$, in the second case. However, the order of the magnitude of the estimate is the same as that of its exact value. It is to be noted that the response representation has been restricted to third order kernels only, in this study. Also, the ensemble size has been restricted to 2000. Increased sample size and/or increased ensemble size can be expected to yield more accurate estimates.

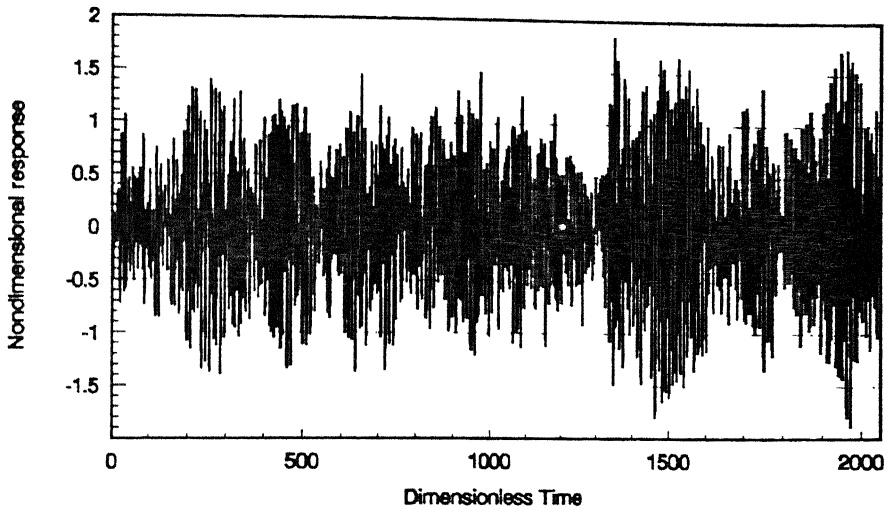

(a) Response, ${}^{x_1}\eta(\tau)$, at station 1.

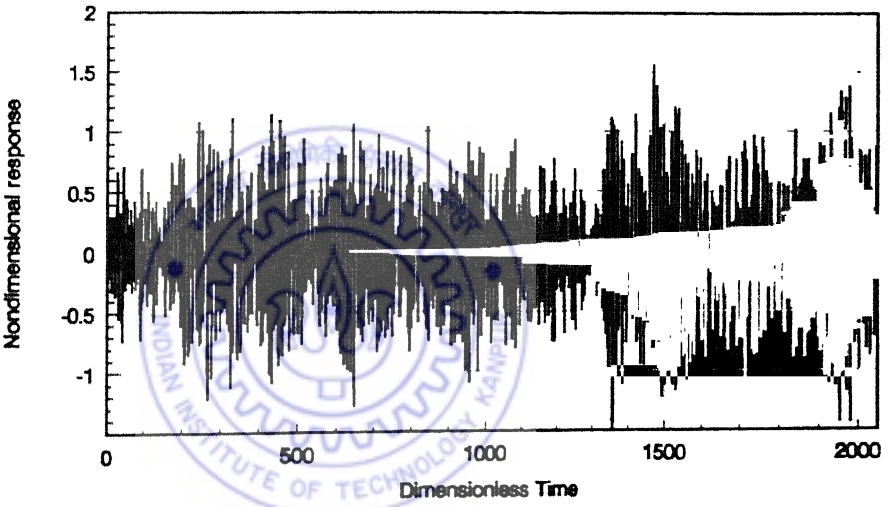

(b) Response, ${}^{x_2}\eta(\tau)$, at station 2.

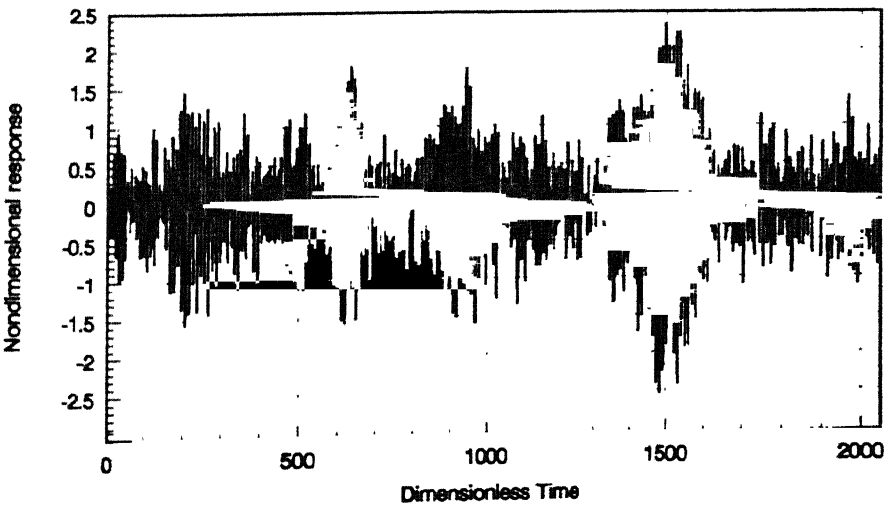

(c) Response, ${}^{x_3}\eta(\tau)$, at station 3.

Fig. 5.12 Typical response samples: Case 2.

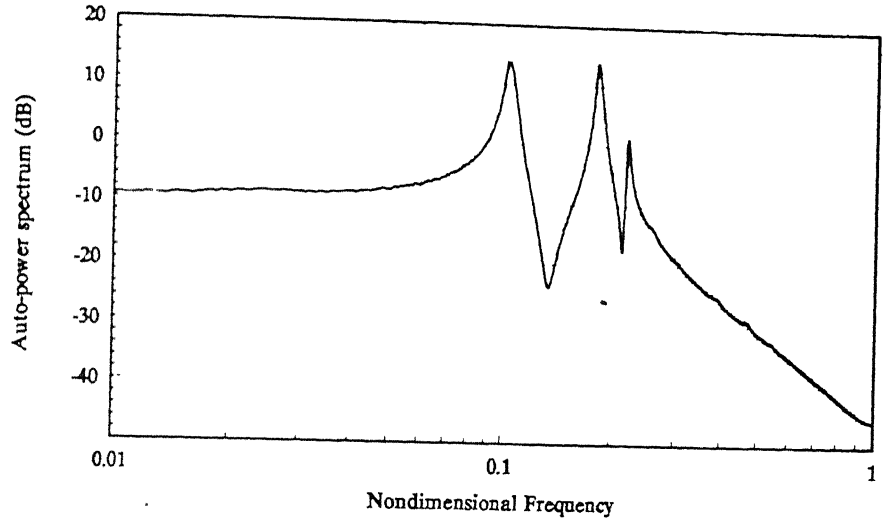

(a) Power-spectrum of ${}^{x_1}\eta(\tau)$.

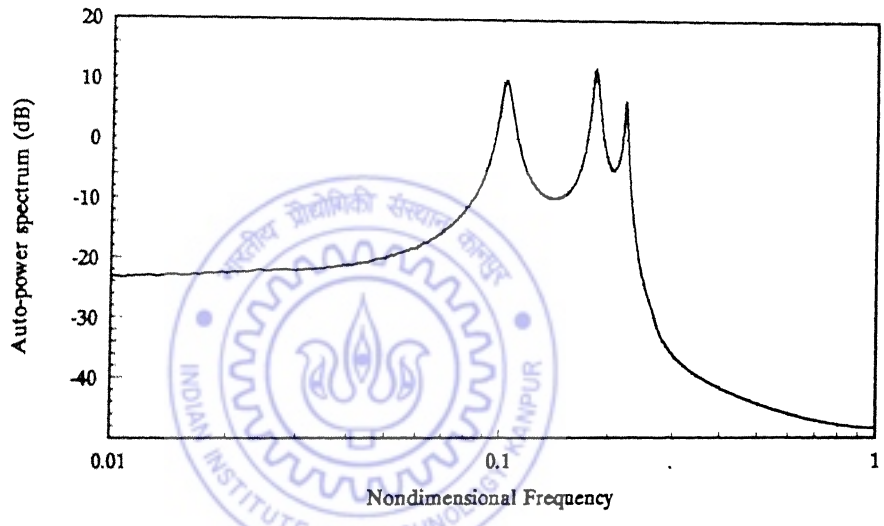

(b) Power-spectrum of ${}^{x_2}\eta(\tau)$.

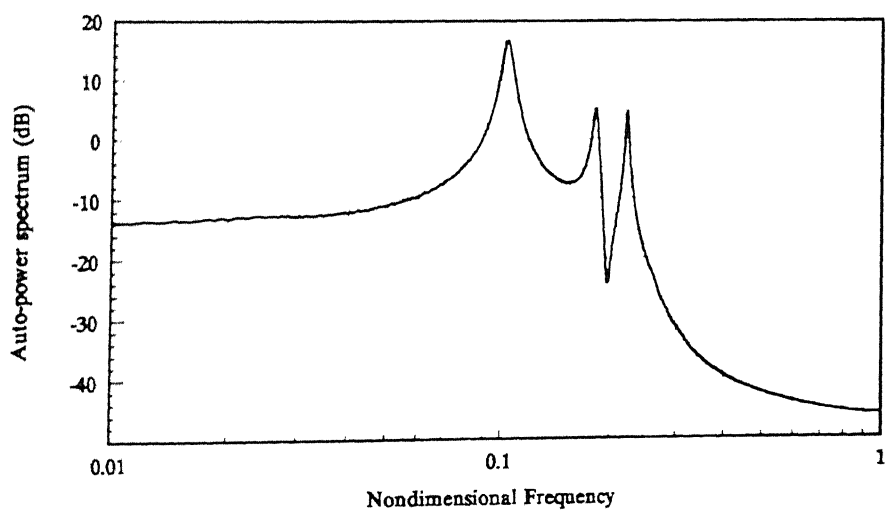

(c) Power-spectrum of ${}^{x_3}\eta(\tau)$.

Fig. 5.13 Power-spectra of the response: Case 2 (averaged over 200 samples).

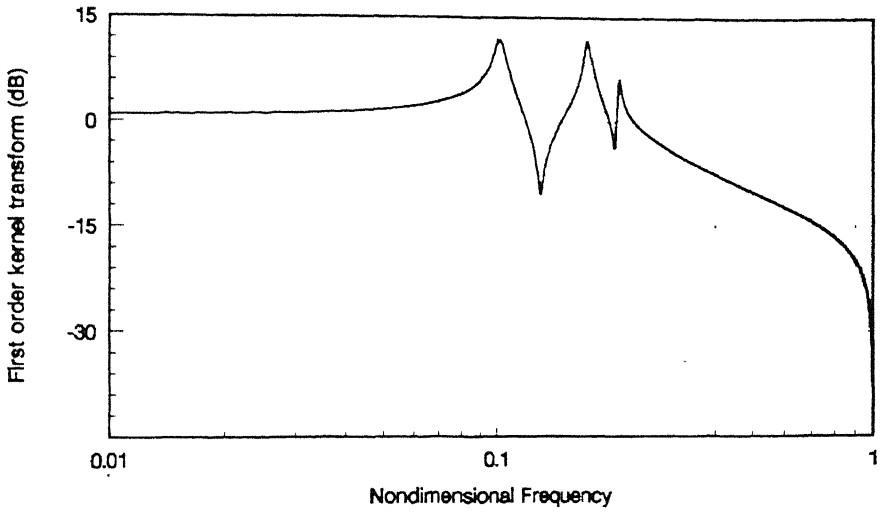

(a) Estimate of ${}^{x_1}H_1^{(1)}(\omega)$.

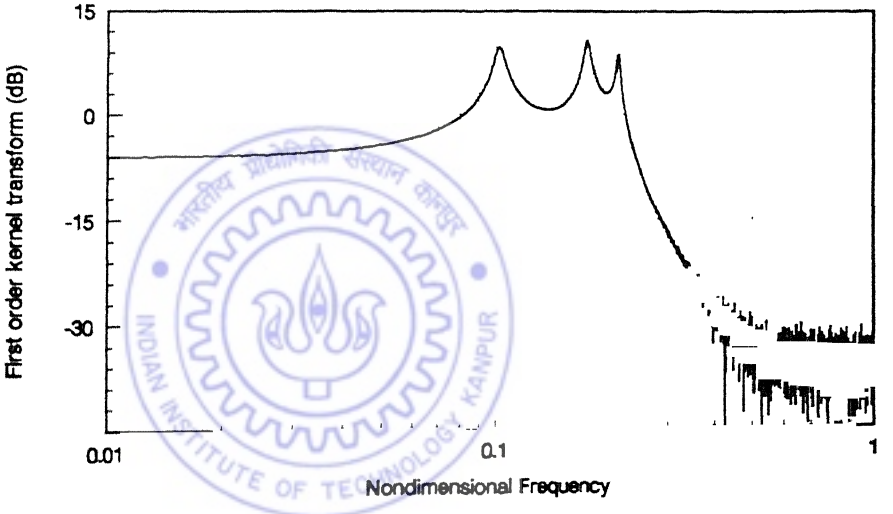

(b) Estimate of ${}^{x_2}H_1^{(1)}(\omega)$.

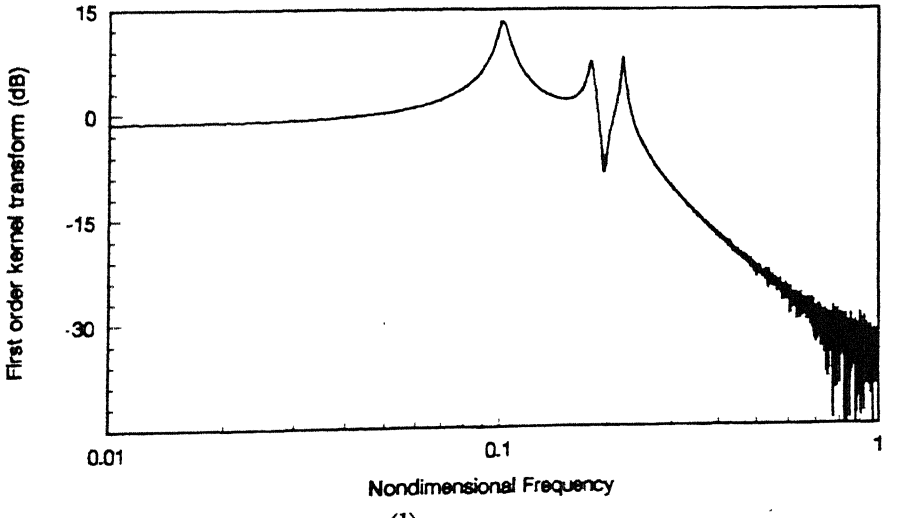

(c) Estimate of ${}^{x_3}H_1^{(1)}(\omega)$.

Fig. 5.14 Estimates of the first order kernel transforms: Case 2 (Contd.)

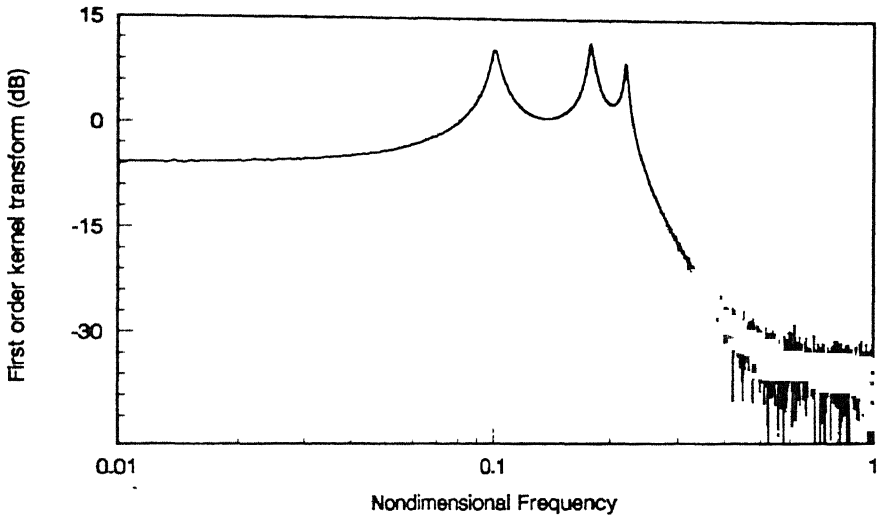

(d) Estimate of ${}^{x_1}H_1^{(2)}(\omega)$.

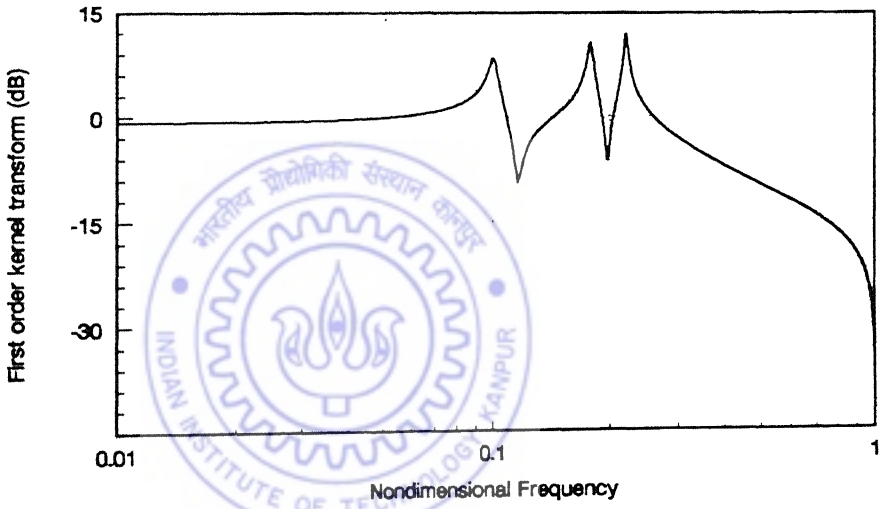

(e) Estimate of ${}^{x_2}H_1^{(2)}(\omega)$.

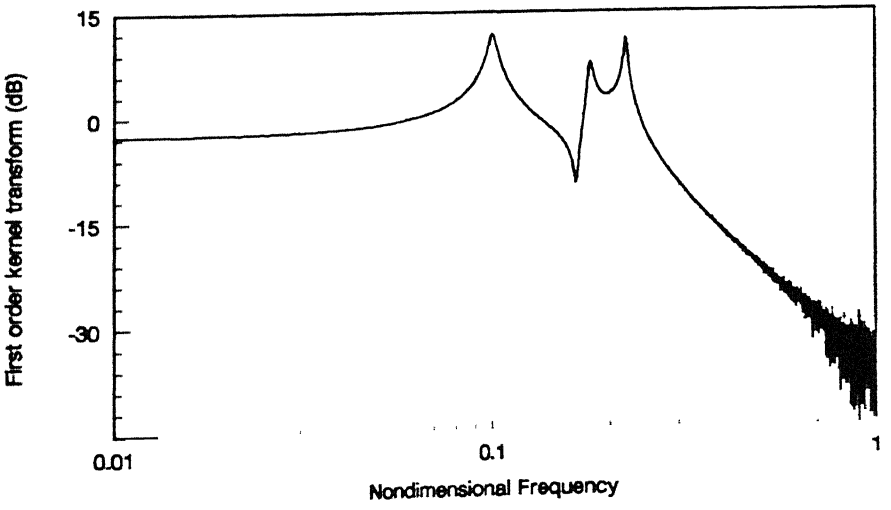

(f) Estimate of ${}^{x_3}H_1^{(2)}(\omega)$.

Fig. 5.14 Estimates of the first order kernel transforms: Case 2.

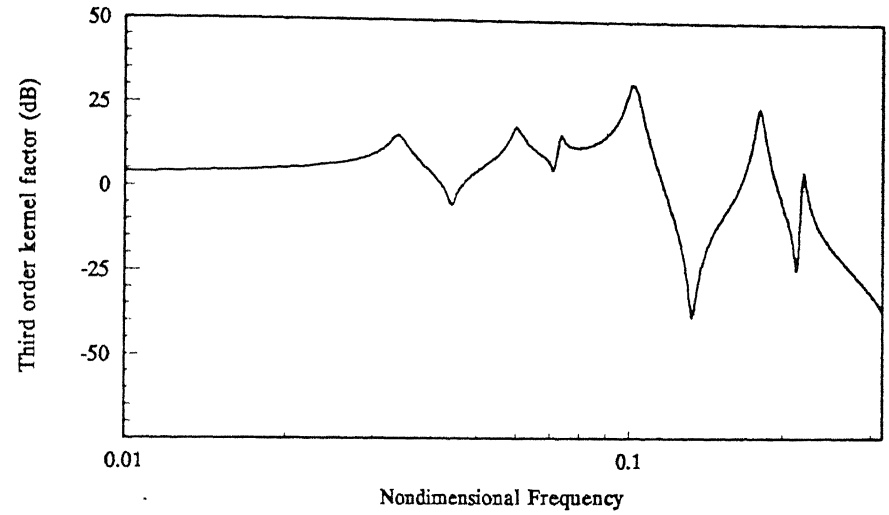

(a) Estimate of ${}^{x_1x_1}\Psi_3^{1-1,1,1}(\omega,\omega,\omega)$.

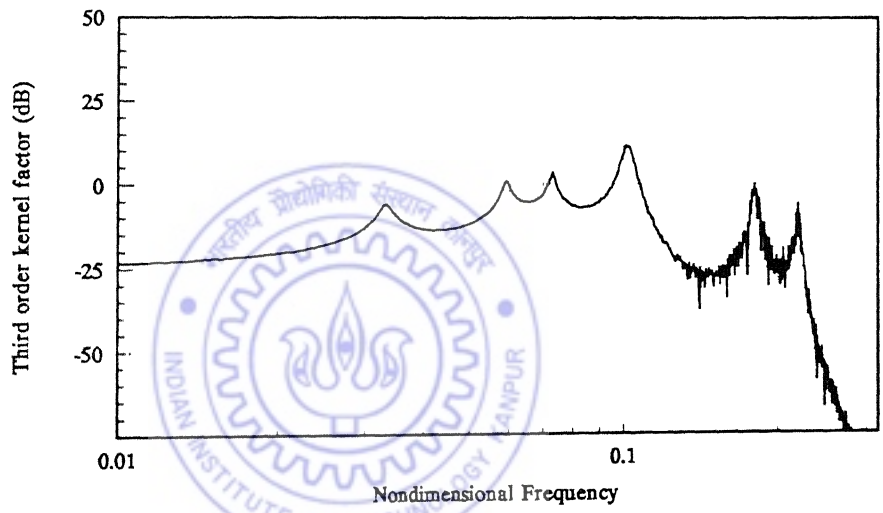

(b) Estimate of ${}^{x_1x_2}\Psi_3^{2-1,1,1}(\omega,\omega,\omega)$.

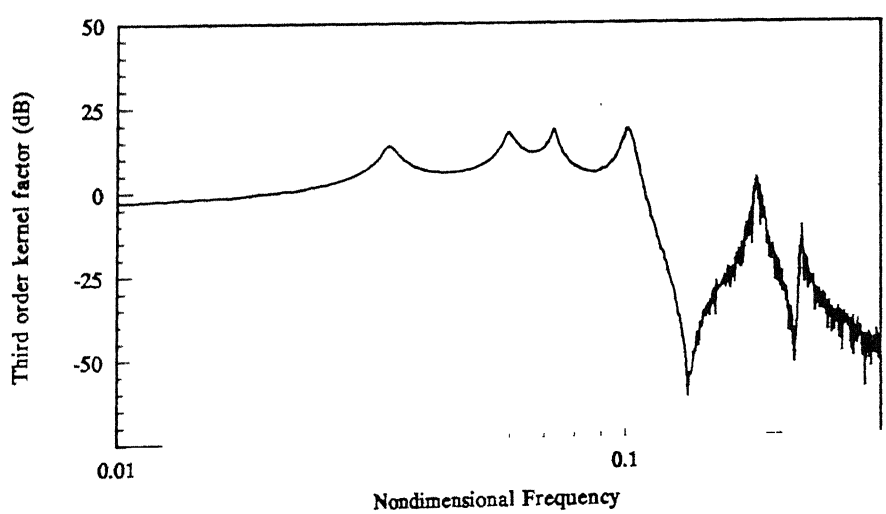

(c) Estimate of ${}^{x_2x_1}\Psi_3^{1-1,1,1}(\omega,\omega,\omega)$.

Fig. 5.15 Third order kernel factors: Case 2 (Contd.)

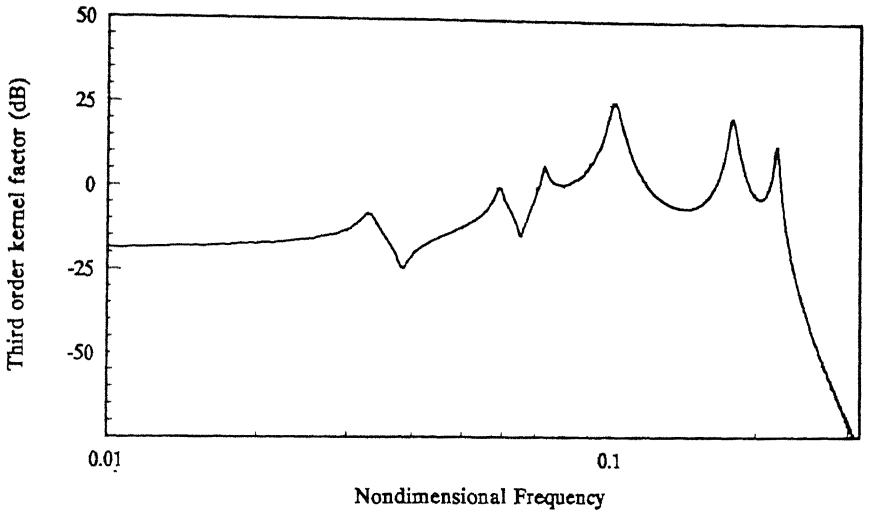

(d) Estimate of ${}^{x_2x_2}\Psi_3^{2-1,1,1}(\omega,\omega,\omega)$.

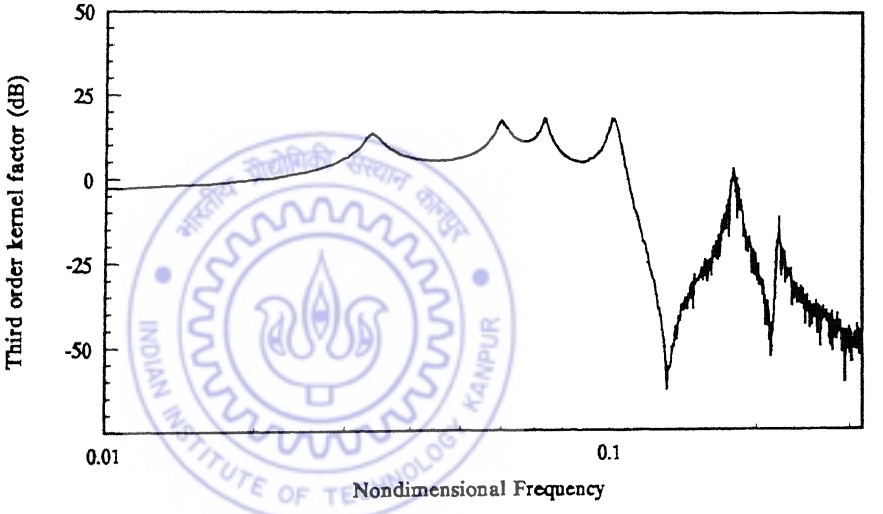

(e) Estimate of ${}^{x_3x_1}\Psi_3^{1-1,1,1}(\omega,\omega,\omega)$.

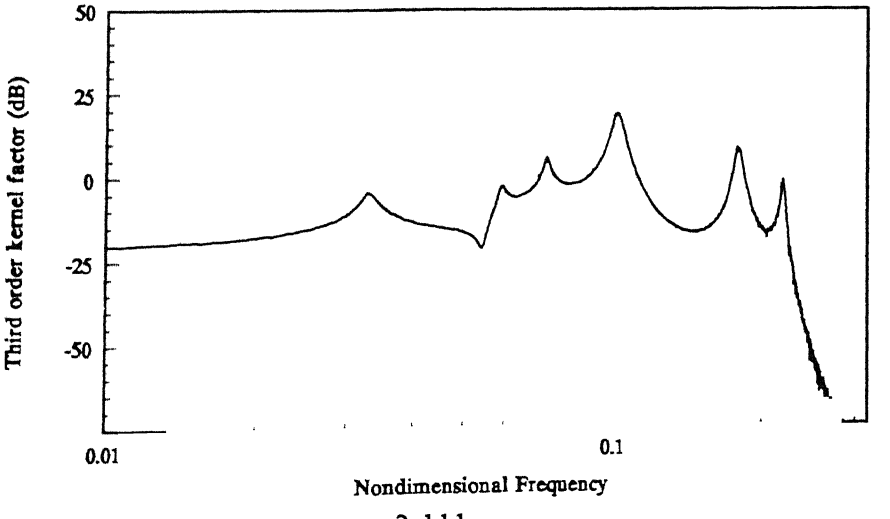

(f) Estimate of ${}^{x_3x_2}\Psi_3^{2-1,1,1}(\omega,\omega,\omega)$.

Fig. 5.15 Third order kernel factors: Case2.

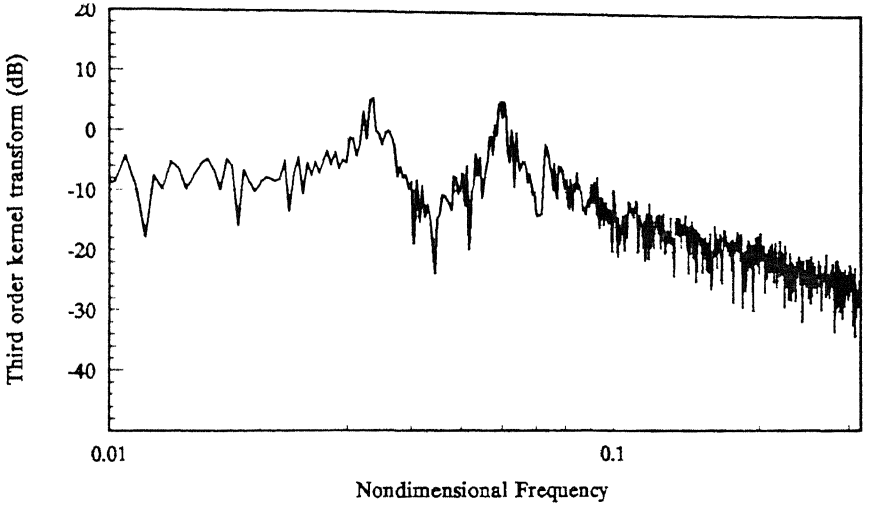

(a) Estimate of ${}^{x_1}H_3^{(1)}(\omega,\omega,\omega)$.

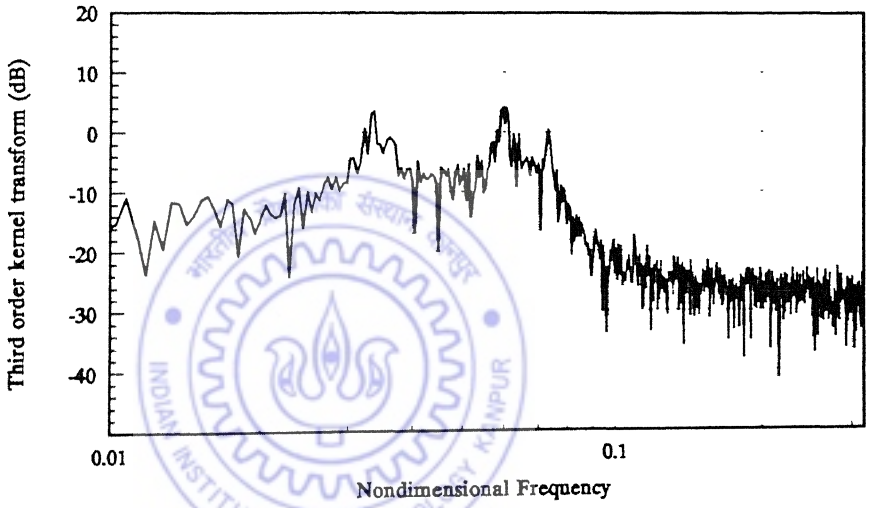

(b) Estimate of ${}^{x_2}H_3^{(1)}(\omega,\omega,\omega)$.

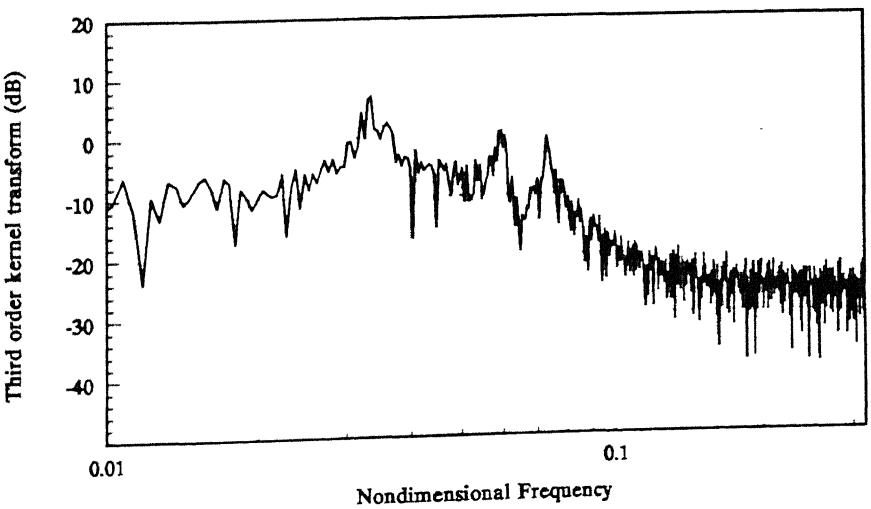

(c) Estimate of ${}^{x_3}H_3^{(1)}(\omega,\omega,\omega)$.

Fig. 5.16 Estimates of third order kernel transforms: Case 2.

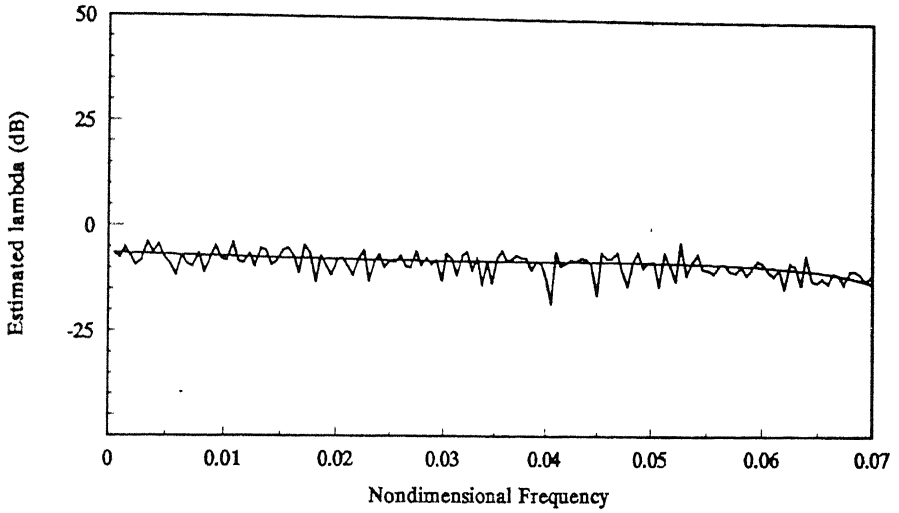

(a) Estimate of λ_{b1}^{N}.

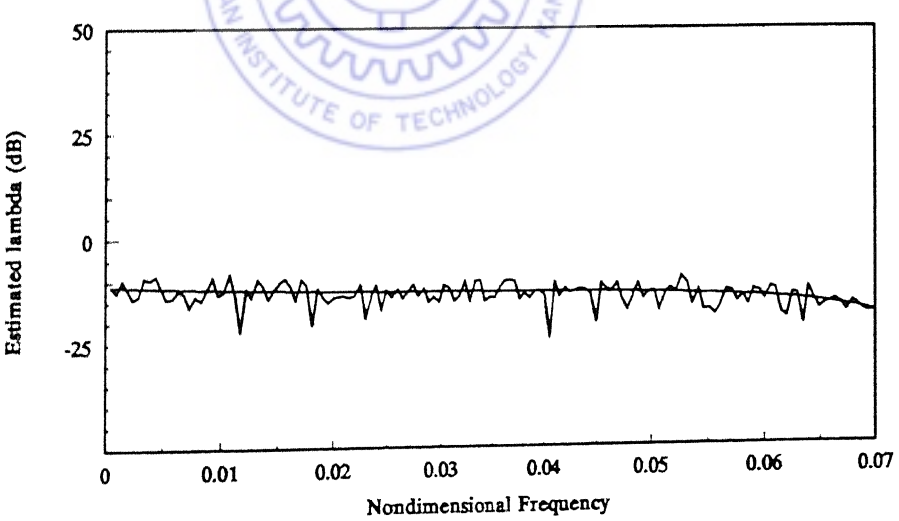

(b) Estimate of λ_{b2}^{N}.

Fig. 5.17 Estimates of the nonlinear parameters: Case 2.

5.6 Remarks

The parameter estimation procedure, developed in the previous chapters for parameter estimation in rigid rotors, has been extended to incorporate shaft flexibility, in this chapter. This has served to illustrate, the general nature of the procedures adopted for nonlinear parameter estimation. Relatively few numerical exercises have been carried out, in this chapter. The accuracies of the estimates with various other nondimensional parameters and measurement noise can be expected to follow trends similar to those in the earlier chapters.

CHAPTER 6

EXPERIMENTAL INVESTIGATIONS

Experimental investigations have been carried out, in addition to the computer simulation described in earlier chapters, for further illustration of the parameter estimation procedures. The experimental studies have been carried out on an existing laboratory rotor-rig. These studies are restricted, due to laboratory constraints, to the case of a rigid rotor supported in ball bearings. For such a bearing, cross-coupling stiffness parameters are negligible in comparison to the direct stiffness coefficients. The experimental rotor-bearing system, if the shaft is rigid, corresponds to the single-degree-freedom system considered in Chapter 3. The rotor-bearing system is set into vibrations by providing white noise excitation at one of the bearing caps. Measurements for excitation force and the resultant vibration response are made simultaneously at the point of force application itself, i.e. at the bearing cap. The measured data is then processed in accordance with the procedure described in Chapter 3, for linear and nonlinear parameter estimation. The experimentation is carried out for various force excitation intensity levels. Variation in the excitation force levels provides with different values of the non-dimensional nonlinear parameter, λ. The rig and the instrumentation are shown schematically in Figure 6.1. A detailed description of the rig, instrumentation and results follows.

6.1 The Rig

The laboratory rig consists of a disc centrally mounted on a shaft supported in two identical ball bearings. The shaft can be driven, if required, through a flexible coupling by a motor. The disc has a mass of 0.815 Kg. The shaft is 0.16 m long with a diameter of 10 mm. The bearings are supported in pedestals, comprising of an upper cap and a lower case. The pedestal is mounted on a steel base, which in turn is bolted to a foundation.

The bearings are SKF make with the following specifications -

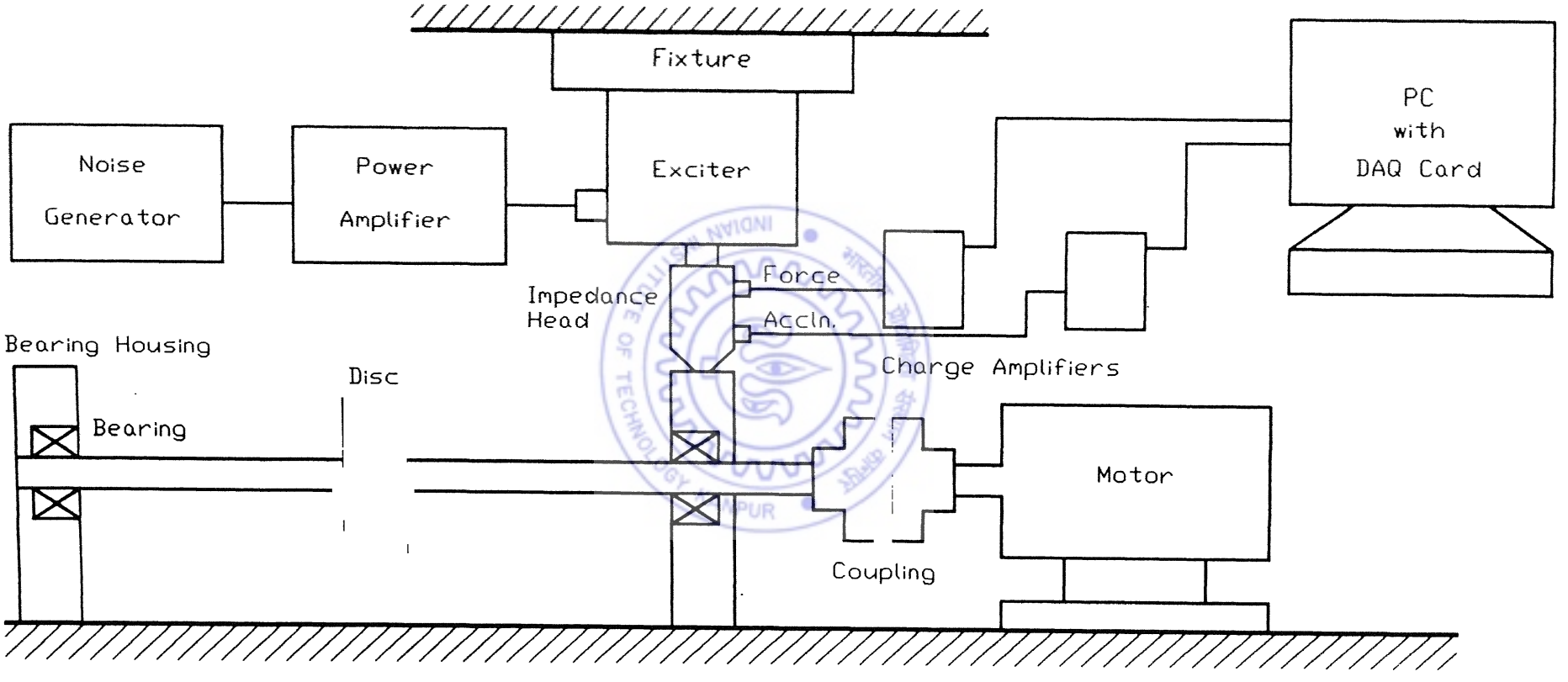

Fig. 6.1 Schematic diagram of the rotor rig.

Ball bearing Type	SKF 6200
Number of balls	6
Ball diameter	6 mm
Bore diameter	10 mm
Outer diameter	30 mm
Pitch diameter	20 mm
Inner ring ball race radius	3.09 mm
Outer ring ball race radius	3.09 mm
Allowable pre-load	0 - 2 μ m
Rotor mass per bearing	0.41 kg

Figure 6.2 shows the overall experimental arrangement. The rotor-bearing is excited through the bearing cap by a electro-dynamic shaker. The shaker is mounted on a specially designed rigid frame. Two-plane rigid-rotor balancing is carried out before proceeding with the experiments.

6.2 Instrumentation

White noise excitation is generated by a random signal generator (Brüel & Kjaer make, Type 1405). This noise generator has a frequency range of 20Hz to 100 kHz and can provide a maximum uniform spectral density of 10^{-4} V^2/Hz upto 50 kHz frequency. The white noise signal is amplified through a power amplifier and fed to the shaker. The Power Amplifier is Brüel & Kjaer make, Type 2706 with a frequency range of 10 Hz to 20 kHz, with a signal distortion limit of approximately 0.2%. The electrodynamic shaker is also of Brüel & Kjaer make, with a frequency range of 0 - 18 kHz and a peak-to-peak force rating ranging upto 10 N and a maximum displacement of 6 mm. The excitation force and response are measured by an impedance head attached between the shaker and the bearing cap. The close up of the rig including the shaker and the impedance head is shown in Figure 6.3. The impedance head is Brüel & Kjaer make, Type 8001 with accelerometer sensitivity of 3 pC/ms^{-2}, force gauge sensitivity of 370 pC/N and 1-

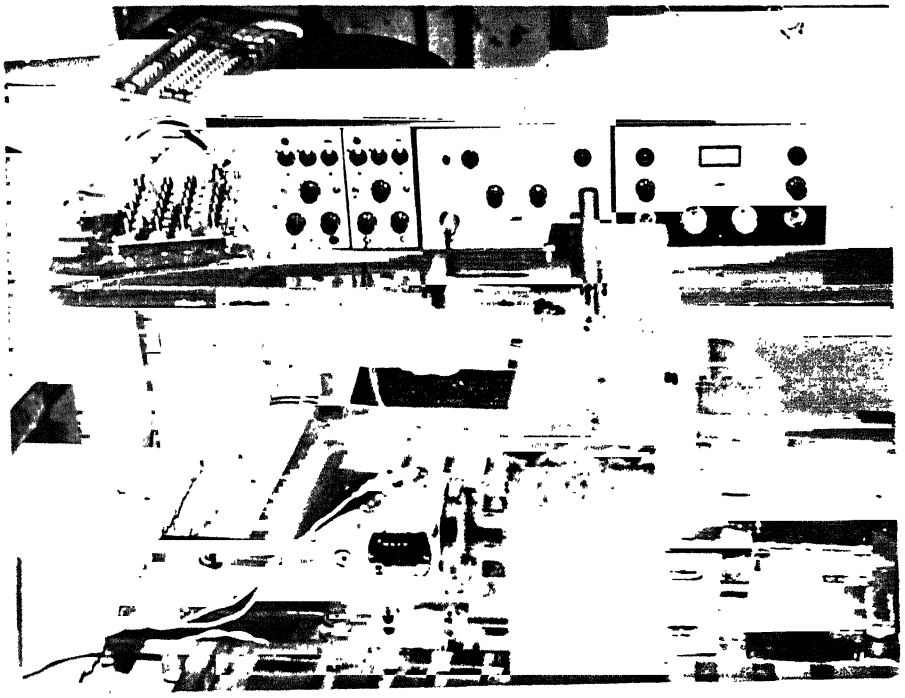

Fig. 6.2 Overall experimental arrangement.

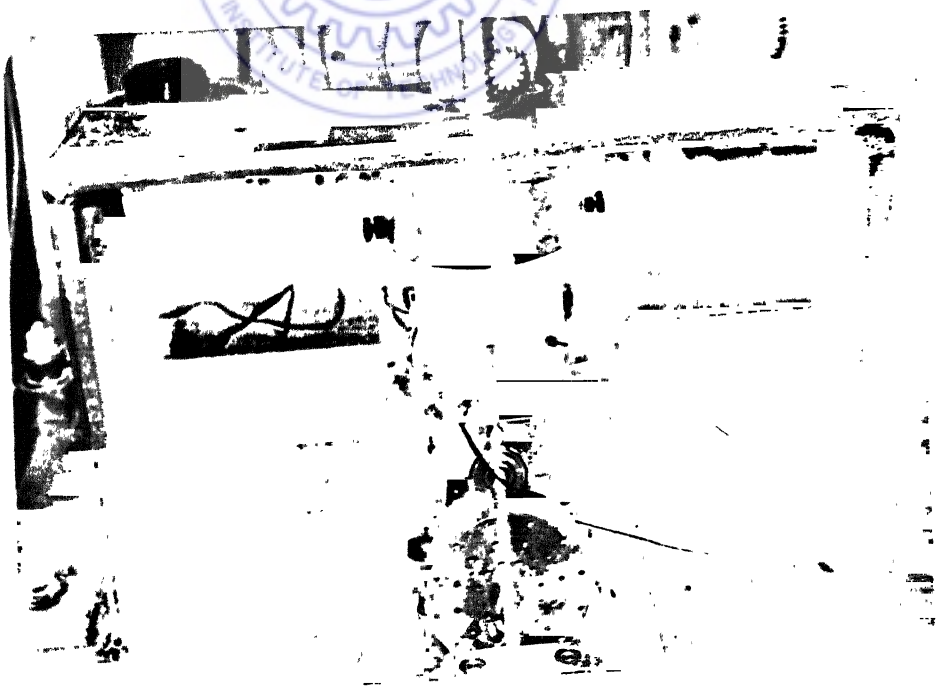

Fig. 6.3 Close-up of the shaker and impedance head.

10,000 Hz frequency range. The signals from the impedance head is fed to a computer through standard Brüel & Kjaer, Type 2635, charge amplifiers.

6.3 Data Acquisition

The analog signals from impedance head through charge amplifier are digitized in the computer through a 32 bit Analog to Digital conversion card. The data is acquired into the computer through a virtual instrumentation (VI) program using LabVIEW software. The data acquisition card (National Instruments, Texas; Type-AT-MIO-16E-10) has a 12 bit resolution and a maximum sampling rate of 100 kS/s. The front panel and back panel of the VI program developed in LabVIEW for the data acquisition are shown in Figures 6.4(a) and 6.4(b). The data for the excitation force and the vibration response is acquired at 4096 number of equispaced time (t) instants, for a total period of 0.32 sec. Such a set of data is treated as a set of force and response *samples*. A total of 2000 such *samples* are collected for both the force excitation and the acceleration response and treated as an *ensemble* of force and response samples. Statistical averaging is carried out over this *ensemble* for further processing.

6.4 Case Studies

As mentioned earlier, experimental studies are carried out for various force excitation intensity levels. These force intensity levels are set by choosing the spectral density level on the white noise generator. The maximum force, F_{max}, obtained in a force *sample*, is incorporated in the definition of the non-dimensional nonlinear parameter λ (ref: equation 3.3). For the same rotor-bearing configuration, different values of F_{max} provide different values of λ and the results obtained for the estimates can be compared in a statistical context, as in Chapter 3.

Case 1:

As a first case the spectral density level on the white noise generator is set such that it gives F_{max} = 3.27 N, as measured by the impedance head on the bearing cap. A typical *sample* of the white noise excitation force is shown in Fig. 6.5 (a). The response in terms

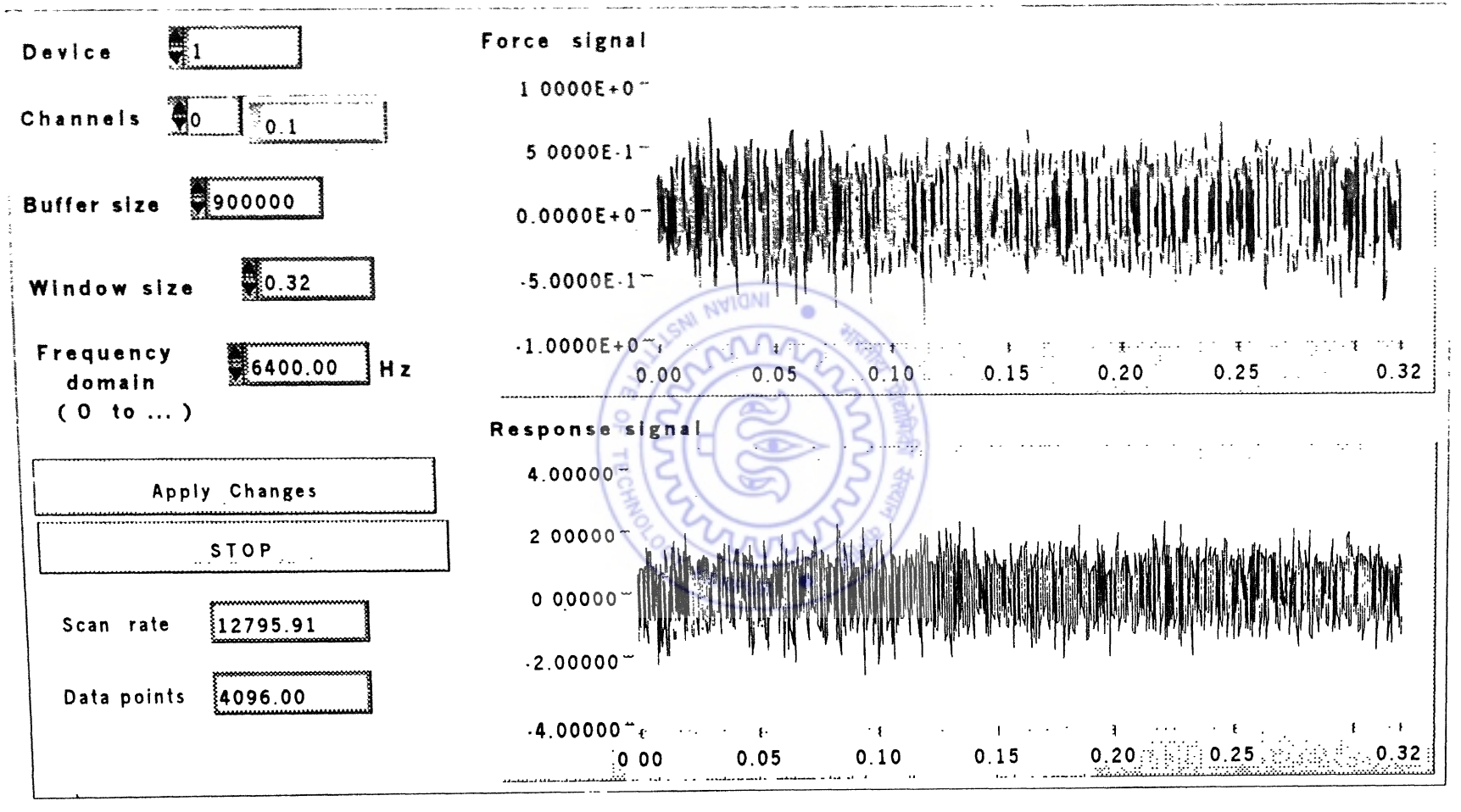

Fig. 6.4(a) Front Panel of the LabVIEW VI for data acquisition.

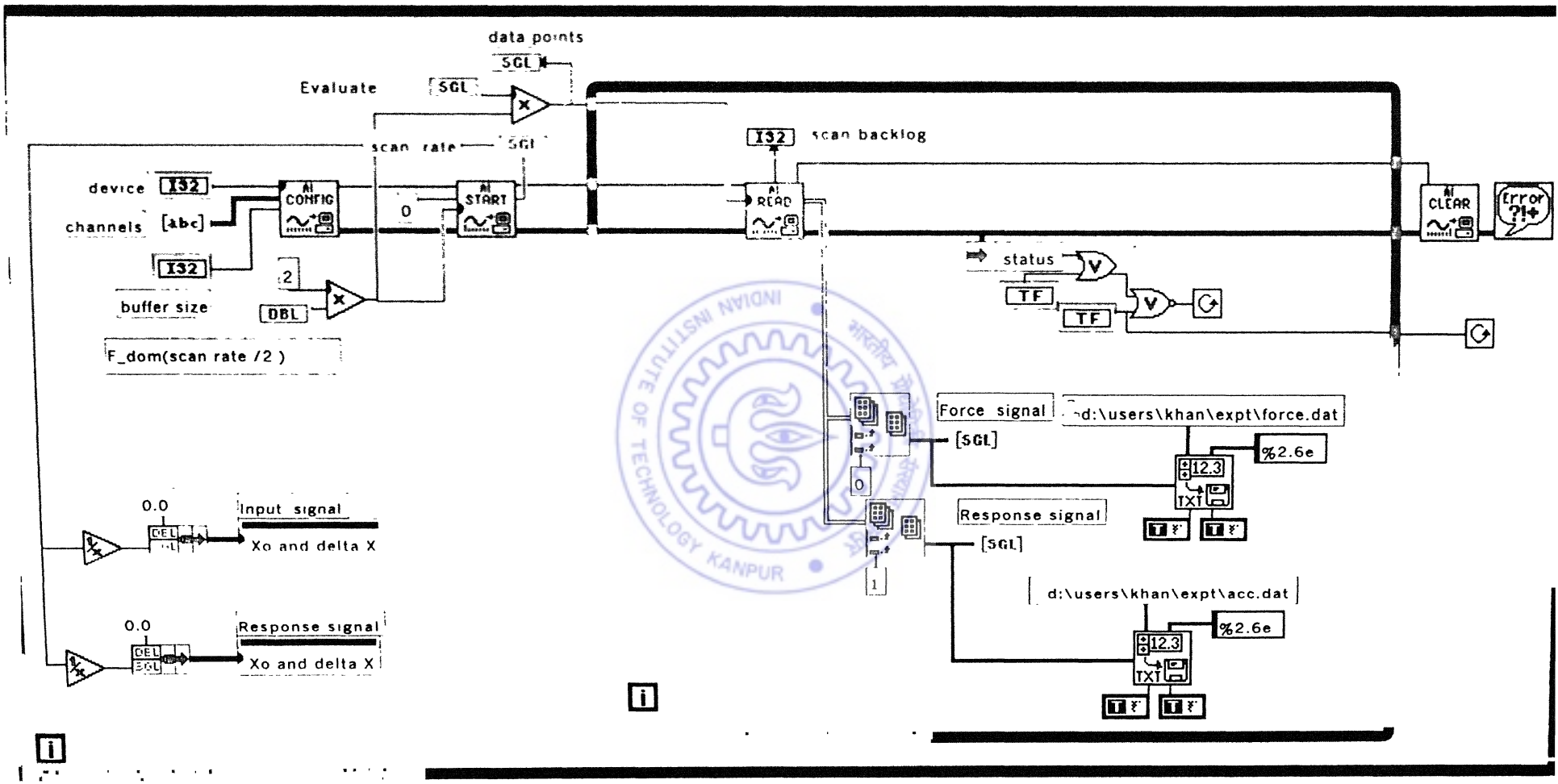

Fig. 6.4(b) Back Panel of the LabVIEW VI for data acquisition.

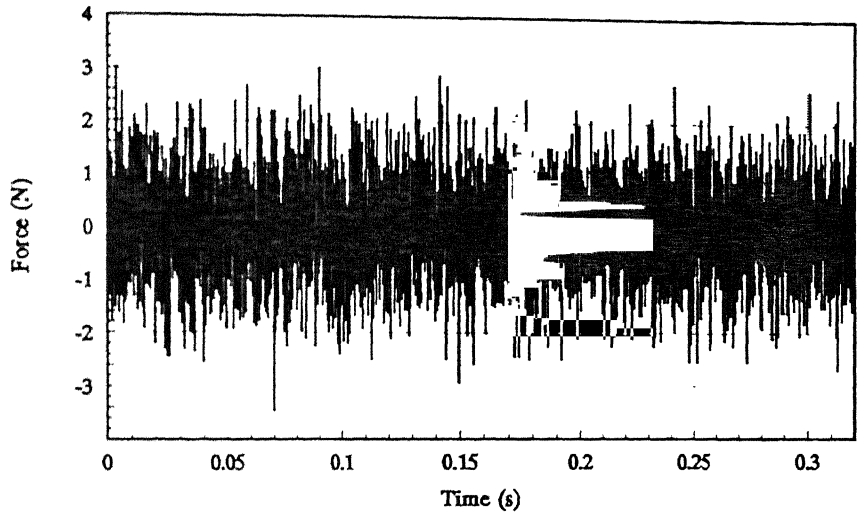

Fig. 6.5(a) Typical sample of the input force: Case1

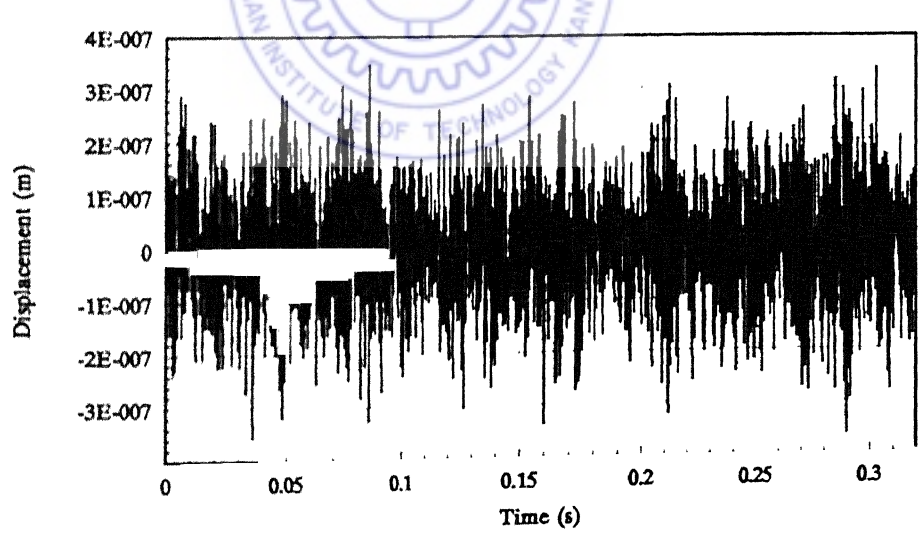

Fig. 6.5(b) Typical sample of the response: Case1

of displacement, is obtained through integration of the acceleration signal. The typical sample of the displacement is shown in Fig. 6.5 (b). In order to check the noise level in the measurements, all the instruments, including the electromagnetic shaker, were put on. The gain of the power amplifier between the signal generator and the shaker was adjusted at the lowest level so as to have no excitation conditions. Typical signals recorded, from the impedance head, under this condition, are shown in Figs. 6.6 (a) and (b). Comparison of these with the force and response signals of Figs. 6.5 (a) and (b) respectively, shows that the noise to signal ratio, in the extreme cases are 2.8% and 3.5% respectively. The influence of measurement noise on the parameter estimation procedure was discussed in Chapter 3 and the procedure was illustrated to be robust in the presence of 5% noise. The present noise levels are rather small and it can be safely assumed that their influence on the estimates will be insignificant. The power spectrum density of the excitation force is obtained by averaging over the *ensemble* formed from 2000 individual samples force signals. The power spectrum density for this case can be seen to be equal to $0.36\,N^2/Hz$ (-4.436dB) from Fig. 6.7 (a). The power spectrum density of the displacement response, similarly averaged over the ensemble is shown in Fig. 6.7 (b). The frequency in these two plots ranges from 0 to 6400 Hz. The two peaks are observed in Fig. 6.7 (b), a prominent one at a frequency equal to 1125 Hz and a minor one at a frequency of 3375Hz. The predominant frequency of 1125 Hz, represents the fundamental frequency of the system. (This was confirmed separately also, through repeated rap-tests, using an impact-hammer.) The minor peak at 3375 Hz suggests the presence of a nonlinearity in the system which can be approximated by a cubic function. That the system nonlinearity is of cubic type was further confirmed by applying a harmonic force on the system, through the Signal Generator, instead of a random white noise. A sweep test with harmonic excitation was performed and the response was noted. It was observed that along with a prominent peak corresponding to the harmonic excitation frequency, the plot of the response contains a minor peak at the 3rd multiple of the harmonic excitation frequency. This observation is displayed in the series of Figures 6.8 (a)-(f).

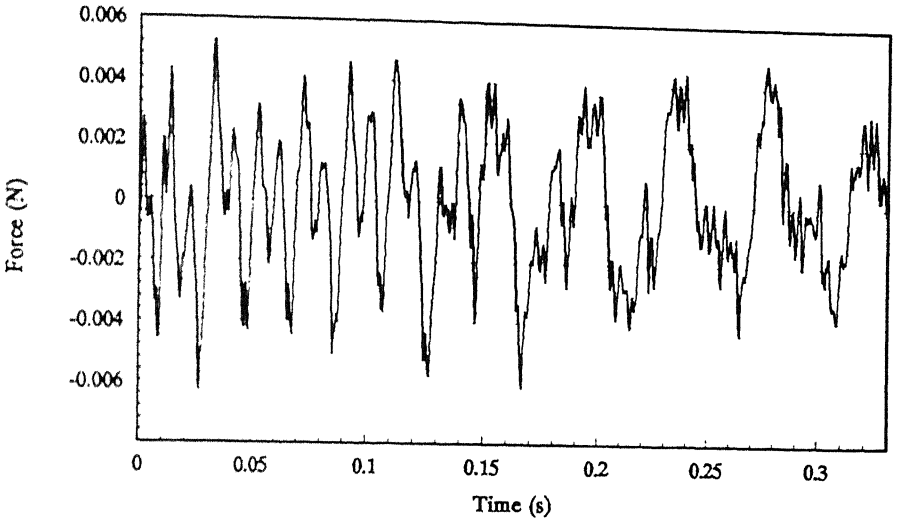

Fig. 6.6(a) Typical sample of noise level in input-force measurement.

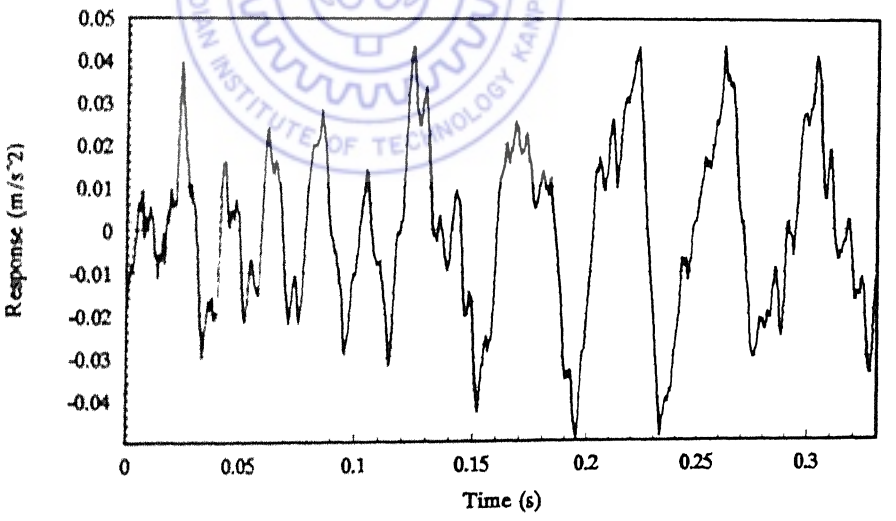

Fig. 6.6(b) Typical sample of noise level in response measurement.

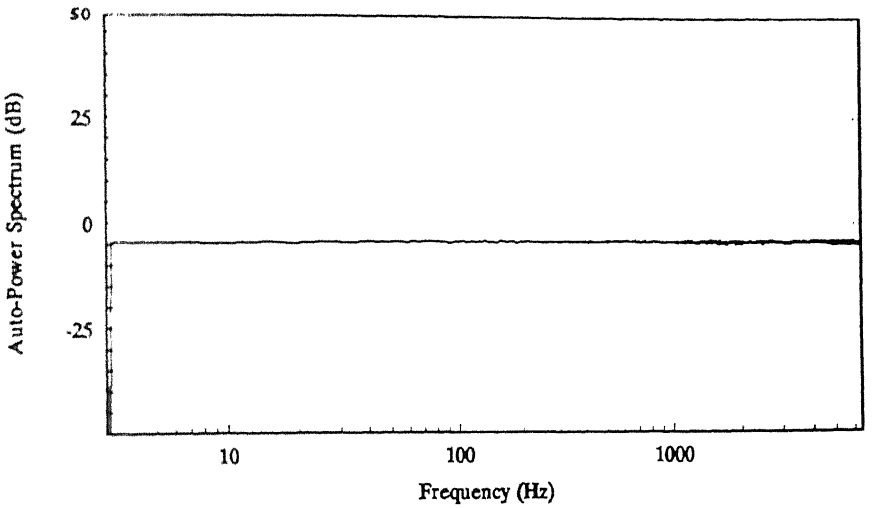

Fig. 6.7(a) Power spectrum of the input force: Case1 (averaged over 2000 samples).

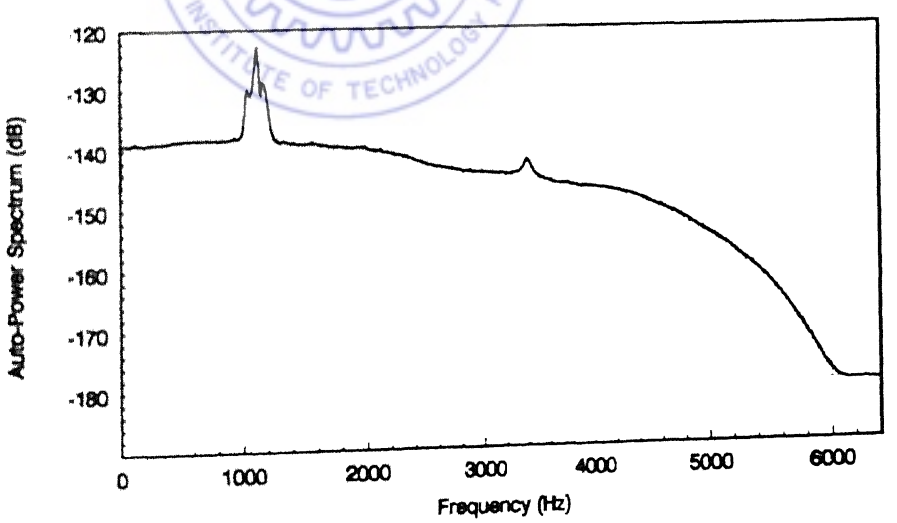

Fig. 6.7(b) Power spectrum of the response: Case1 (averaged over 2000 samples).

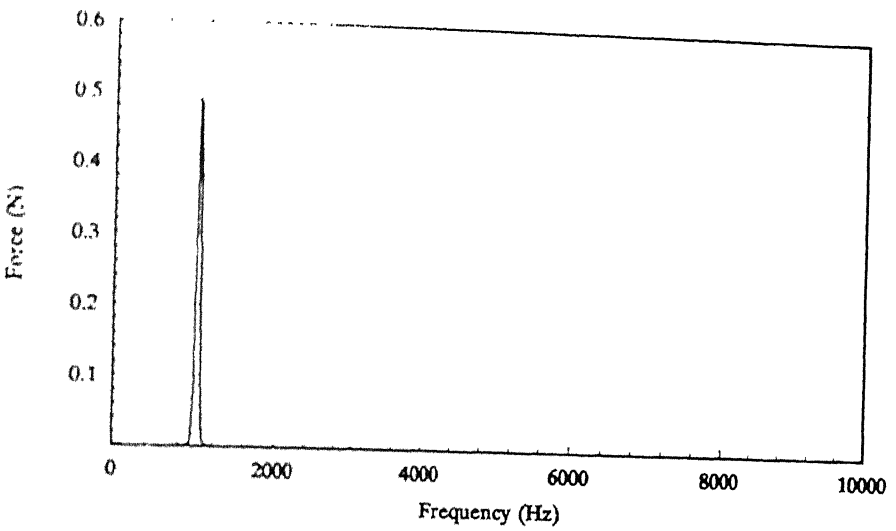

Fig. 6.8(a) Harmonic excitation at $\omega = 1000$ Hz.

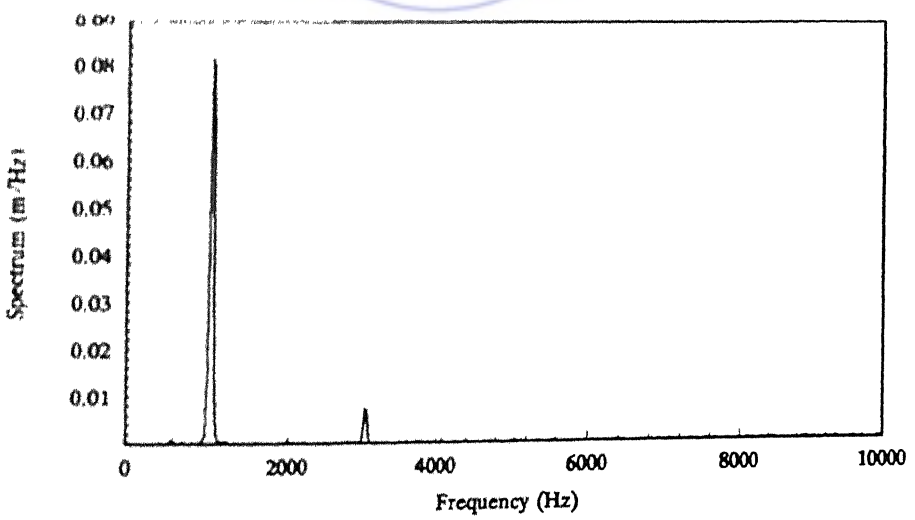

Fig. 6.8(b) Response to the harmonic excitation of (a) above.

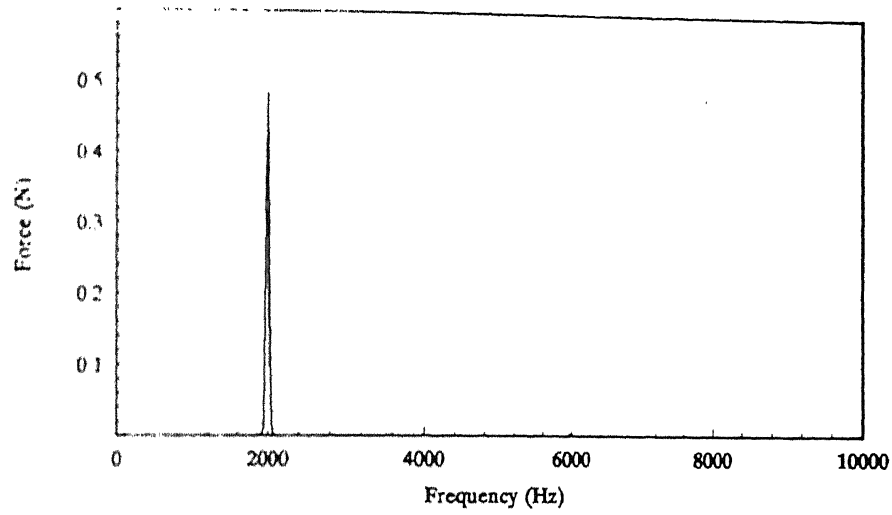

Fig. 6.8(c) Harmonic excitation at $\omega = 2000$ Hz.

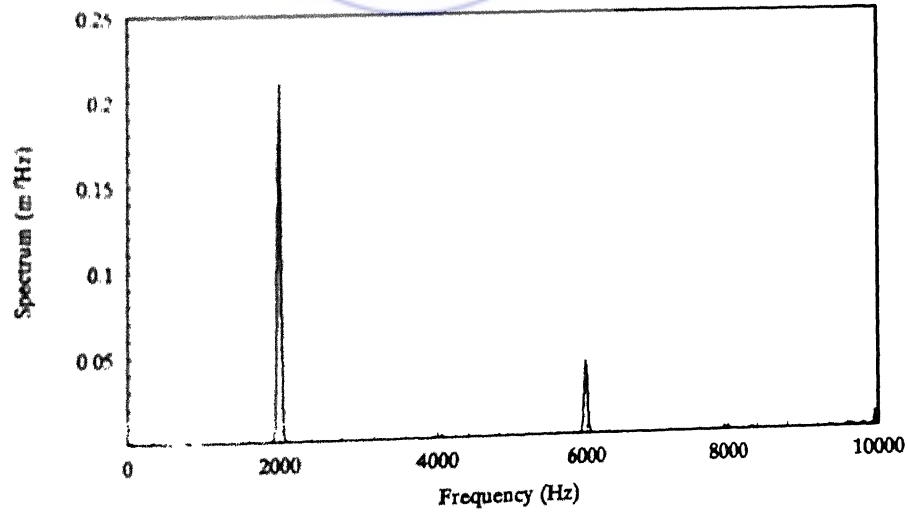

Fig. 6.8(d) Response to the harmonic excitation of (b) above.

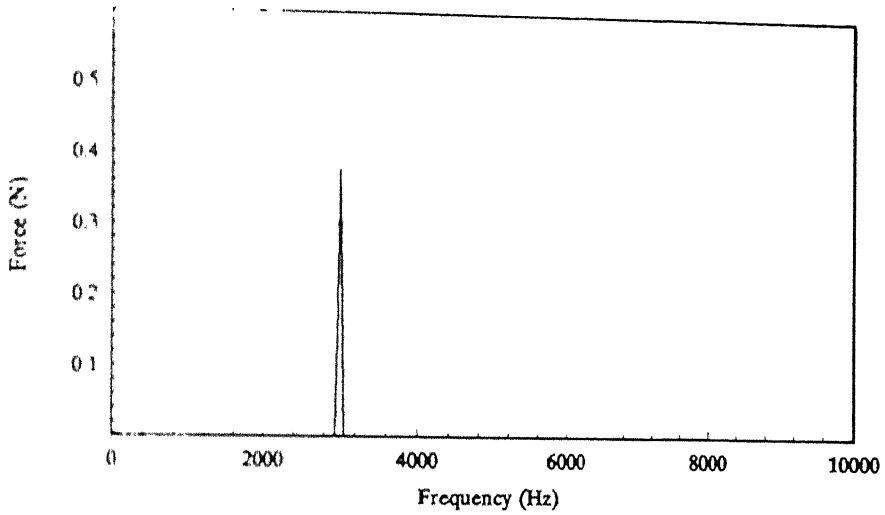

Fig. 6.8(e) Harmonic excitation at $\omega = 3000$ Hz.

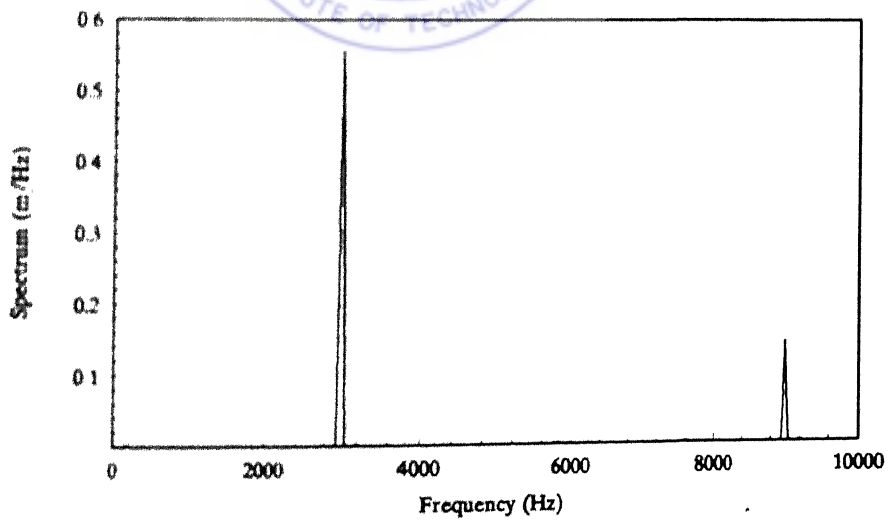

Fig. 6.8(f) Response to the harmonic excitation of (e) above.

The white noise excitation and the response measurements are employed to construct the first order Volterra kernel transform $H_1(\omega)$, through use of equations (3.34) and (3.42)-(3.43). The first order Volterra kernel transform $|H_1(\omega)|$, thus obtained is shown in Fig. 6.9. The algebraic form of $H_1(\omega)$ from equation (3.12) is

$$H_1(\omega) = \frac{1}{m\omega^2 + jc\omega + k} = \frac{1/m}{(\omega_n^2 - \omega^2) + j2\xi\omega\omega_n} \tag{6.1}$$

The linear parameters ω_n and ξ are estimated from $H_1(\omega)$. The natural frequency has been readily identified as

ω_n = 1125 Hz = 7068.58 rad/s

The estimate of damping, using a least square fit of the curve of Fig. 6.9 with equation (6.1), is found to be

ξ = 0.008.

The third order kernel factor $\Psi_3(\omega,\omega,\omega)$ is synthesised from the first order Volterra kernel transform $H_1(\omega)$ of Fig. 6.9, in accordance with equation (3.20). The absolute values of $\Psi_3(\omega,\omega,\omega)$ and $H_3(\omega,\omega,\omega)$ are shown in Fig. 6.10 (a), (b). As in the case of the computer simulation of Chapter 3, it can be observed, from the Figs. 6.10 (a),(b) that while the measured third order kernel transform $H_3(\omega,\omega,\omega)$ is reasonably accurate in showing the harmonic at $\omega_n/3$ (=375 Hz.), the identification of the harmonic at ω_n (= 1125 Hz) is weak. Improvement in these plots can be expected if the number of samples in the ensemble, over which averaging is carried out, is increased. In the present study, however, due to data storage limitations in the computer, the number of samples in the ensemble has been restricted to 2000. The estimation of λ, from these kernel transforms, is therefore restricted to the frequency zone of 0-1000 Hz. The nonlinear stiffness k^N is obtained from the plots of $\Psi_3(\omega,\omega,\omega)$ and $H_3(\omega,\omega,\omega)$, by employing equation (3.44). The estimate of k^N, thus obtained is plotted in Fig. 6.11. A fourth order

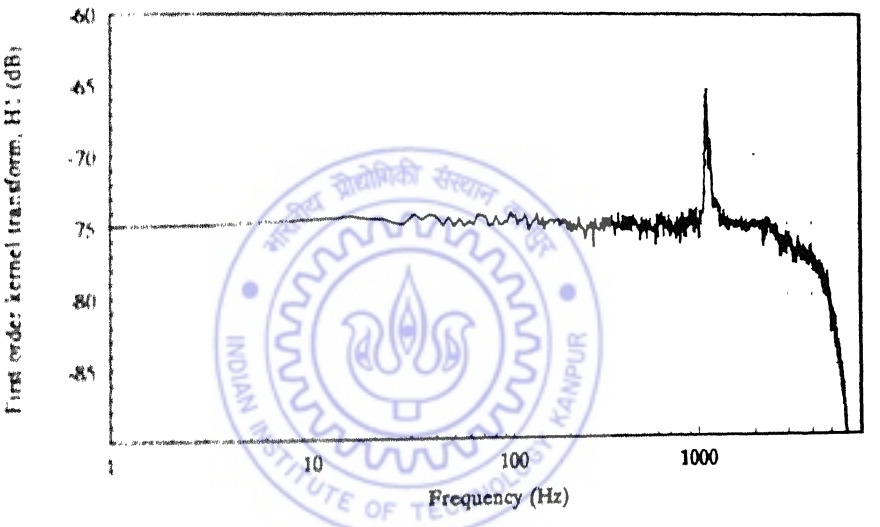

Fig. 6.9 Estimate of first order kernel transform, $H_1(\omega)$: Case 1

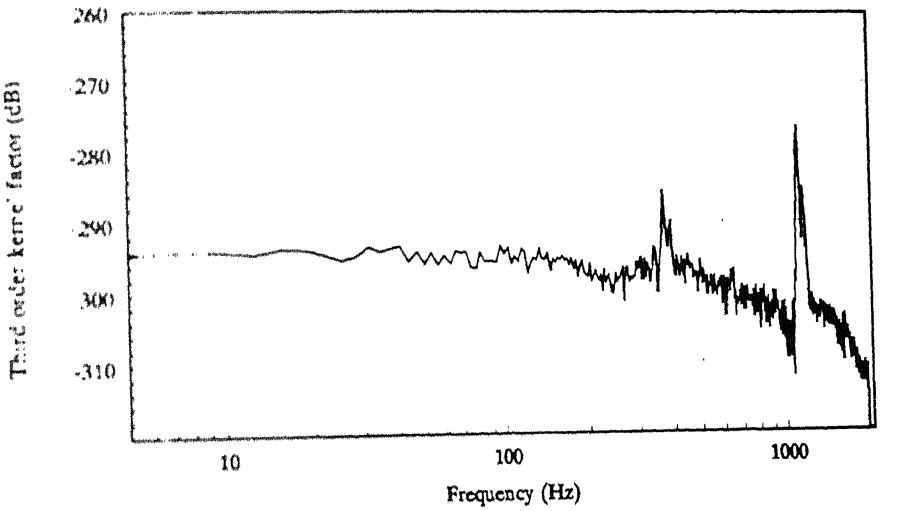

(a) Estimate of $\Psi_3(\omega,\omega,\omega)$.

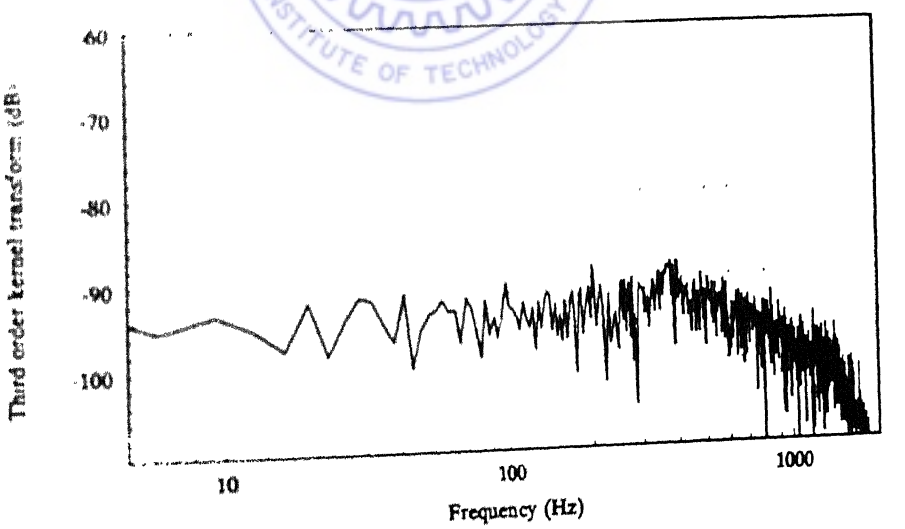

(b) Estimate of $H_3(\omega,\omega,\omega)$.

Fig. 6.10 Third order estimates: Case 1.

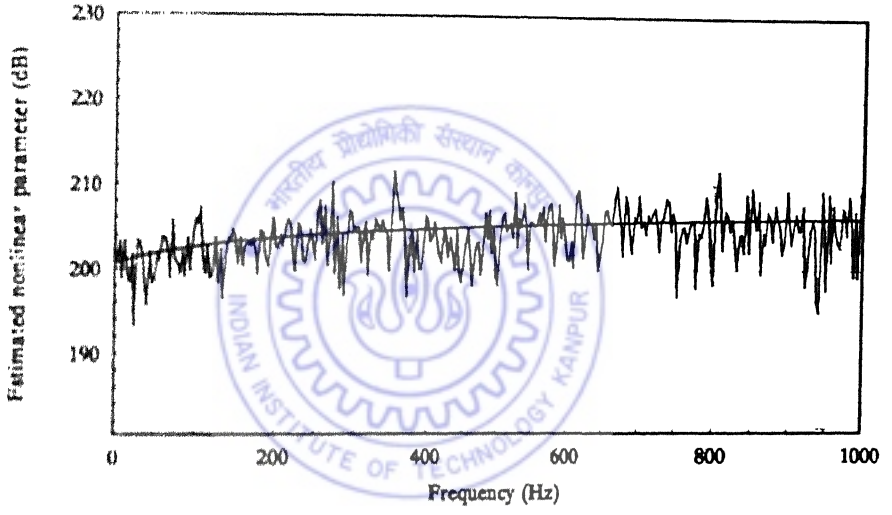

Fig. 6.11 Estimate of the nonlinear parameter, k^N : Case 1

polynomial curve regressed through the estimates of k^N over the frequency range, is also shown in Fig. 6.11. The mean value of the estimates of k^N is found to be 2.99 x 10^{20} N/m^3. Assuming that both the bearings are identical and act parallely, the nonlinear stiffness k^N of each bearing can be written as 1.49 x 10^{20} N/m^3. The corresponding value of the nondimensional nonlinear parameter λ is calculated as 0.366.

The sign of k^N can be readily identified as negative, from the discussion of Section 3.6.6, and by observing the signs of $\omega_n/3$ peaks of the real and imaginary components of $\Psi_3(\omega,\omega,\omega)$ and $H_3(\omega,\omega,\omega)$ shown in Figs. 6.12 and 6.13.

Case 2:

As the next case, the excitation force level is lowered down, such that F_{max} = 1.1 N. Typical samples of the excitation force and the displacement response are shown in Figs.6.14 (a),(b) respectively. The power spectrum density of the excitation force (Fig. 6.15(a)) is 0.038 N^2/Hz (-14.2dB), in this case. The power spectrum of the displacement response, shown in Fig.6.15(b), as in Case 1, shows a major peak at 1125 Hz and a minor one at 3375 Hz. The first order Volterra kernel transform, $H_1(\omega)$ is shown in Fig.6.16. The natural frequency identified from the plot of $H_1(\omega)$ is

ω_n = 1125 Hz = 7068.58 rad/s

while damping has been estimated as

ξ = 0.0078.

The third order kernel factor, $\Psi_3(\omega,\omega,\omega)$ and the third order Volterra kernel transform $H_3(\omega,\omega,\omega)$ have been plotted in Fig. 6.17 (a) and 6.17 (b), respectively. The estimate of the nonlinear stiffness, k^N, is shown in Fig. 6.18. The mean value of k^N for each bearing, in this case, has been found to be 3.58 x 10^{20} N/m^3. It can be observed, through a comparison between the plots of Cases 1 and 2, that while the identification of the $\omega_n/3$ peak is sharper in $H_3(\omega,\omega,\omega)$ if the excitation force level is lower (Case 2),

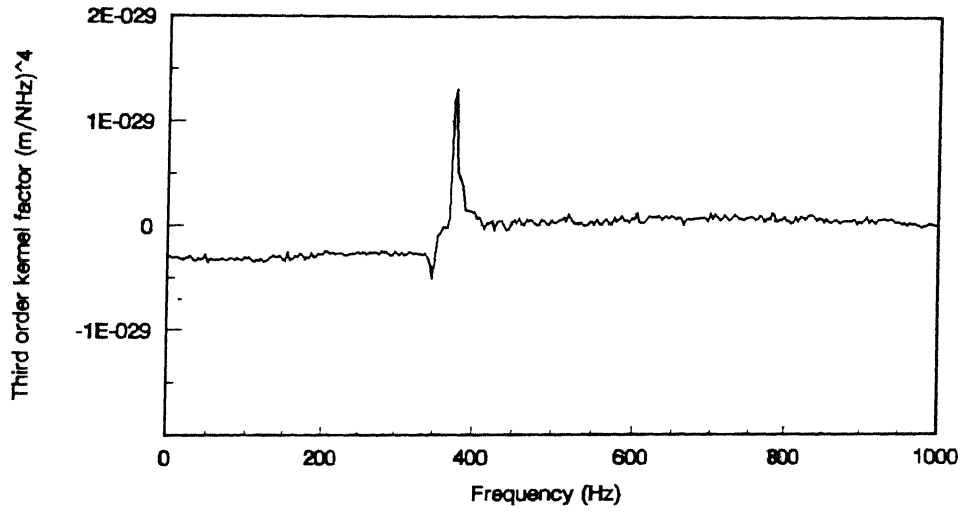

(a) Real component.

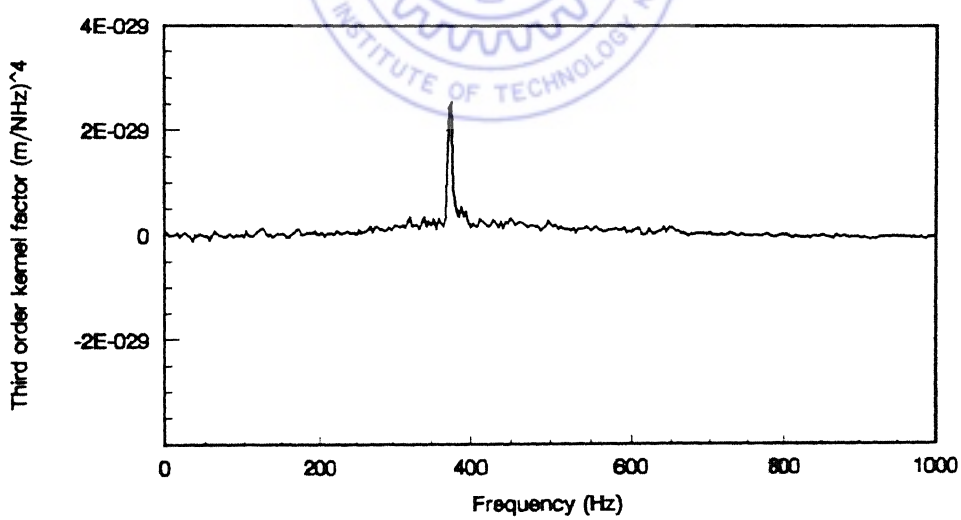

(b) Imaginary component.

Fig. 6.12 Estimate of third order kernel factor $\Psi_3(\omega,\omega,\omega)$.

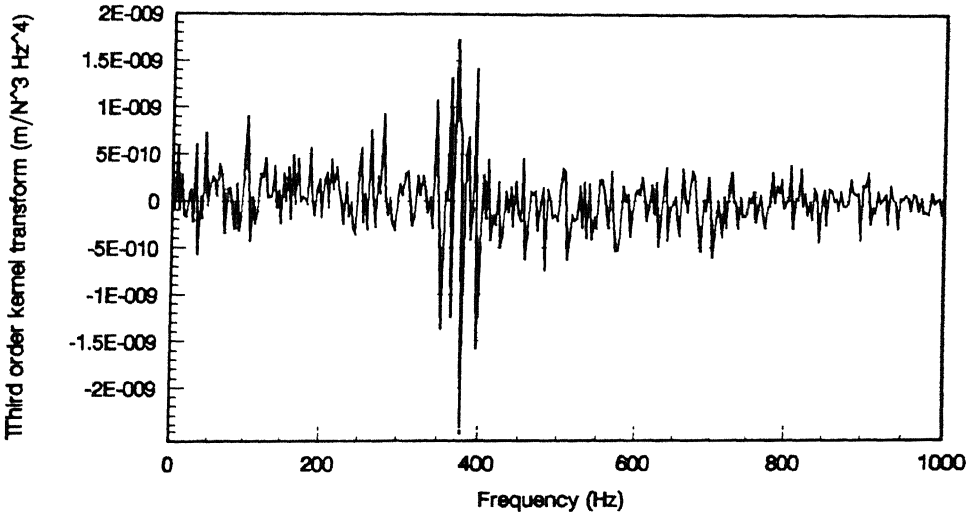

(a) Real component.

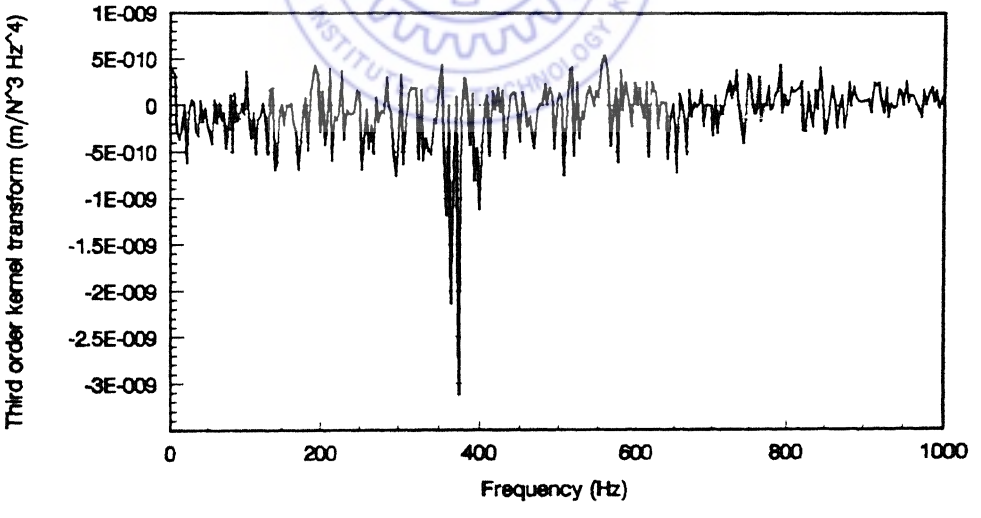

(b) Imaginary component.

Fig. 6.13 Estimate of the third order kernel transform, $H_3(\omega,\omega,\omega)$.

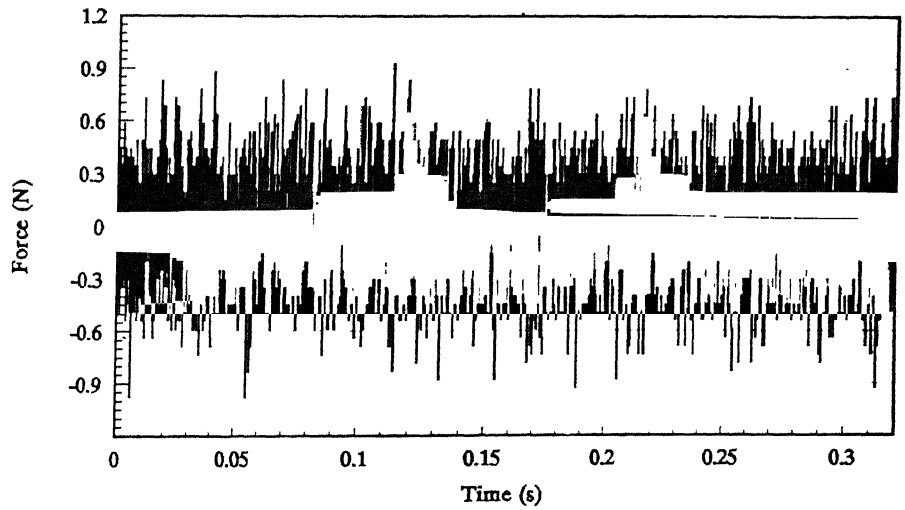

Fig. 6.14(a) Typical sample of the input force: Case2

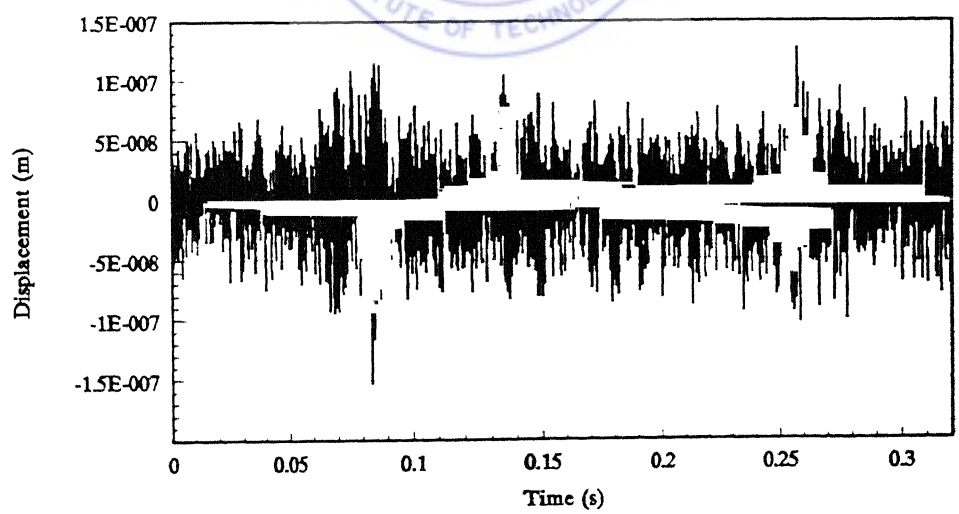

Fig. 6.14(b) Typical sample of the response: Case2

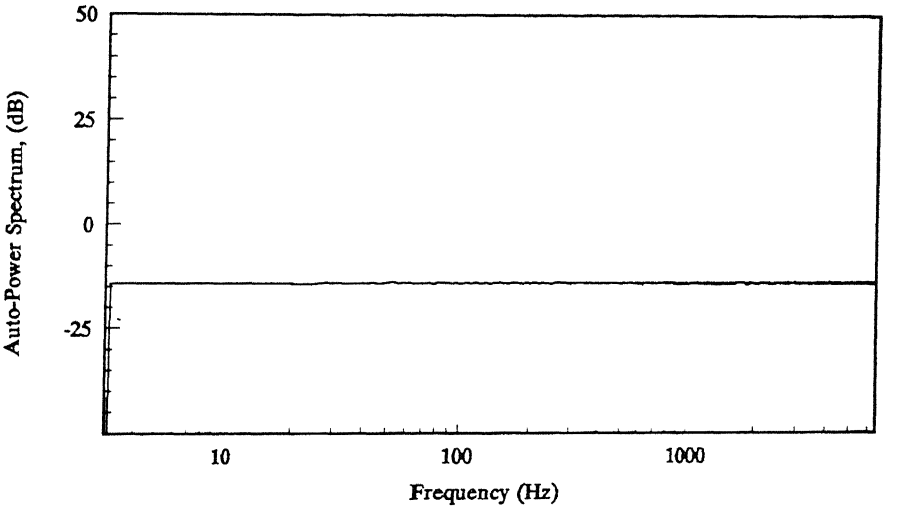

Fig. 6.15(a) Power spectrum of the input force: Case 2

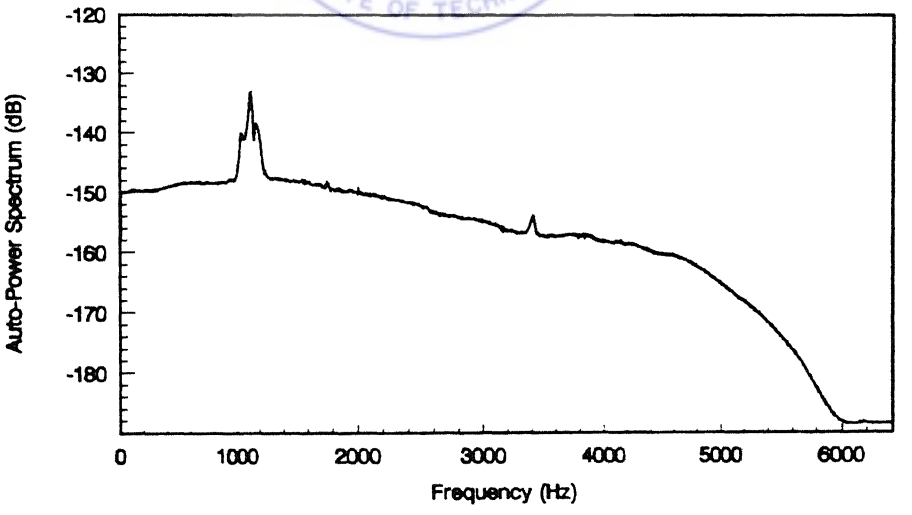

Fig. 6.15(b) Power spectrum of the response: Case 2

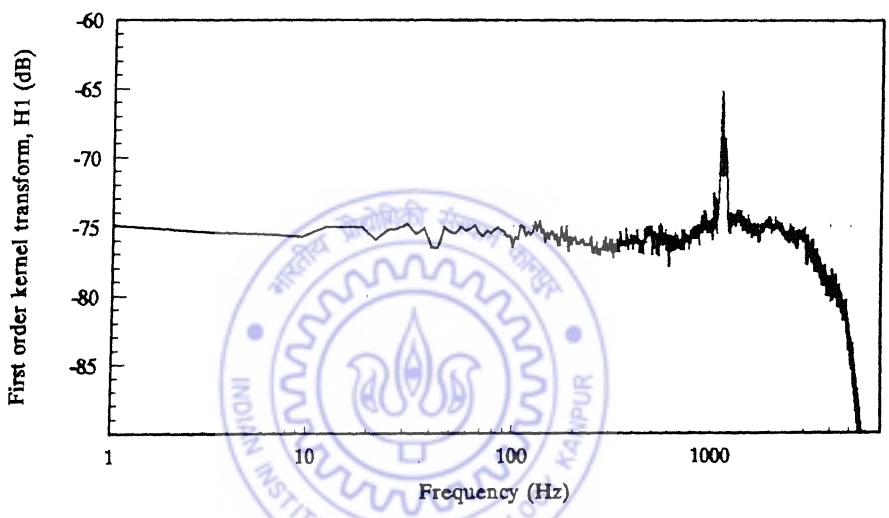

Fig. 6.16 Estimate of first order kernel transform, $H_1(\omega)$: Case 2

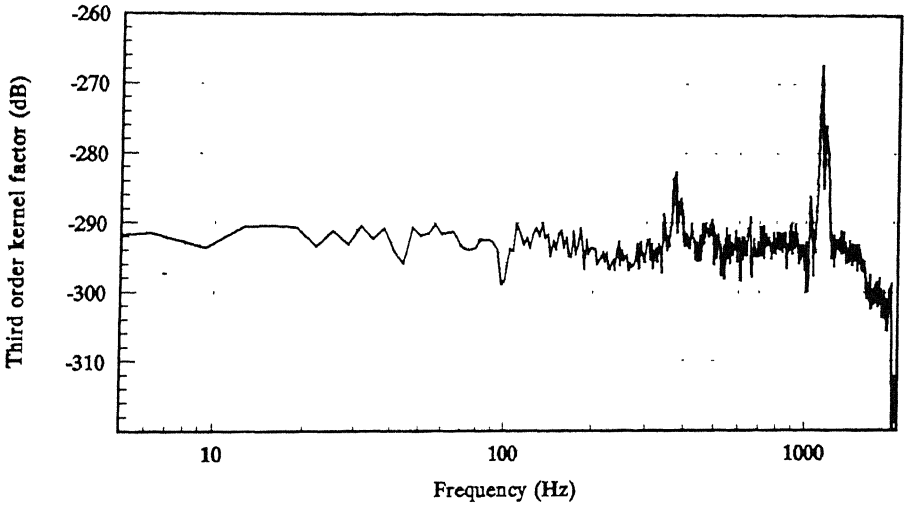

(a) Estimate of $\Psi_3(\omega,\omega,\omega)$

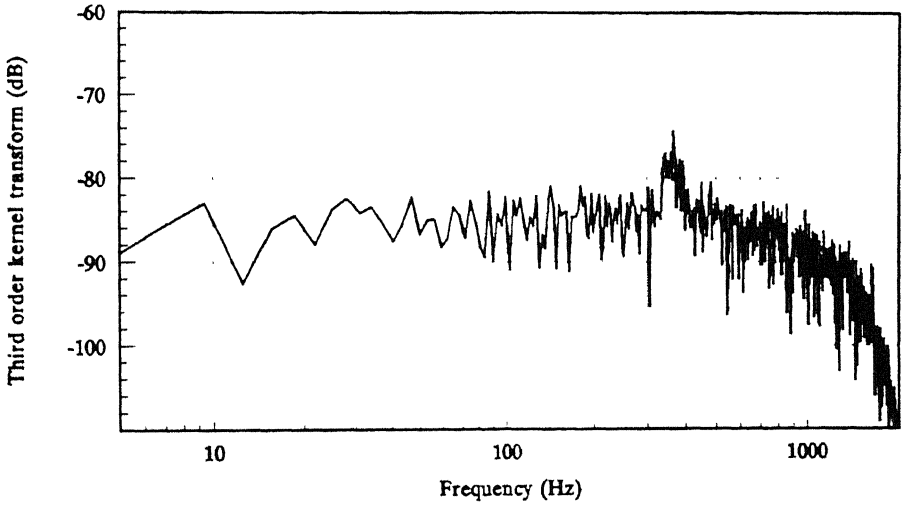

(b) Estimate of $H_3(\omega,\omega,\omega)$

Fig. 6.17 Third order estimates: Case2

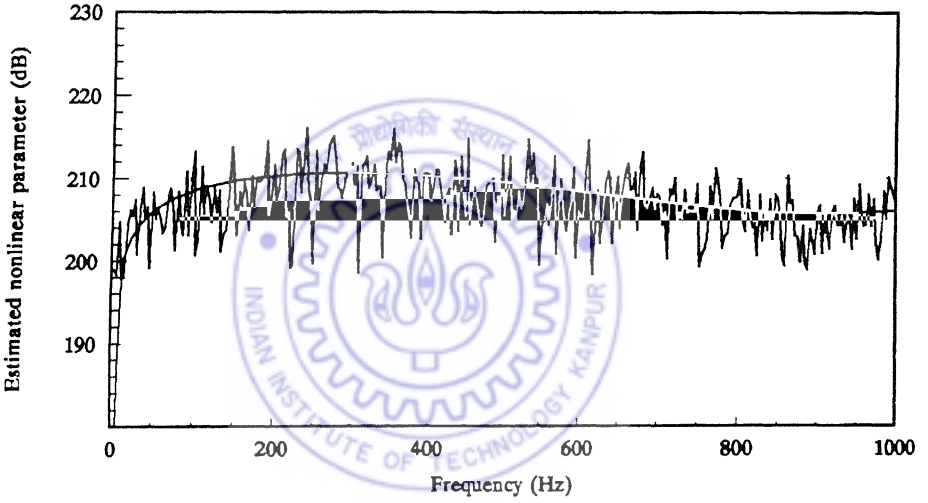

Fig. 6.18 Estimate of the nonlinear parameter, k^N : Case 2.

the estimate of the nonlinear parameter, k^N, shows better uniformity over the frequency range for a higher excitation force level (Case 1). The corresponding value of the nondimensional nonlinear parameter λ is calculated in this case as 0.114.

Case 3:

As a third case, the excitation force level is lowered down still further, such that F_{max} = 0.288 *N*. Figs.6.19 (a),(b) respectively shows typical samples of the excitation force and the displacement response. The power spectrum density of the excitation force (Fig. 6.20(a)) is 0.003 N^2/Hz (-25.68dB), in this case. The power spectrum of the displacement response is shown in Fig.6.20 (b), while the first order Volterra kernel transform, $H_1(\omega)$ is shown in Fig.6.21. The natural frequency identified from the plot of $H_1(\omega)$ is

ω_n = 1128 Hz = 7068.58 rad/s

while damping has been estimated as

ξ = 0.0079.

The third order kernel factor, $\Psi_3(\omega,\omega,\omega)$ and the third order Volterra kernel transform $H_3(\omega,\omega,\omega)$ have been plotted in Fig. 6.22 (a) and 6.22 (b), respectively. The estimate of the nonlinear stiffness, k^N, is shown in Fig. 6.23. The mean value of k^N for each bearing, in this case, has been found to be 9.50 x 10^{20} N/m^3. The corresponding value of the nondimensional nonlinear parameter λ is calculated in this case as 0.0199.

As in the first two cases, the trends observed in this case seem to be similar, that while the identification of the $\omega_n/3$ peak is sharper in $H_3(\omega,\omega,\omega)$ if the excitation force level is low, the estimate of the nonlinear parameter, k^N, shows better uniformity over the frequency range for a higher excitation force level. Similar observations were made in Chapter 3, during the computer simulation of the procedure. The computer simulation was carried out for three values of the nondimensional parameter, λ (1.0, 0.1 and 0.01), and the accuracy of the estimates was seen to be the best in the case of λ = 1.0. The

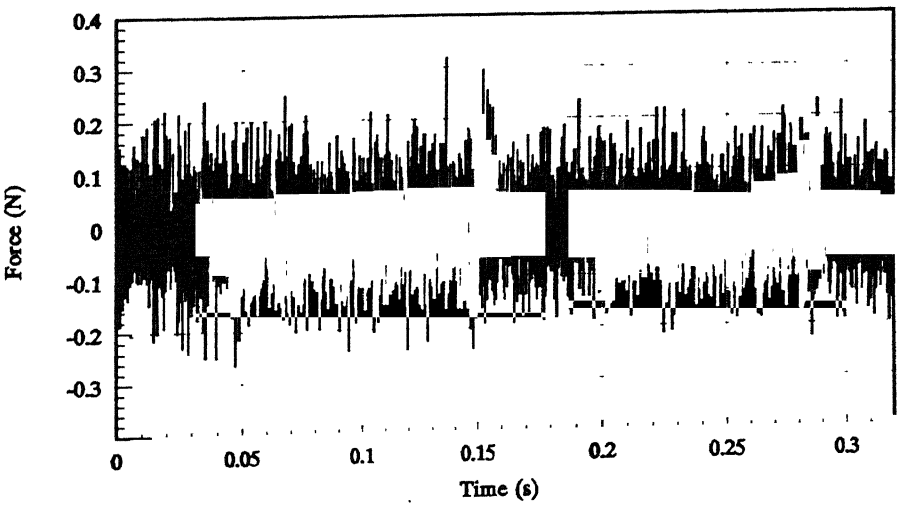

Fig. 6.19(a) Typical sample of the input force: Case3

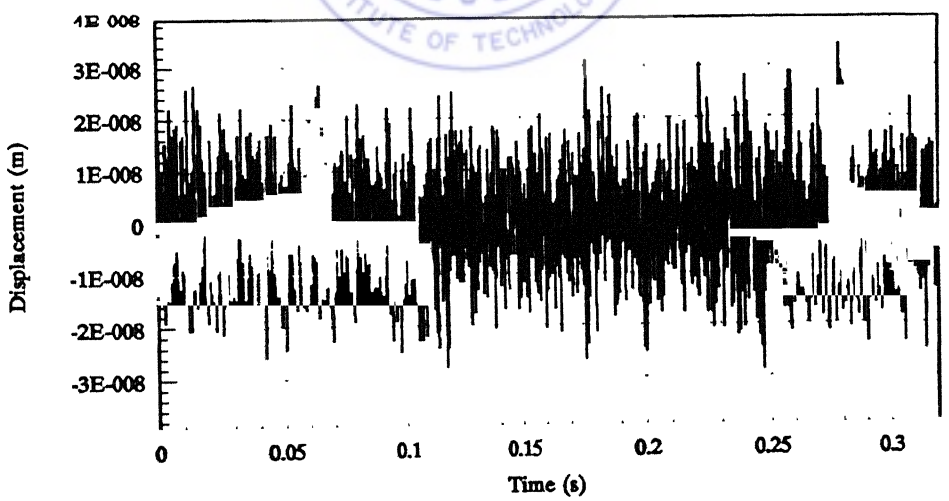

Fig. 6.19(b) Typical sample of the response:Case3

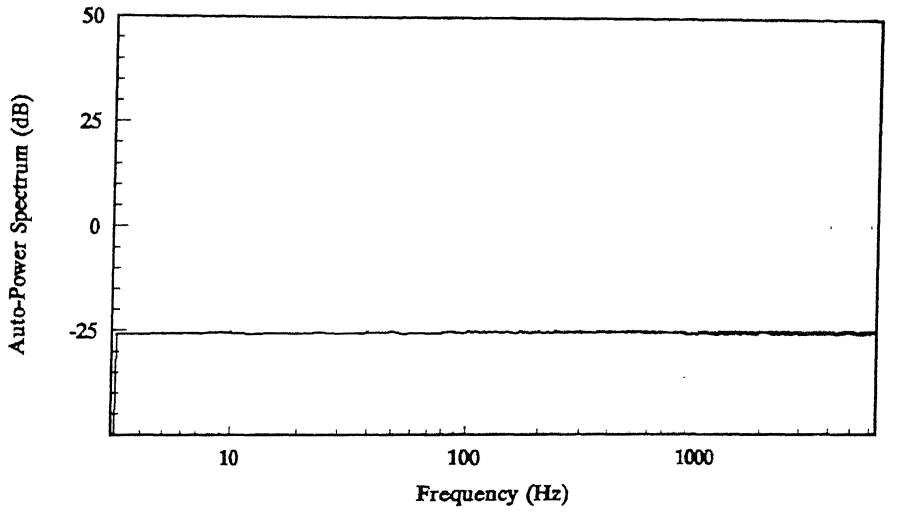

Fig. 6.20(a) Power spectrum of the input force: Case 3 (averaged over 2000 samples).

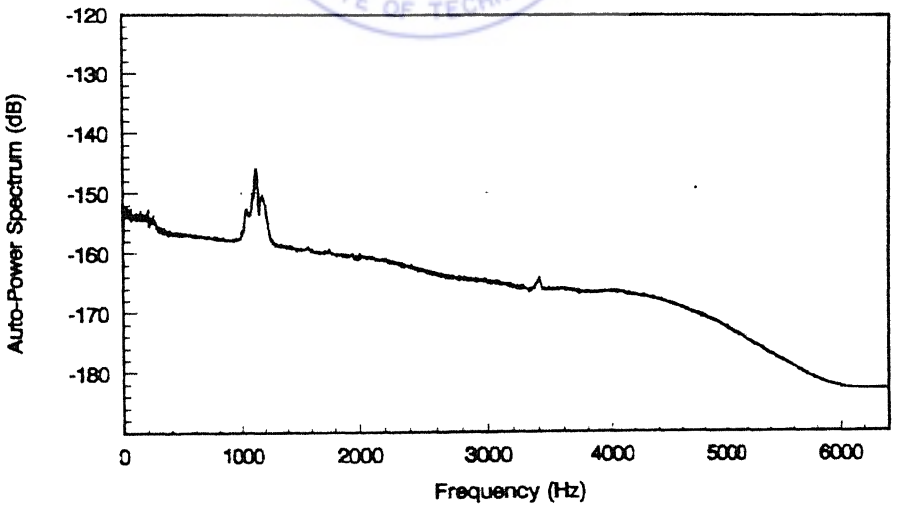

Fig. 6.20(b) Power spectrum of the response: Case 3 (averaged over 2000 samples).

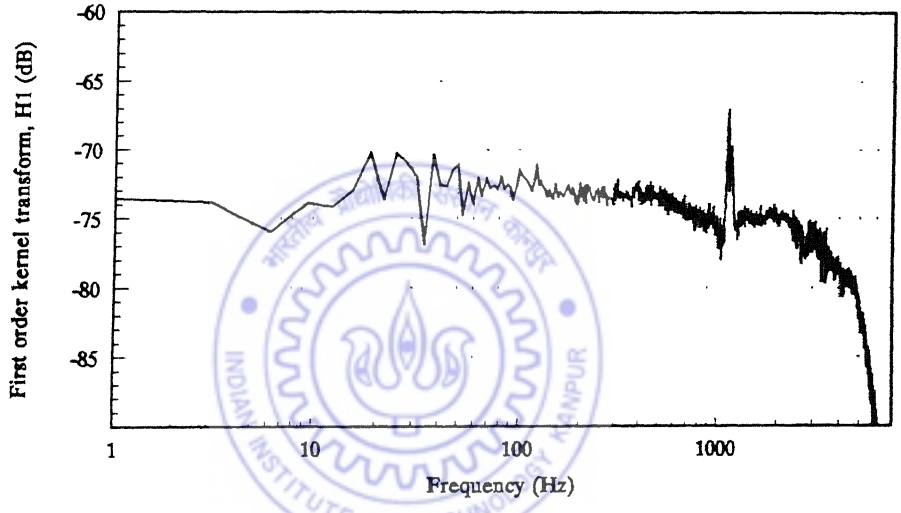

Fig. 6.21 Estimate of first order kernel transform, $H_1(\omega)$: Case 3

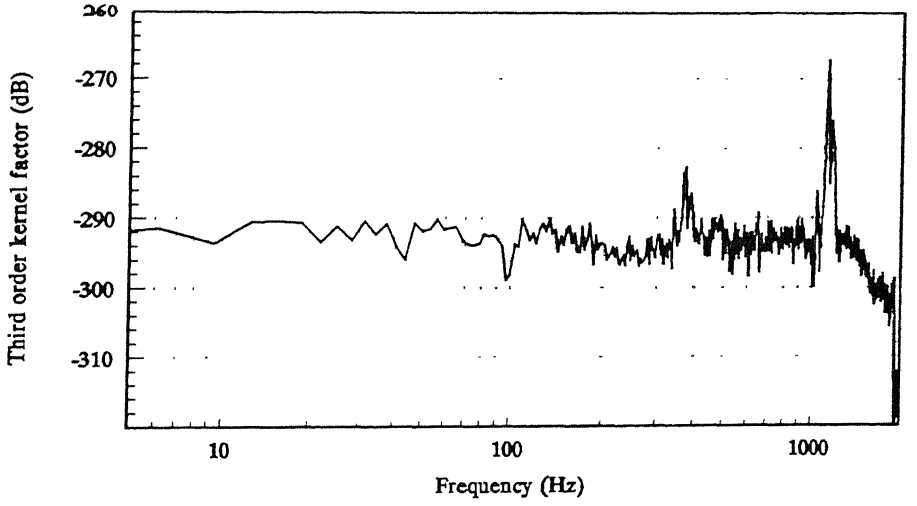

(a) Estimate of $\Psi_3(\omega,\omega,\omega)$.

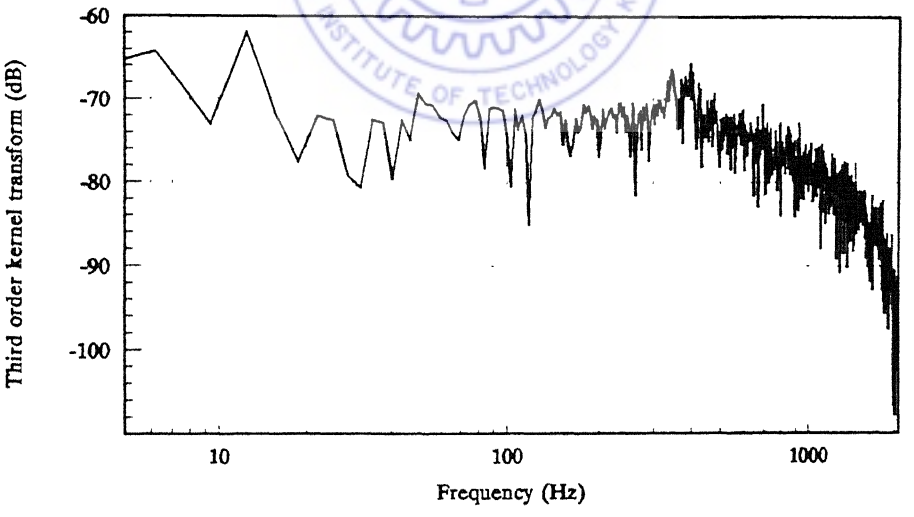

(b) Estimate of $H_3(\omega,\omega,\omega)$.

Fig. 6.22 Third order estimates: Case3

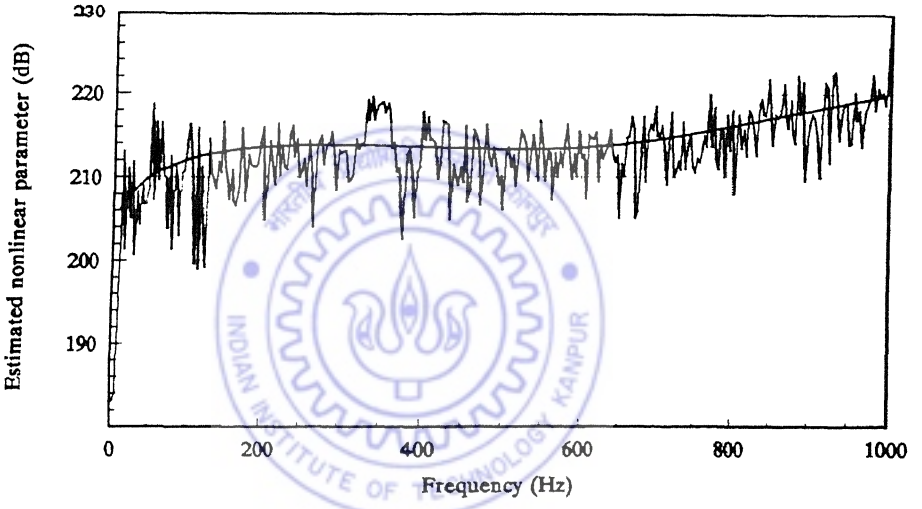

Fig. 6.23 Estimate of the nonlinear parameter, k^N : Case 3.

values of the nondimensional nonlinearity parameter, λ, in the three cases during experimental investigations have been 0.366, 0.114 and 0.0199 and the mean values of the estimates of the nonlinear stiffness k^N in the three cases have been 2.99 x $10^{20}\ N/m^3$, 7.16 x $10^{20}\ N/m^3$ and 19.0 x $10^{20}\ N/m^3$, respectively. The order of the nonlinearity of k^N can be concluded to be as $10^{20}\ N/m^3$ from the three results, while on the basis of the computer simulation results of Chapter 3 and the uniformity of the estimates over a frequency range in the experimental investigations, the correct magnitude appears to be one in the range suggested by the first two values (1.49, 3.58) rather than the third (9.50). The major source of error, apart from experimental noise, as mentioned in Chapter 3, is that the estimation procedure is restricted to kernels up to the third order only, in order to keep the computations to a manageable level. Inclusion of higher order kernels (5^{th}., 7^{th} order) in the response representation can be expected to improve the accuracy of the estimates at increased computational effort. Another source of inaccuracy in the estimates is the finite length of samples and the ensemble size.

6.5 Validation

An independent check is carried out to validate the estimates of the nonlinear stiffness. This check is based on the analytical formulations of Harris (1984) and Ragulskis et al. (1974), which treat the bearing in isolation of the shaft and employ the Hertzian contact theory.

Referring to Fig.6.24, the total elastic force at the points of contact of the *i*th ball with the inner and outer races is expressed as

$$F_i = K_n(g + x\cos\eta_i + y\sin\eta_i)^{3/2} \tag{6.2}$$

and its projection along the line of action of the applied force is

$$F_i = K_n(g + x\cos\eta_i + y\sin\eta_i)^{3/2}\cos\eta_i \tag{6.3}$$

where g is the radial preload or preclearance between the ball and the races and x and y are the displacements of the moving ring in the direction of the radial load and perpendicular to the direction of the radial load respectively. η_i is the angle between the

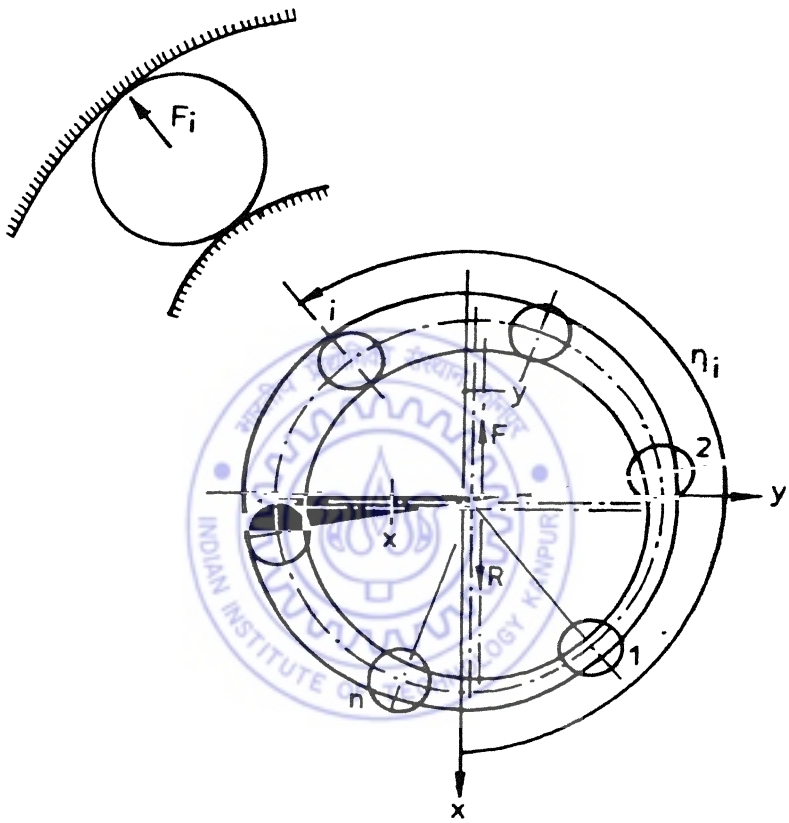

Figure 6.24 Schematic diagram of a loaded bearing

lines of action of the radial load (direction of displacement of the moving ring) and the radius passing through the center of the *i*th ball. K_n is a coefficient of proportionality depending on the geometric and material properties of the bearing. The value of K_n, for the test bearing is estimated by the method suggested by Harris (1984) as 2.82×10^5 N/mm$^{1.5}$.

The total elastic force in the direction of the applied force is

$$F = \sum_{i=1}^{n} F_i \tag{6.4}$$

where n is the total number of balls in the bearing.

Using the condition of zero elastic force in the direction perpendicular to the elastic load, the deformation, y, perpendicular to the radial force line is expressed as

$$y = \sum_{i=1}^{n} [g + x\cos(\eta_i)]^{3/2} \sin(\eta_i) \Big/ \sum_{i=1}^{n} [g + x\cos(\eta_i)]^{1/2} \sin^2(\eta_i) \tag{6.5}$$

Equations (6.3) and (6.5) are used in equation (6.4) and the bearing stiffness is determined as a function of the deformation x as

$$k(x) = \partial F / \partial x \tag{6.6}$$

It can be seen that the bearing stiffness is critically dependent on the preloading, g, of the balls. While the manufacturer, may, at times, provide the preload range, the exact value of the preloading of the bearing balls in the shaft-casing assembly, especially during operations which have involved wear and tear, would be difficult to determine. The stiffness of the test bearing is plotted in Fig. 6.25 as a function of the radial deformation, x, for various allowable preload values, g.

The same experimental rotor-bearing set-up was employed by Tiwari (1995), for linear and nonlinear parameter estimation. He adopted a Markov process approach and modeled the governing equations of the system into a Fokker-Planck equation. No external excitation was given to the system and the random disturbances during the rotation of the shaft, caused due to imperfections and deterioration of the rolling surfaces as well as

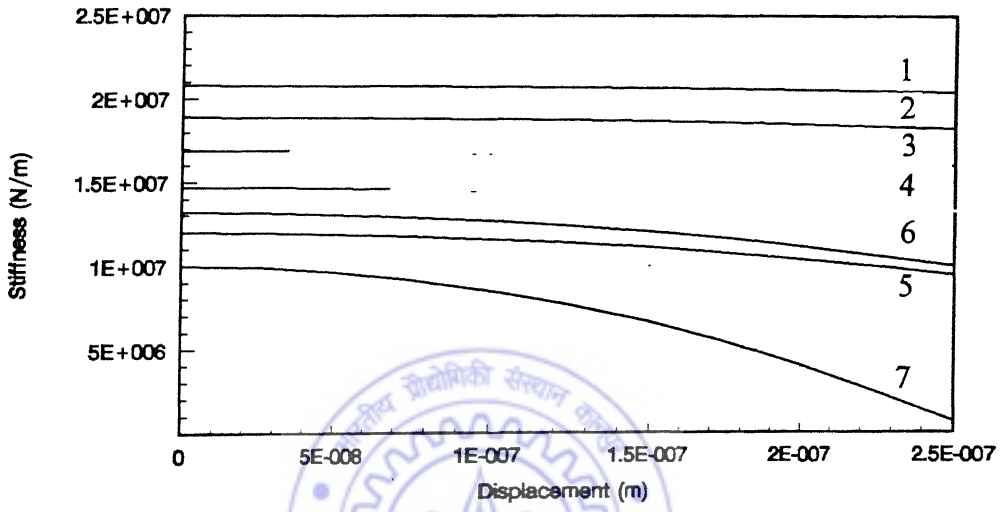

Fig. 6.25 Stiffness comparision

7 - Present study

1-5 Harris (1984) and Regulskis et al (1974) with preload 0.2, 0.3, 0.4, 0.5 and 0.6 μm respectively

6 - Tiwari (1995).

from other random sources, like inaccuracies in alignment etc., were approximated in an engineering sense as white and Gaussian. An exact solution of the Fokker-Planck equation was obtained, in terms of the probability density functions of the response, a curve fitting algorithm was developed to process the solution for parameter estimation. The results obtained by Tiwari (1995) along with those from the present procedure are also plotted in Fig. 6.25. This comparison is also listed in Table 6.1. The expressions for the theoretical stiffness in Table 6.1 have been obtained by curve fitting the stiffness values obtained from equation (6.6), through a quadratic in x.

Table 6.1 Comparison of bearing stiffness parameters

	Hertzian Contact Theory (isolated bearing)					**Tiwari (1995)**	**Present Study**		
	Preload (microns)						Case 1	Case 2	Case 3
	0.2	0.3	0.4	0.5	0.6				
k (MN/m)	12.0	14.7	16.9	18.9	20.8	22.3	10.0	10.0	10.3
k' $(EN/m^3)^*$	-40.1	-21.8	-14.2	-10.2	-6.1	-85.0	-149.0	-358.0	-950.0

* $EN/m^3 = exa\text{-}Newton/m^3 = 10^{18}\ Newton/m^3$

6.6 Remarks

A good resemblance can be observed between the results obtained in the present study and those obtained by Tiwari and the theoretically possible values. While there is variation in the exact magnitude of the estimates, the order of the magnitudes is practically identical. This serves to illustrate the correctness of the experimental exercise and the practical application aspects of the estimation procedures.

CHAPTER 7

CONCLUSION

The present study has concerned itself with the inverse problem of parameter estimation in nonlinear rotor bearing systems. Volterra and Wiener theories of nonlinear analysis have been employed as the theoretical platforms for analytical development of procedures. A frequency domain approach has been adopted and nonlinear response of the system is expressed through first and higher order Volterra and Wiener kernel transforms. The procedure involves extraction of Wiener kernels from measurements of the applied white noise (broadband in practice) excitation and the resultant response of the systems. The Wiener kernels are transformed to Volterra kernels, which are then processed for parameter estimation. The following rotor systems were considered

(i) Rigid Rotor in bearings without cross-coupling

(ii) Rigid Rotor in bearings with cross-coupling

(iii) Flexible Rotor

The procedure was developed in steps – the first rotor configuration mentioned above, was treated as a single-degree-freedom-system; the next two cases involved more than one degrees of freedom, where the cross-kernel concept was developed through Laplace transforms. The procedures have been extensively illustrated through numerical simulation. Reasonably good estimates have been obtained for both – linear and nonlinear stiffness parameters.

One major approximation in the present study was the restriction of response representation, to include kernels upto the third order only. This has been done in order to keep the algebra at a manageable level. The accuracy of estimates is related to the accuracy of response representation through kernels upto third order. The check, in the present study is carried out by performing numerical simulation for various values of the nondimensional nonlinear parameters. This nondimensional nonlinear parameter includes the linear stiffness and force magnitude terms, in addition to the nonlinear stiffness terms. The nonlinear parameters were found to be estimated within the correct order of the magnitudes of their exact values, though the accuracy of the values vary with the values

of the nondimensional parameters chosen for computer simulation. The present study can be usefully employed to design experiments to choose appropriate excitation force levels for an expected set of values of the stiffness parameters. However, it would be worthwhile, as a future exercise, to the extend the procedure to include kernels of higher order. This can be done for a single-degree-freedom-system, without a great deal of additional algebra. However, for systems, with more than one degree of freedom, it would help to first develop some generic forms for response and kernel expression.

Despite the fact that the expressions look formidable with Volterra and Wiener series (this would be the case, anyway, for a nonlinear analysis) the computer implementation of the algorithms is rather simple and quick. The ensemble size of the force and response samples, in the present study, is kept at 2000, due to data storage limitations of the computer (A large amount of data was to be stored and retained in the computer, during the entire course of the study). The accuracy of the estimated first order kernel transforms was checked and the parameter estimation was restricted to a frequency range, upto which the errors were low. An attempt can be made, as a future exercise to work with a larger ensemble size to improve the accuracy and thereby also increase the usable frequency range for parameter estimation.

The analytical development, in the present study, has been carried out for cubic form of nonlinearities. However, the procedures can deal with any general polynomial form of nonlinearity. Damping was treated to be linear during this entire exercise. Damping nonlinearity can be incorporated in the analysis, though with increased algebraic effort. The accuracy of the nonlinear damping estimates, with the present form of response representation and the sample and ensemble specifications, can be discussed and reviewed only after such a study is made.

The present study also attempted to implement the algorithms developed on a laboratory rotor-rig. The study was carried out with the existing facilities and constraints. The results were satisfactory and further strengthened the applicability of the procedures. However, the experimental study was restricted to ball bearings. Further experimental work needs to carry out on rotors in fluid film bearings, in order to fully investigate the utility of the procedures developed during the course of this study.

REFERENCES

Amorocho, J., and Orlob, G., 1961, "*Nonlinear Analysis of Hydrologic Systems*", Water Resour. Cent. Contrib. 40, Univ. of Calif., Los Ang.

Ariaratnam, S. T., 1960, "*Random Vibration of Non-linear Suspensions*", Journal Mechanical Engineering Science **2**(3), pp. 195-201.

Arumugam, P., Swarnamani, S., and Prabhu, B. S., 1997, "*An Experimental Investigation on Static and Dynamic Characteristics of Journal Bearings Under the Influence of Twisting Misalignment*", Transactions of ASME, Journal of Tribology, **119**, pp. 188-192.

Baheti, S. K., and Kirk, R. G., 1994, "*Thermo-Hydrodynamic Solution of Floating Ring Seals for High Pressure Compressors using the Finite Element Method*", STLE Tribology Transactions, **37**(2), pp. 336-346.

Baheti, S. K., and Kirk, R. G., 1994a, "*Finite-Element Thermo-Hydrodynamic Analysis of a Circumferencially Grooved Floating Oil Ring Seal*", STLE 94-AM-8D-2.

Barret, J. F., 1963, "*The Use of Functionals in the Analysis of Nonlinear Physical Systems*", J. Electronic Control, **15**, pp. 567-615.

Bedrosian, E., and Rice, S. O., 1971, "*The Output Properties of Volterra Systems (Nonlinear System With Memory) Driven by Harmonic and Gaussian Inputs*", Proceedings of the IEEE, **59**(12), pp. 1688-1707.

Bedrosian, E., and Rice, S., 1975, "*Application of Volterra-System Analysis, Proceedings of Ist Symposium on Test and Identification of Nonlinear Systems*", pp. 15-27.

Bendat, J. S., 1983, "*Statistical Errors for Nonlinear System Measurements Involving Square-Law operations*", Journal of Sound and Vibration, **90**(2), p. 275.

Bendat, J. S., 1990, "*Nonlinear System Analysis and Identification from Random Data*", New York: John Wiley.

Bendat, J. S., 1998, "*Nonlinear System Techniques and Applications*", New York: John Wiley.

Bendat, J. S., and Piersol, A. G., 1982, "*Spectral Analysis of Nonlinear Systems Involving Square Law Operations*", Journal of Sound and Vibration, **81**(2), pp. 199-213.

Bendat, J. S., and Piersol, A. G., 1986, "*Random Data: Analysis and Measurement Procedures*", 2nd Edition, Wiley-Interscience, New-York.

Bendat, J. S., and Piersol, A. G., 1993, "*Engineering Applications of Correlation and Spectral Analysis*", New York: John Wiley.

Billings, S. A., 1980, "*Identification of Nonlinear Systems-A Survey*", Proceedings of IEE, **127**(6), pp. 272-285.

Billings, S. A., and Fakhouri, S. Y., 1978, "*Theory of Separable Processes With Applications to the Identification of Nonlinear Systems*", Proceedings of IEE, **125**(9), pp. 1051-1058.

Blok, H., 1965, "*Toplogical Aspects and the Impulse/Whirl Angle Method in the Orbital Hydrodynamics of Dynamically Loaded Journal Bearing*", Lecture Notes (Condensed English Version), Delft, The Netherlands.

Bolotin, V. V., 1979, "*Random Vibration in Elastic Systems*", Nauka, Moscow (in Russian).

Booker, J., 1965, "*Dynamically Loaded Journal Bearings: Mobility Methods of Solution*", Journal of Basic Engineering, pp. 537-546.

Boyd, S., Tang, Y. S., and Chua, L. O., 1983, "*Measuring Volterra Kernels*", IEEE Transactions on Circuits and Systems, **CAS-30**(8), pp. 571-577.

Brilliant, M. B., 1958, "*Theory of the Analysis of the Nonlinear systems*", MIT Res. Lab. of Elect., Technical report, 304.

Brillinger, D. R., 1970, "*The Identification of Polynomial Systems by means of Higher order Spectra*", Journal of Sound and Vibration **12**(3), pp. 301-313.

Burrows, C. R, Sayed-Esfahani, R., and Stanway, R., 1981, "*A Comparison of Multifrequency Techniques for Measuring the Dynamics of Squeeze Film Bearings*", Transactions of ASME, Journal of Lubrication Technology, **103**, pp. 137-143.

Burrows, C. R., and Sahinkaya, M. N., 1982, "*Frequency Domain Estimation of Linearised Oil Film Coefficients*", Transactions of ASME, Journal of Lubrication Technology, **104**, 210.

Cai, G. Q. and Lin, Y. K., 1988, "*A New Approximate Solution Technique for Randomly Excited Non-Linear Oscillators*", International Journal of Non-linear Mechanics, **23**, pp. 409-420.

Caughey, T. K., 1963, "*Derivation and application of the Fokker-Planck Equation to Discrete Non-Linear Dynamic Systems Subjected to White Random Excitation*", Journal of Acoustical Society of America, **35**(11), pp. 1683-1692.

Caughey, T. K., 1971, "*Nonlinear Theory of Random Vibrations*", Advances in Applied Mechanics, **11**, pp. 209-253, Academic Press, New York.

Caughey, T. K., 1986, "*On the Response of Non-Linear Oscillators to Stochastic Excitation*", Probabilistic Engineering Mechanics, **1**, pp. 2-4.

Caughey, T. K. and Ma, F., 1983, "*The Exact Steady State Solution of a Class of Nonlinear Stochastic Systems*", International Journal of Nonlinear Mechanics, **17**, pp. 137-142.

Chen, J. H., and Lee, A. C., 1997, "*Identification of Linearised Dynamic Characteristics of Rolling Element Bearings*", Transactions of ASME, Journal of Vibration and Acoustics, **119**, pp. 60-69.

Childs, D., 1993, "*Turbomachinery Rotordynamics: Phenomena, Modeling and Analysis*", New York: A Wiley-Interscience Publication.

Childs, D., Moes, H., and Van Leeuwen, H., 1977, "*Journal Bearing Impedance Description for Rotor Dynamic Applications*", Transactions of ASME, Journal of Lubrication Technology, pp. 198-214.

Choi, D., Miksad, R. W, and Powers, E. J, 1985, "*Application of Digital Cross-Bispectral Analysis Techniques to Model the Nonlinear Response of a Moored Vessel System in Random Seas*", Journal of Sound and Vibration, **99**, pp. 309-326.

Choy, F. K., Braun, M. J. and Hu Y., 1992, "*Nonlinear Transient and Frequency Response Analysis of a Hydrodynamic Journal Bearing*", Transactions of the ASME, Journal of Tribology **114**, pp. 448-454.

Chu., C. S., Wood, K. L., and Busch-Vishniac, I. J., 1998, "*A Nonlinear Dynamic Model With Confidence Bounds for Hydrodynamic Bearings*", Transactions of ASME , Journal of Tribology, **120**, pp. 595-604.

Chua, L. O., and Ng., C. Y., 1979, "*Frequency Domain Analysis of Nonlinear Systems: General Theory*", IEE Journal on Electronic Circuits and Sys., **3**(4), pp. 165-185.

Chua, L. O., and Ng., C. Y., 1979a, "*Frequency Domain Analysis of Nonlinear Systems: Formulation of Transfer Functions*", IEE Journal on Electronic Circuits and Systems, **3**(6), pp. 257-267.

Crandall, S. H., 1963, "*Perturbation Techniques for Random Vibrations of Nonlinear Systems*", Journal of Acoustical Society of America, **35**(14), pp. 1700-1705.

Crandall, S. H., 1966, "*Applied Mechanics Surveys*", Random vibration, Abramson, H. N., Liebowitz, H., Crowley, J. M., and Juhasz, S., eds., Sparton Books, Washington, D. C., pp. 681-689.

Crandall, S. H., 1985, "*Non-Gaussian Closure Techniques for Stationary Random Vibration*", International Journal of Non-linear Mechanics, **20**, pp. 1-8.

Crum, L., 1975, "*Simultaneous Reduction and Expansion of Multidimensional Laplace Transform Kernels*", Proceedings of Ist Symposium on Test and Identification of Nonlinear Systems, pp. 89-105.

DeFigueiredo, R., and Dwyer, T., 1980, "*A Best Approximation Framework and Implementation for Simulation of Large Scale Nonlinear Systems*", IEEE Transactions on Circuits and Systems, **CAS-27**, pp. 1005-1014.

Dimentberg, M. F., 1980, *Nonlinear Stochastic Problems of Mechanical Vibrations*, Nauka, Mascow (in Rassian).

Dimentberg, M. F., 1988, "*Statistical Dynamics of Nonlinear and Time-Varying Systems*", Research studies press limited, John Wiley and Sons Inc., New York.

Dimentberg, M. F. and Sokolov, A. A., 1991, "*Identification of Restoring Force Non-Linearity from a System's Response to a White-Noise Excitation*", International Journal of Nonlinear Mechanics, **26**(6), pp. 851-855.

Elsermans, M., Hongerloot, M. and Snokeys, R., 1975, "*Damping in Taper Rolling Bearings*", Proc. 16th MTDR Conference, p. 223, Manchester, 10-12 September.

Eschmann, P., Hasbargen, I. and Weigand, K., 1985, "*Ball and Roller Bearings, Theory, Design and Application*", John Wiley and Sons: New York.

Ewins, D. J., 1984 "*Modal Testing :Theory and Practice*", Lectchworth, England: Research Studies Press.

Eykhoff, P., 1974, "*System Identification: Parameter and State Estimation*", Wiley, New York, pp. 94-104.

Eykhoff, P., Grinten, P. M. Van Der, Naak, H. K., and Veltman, B. P., 1966, "*System Modeling and Identification*", Proc. IIIrd IFAC Congress, London.

Fakhouri, S. Y., 1980, "*Identification of a Class of Nonlinear Systems With Gaussian Non-White Inputs*", International Journal of Systems Science, **11**(5), pp.-541-555.

Fakhouri, S. Y., and Billings, S. A., 1980, "*Identification of Nonlinear Systems Using Correlation Analysis and Pseudorandom Inputs*", International Journal of Systems Science, **11**(3), pp.-261-279.

Fakhouri, S. Y., Billings, S. A., and Wormald, C. N., 1981, "*Analysis of Estimation Errors in the Identification of Nonlinear Systems*", International Journal of Systems Science, **12**(2), pp. 205-225.

Falsone G., 1992, "*Stochastic Linearisation of MDOF Systems Under Parametric Excitations*", International Journal of Nonlinear Mechanics **27**(6), pp. 1025-1037.

Flake, R. H., 1963, "*Volterra Series Representation of Nonlinear Systems*", IEEE Transactions on App. Ind., **81**, pp. 330-335.

Fokker, A. P., 1914, "*Die mittlere energie rotierender electricher dipole im stahlungsfeld*", Annals Phys., **43**, pp. 810-815.

Fredriksson, B., 1980, "*Three-Dimentional Roller-Raceway Contact Stress Analysis*", Advanced Engineering Corp. Report, Sweden.

French, A. S., and Butz E. G., 1973, "*Measuring the Wiener Kernels of a Nonlinear System using the Fast Fourier Transform Algorithm*", International Journal of Control, **17**(3), pp. 529-539.

French, A. S., and Butz, E. G., 1974, "*The use of Walsh Functions in the Wiener Analysis of Nonlinear Systems*", IEEE Transactions on Computers, **C-23** (3), pp. 225-232.

Fretchet, M., 1910, "*Sur les fonctionnels continues*", Ann. Ec. Norm. Sup., **27**, pp. 193-219.

Fuller, A. T., 1969, "*Analysis of Nonlinear Stochastic Systems by means of the Fokker-Planck Equation*", International Journal of Control, **9** (6), pp. 603-655.

Fuller, D. D, 1984, "*Theory and Practice of Lubrication for Engineers*", second edition, New York: A Wiley-Interscience Publication.

George, D. 1959, "*Continuous Nonlinear Systems*", Res. Lab. Electron., M.I.T., Cambridge, Mass., Tech. Rep. 355.

Gifford, S. J., and Tomlinson, G. R., 1989, "*Recent Advances in the Application of Functional Series to Nonlinear Structures*", Journal of Sound and Vibration, **135**(2), pp. 289-317.

Glienicke, J., 1966, "*Experimental Investigation of the Stiffness and Damping Coefficients of Turbine Bearings and their Application to Instability Prediction*", Proceedings of Institute of Mechanical Engineers **181** (3b), p. 116.

Goodwin, M. J., 1991, "*Experimental Techniques for Bearing Impedance Measurement*", Transaction of ASME, Journal of Engineering for Industry, **113**, pp. 335-342.

Goodwin, M. J., Ogrodnik, P. J., Roach, M. P., and Fang, Y., 1997, "*Calculation and Measurement of the Stiffness and Damping Coefficients for a Low Impedance Hydrodynamic Bearing*", Trans. of ASME, Journal of Tribology, **119**, pp. 57-63.

Gross, W., 1962, "*Gas Film Lubrication*", New York: Wiley.

Gustavsson, O. and Tallian, T., 1962, "*Detection of Damage in Assembled Rolling Element Bearings*", Trans. of American Society of Locomotive Engineers **5**.

Hagg, A. C., 1946, "*The Influence of Oil Film Journal Bearings on the Stability of Rotating Machines*", Transactions of ASME, Journal of Applied Mechanics, **13**, pp. A211-A220.

Halme, A., Orava, J., and Blomberg, H., 1971, "*Polynomial Operators in Nonlinear Systems Theory*", International Journal of System Sciences, **2**(1), pp. 25-47.

Harris, G. H., and Lapidus, L., 1967, "*The Identification of Nonlinear Systems*", Industrial and Engineering Chemistry, **59**(6), pp. 66-81.

Harris, T. A., 1984, "*Rolling Bearing Analysis*", New York: Wiley.

Hertz, H., 1896, "*On the Contact of Rigid Elastic Solids and on Hardness*", Miscellaneous Papers, Macmillan, London, pp. 163-183.

Hess, D. P., Soom, A. and Kim, C. H., 1992, "*Normal Vibrations and Friction at a Hertzian Contact Under Random Excitation: Theory and Experiments*", Journal of Sound and Vibration **153** (3), pp. 491-508.

Ho, D., and Stark, L, 1973, "*Identification of Biological Systems by Volterra Series*", Proceedings of 4th Symposium on Nonlinear Estimation Theory and its Application.

Honrath, K., 1960, "*Concerning the Stiffness of Machine Tool Spindles and Their Bearings*", Thesis submitted for Dicktor Ingenieur at the Technical University of Aachen.

Hummel, C., 1926, "*Kristische Drehzahlen Als Folge Der Nachgiebigkeit Des Schmiermittels Im Larger*", VDI-Forschungsheft, 287.

Hung, G., and Stark, L., 1977, "*Introductory Review: The Kernel Identification Method: Review of Theory, Calculation, Application, and Interpretation,*" Mathematical Biosciences, **37**, pp. 135-190.

Hung, G., Stark, L., and Eykhoff, P., 1977, "*On the Interpretation of Kernels. I. Computer Simulation of Responses to Impulse Pairs*", Annals of Biomedical Engineering, **5**, pp. 130-143.

Ibrahim, R. A. and Roberts, J. W., 1978, "*Parametric Vibrations, Part 5: Stochastic Problems*", Shock and Vibration Digest, **10**, pp. 17-38.

Jacoby, S., 1966, "*A Mathematical Model for Nonlinear Hydrologic Systems*", J. Geophys. Rev., **71**, pp. 4811-4824.

Kalker, K., 1982, "*Numerical Calculation of the Elastic Field in a Half-Space due to an Arbitrary Load Distributed Over a Bounded Region of the Surface*", SKF Engineering and Research Center report NL82D002 (Appendix).

Katzenelson J., Gould, L., 1962, "*The Design of Nonlinear Filters and Control Systems*", Part I, Inf. Control, **5**, pp. 108-143.

Khasminskii, R. Z., 1966, "*A Limit Theorem for the Solutions of Differential Equations With Random Right-Hand Sides*", Theory of Probability and Applications, **11**, pp. 390-405.

Kim, K. I., and Powers, E. J., 1988, "*A Digital Method for Modeling Quadratically Nonlinear Systems with a General Random Input*", IEEE Transactions on Acoustics, Speech and Signal Processing, **ASSP-36**, pp. 1758-1769.

Kirk, R. G., and Gunter E. J., 1970, "*Transient Journal Bearing Analysis*", NASA CR 1599.

Kirk, R. G., and Gunter E. J., 1975, *"Short Bearing Analysis Applied to Rotor Dynamics, Part I: Theory"*, ASLE-ASME Joint Lubrication Conference 75-Lub-30.

Kirk, R. G., and Gunter E. J., 1975a, *"Short Bearing Analysis Applied to Rotor Dynamics, Part II: Results of Journal Bearing Response"*, ASLE-ASME Joint Lubrication Conference 75-Lub-31.

Klein, S., and Yasui, S., 1976, *"Nonlinear Systems Analysis with General Non-Gaussian Stimuli"*, Tech. Rep. Div. Of Biol., Calif., Inst. Of Technol.

Koh, T., and Powers, E. J., 1985, *"Second Order Volterra Filtering and its Application to Nonlinear System Identification"*, IEEE Transactions on Acoustics, Speech and Signal Processing, **ASSP-33**, pp. 1445-1455.

Kolmogorov A., 1931, *"Uber Die Analytischen Methoden in Wahrsheinlicheitsrechnung"*, Mathematische Annalen, **104**, pp. 415-458.

Kononenko, V. O. and Plakhtienko, N. P., 1970, *"Determination of Nonlinear Vibration System Characteristics from Analysis of Vibrations"*, Prikladnaya Mekhanika, **6**, Vyp. 9.

Korenberg, M. J., 1973, *"Identification of Nonlinear Differential Systems"*, JACC, pp. 597-603.

Korenberg, M. J., and Hunter, I. W., 1990, *"The Identification of Nonlinear Biological Systems: Wiener Kernel Approaches"*, Annals of Biomedical Engineering, **18**, pp. 629-654.

Kraus, J., Blech, J. J. and Braun, S. G., 1987, *"In Situ Determination of Rolling Bearing Stiffness and Damping by Modal Analysis"*, Transaction of ASME, Journal of Vibration, Acoustics, Stress, and Reliability in Design, **109**, pp. 235-240.

Krausz, H. I., 1975, *"Identification of Nonlinear Systems using Random Impulse Train Input"*, Biological Cybernetics **19**, pp. 217-230.

Krodkiewski, J. M., and Ding, J., 1993, *"Theory and Experiment on a Method for On-Site Identification of Configurations of Multi-Bearing Rotor Systems"*, Journal of Sound and Vibration, **164**(2), pp. 281-293.

Krodkiewski, J. M., and Ding, J., 1993a, *"Inclusion of Static Indetermination in the Mathematical Model for Nonlinear Dynamic Analyses of Multi-Bearing Rotor System"*, Journal of Sound and Vibration, **164**(2), pp. 267-280.

Kunert, K., 1961, "*Spannungsverteilung im halbraum bei elliptischer flchenpressungsverteilung ber einer rechteckigen druckfl,,che*", Forsch. Geb. Ingerieurwes **27** (6), pp. 165-174.

Lee, Y. W., Levinson, N., and Martin, W.T., 1964, "*Selected Papers of Norbert Wiener*", Published Jointly by Society for Industrial and Applied Mathematics and the M. I. T. Press, Cambridge, Massachusetts.

Lee, Y. W., and Schetzen, M., 1965, *"Measurement of Wiener Kernels of Nonlinear System by Crosscorrelation*", International Journal of Control, **2**(3), pp. 237-254.

Leon, B. J., and Schaefer, D. J., 1978, *"Volterra Series and Picard Iteration for Nonlinear Circuits and Systems*," IEEE Transactions on Circuits and Systems, **CAS-25**, pp. 789-793.

Lesiak, C., and Krener, A. J., 1978, "*Existence and Uniqueness of Volterra Series*," IEEE Transactions on Automatic Control, **AC-23**, pp. 1090-1095.

Levy, E. C., 1959, "*Complex-Curve Fitting.*" IRE Transactions on Automatic Control, **AC-4**, pp. 37-44.

Lim, T. C. and Singh, R., 1990a, "*Vibration Transmission Through Rolling Element Bearings, Part I: Bearing Stiffness Formulation*", Journal of Sound and Vibration **139** (2), pp. 179-199.

Lim, T. C. and Singh, R., 1990b, "*Vibration Transmission Through Rolling Element Bearings, Part II: System Studies*", Journal of Sound and Vibration **139** (2), pp. 201-225.

Lim, T. C. and Singh, R., 1991, "*Vibration Transmission Through Rolling Element Bearings, Part III: Geared Rotor System Studies*", Journal of Sound and Vibration **151** (1), pp. 31-54.

Lim, T. C. and Singh, R., 1992, "*Vibration Transmission Through Rolling Element Bearings, Part IV: Statistical Energy Analysis*", Journal of Sound and Vibration **153** (1), pp. 37-50.

Lim, T. C. and Singh, R., 1994, "*Vibration Transmission Through Rolling Element Bearings, Part V: Effect of Distributed Contact Load on Roller Bearing Stiffness Matrix*", Journal of Sound and Vibration **169** (4), pp. 547-553.

Lin, Y. K. and Cai, G. Q., 1995, *Probabilistic Structural Dynamics. Advanced Theory and Applications*. New York: McGraw-Hill.

Lohman, G., 1953, "*Untersuchung des Laufgerausches von Walzlgern*", Konstruktion **5**.

Lubbock, J. K. and Bansal V. S., 1969, "*Multidimensional Laplace Transforms for Solution of Nonlinear Equations*", Proceedings of IEE, **116**(12), pp. 2075-2082.

Lund, J. W., 1968, "*Calculation of Stiffness and Damping Properties of a Gas Bearings*," Transactions of ASME, Journal of Lubrication Technology, pp. 793-803.

Lund, J. W., 1987, "*Review of the Concept of Dynamic Coefficients for Fluid Film Bearings*," Transactions of ASME, Journal of Tribology, **109**, pp. 37-41.

Lund, J. W., and Sternlicht, B., 1962, "*Rotor Bearing Dynamics with Emphasis on Attenuation*", Transactions of ASME, Journal of Basic Engineering, pp. 491-502.

Marmarelis, P., and Naka, K. I., 1973, "*Nonlinear Analysis and Synthesis of Receptive Field Responses in the Cat-Fish Retina-I: Horizontal Cell Ganglion Cell Chain*", J. Neurophysiol., **36**, pp. 605-618.

Marmarelis, P., and Naka, K. I., 1973b, "*Nonlinear Analysis and Synthesis of Receptive Field Responses in the Cat-Fish Retina-II: One Input White Noise Analysis*", J. Neurophysiol, **36**, pp. 619-633.

Marmarelis, P., and Naka, K. I., 1973c, "*Nonlinear Analysis and Synthesis of Receptive Field Responses in the Cat-Fish Retina-III: Two Input White-Noise Analysis*", J. Neurophysiol, **36**, pp. 634-648.

McFadden, P. D. and Smith, J. D., 1984, "*Vibration Monitoring of Rolling Element Bearings by the High-Frequency Resonance Technique - A Review*", International Journal of Tribology, **17**, pp. 3-10.

McFadden, P. D. and Smith, J. D., 1985, "*The Vibration Produced by Multiple Point Defects in a Rolling Element Bearing*", Journal of Sound and Vibration, **98** (2), 263-273.

Morton, P. G., 1971, "*Measurements of Dynamic Characteristics of a Large Sleeve Bearings*", Transactions of ASME, Journal of Lubrication Technology, 143.

Muszynska, A. and Bently, D. E., 1990, "*Frequency-Swept Rotating Input Perturbation Techniques and Identification of the Fluid Force Models in Rotor/Bearing/Seal Systems and Fluid Handling Machines*", Journal of Sound and Vibration, **143** (1), pp. 103-124.

Myrick, T. Jr., and Rylander H. G., 1975, "*Analysis of Flexible Rotor*", ASME Design Engineering Technology Conference, Washington D.C. 75-Det-39.

Nam, S. W., Kim, S.B., and Powers, E. J., 1990, "*Nonlinear System Identification With Random Excitation Using Discrete Third Order Volterra Series*", Conference Proceedings of 8th International Modal Analysis, pp. 1278-1283.

Newkirk, B. L., 1925, "*Shaft Whipping*", General Electric Review, 169.

Newkirk, B. L., and Taylor, H. D., 1924, "*Shaft Whipping Due to Oil Action in Journal Bearings*", General Electric Review, pp. 559-568.

Nikias, C. L., and Raghuveer, M. R., 1987, "*Bispectral Estimation: Digital Signal Processing Framework*", Proceedings of IEEE, 75, pp. 869-891.

Nordman, R., and Schollhorn, K., 1980, "*Identification of Stiffness and Damping Coefficients of Journal Bearings by Means of Impact Method*", Institution of Mechanical Engineers Conference, Vibration of Rotating Machinery, Cambridge.

Ocvirk, F., 1952, "*Short Bearing Approximations for Full Journal Bearings*", NASA Tech. Note 2808.

Odiari, E. A., and Ewins, D. J., 1992, "*Parameter Identification for Nonlinear Rotor-Stator Systems- the Volterra/Wiener Based Approach*", Conference Proceedings of Institution of Mechanical Engineers (IMechE), Vibrations in Rotating Machineries, pp. 193-202.

Orabi, I. I., and Ahmadi, G., 1987, "*A Functional Series Expansion Method For Response Analysis of Nonlinear Systems Subjected to Random Excitations*", International Journal of Nonlinear Mechanics, **22**(6), pp. 451-465.

Orcutt, F. K., Arwas, E. B., 1967, "*The Steady State and Dynamic Characteristics of Full Circular Bearing and a Partial Arc Bearing in Laminar and Turbulent Flow Regimes*", Transactions of ASME, Journal of Lubrication Technology 89 Series **F(2)**, pp. 143-153.

Palmgren, A., 1959, "*Ball and Roller Bearing Engineering*", Third Edition, Burbank.

Papanicolaou, G. C., and Kohler, W., 1974, *"Asymptotic Theory of Mixing Stochastic Ordinary Differential Equations"*, Comm. on Pure and Applied Mathematics, **27**, pp. 614-668.

Planck, M., 1917, "*Uber einen satz der statischen dynamik und seine erweiterung in der quanten-theorie*", Sitzungber, Preuss. Akadamie Weiss, pp. 324-341.

Powers, E. J., and Miksad, R. W., 1987, *"Polyspectral Measurement and Analysis of Nonlinear Wave Interactions in Fluids"*, ASME Winter Annual Meeting, Boston.

Pradlwarter, H. J., Bucher, C. G. and Schueller G. I., 1991, "*Structural Dynamics, Recent Advances*", *Editor Schueller, G. I.*, New York: Springer - Verlag.

Raemer, H. R., 1969, "*Statistical Communication Theory and Applications*", Englewood Cliffs, New Jersey: Prentice-Hall.

Ragulskis, K. M., Jurkauskas, A. Yu., Atstupenas, V. V., Vitkute, A. Yu., and Kulvec, A. P., 1974, "*Vibration of Bearings*", Vilnyus: Mintis Publishers.

Rao, J. S., 1998, "*Rotor Dynamics*", Third Edition, New Age International (P) Limited Publishers.

Reusner, H., 1977, "*Druckfl,,chenbelastung und Overfluchenverschiebung in W,,lzkontakt von Rot,,tionskurpern*", Dissertation, Schweinfurt, West Germany.

Rice, H. J., and Fitzpatrick, J. A., 1988, "*A Generalised Technique For Spectral Analysis of Nonlinear Systems*", Mechanical Systems and Signal Processing **2**(2), pp. 195-207.

Rice, H. J., and Fitzpatrick, J. A., 1991, "*A Procedure for the Identification of Linear and Nonlinear Multi-Degree of Freedom Systems*", Journal of Sound and Vibration, **149**(3), pp. 397-411.

Roberts, J. B., 1981, "*Response of Nonlinear Mechanical Systems to Random Excitation, Part 1: Markov Method*", Shock and Vibration Digest, **13** (4), pp. 17-28.

Roberts, J. B., 1983, "*Energy Method for Nonlinear Systems With Non-White Excitation*", Proceedings IUTAM Symposium Random Vibrations and Reliability, K. Hennig, Ed, Akademie, Berlin, pp. 285-294.

Robertson, D., 1946, "*Whirling of a Journal in a Sleeve Bearing*", Philosphical Magazine, **15**(7), pp. 113-130.

Rouvas C. and Childs D. W., 1993, "*A Parameter Identification Method for the Rotordynamic Coefficients of a High Reynolds Number Hydrostatic Bearing*", Transactions ASME, Journal of Vibration and Acoustics, **115**, pp. 264-270.

Roy, R. V., and Spanos, P. D., 1990, "*Wiener-Hermite Functional Representation of Non-Linear Stochastic Systems*", Journal of Structural safety.

Rubinstein, R. Y., 1981, "*Simulation and the Monte Carlo Method*", Wiley, New York.

Rugh, W. J., 1981, "*Nonlinear System Theory: The Volterra/Wiener Approach*", Johns Hopkins University Press, Baltimore, Maryland.

Sahinkaya, M. N., and Burrows, C. R., 1984, "*Estimation of Linearised Oil Film Parameters from Out of Balance Response*", Proceedings of Institute of Mechanical Engineers **198c**(8), 131.

Sandberg, I. W., 1982, "*Expansions for Nonlinear Systems*", Bell System Tech. J., **61** pp. 159-200.

Sayler, R., deSilva, G., Leather, J., Anderson, J. and MacPherson, P., 1981, "*Elastic Conformity in Hertzian Contacts*", Tribol. Int., pp. 315-322.

Schetzen, M., 1965, "*Measurement of the Kernels of a Nonlinear System of Finite Order,*" International Journal of Control, **1**(3), pp. 251-263.

Schetzen, M., 1965a, "*Synthesis of a Class of Nonlinear Systems,*" International Journal of Control, **1**(5), pp. 401-414

Schetzen, M., 1974, "*A Theory of Nonlinear System Identification,*" International Journal of Control, **20**(4), pp. 577-592.

Schetzen, M., 1980, "*The Volterra and Wiener Theories of Nonlinear Systems*", New York: John Wiley and Sons.

Shinozuka, M., 1972, "*Monte Carlo Solution of Structural Dynamics*", Computers Structures, **2**, pp. 855-874.

Simandri, S., and Hahn, E. J., 1975, "*Effect of Pressurization in the Vibration of Isolation Capability of Squeeze Film Bearings*", ASME Design Engineering Technology Conference, Washington D. C., 75-Lub-70.

Soong, T. T. and Grigoriu, M., 1993, *Random Vibration of Mechanical and Structural Systems*. New Jersy: Prentice-Hall.

Spanos, P. D., 1981, "*Monte Carlo Simulations of Responses of Non-Symmetric Dynamic Systems to Random Excitations*", Computers Structures, **13**, pp. 371-376.

Spanos, P. D., 1983, "*Approximate Analysis of Random Vibration Problems Through Stochastic Averaging*", Proceedings IUTAM Symposium Random Vibrations and Reliability, K. Hennig, Ed, Akademie, Berlin, pp. 327-337.

Spanos P. D. and Donley M. G., 1991, "*Equivalent Statistical Quadratization for Non-Linear Systems*", Journal of Engineering. Mechanics, **117**(6), pp. 1289-1310.

Spanos P. D. and Donley M. G., 1992, "*Non-Linear Multi-Degree-of-Freedom-System Random Vibration by Equivalent Statistical Quadratization*", International Journal of Non-Linear Mechanics, **27**(5), pp. 735-748.

Spanos, P. D. and Mignolet, M. D., 1989, "*ARMA Monte Carlo simulation in probabilistic structural analysis*", Shock Vibration Digest, **21**, pp. 3-14.

Stanway, R., Burrows, C. R., and Holmes, R., 1979, I. Mechanical Engineering Science, Institute of Mechanical Engineers, **21**(6).

Stodola, A., 1925, "*Kristiche Wellenstorong Infolge Der Nachgiebigkeit Des Oelpolsters Im Larger*", Schweizerische Bauzeiting, **85**, pp. 265-266.

Stoker, J. J., 1950, "*Non-linear Vibrations*", Interscience Publishers.

Stolarski, T. A., 1990, "*Tribology in Machine Design*", Oxford: Heinemann Newnes.

Stratonovitch, R. L., 1967, "*Topics in the Theory of Random Noise*", **2**, Gordon and Breach, New York.

Su, Y. T., Lin, M. H., and Lee M. S., 1993, "*The effects of Surface Irregularities on Roller Bearing Vibrations*", Journal of Sound and Vibration, **165** (3), pp. 455-466.

Sunnesjo, C. S., 1985, "*Rolling Bearing Vibrations - The Effects of Geometrical Imperfections and Wear*", Journal of Sound and Vibration, **98** (4), pp. 455-474.

Swanson, E. E., and Kirk, R. G., 1997, "*Survey of Experimental Data for Fixed Geometry Hydrodynamic Journal Bearings*", Transactions of ASME, Journal of Tribology, **119**, pp. 704-710.

Tick, L., 1961, "*The Estimation of Transfer Functions of Quadratic Systems*", Technometric **3**(4) pp. 563-567.

Tiwari, R. and Vyas, N. S., 1995, "*Estimation of Nonlinear Stiffness Parameters of Rolling Element Bearings from Random Response of Rotor Bearing Systems*", Journal of Sound and Vibration, **187**(2,) pp.229-239.

Tiwari, R. and Vyas, N. S., 1997, "*Nonlinear Bearing Stiffness Parameter Extraction from Random Response in Flexible Rotor-Bearing Systems*", Journal of Sound and Vibration, **203**(3), pp. 389-408.

Tiwari, R. and Vyas, N. S., 1997a, "*Parameter Estimation in Imbalanced Nonlinear Rotor-Bearing Systems from Random Response*", Journal of Sound and Vibration, **208**(1), pp. 1-14.

Tiwari, R. and Vyas, N. S., 1998, "*Stiffness Estimation from Random Response in Multi-Mass Rotor-Bearing Systems*", Probabilistic Engineering, Mechanics, **13**(4), pp. 255-268.

Tonneson, J., 1975, "*Experimental Parametric Study of a Squeeze Film Bearing*", ASLE-ASME Joint Lubrication Conference, Miami Beach, Fla., 75-Lub-42.

Vance, J. M., and Kearton, A. J., 1975, "*Experimental Measurement of the Dynamic Force Response of a Squeeze Film Damper*", ASME Design Engineering Technology Conference, Washington D.C., 75-DET-39.

Vandiver, J. K., and Jong, J. Y., 1986, "*The Relation Between in Line and Cross Flow Vortex Induced Vibration of Cylinders*", Proceedings of Ist OMAE Symposium on Offshore and Arctic Frontiers, ASME, pp. 299-309.

Vasta M, 1995, "*Exact Stationary Solution for a Class of Non-Linear Systems Driven by a Non-Normal Delta-Correlated Process*", International Journal of Non-Linear Mechanics, **30**(4), pp. 407-418.

Volterra, V., 1889, "*Surr une generlisation de la theorie des functions d'une variable imaginaire. Ler Memoire.*", Acta Math., Stockh., **12**, pp. 233-286.

Volterra, V. 1930, "*Theory of Functionals*", Blackie and Sons, Glasgow.

Volterra, V., 1959, "*Theory of Functionals and of Integral and Integro-Differential Equations*", Dover Publications, Inc., New York.

Walford, T. L. H. and Stone B. J., 1980, "*The Measurement of the Radial Stiffness of Rolling Element Bearings Under Oscillation Conditions*", Journal of Mechanical Engineering Science **22** (4), pp. 175-181.

Warner. P. C., 1963, "*Static and Dynamic Properties of Partial Journal Bearings*", Transactions of ASME, Journal of Basic Engineering, **85**(D), pp. 247-257.

Watanabe, A., 1975, "*The Volterra Series Expansion of Nonlinear Functionals Which are Defined on the Product of two Finite- Dimensional Vector Spaces, and its Application to Characterisation of Two Input Systems*", Summer Comput. Simulation Conference.

Watanabe, A., and Stark, L., 1975, "*Kernel Method for Nonlinear Analysis: Identification of a Biological Control System*", Math. Biosci., **27**, pp. 99-108.

While, M. F., 1979, "*Rolling Element Bearing Vibration Transfer Characteristics: Effect of Stiffness*", Journal of Applied Mechanics, Trans. of ASME, **46**, pp. 677-684.

Wiener, N., 1958, "*Nonlinear Problems in Random Theory*", The Massachusetts Institute of Technology and John Wiley and Sons ,Inc., New York.

Worden, K., Manson, G. and Tomlinson, G. R., 1997, "*A Harmonic Probing Algorithm for the Multi-Input Volterra Series*", Journal of Sound and Vibration, **201**(1), pp. 67-84.

Yamamouchi, Y., 1974, "*Ship's Behaviour in Waves as a Stochastic Process*", Dynamics of Marine Vehicles and Structures in Waves (Ed. R.E.D. Bishop and W.G. Price) London: Institution of Mechanical Engineers,

Zhou R. S. and Hashimoto F. 1995, "*A New Rolling Contact Surface and "No Run-In" Performance Bearings*", Transactions of the ASME, Journal of Tribology, **117**, pp. 166-170.

Zhu, W. Q. and Yu, J.S., 1989, "*The Equivalent Nonlinear System Methods*", Journal of Sound and Vibration, **129**, pp. 385-395.

Zhu, W. Q., 1983, "*Stochastic Averaging of the Energy Envelope of Nearly Lyapunov Systems*", Proceedings IUTAM Symposium Random Vibrations and Reliability, K. Henning, Ed, Akademie, Berlin, pp. 347-357.

Zwilein, O. and Schlicht, 1980, "*Werkstoffanstrengung bei walzbeanspruchung - einfluss von reibung und eigenspannungen*", Werkstofftech, **11**, pp. 1-14.

LIST OF PAPERS PUBLISHED/COMMUNICATED FROM THE PRESENT STUDY

Khan, A. A., and Vyas, N. S., 1998, "*Nonlinear Parameter Estimation Using Volterra and Wiener Theories*", (in print), Journal of Sound and Vibration.

Khan, A. A., and Vyas, N. S., 1998, "*Parameter Estimation in a Nonlinear Coupled System Through Volterra and Wiener Kernels*", communicated to Journal of Sound and Vibration.

Khan, A. A., and Vyas, N. S., 1999, "*Nonlinear Bearing Stiffness Parameter Estimation in Flexible Rotor-Bearing Systems Using Volterra and Wiener Approach*", communicated to Probabilistic Engineering Mechanics.

Khan, A. A., and Vyas, N. S., 1999, "*Analytical and Experimental Investigations for Nonlinear Rotor Bearing Stiffness Estimation Through Volterra and Wiener Kernels*", communicated to Mechanism and Machine Theory.